An Optical Biosensor and Immunoassay Framework Suitable for On-Site Measurement of Progesterone Concentration in Bovine Milk

Mr. Arash Ghadar

BEng (Hons.), MSc (Distinction)

A thesis is submitted in partial fulfilment of the requirements for the degree of

Doctor of Philosophy in Engineering

University of Warwick

School of Engineering

May 2017

TABLE OF CONTENTS

ACKNOWLEDGMENT

I would like to express my gratitude to my supervisor Prof. Julian Gardner, who helped me to shape the project, offered wise guidance throughout and facilitated the use of university resources.

I am also very grateful for the valuable advice that Prof. Chris Dowson offered on the biological aspects, as well as the lab space and biological samples he kindly provided.

Furthermore, I would like to thank Prof Dave Hutchins, the chair of review committee, for his valuable suggestions; Datalink Electronics for their support in particular during the final days of the PhD when I needed more time; the staff at the school of engineering for their support in making the prototype units; and finally PhD students and staff at the school of life sciences for their input while working on the experiments.

I have been lucky to have a loving and caring family who supported me all the way in this journey. I appreciate their love and support when I was not able to spend as much time as I would have loved to with them. My son, Artin always found a way to make me happy, give me boost of energy and comfort me with his little heart and warm cuddles. Above all, my wife, Armaghan, my soulmate and my best friend, has always been a great source of aspiration, and desire to achieve high ambitions.

ABSTRACT

This PhD provides a novel design for a fluorescence-based biosensor and the associated immunoassay framework. It offers a solution for measuring progesterone concentration in bovine milk that can be used as an integral part of a dairy farm's reproductive management, with a direct impact on the farm profitability. A cow needs to give birth in regular intervals in order to produce a healthy amount of milk. A high pregnancy rate requires an accurate estimate of the onset of oestrus to achieve an effective insemination and therefore a high conception rate. Progesterone concentration in bovine milk reaches a minimum at around $2\ \mathrm{ng/ml}$, approximately 72 hours before oestrus, a characteristic that can be used to detect the onset of oestrus. The majority of methods currently employed for progesterone measurement require expensive laboratory-based instruments and time-consuming preparation stages. This thesis, however sets out the case for the design of a portable commercially-viable biosensor, capable of measuring progesterone concentration on-site at dairy farms.

The proposed solution features a unique adaptive offset cancellation mechanism, which compensates for the effect of varying background LED light and provides a wide dynamic range. The design eliminates the need for the expensive optical components such as lens, collimator and dichroic mirror. Furthermore, the innovative design of the casing substantially reduces the effect of background light on the detector circuit, whilst improves the fluorescent excitation within the sample and subsequent detection by the sensor. This thesis also provides a novel framework for a competitive homogeneous immunoassay based on Fluorescence Resonance Energy Transfer (FRET). Three specific immunoassay procedures are proposed, offering a trade off on hardware cost versus running cost as well as procedural and algorithmic complexity.

Following a thorough analysis of the hardware design and immunoassay framework and the optimisation of the key system parameters, a prototype biosensor was developed. Numerous experiments were carried out and the performance was verified against CLARIOstar spectrofluorometer. The outcome demonstrates the effectiveness of the immunoassay framework and the ability of the biosensor to measure fluorophore concentration with an accuracy of $\pm 250\ \mathrm{pM}$, which is suitable for detecting the onset of oestrus.

ABBREVIATIONS

BFP Blue Fluorescent Protein

BLG Beta Lacto-Globulin

BSA Bovine Serum Albumin

FRET Fluorescence Resonance Energy Transfer

GFP Green Fluorescent Protein

LED Light emitting Diode

OEM Original Equipment Manufacturer

PBS Phosphate Buffered Saline

RFP Red Fluorescent Protein

SPR Surface Plasmon Resonance

TIR Total Internal Reflection

LIST OF FIGURES

1 THE CASE FOR A PORTABLE COMMERCIALLY-VIABLE IMMUNOASSAY

1.1 Introduction

The aim of this PhD is to propose a solution for an economically-viable portable biosensor and the associated immunoassay framework that can be used for on-site measurement of progesterone concentration in bovine milk. The need for progesterone measurement arises from the fact that progesterone can be used as a key indicator for an effective reproductive management. Reproductive management is an essential part of most modern dairy farms, with a direct impact on their profitability. It focuses on maximising the pregnancy rate of the cows, in order to ensure they give birth in regular intervals and consequently produce a healthy volume of milk. A key factor in achieving a high pregnancy rate is an accurate estimate of onset of oestrus. This ensures an effective insemination and as a result a high conception rate.

Progesterone is an essential hormone in mammals' reproductive cycle. The molecule signals the body, in particular the uterus, to provide the necessary condition for enabling and maintaining pregnancy should the sperm reach the egg and form an embryo. Studies show that progesterone concentration goes through a cyclic period. In a cycle, the concentration is low during the follicular period and high while in the luteal phase. The progesterone concentration reaches a minimum of around $2\,\mathrm{nM}$, approximately 72 hours before oestrus. This is the feature that enables the use of progesterone concentration as an indicator for determining the onset of oestrus.

Although there are a variety of methods for measuring progesterone level in milk, these systems often require expensive laboratory-based instruments and extensive

sample preparation and user involvement during the test. As a result such systems are neither cost-effective nor practical for use at dairy farms.

This PhD aims to address these issues by providing a solution suitable for a portable, commercially-viable and easy to use immunoassay that can be employed on-site at dairy farms. The thesis has been broken down in a number of chapters, starting with a rationale for the proposed work, followed by a detailed review of the existing immunoassays, in particular the fluorescence-based methods. The details of the hardware design, immunoassay framework and analysis of molecular interactions are explained in the subsequent chapters. The system design and methodology have been the basis for a publication in IEEE Sensors (Ghadar, et al., 2013). Finally, critical parameters of the system are evaluated and optimised, and the results of experiments are presented to verify the performance and demonstrate the effectiveness of the proposed solution.

This chapter starts with describing the reproductive cycle and the role of oestrogen and progesterone molecules as the two important hormones controlling this process. This will then be followed by a review of reproductive management, the associated economic benefits and various ways of accomplishing an effective management, in particular the business case for having a portable economically-viable progesterone measurement assay. Finally, the chapter outlines the scope of this PhD work, along with the aims, objectives and contributions made throughout this study.

1.2 Reproductive Cycle

Female mammals go through regular reproductive cycles, consisting of a repeated sequence of fertility and non-fertility phases as shown in Figure 1.1 (DeJarnette & Nebel, 2016). The fertile phase, or the follicular phase, is where the female mammal is sexually receptive. The female body during this phase gets ready to release an egg into the uterus and accept sperm in order to form an embryo. During the subsequent non-

fertile phase, referred to as the luteal phase, the female body prepares to maintain the pregnancy in case the embryo is formed. In mammals with menstrual cycle (humans) this phase ends by the disposal of endometrium (the inner membrane of the mammalian uterus) during menstruation. In other mammals with oestrus cycles (e.g. cows) the endometrium is absorbed by the animal body at the end of this phase. The number and frequency of oestrus cycle vary amongst animals. For instance, a white-tailed deer or fox goes through oestrus once a year in a particular season; sheep and horses have a series of cycles in a year; while mice, cows and pigs have regular oestrus cycles (Encylopedia, 2011). This thesis is focused on cows' oestrus cycle and progesterone measurement as a method of detecting the onset of oestrus.

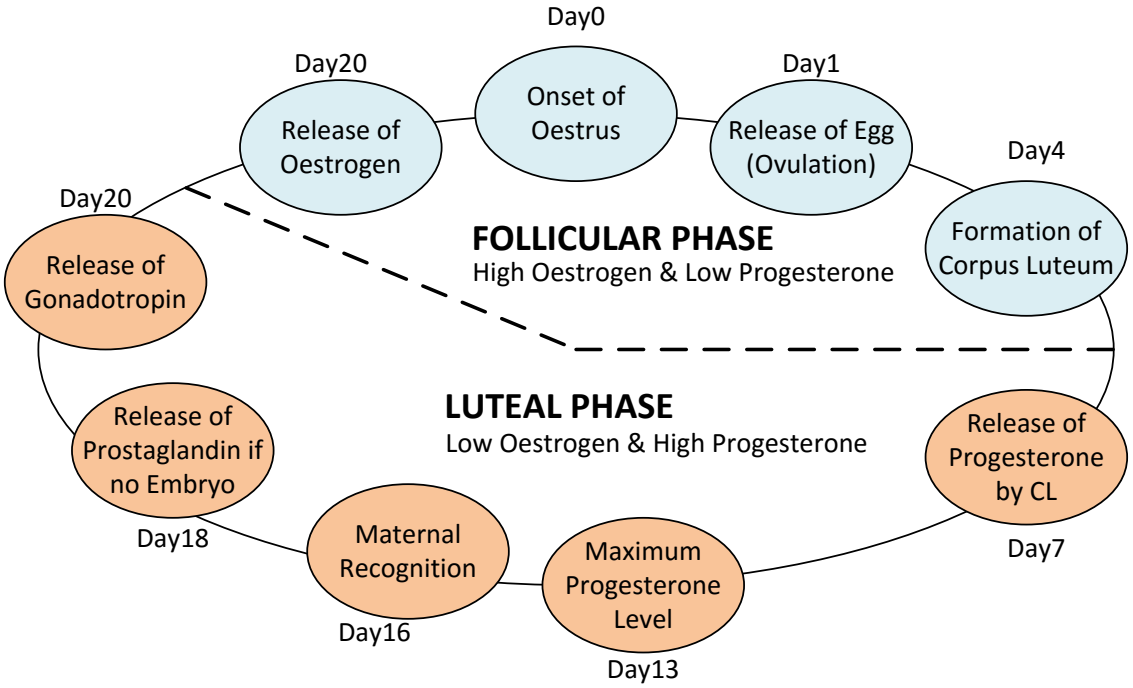

Figure 1.1 Reproductive cycle (DeJarnette & Nebel, 2016)

1.3 Progesterone and Physiological Changes during Oestrus Cycle

Prior to oestrus, a number of follicles begin to grow on the cows' two ovaries (see Figure 1.2). The ovaries produce eggs as well as oestrogen and progesterone hormones. Hormones are certain types of biomolecules used by the body for

regulating physiological and behavioural functions of organs and tissues. Metabolism, reproduction, growth and mood control are examples of such functions (Neave, 2008). The regulating effect takes place in tandem with the presence of hormone receptors on the surface or inside a cell. When the receptor binds to its specific hormone, it triggers a biochemical chain of events, which results in the associated physiological and behavioural effects. Both oestrogen and progesterone molecules are steroid hormones, which are cyclic organic compounds containing carbon, oxygen and hydrogen atoms in their base structure.

Oestrogen prepares the animal's reproductive organs for breeding by enabling the cervix to secrete mucus for lubricating the vagina, making uterus sexually sensitive and helping the passage of semen during insemination (DeJarnette & Nebel, 2016). During this period typically one of the follicles on the ovaries grows significantly larger than the others, which then ruptures and releases an egg, resulting in ovulation.

After ovulation the oestrogen level falls and luteal cells grow in place of the ruptured follicles, which subsequently turn into Corpus Luteum (CL), normally within 5-6 days (see Figure 1.2). CL is responsible for producing progesterone. Progesterone is a steroid hormone with molecular formula of $C_{21}H_{30}O_2$ and specific weight of $314.4617\ \mathrm{ng/ml}$ (Biotechnology Information, 2015). This hormone triggers uterus to produce uterine milk as a nourishing substance for the embryo. It also enables the formation of a thick mucus plug for blocking the cervix and protecting the uterus from viruses and bacteria. In addition, progesterone helps maintaining the pregnancy by regulating the release of gonadotropins from the pituitary gland in the brain (DeJarnette & Nebel, 2016).

During an oestrus cycle the level of progesterone increases from its minimum level at oestrus to the maximum level at around day 13. A few days later, typically at day 16, the uterus looks for embryo (maternal recognition) and if none is detected produces prostaglandin hormone, which destroys the CL. The lack of functioning CL enables the

pituitary gland to increase the secretion of gonadotropin, resulting in the production of oestrogen by the dominant follicle and consequently start of another oestrus cycle after 21 days.

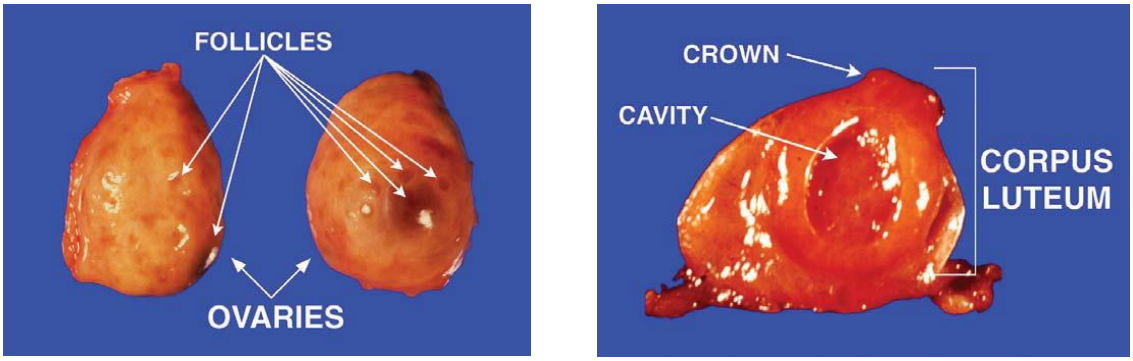

Figure 1.2 Ovaries and the egg producing follicles (left). Cross section of the ovary and the Corpus Luteum (right) (DeJarnette & Nebel, 2016)

The oestrus cycle is often described in two subsequent and complimentary phases; namely, follicular and luteal (see Figure 1.1). During the follicular phase the oestrogen level is high and progesterone level is low, providing a suitable condition for insemination. The luteal phase is associated with low oestrogen and high progesterone levels in order to provide a suitable condition for the growth and development of embryo, if one is formed. This phase starts with the formation of CL (day 5-6) and ends with the destruction of CL (day 17-19). Figure 1.3 shows the typical progesterone level profile during oestrus cycle. The figures shows progesterone level is low a few days before and after oestrus then gradually rises to its maximum level at day 13. After that if the embryo is formed the progesterone level remains high, otherwise it falls to near-zero level by day 21, indicating the start of a new oestrus cycle.

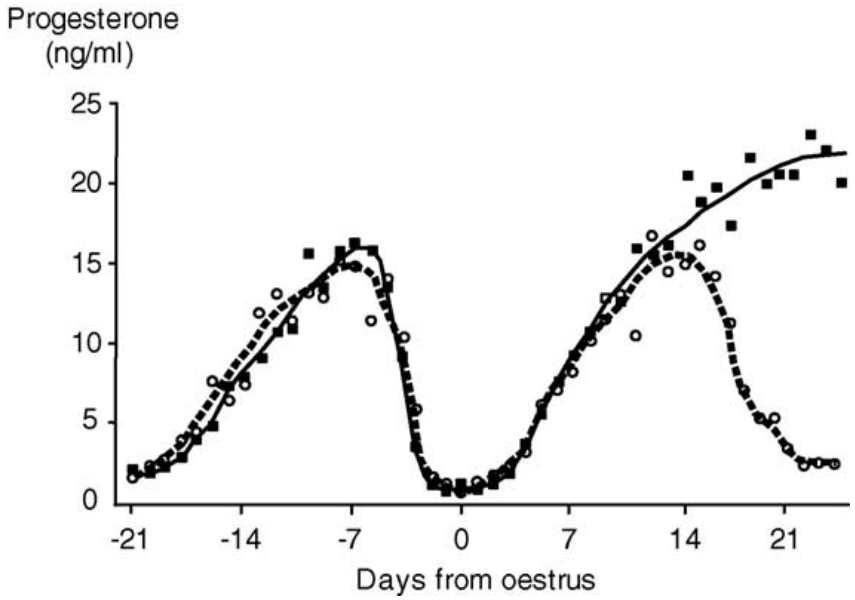

Figure 1.3 Concentration of milk progesterone around oestrus, shown by day 0. The squares represent the case where the cow conceived, whereas the circles show the case where it did not conceive (Friggen & Chagunda, 2005)

1.4 Reproductive Management

Profitability of a dairy farm has a direct relationship to the amount of milk produced per cow. A dairy cow is a mammal therefore needs to give birth in order to produce milk. The gestation period for a cow is around 9 months. Towards the end of this period prolactin and uterine lactogenic hormone levels increase, which trigger the development of mammary glands. After gestation, the lactation (secretion of milk by mammary glands) starts which typically lasts for 12 months. Milk production is normally at the highest level between 30 to 150 Days in Milk (DIM) (Poock, et al., 2009). After each pregnancy, farmers consider a 2-3 months period of rest, allowing the cow's body to get ready for another round of pregnancy and lactation (Giordano, et al., 2011). Once this period is over, the cow needs to be impregnated as soon as possible in order to minimise the unnecessary delay in milk production.

1.4.1 Factors Affecting Milk Production

In general optimised milk production relies on two main factors; namely, successful pregnancy in a timely fashion; and optimised milk yield per cow. The latter depends on various conditions such the breed, food and health of the cow. These factors are outside the scope of this PhD work and are not discussed here.

On the other hand in order to achieve a successful pregnancy in a timely fashion two aspects need to be considered. Firstly an appropriate insemination technique must be employed to generate a high conception rate. Secondly, the insemination must be carried out at an appropriate time in order to achieve a high pregnancy rate. These aspects are discussed in the subsequent sections.

1.4.2 Insemination

The insemination can be carried out either by Natural service Sires (NS), or using Artificial Insemination (AI). AI has several advantages over NS. It generally leads to a higher conception rate (Grimard, et al., 2006); eliminates the venereal diseases; is a much safer operation to carry out (Vishwanath, 2003); has significant genetic benefits (Lima, et al., 2010); and results in an improved milk production by delivering heifers from more-productive breeds (Overton, 2005).

The timing of insemination is of significant importance in order to achieve a high pregnancy rate. The appropriate time of insemination can be determined by anticipating the onset of oestrus as outlined in Section 1.4.3. Currently there are two methods to achieve this goal. The first method is based on synchronised insemination, where the reproductive activities of a group of cows are synchronised as a result of injection of certain hormones. This leads to synchronised oestrus cycles for the cows in the same synchronised group, all starting oestrus at the same known time. This method is currently employed in some industrial farms; however there is an extra cost

associated with the injection of various hormones at different stages. Furthermore, the presumed time of oestrus is not always precise and certain level of oestrus monitoring, albeit over a shorter period of time, is still required.

The second method is based on accurate detection of onset of oestrus. Oestrus detection is the focus of this PhD work and will be reviewed in Section 1.4.4.

1.4.3 Milk Progesterone and Optimum Time of Insemination

Milk, blood, faeces and saliva all provide noticeable progesterone profiles. Some studies have been conducted on the time of oestrus and its relation to progesterone level in milk and blood (Posthuma-Trumpie, et al., 2009). In a study carried out by Roelofs, et al., twenty sets of data for milk and eighteen sets for plasma progesterone concentration were collected (Roelofs, et al., 2006). Each data set consisted of a progesterone profile from its maximum concentration to when the progesterone level fell below $2\ \mathrm{ng/ml}$. Table 1.1 presents the results of these experiments, showing that on average milk progesterone level declined from $15\ \mathrm{ng/ml}$ to $5\ \mathrm{ng/ml}$ in 18 hours, with a subsequent decline from $5\ \mathrm{ng/ml}$ to $2\ \mathrm{ng/ml}$ in the next 9 hours.

Table 1.1 Milk progesterone and time to oestrus

Milk progesterone concentration ($\mathrm{ng/ml}$)	Time to oestrus Mean $\pm$ SD (hours)
<15	97.7±17.8
<5	79.7±11.2
<2	70.7±16.8

In another study Dransfield, et al., carried out several experiments over 2661 artificial inseminations in 17 herds in order to determine the optimum timing for AI in dairy cows (Dransfield, et al., 1998). Table 1.2 shows the most effective time for insemination is a 12-hour window, between 4 to 16 hours from the onset of oestrus.

Generally the best results are achieved if the cow is inseminated 3 days after the fall of milk progesterone level below $5\ \mathrm{ng/ml}$ (Velasco-Garcia & Mottram, 2003).

Table 1.2 AI timing vs conception rate (Velasco-Garcia & Mottram, 2003).

Number of hours from the onset of oestrus to AI	Number of AIs	Conception Rate %
0-4	327	43
4-8	735	51
8-12	677	51
12-16	459	46
16-20	317	28
20-24	139	32
24-28	7	14

1.4.4 Oestrus Detection

Oestrus detection is achieved by a variety of methods, each offering a different level of accuracy. Some techniques consider the physiological changes and others focus on the behavioural aspects (Firk, et al., 2002). The presence of mounting activity, restlessness, reduced milk yield, increased body temperature and reduced electrical resistance of vaginal mucus are some of the signs that may be used for detecting the onset of oestrus (Rao, et al., 2013).

Mount activity is the more-widely used behavioural method, which is based on the principle that a cow in heat has the tendency to stand and encourage the male cows to mount (Ball & Peters, 2004). HeatWatch developed by Cow Chips LLC (Watch, 2006), is a commercial system, which uses mount activity for detecting oestrus. This is based on a special mount sensor attached to the cow, which monitors the mount activity and sends necessary signals wirelessly to a central computer. The computer implements sophisticated algorithms to detect the mount activity.

The above mentioned methods only apply to small farms, are not accurate and/or require substantial infrastructure at a significant cost. In the contrary, earlier in this chapter, it was stated that progesterone level is an accurate indicator of oestrus. The progesterone measurement can be done using easily-obtainable milk samples. Such systems do not require a sensor per cow (only a few per farm) and can be conveniently scaled up across large farms. The downside however is the cost of current progesterone measurement methods. These methods are reviewed in details in chapters 2 and 3. The purpose of this PhD is to introduce an economically-viable progesterone biosensor design, which can be used on-site by the farmers in order for benefit from the accuracy of progesterone-based oestrus detection at an affordable cost.

1.5 Economic Benefits and Business Rationale

In order to understand the business rationale behind this proposal, the economic benefits of accurate oestrus detection needs to be investigated. University of Missouri produced a report for the Missouri Dairy Growth Council in 2009 (Poock, et al., 2009), stating that the US national average for Oestrus Detection Rate (ODR) and the Pregnancy Rate (PR) are 35% and 14%, respectively. The Pregnancy Rate (PR) is the Conception Rate (CR) multiplied by oestrus detection rate. The average conception rate starts from 43% in the first service, declining to 40% for the third service (Ferguson & Skidmore, 2013). As mentioned before oestrus detection is of prime importance for a dairy farm. It results in an improved pregnancy rate and better-controlled pregnancy intervals, therefore profitable yet healthy cows (Friggen & Chagunda, 2005).

Using the tool provided by Scott Poock (Poock, 2009), considering 35% oestrus detection rate and 40% conception rate, a 10% increase in the detection rate results in a 4% increase in the pregnancy rate (from 14% to 18%). Scott Poock estimated $35 economic benefits per cow per a percentage increase in the pregnancy rate. Therefore

a 4% increase for a herd of 100 cows could potentially generate an additional annual economic benefit of $14K (£11K) for a herd with 100 cows.

1.5.1 Market Size

In order to estimate the potential economic benefits of the proposed technology in the UK, the first issue to be considered is the size of this industry. The number of dairy cows in the UK was estimated to be around 1.8M in 2015 (DEFRA, 2015), while the number of UK milk producers was approximately 10K (Agency, 2015). The average farm size is therefore assumed to be 180 cows.

Considering the pregnancy rate of 35%, on average a cow gets pregnant after several inseminations over 3 oestrus cycles. During each cycle, in order to follow the progesterone profile and detect the minimum as specified in Table 1.1 , regular progesterone measurement over 5 days prior and 5 days after the expected oestrus is required. Dairy cows are normally milked 4-5 times a day. The progesterone level therefore needs to be measured 40-50 times during each cycle, 120-150 times annually, on average 135 times.

Assuming that a progesterone sensor can measure the progesterone level in a sample within 30 minutes, including preparation time, it can take 48 measurements every day, in total 17520 measurements over a year. In a perfect scenario where the oestrus cycles of all cows are perfectly staggered , each sensor on average can test milk samples from 130 cows (assuming 135 tests per cow per year). This means on average two sensors will be required to deal with an average size farm of 180 cows. In reality however this is not the most probable scenario and at least a third sensor will be needed to run alongside the other two. In addition there will be a need for a fourth one to ensure there are at least three fully operational sensors, while one is going through maintenance and repair. Therefore in total four sensors are considered for each average size farm, leading to 40K potential market size to cover all the farms in

the UK. Considering a 50% adoption rate over a 5-year period the annual requirement for the first 5 years will be around 4K sensors.

The number of UK dairy cows increases 50K (2.5-3%) a year (DEFRA, 2015). Also as commercial devices go through a development cycle once every 5 years, at least to offer new user interface and connectivity features, it is plausible to envisage some customers would like to replace some of their current devices with the new version. Considering a modest 2.5% replacement rate, in total there will be a need for manufacturing an extra 5% unit, 1000 sensors from year 6 onwards. These figures are for the UK alone, which only has 2% of the worldwide milk production market (FAO, 2015).

1.5.2 An Indicative Estimate of the Potential Revenue

The estimated market size above is based on the transducer only. However, the main benefit is in the consumables, automation and database management software, which will have long-term economic benefits and generate steady stream of revenue. Considering the current number of cows at 1.8M, 50% adoption after 5 years, and 135 tests per cow every year, the total annual number of consumables will be in the region of 120M. Assuming that a scaled down version of the sensor as suggested in the future work section is used, due to the small amount of biosamples required for each test, the selling price of the consumables per test is estimated to be lower than 20p, resulting in a consumable revenue of £24M in the UK.

The consumable cost for an average 180-cow farm, based on 135 tests per cow every year, would be £4.8K. Looking back at the beginning of this section, effective oestrus detection can bring an additional £11K saving per 100-cow herd (for 4% improvement in pregnancy rate), or £20K for an average farm. Taking away the cost of consumables, the farm could potentially make a saving of £15K a year. If £5K is considered for purchasing 4 sensors (£1250 each), there will be £10K saving in the first year and £15K

thence. The potential saving would increase if the pregnancy rate improves beyond 4%. In addition, a high production volume is expected to significantly reduce the selling price of the consumables, while improving the business profitability.

The manufacturing cost of the sensor at annual production volumes of 1K or more is estimated to be in the region of £400-500. Normally an Original Equipment Manufacturer (OEM) operates on the basis that 30-40% of the selling price constitutes the manufacturing cost and the remaining running costs of the business including admin, R&D, finance, sales, marketing and profit. Therefore, depending on the production volume, an average selling price of £1250 can be envisaged for this product. This is in fact cheaper than the least expensive quality handheld fluorometer in the market.

The development, verification, field trial and certification are anticipated to take 2-3 years and cost in the region of £500K. As the new company will likely to be the market leader it is plausible to consider a minimum of 25% market share. This will result in the sales of 5K devices and 90M consumables in total during the first 5 years, followed by an annual device sales of 250 and a 5% increase in consumables sales. The total revenue after 5 years for the sales of devices (£1250 per device) will be £6.25M and for the consumables (20p each), £18M. At 5% net profit the company can potentially make £1.2M profit over the first 5 years, enough to pay for the initial investment, including interest charge. Once the market is established the annual revenue based on the sales of new and replacement devices will be £300K, while the consumables will continue to sell for all the new and existing farms..

The figures and estimates stated in this section only provide an indication of the market size and revenues for the company, demonstrating the potentials for establishing a high growth company with healthy profit margins to attract investors for developing the commercial product.

1.6 Problem Formulation, Objectives and Contributions

The aim of this PhD work is to design an economically-viable portable biosensor and the associated immunoassay framework for the on-site measurement of progesterone concentration in bovine milk. The proposed system is based on the principle of competitive homogeneous fluorescence-based immunoassay where tagged antigens compete with the native antigen, as the analyte of interest, in order to bind with the immunoassay-specific antibody. Fluorescence Resonance Energy Transfer (FRET) is used to separate the antigens of interest and measure the concentration of native antigen. This led to the following objectives:

- To review the literature on existing sensors and immunoassays, which can be used for measuring progesterone.
- To review the literature on the principles of fluorescence spectroscopy and how they can be applied to the sensor design.
- To design and develop a cost-effective and sensitive electronic circuitry in order to accurately control the LED and measure photodiodes output. To design and develop an enclosure that reduces the effect of background light, while offering a good degree of thermal conductivity and protection against ambient light.
- To develop the measurement methodology and the theoretical framework based on FRET for measuring concentration of progesterone.
- To review and analyse the main constituents and molecular behaviour of milk and how they can affect the performance of the immunoassay.
- To verify the design of the transducer using standard fluorophores and compare that against a standard high performance lab-based spectrometer.
- To review the outcome of the research and suggest ideas for future work and direction of research.

Following a thorough investigation into the current design of fluorometers, immunoassays and the associated biomolecular aspects, a transducer design was

proposed that can be manufactured as an economically-viable product for widespread use. The transducer provides the necessary platform for the application of a homogenous competitive immunoassay in order to measure the concentration of the analyte of interest. These aspects formed a major part of the subsequent work carried out for this PhD. A complete system was then developed and evaluated. The simulation and empirical results demonstrated the effectiveness and validity of the proposed solution. In order to achieve the aims and objectives of this PhD, a number of novel methods and approaches were proposed, analysed and implemented, resulting in significant contributions to this field as detailed below.

A novel design without the need for optical components

The current commercial fluorometers require a range of optical components including collimators, lenses, mirrors, prisms and filters, either as a dichroic one or an optical monochromator (see Chapter 3). The proposed solution however eliminates the need for these expensive and often inefficient items yet provides the necessary measurement accuracy by the use of a combination of novel mechanical and electronic designs (see Chapter 4).

Adaptive background offset cancellation

The transducer benefits from an adaptive background offset cancellation method, without a need for a DC offset. The system uses a set of two photodiodes and the associated electronic circuitry, offering a wide dynamic range over several orders of magnitude change in the photodiode current (see Chapter 4). The transducer can measure the photodiodes output without changing the circuit settings from the case of no test tube in the chamber to the case where the test tube contains full fat milk and the fluorophore of interest (see Chapter 7). This is particularly useful for applications such as oestrus detection, where progesterone level needs to be measured and profiled over a range of fluorescence levels in order to detect the minimum and onset of oestrus.

Novel geometric design for background light reduction and scalability

The transducer features a unique mechanical design, (including light channels, test tube chamber, and electronics mounting arrangement) that significantly reduces the effect of LED background light on the photodiodes (see Chapter 4). In addition, the symmetrical design of the enclosure allows for the installation of a second set of photodiodes and LEDs, providing the necessary means for the application of ratio-metric measurement and simplification of the assay procedures (see Chapter 5). The design is also easy to manufacture and can be scaled down in order to miniaturise the system as a commercial product.

Generic solution for a wide range of applications

The transducer design including the electronic and mechanical features are not specific to progesterone measurement and can be utilised for the design of a generic fluorometer. In addition, the proposed solution including the transducer as well as the general immunoassay framework can be applied to a wide range of biomolecules in liquid samples other than milk.

Modelling and Optimisation

A statistical model of the competition between various elements of the immunoassay, based on the formation of FRET pairs, was presented and an in-depth analysis carried out (see Chapter 5). Furthermore, the key parameters of the model, including the concentration of antigens and antibody were evaluated and the optimum values were determined. This approach is in contrast with the current study trend in this field, which is mainly focused on gathering empirical results and then trying to fit a model to the system behaviour. The approach presented in this work is based on a detailed theoretical framework for the behaviour of the system, followed by data collection and verification. This is anticipated to add another dimension to the direction of research in this area.

Biomolecular Interaction Analysis

Milk is a complex medium, consisting of a wide range of molecules with different shapes, sizes and manner of interaction. In order to understand the binding behaviour of immunoassay biomolecules, an in-depth study of all key molecules of milk and their effects on the formation of FRET pairs was carried out. The focus in particular is on the affinity and probability of interference based on the concept of zeta potential and pH level. This type of theoretical analysis on milk to the best of author's knowledge has not been carried out to date.

Measurement Procedure

The immunoassay requires antibody and two types of tagged antigen molecules in order to form FRET pairs in competition with milk progesterone. Three measurement procedures consisting of two, four and five stages are proposed, providing options based on hardware cost versus complexity of algorithm, accuracy, running cost and ease of use.

1.7 Thesis Outline

The remaining chapters of this PhD have been organised as follows.

Chapter 2 provides an overview of the principles behind an immunoassay covering main aspects such as competitive versus non-competitive, separation mechanisms (homogeneous versus heterogeneous) and detection methods. This is then followed by a review of the current immunoassay methods and those used in progesterone measurement.

Chapter 3 reviews various aspects of fluorescence spectroscopy including different types of photon emission from a substance, fluorescence properties such as quantum yield and quenching and finally the fundamentals of Fluorescence Resonance Energy Transfer (FRET). This chapter also gives a brief overview of the existing commercial

spectrometers and fluorescence-based immunoassays used for measuring progesterone concentration.

Chapter 4 provides a complete account of the transducer design, including enclosure, emitter and detector. The enclosure section describes the novel geometric design that minimises the effect of LED background light on the photodiode. The Emitter section covers the characteristics of the LED and the associated control circuit. The LED voltage, current and junction temperature can affect the wavelength and luminous power of the LED. These aspects and the appropriate control and measurement methods are reviewed in this chapter. Finally, the details of the detector circuit, including the photodiodes, the associated circuit and offset current and voltage are described. The principle behind dynamic offset cancellation method is also presented in this chapter.

Chapter 5 details the system model describing the formation of FRET and the relationship between FRET signal and progesterone concentration. In this chapter the excitation and emission spectra of LED, donor tagged progesterone, acceptor tagged progesterone and their effects on the photodiodes detection are analysed and formulated. At the end, three methods of progesterone measurement are proposed. These methods demonstrate the relationship between hardware cost, algorithm complexity, running cost and ease of use.

Chapter 6 presents a study of the major constituents of milk, including lactose, casein, whey and lipids. The structure and properties of all these molecules are investigated and their effects on the performance of the immunoassay are assessed. The concept of zeta potential and how it affects the intra-molecular interactions within milk, in particular in relationship to progesterone, is presented and the pertaining factors affecting the competitive binding of progesterone and antibody molecules are analysed.

Chapter 7 first focuses on optimising various parameters of the biomolecular model of the immunoassay, including the effect of concentration of donor and acceptor tagged antigen as well as antibody on the strength of FRET signal. Using LED, fluorophores and photodiodes spectra the best combination of LED, FRET fluorophores and photodiode colours are determined. The chapter then covers a wide range of experimentation on the effects of LED current, dynamic background cancellation and type of samples on the transducer output. This is then followed by collecting data for Fluorescein and Green Fluorescent Protein (GFP) dilutions, verified against the data gathered for the same dilutions by CLARIOstar, a high-performance microplate reader spectrometer. Finally, a number of experiments were carried out to demonstrate the formation of FRET on antibody-antigen complexes.

Chapter 8 covers the summary and conclusion of the thesis, a discussion on all key aspects of the immunoassay, followed by suggestions for future work.

The Appendix provides the paper published by the author on a part of the work carried out during this PhD programme. It is anticipated that a number of patents in particular on the hardware design and immunoassay framework can be registered, followed by further academic publications in relation to this work.

2 A REVIEW OF IMMUNOASSAYS AND THEIR APPLICATIONS TO PROGESTERONE MEASUREMENT

2.1 Introduction

Immunoassay is an established technique for detecting the existence or measuring the concentration of molecules of interest in a bio-chemical solution. An immunoassay uses specific antibody and antigen molecules in order to create an immuno-reaction, that can generate certain conditions or effects and consequently be detected or measured via a specific recognition system. There are numerous types of immunoassays which vary in the number and type of antibodies and antigens; the medium and circumstances that lead to the immuno-reaction; and finally the system and sensory mechanisms for qualitative or quantitative assessment of the reaction.

In this chapter, the principles behind immunoassays are reviewed, covering important aspects such as competitive versus non-competitive, separation mechanism, as well as label types and detection methods. This will then be followed by a review of current progesterone immunoassays, excluding fluorescence based immunoassays which will covered in the next chapter as it constitutes the main theme of this PhD.

2.2 Principle of Immunoassay

As mentioned before an immunoassay uses antibodies and antigens to form a complex that can be detected by the detection system. An antibody, or Immunoglobulin (Ig), is a form of protein used by the immune system to neutralise its associated antigen. An antibody in essence is a Y shape molecule, with heavy and light chains referred to as Fc (Crystallisable Fragment) and Fab (Antigen Binding Fragment) regions, respectively. The Y shape antibody provides two antigen binding sites as shown in Figure 2.1.

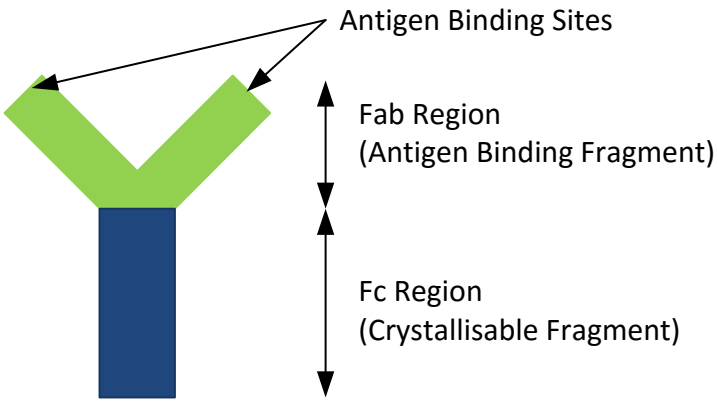

Figure 2.1 Antibody Binding Sites

The antibody can either be monoclonal or polyclonal. The Fab region of the monoclonal antibody can only bind to one epitope (binding site) of the antigen, whereas polyclonal antibodies can recognise multiple epitopes of an antigen. As a monoclonal antibody only binds to one specific epitope of an antigen, the antibodies produced during the manufacturing process are identical. The high specificity of a monoclonal antibody also results in assays with low background noise and low cross reactivity. These benefits however come at an increased manufacturing cost. A polyclonal antibody on the other hand produces higher signal level due to the possibility of binding to multiple binding sites. These antibodies are less sensitive to antigen variations and cheaper to manufacture (Abcam, 2015).

There are a number of antibody isotypes referred to as IgA, IgD, IgE, IgG and IgM, reflecting the structure of the heavy chain and the number of Y shape molecules in the structure. IgD, IgE and IgG are monomers, IgA is a dimer and IgM a pentamer, consisting of 1, 2 and 5 Y-shape molecules, respectively. A detailed review of various antibody isotypes is outside the scope of this PhD work. The isotype used in this thesis is a monomer monoclonal IgG antibody, as it is the key component of all isotypes.

An immunoassay can be used for detecting either antigen or antibody. In essence all immunoassays operate based on binding of an antigen or antibody of interest to its

specific antibody or antigen, respectively. When the analyte is antigen, a matching antibody is needed for detecting the analyte, and vice versa. Progesterone is an antigen, therefore in this PhD the focus has been on the immunoassay designs for antigen detection, although similar principles can also apply to the immunoassays used for detecting antibody as the analyte.

There are three main aspects which need to be considered in an immunoassay design; namely binding methodology, separation mechanism and detection technique. These aspects are discussed in some detail in the following sections.

2.2.1 Formation of an Antibody-Antigen Complex - Competitive vs Non Competitive

An immunoassay can be developed as either a competitive or non-competitive (sandwich) test. In the competitive format the analyte competes with its labelled version to form an antibody-antigen complex. In a non-competitive or sandwich approach the analyte is sandwiched between a labelled and un-labelled antibody or antigen depending on the type of analyte.

The basic method for the application of non-competitive approach is to immobilise antigen-specific antibody molecules on a surface such as microtiter plate (Wild, 2013). A second antibody, which can bind to another epitope of the same antigen is labelled with a detectable tag suitable for the chosen detection system, as described in Section 2.2.2. The sample containing the antigen of interest together with the second antibody is added to the plate and left to incubate. At the end of this process each antigen molecule will be sandwiched between two types of antibody molecules (see Figure 2.2). The solution then needs to be washed in order to remove the unbound molecules through a process referred to as separation. The bound antibody-antigen complexes are then put under the detection system so that the concentration level of antigen can be measured.

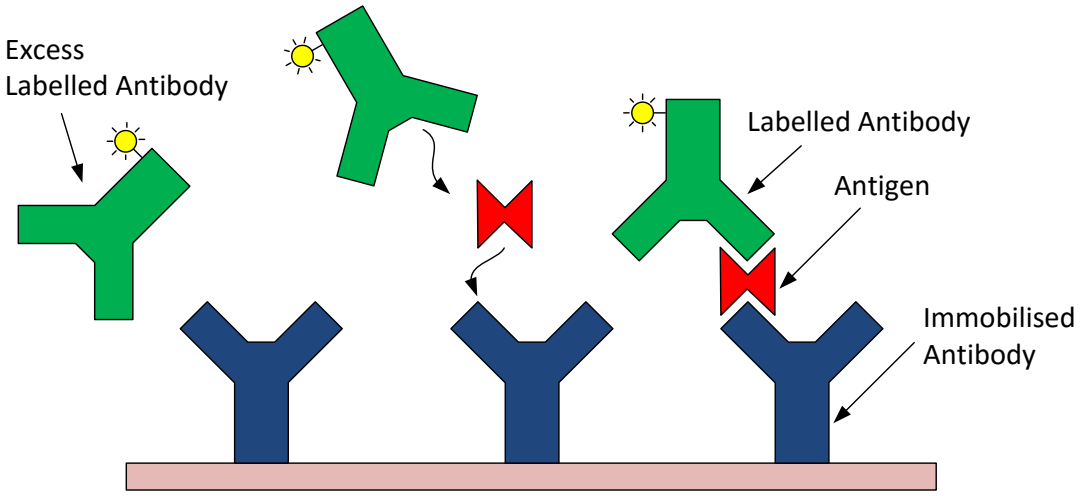

Figure 2.2 Sandwich immunoassay

In a basic competitive approach, instead of using a second labelled antibody, a labelled antigen the same as the sample antigen is used. As both original and labelled antigen molecules have equal chance of binding to the immobilised antibody binding sites, they will compete to do so (see Figure 2.3). After the separation stage the immobilised antibody-antigen complexes remain, which will be then be put under the detection system. The concentration of the original antigen has an inverse relationship to the concentration of labelled antigen, meaning that high level of labelled antigen in the antigen-antibody complexes represent low level of original antigen, and vice versa.

The sandwich approach is normally used for large antigen molecules with several epitopes allowing for two different antibodies to bind. It also generally results in a higher signal level, which will be easier to measure. This approach however requires antibody concentration to be significantly higher than the antigen's in order to ensure all antigen molecules have a chance of binding. The competitive approach on the other hand is more suitable for small molecules and also when the excess level of antibody is not available or economically viable. This method is therefore employed in this PhD for measuring the concentration of progesterone, which is a small molecule compared to normal biomolecules.

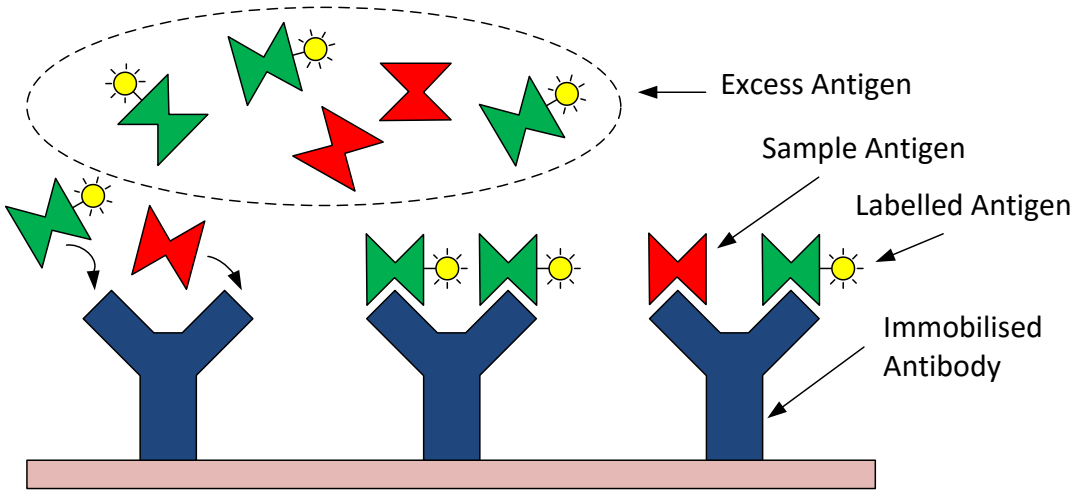

Figure 2.3 Competitive immunoassay

The diagrams shown in this section are the simplified versions of the tests normally carried out in practice, with the intention to help visualise and better understand the principles. In practice, however often a secondary antibody is used for signal generation. This has been described in more details in Section 2.3.1.

2.2.2 Label Types and Detection Methods

Once an antibody-antigen complex is formed, a suitable detection method is required to provide a qualitative or quantitative measure of the level of analyte of interest by detecting the labelled or tagged biomolecules in the sample. The majority of lab-based tests are carried-out using microtiter plates, which come in a variety of shapes and sizes. These plates consist of a large array of small wells, designed to contain a small volume of sample, while being analysed by a microtiter plate reader with a suitable detection mechanism. The biosensors in contrast have a specifically designed structure, including a suitable sample handling and detection mechanism.

There are a number of methods widely used for this purpose. A radio immunoassay benefits from radioactive tags that can be detected by a gamma detector (Szpocińska & Markiewicz, 2007). An enzyme-based immunoassay operates on the basis of change of colour when a substrate is added to the solution (Gan & Patel, 2013). A fluorescence-based immunoassay utilises fluorescent tags that can be detected by spectrofluorometry. Electrochemical immunoassays require nano-particles such as gold and the use of voltammetry to measure the electrochemical characteristics in relation to the concentration of analyte (Monerris, et al., 2012). Liquid chromatography mass spectroscopy operates based on the separation of various elements of the sample using a high pressure mechanism and then measuring the outcome using mass spectroscopy (Regal, et al., 2010) (Keski-Rahkonena, et al., 2011). A magnetic immunoassay needs magnetic beads and some form of sensitive magnetometer in order to detect magnetically-tagged biomolecules (Ivanovaa & Godjevargova, 2015). The methods that have been used in progesterone measurement and are pertinent to the design of a portable immunoassay, are reviewed in more details in Section 2.3.

2.2.3 Separation Method - Heterogeneous vs Homogeneous

In order to measure the concentration of analyte, a separation stage is required. This is carried out by either physically separating the free moving labelled molecules from the antibody-antigen complexes through a wash process, or by introducing an additional measure to separate the signal generated by the unbound labelled biomolecules from the one produced by the labelled biomolecules within the antibody-antigen complex.

Immunoassays based on physical separation are referred to as heterogeneous, whereas those that operate based on signal separation are referred to as homogeneous.

A heterogeneous immunoassay normally provides a higher signal level, however requires a careful wash process to ensure all unbound molecules are removed and the antigen-antibody complexes remain immobilised. This will lead to extra labour cost and generally longer test time. Furthermore, some of the bound antibody-antigen complexes may be removed during the wash stage resulting in variations and inaccuracies in the outcome. A homogeneous system on the other hand produces a weaker signal level under a high background noise, making it more difficult to measure. It also requires additional measures to ensure free moving labelled antibody or antigen molecules do not influence the results (Ullman, 2013). The equipment required for homogeneous assays are generally significantly more complex and expensive, although the labour involvement and test time are relatively lower, resulting in a more repeatable and reliable process.

The system proposed in this PhD work is based on homogeneous approach, which is more suitable for an automated system, as it does not require physical separation and offers a higher degree of repeatability and reliability at a lower operational cost.

2.3 Progesterone Immunoassays

Over the years various immunoassay concepts have been applied to the measurement of progesterone level, either as lab-based test or on-site at the milk parlour. Lab-based systems are generally expensive and time consuming, however offer a more accurate measurement. On-site systems are normally targeted for specific molecules and can either be a simple immunoassay like a test strip, or a complete biosensor providing a full package of sensing, transduction, analysis and user interface. This section provides an overview of the key methods used for progesterone measurement.

2.3.1 Enzyme Immunoassay

Enzyme Immuno-Assay (EIA) or Enzyme Linked Immunosorbent Assay (ELISA) is one of the most widely used assays in the industry. This type of test is normally carried out using a microtiter plate in conjunction with a microplate reader. An ELISA test can be performed on the basis of direct or indirect methodology, referring to the mechanism for capture and detection (Thermo Scientific, 2011).

In the direct method the sample is directly absorbed on the bottom of a microtiter plate's well. An enzyme-labelled antibody is then added to the well and left to incubate (see Figure 2.4). After a wash stage, chromogenic or fluorogenic enzyme substrate is added resulting in a change of colour due to the presence of enzyme in the enzyme-labelled antibody-antigen complexes (Gan & Patel, 2013).

For qualitative assays a colour chart can be used to determine whether the concentration is above or below a threshold level. For quantitative analysis, spectroscopy can be used to determine the exact concentration of the analyte of interest.

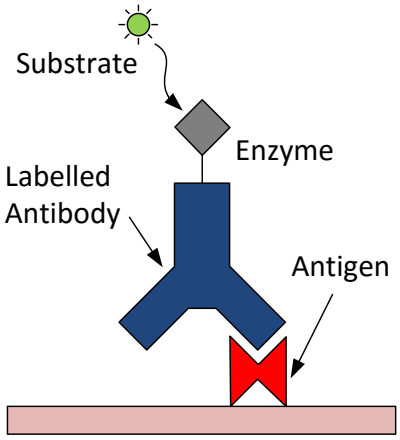

Figure 2.4 Direct ELISA with immobilised antigen and enzyme-labelled primary antibody

In an indirect method the capture is done indirectly by immobilised antibodies, incubated over a relatively long period of time on the bottom of a well (see Figure 2.5).

The sample and also another primary antibody that can bind to a different epitope of the antigen is added and left to incubate. The excess biomolecules are then washed and an enzyme-labelled secondary antibody is added to the mixture. After a while the mixture is washed again and enzyme substrate is added.

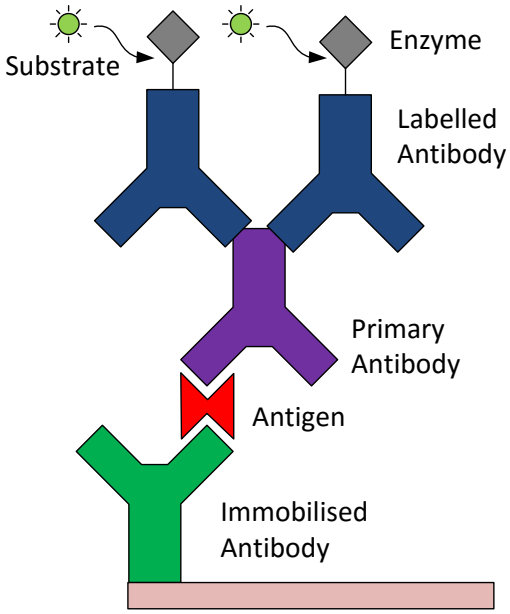

Figure 2.5 Indirect ELISA with immobilised antibody, a second primary antibody and enzyme-labelled secondary antibody

The ELISA can use the competitive format, where a secondary antibody is immobilised first. The sample, enzyme-labelled antigen, and a primary antibody is added to the well and left for some time to incubate. The labelled and unlabelled antigens compete with each other to bind with the primary antibody, which in turn binds with the secondary immobilised antibody. After a period of time, the well is washed and substrate is added. As this is a competitive format the signal produced has an inverse relationship to the actual concentration of the antibody.

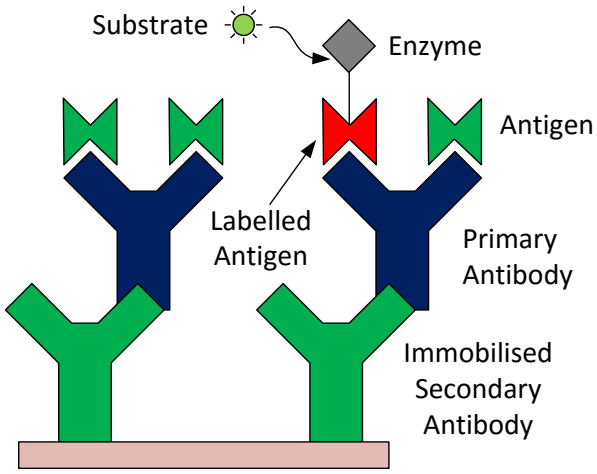

Figure 2.6 Competitive ELISA with immobilised secondary antibody, a primary antibody and enzyme-labelled antigen

ELISA has been used for measuring progesterone in milk, in particular by Waldmann in a sandwich-based assay using monoclonal antibody (Waldmann, 1993). Banu, et al., used the competitive approach for measuring progesterone as a tool to investigate ovarian cyclicity (Banu, et al., 2012). Mitchell, et al., used a 18-atom linker for protein conjugation in ELISA format and benchmarked the test against Radio Immuno-Assay (RIA), achieving a detection limit of 0.1 $\mathrm{ng/ml}$ (Mitchell, et al., 2004). Claycomb, et al., designed a complex automated fluid handling system for implementing a rapid EIA test (Claycomb, et al., 1998), which although offered the required accuracy for oestrus detection at a relatively fast turnaround, the immunoassay still needed the incubation period and wash stage, albeit through the use of a complex fluid handling system (Claycomb & Delwiche, 1998).

2.3.2 Lateral Flow Immunoassay (LFIA)

A Lateral Flow Assay (LFA) is based on the use of a test strip with an appropriate dry reagent. The reagent is activated when the sample is applied (Posthuma-Trumpie, et al., 2009). LFIA is normally used where a qualitative outcome is required such as a pregnancy test to give a positive or negative result. Similarly to ELISA, LFIA can be of a competitive or sandwich type. There have been several studies on the use of lateral

flow for on-site progesterone measurement. In one of the early attempts of using lateral flow for progesterone measurement, Laitinen, et al., used a competitive assay format with monoclonal anti-progesterone antibody and a progesterone-protein conjugate labelled with colloidal gold particles (Laitinen & Vuento, 1996a), (Laitinen & Vuento, 1996b). The reported accuracy was $5\ \mathrm{ng/ml}$. In recent years Samsonova, et al., created an assay format which benefited from the pricniples of ELISA (enzyme immunoassay) as well as speed and ease of use of lateral flow to measure progesterone in bovine whole milk (Samsonova, et al., 2015). Figure 2.7 shows the test strip developed for this purpose. The detection level reported for this test is $7\ \mathrm{ng/ml}$, which although can be used for detecting pregnancy, the accuracy level is not suitable for detecting the time of oestrus, which requires detection level of $2\ \mathrm{ng/ml}$.

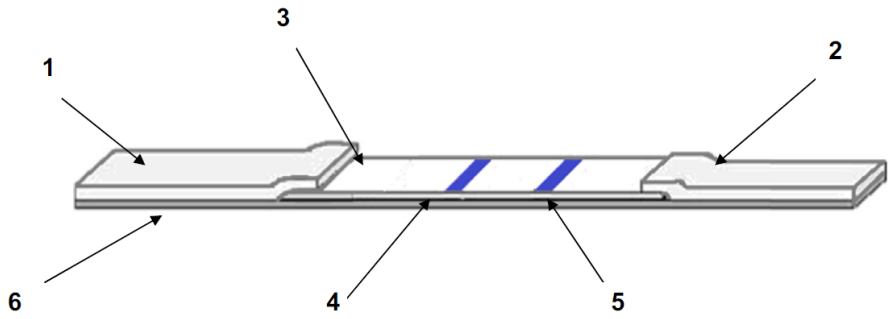

Figure 2.7 A LFEIA test strip consists of sample and absorbent pads (1 and 2) mounted on a plastic substrate (6). The analytical membrane (3) with the test and control lines (4 and 5) display and confirm the results (Samsonova, et al., 2015)

2.3.3 Magnetic Immunoassay

Magnetic immunoassay refers to the use of magnetic particles in labelling biomolecules that form the immunoassay. Ivanovaa & Godjevargova used this method to label the anti-progesterone antibodies in an ELISA format (Ivanovaa & Godjevargova, 2015). ELISA requires the antibodies to be immobilised on a substrate through a time-consuming incubation period which is typically done overnight. The wash process is also likely to wash away the antibody-antigen complex. The method Ivanovaa & Godjevargova developed does not not require antibody immobilisation.

Instead the magnetic-labelled antibody is first added to the sample solution, followed by waiting for 30 minutes to incubate. Magnatic field is then applied in order to keep the antibody-antigen complexes with the attached magnetic particle to one side while the sample is being washed. In the next stage progetserone enzyme conjugate is added, followed by waiting for a further $30\ \mathrm{min}$ to incubate. Magnetifc field is used again during the wash process. Finally enzyme substrate is added. After leaving the sample for a further $15\ \mathrm{min}$, the results are studied using a RT 2100C spectrometer at $450\ \mathrm{nm}$ wavelength (see Figure 2.8). The application of this method resulted in an accuracy of $0.1\ \mathrm{ng/ml}$. Although this method provides an accurate result and is faster than standard ELISA, still requires significant manual opeartion and takes a number of hours to complete.

Figure 2.8 Rayto RT 2100C microplate reader

2.3.4 Radio Immunoassay

A Radio Immuno-Assay (RIA) requires radioactive labelling of the antigen or antibody using a radioisotope, often a gamma radioisotope of iodine. The gamma radiation is

detected using a gamma detector. This type of immunoassay is suitable for laboratory use as the equipment is expensive, requires careful safety considerations due to the use of radioactive material and needs specially trained personnel in order to carry out the test. RIA tests however are very specific and sensitive (Szpocińska & Markiewicz, 2007). This type of immunoassay is normally considered in heterogeneous setup where a separation stage is required for moving the analyte of interest away from the labelled antibody or antigen molecules. Progesterone measurement in milk using a competitive heterogeneous setup has been successfully carried out, showing an accuracy level of $0.25\ \mathrm{ng/ml}$ (Szpocińska & Markiewicz, 2007). Colazo, et al., also compared two types of EIA tests against RIA for measuring progesterone level in milk and verified that RIA provides a greater degree of accuracy and repeatability based on the data gathered for 72 samples from 24 cows (Colazo, et al., 2008).

2.3.5 Electrochemical Immunoassay

These methods operate based on a change in the electrical characteristics of a sensor in the presence of analyte. Pemberton, et al. used a competitive enzyme-based assay and utilised potentiostat circuit to measure the concentration of progesterone (Pemberton, et al., 2001). The assay had a limit of detection of $0.8\ \mathrm{ng/ml}$. Xu, et al., based on a similar set up, carried out a quantitative analysis using absorption level at $405\ \mathrm{nm}$ and were able to measure a progesterone level less than $0.1\ \mathrm{ng/ml}$ by means a microplate reader (Xu, et al., 2005). Monerris, et al., used a specially designed electrochemical sensor for measuring progesterone in bovine milk using gold nanoparticles (Monerris, et al., 2012). Their method is based on immobilising antibody on a gold disk electrode that has gold nanoparticles deposited on a cysteamine layer. The horseradish Peroxidase (HRP) enzyme conjugated progesterone molecules then compete with the native progesterone to bind with the antibody. This is followed by a wash stage and then the addition of pyrocatechol ($\mathrm{H_2Q}$) and $\mathrm{H_2O_2}$. Once the gold disk is activated via cyclic voltammetry, the counter electrode is formed in order to facilitate measurement using Autolab PGSTAT 30 potentiostat. The system creates a

response as a result of sinewave voltammetry that is proportional to the concentration of progesterone in the milk serum. The immunoassay offers $0.5\ \mathrm{ng/ml}$ measurement limit in milk.

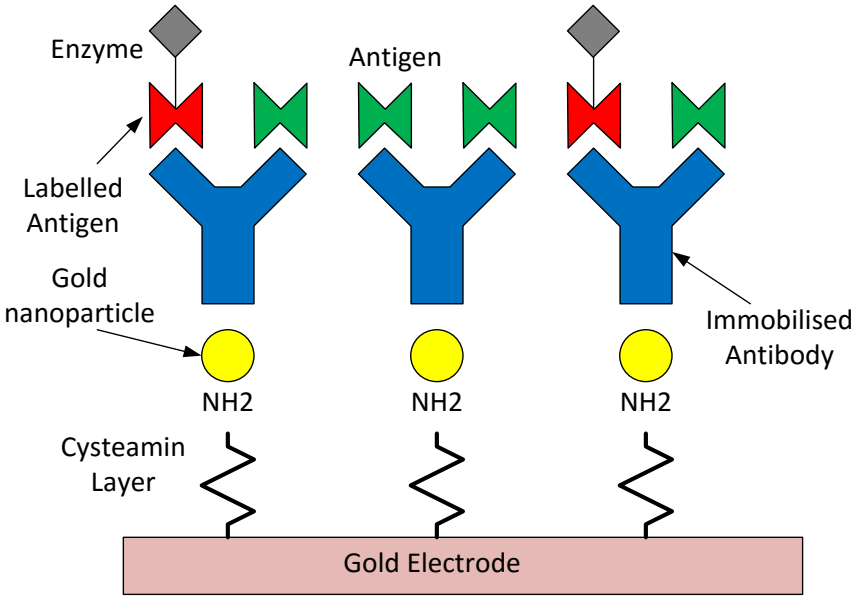

Figure 2.9 Electrochemical immunoassay process used for measuring progesterone (Monerris, et al., 2012)

2.3.6 Fluorescence-Based Immunoassay

This category consists of a wide range of methods mainly based on polarisation, fluorescence resonance energy transfer, time-resolved spectroscopy, total internal reflection and surface plasmon resonance. As the main theme of this PhD work is on the design of a fluorescence-based immunoassay, the principles of fluorescence spectroscopy along with a review of fluorescence-based progesterone immunoassays and the current commercial fluorometers are reviewed in more details in Chapter 3.

2.4 Summary

This chapter provided an overview of the main aspects of an immunoassay, focusing on separation mechanism, being heterogeneous or homogeneous; the manner of

antibody-antigen binding as in competitive versus non-competitive; and the detection system based on enzyme, radioactive tag, fluorescent tag, magnetic particles, gold nano particles and so on. This was then followed by a review of current immunoassays applied to the measurement of progesterone in milk. Table 2.1 shows a summary of the immunoassay methods mentioned in this chapter. Fluorescence immunoassays are covered in the next chapter. As demonstrated in this table the only test suitable for use outside a lab environment is LFIA. This test however does not have the accuracy required for detecting time of oestrus.

Table 2.1 Immunoassays used for measuring progesterone level

Name	Label Type	Wash Stage?	Incubation	Accuracy	Use case
ELISA	Enzyme	Yes	Yes	0.1 ng/ml	Lab based
LFIA	Enzyme	No	Yes	5 ng/ml	Portable
MIA	Magnetic	Yes	Yes	0.1 ng/ml	Lab based
RIA	Radioactive	Yes	Yes	0.25 ng/ml	Lab based
EIA	Nano particles	Yes	Yes	0.1 ng/ml	Lab based

The results for the immunoassay outlined in this chapter show that the majority can provide a means of progesterone measurement accurate enough for oestrus detection. The downside is that almost all methods require significant operator involvement, are slow to apply and need expensive lab-based equipment to capture the output and provide a representative data. Methods such as ELISA are time-consuming and require significant level of manual intervention and sample handling. Although qualitative colourimetric analysis is possible without the use of such equipment, for quantitative analysis the use of a spectrofluorometer which is an expensive lab-based analysis tool is essential. Radioimmunoassay offers a good accuracy level but is expensive and has safety concerns. Although the use of electrochemical immunoassay seems hopeful, the current available methods still require significant manual intervention and need lab-based voltammetry equipment. The methods based on fluorescence measurement offer a suitable platform for the

design of a compact assay due to the range of features and diversity of approach they can offer.

Next chapter will provide a detailed description of fluorescence spectroscopy, the associated principles, current commercial equipment and methods used to date for measuring progesterone level using fluorescence effect.

3 A REVIEW OF FLUORESCENCE SPECTROSCOPY

3.1 Introduction

Fluorescence spectroscopy provides the means of studying fluorescence effect of a fluorescent substance, referred to as fluorophore. It incorporates ways of illuminating the substance in order to instigate the fluorescence effect in a controlled manner and consequently measuring or monitoring its emission response. This is a particularly useful tool in biological studies where a fluorophore is used as a biomarker to indicate the presence of a biomolecule in the sample. This chapter provides an overview of the principles behind fluorescence spectroscopy, methods that can be employed for carrying out such studies, the structure of a basic spectrometer, a review of some currently available instruments for fluorescence spectroscopy and finally the fluorescence-based immunoassays employed for measuring progesterone level in milk.

3.2 Fluorescence

A substance whose electronic state has been excited following the absorption of incident photons, often releases it excess energy by emitting photons through a process referred to as luminescence. Jablonski diagram depicts this process as shown in Figure 3.1.

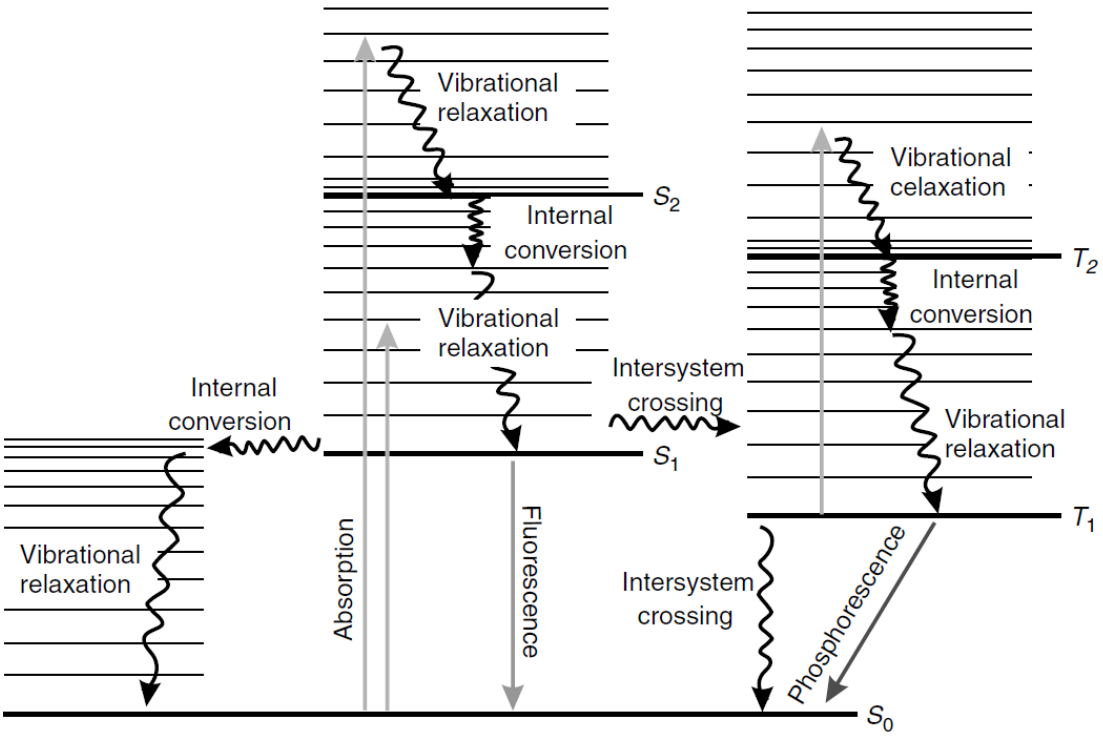

Figure 3.1 Jablonski diagram (Sauer, et al., 2011)

The wavelength of the emitted light and the length of time between excitation and emission depend on the manner of transition from the excited state to the ground level. In general a fluorophore is excited from the ground level, S_0, to a higher singlet state, S_1 or S_2. Each singlet state has a number of vibration levels shown by horizontal lines in the Jablonski diagram. A molecule in the second excited state, S_2, normally goes through internal conversion and within 10 ps relaxes to the first excited state, S_1. The lowest vibrational level represents the thermal equilibrium for each state. The transition from the lowest vibrational level of S_1 to ground level results in the emission of a photon at a higher wavelength than the excitation wavelength. This process is referred to as fluorescence, which normally takes place within 10 ns of excitation. The energy level of an emitted photon is always less than the energy of the absorbed one, hence the reason for emission at a higher wavelength. The difference between absorption and emission wavelengths is referred to as Stoke shift. The emission wavelength is normally independent of excitation.

When a molecule is in state S_1 it can experience spin conversion and go to T_1 triplet state and then relax to the lowest vibrational level of T_1. The molecule can then relax to the ground state by emitting photons through a process referred to as phosphorescence, which often takes place in the range of milliseconds to seconds, in some cases minutes or hours after excitation. This phenomenon is not common in liquid solutions as the molecule is more likely to relax through non-radiative decay or quenching (Lakowicz, 2006).

3.2.1 Depopulation Pathways of Excited Fluorophores

The depopulation of an excited fluorophore can take place in different ways, mainly through internal conversion, vibrational relaxation, secondary absorption, intersystem crossing, fluorescence and phosphorescence. Fluorescence and phosphorescence are the radiative depopulation pathways, resulting in the emission of a lower energy photon, compared to the photon energy of the incident light.

Internal conversion can either be a fast transition from a high energy singlet or triplet state to the corresponding lowest excited state or otherwise a slow non-radiative transition from the lowest excited state to the ground state. Vibrational relaxation is a fast process, during which molecules relax from a high vibrational level to the lowest level by losing their energy to other molecules through collision. Secondary absorption is the absorption of photons by the molecule at the lowest singlet or triplet excited state to a higher energy state. Intersystem crossing refers to the non-radiative transition from singlet state to a lower energy level triplet state through spin reversal. The same can also occur for the lowest excited triplet state to the ground state. As the triplet to singlet transition is spin-forbidden, molecules can stay in triplet state for many seconds as opposed to the lifetime of $100\ \mathrm{ns}$ to $1\ \mathrm{ns}$ for molecules in the singlet excited state.

3.2.2 Fluorescence Quantum Yield and Life Time

The fluorescence intensity depends on the quantum yield (Φ_F) of the fluorophore, a property which is defined as the ratio of number of emitted photons to the absorbed ones. This can be described by the rate of radiative and non-radiative emissions, k_F and k_{nr}, respectively. The k_{nr} constant captures all deactivation scenarios, including quenching, internal conversion and intersystem crossing (Jue, et al., 2009).

$$\Phi_F = \frac{k_F}{k_F + k_{nr}} \tag{3.1}$$

The radiative lifetime, τ_R, of the excited state is the inverse of the fluorescence rate constant.

$$\tau_R = \frac{1}{k_F} \tag{3.2}$$

After considering the effect of non-radiative decays the actual fluorescence decay time, τ_F, will be calculated based on the radiative and non-radiative rates.

$$\tau_F = \frac{1}{k_F + k_{nr}} \tag{3.3}$$

Considering equation (3.1), fluorescence decay time will be expressed as follows:

$$\tau_F = \Phi_F \tau_R \tag{3.4}$$

The fluorescence decay time for most commercial fluorescent molecules is between 1 ns to 10 ns, with a quantum yield in the region of 30 to 90 percent (Jue, et al., 2009). The quantum yield of green fluorescent protein used in the experimentation chapter of this PhD is 60% (Shcherbo, et al., 2009).

3.2.3 Fluorescence Quenching

A fluorophore may relax to an unexcited state through a process referred to as quenching, taking place when a quenching molecule, a quencher, interacts with the fluorophore. Quenching is often as a result of collision between the fluorophore and quencher. It may also be due to the formation of a stable complex consisting of quencher and fluorophore. There are a variety of mechanisms for collisional quenching, for example halogen quenching because of intersystem crossing to triplet state due to spin-orbit coupling (Lakowicz, 2006). The collisional quenching can be formulated using Stern-Volmer equation below (Jue, et al., 2009):

$$\frac{F_0}{F - F_0} = 1 + \frac{1}{k_q[Q]} \tag{3.5}$$

F and F_0 represent the intensity of fluorescence after and before quenching. $[Q]$ and k_q are the quencher concentration and quenching constant. The constant k_q shows the strength of quencher in relation to the fluorophore. Often fluorophores contained within a macrostructure, for example green fluorescent protein in a beta barrel (see Section 6.4.2), are less susceptible to quenching. In contrast fluorophores that freely move in a solution or present on the surface of a biomolecules have a higher quenching rate.

3.2.4 Fluorescent Labels

There are a variety of fluorescent labels that can be used for fluorescence spectroscopy. Fluorescent proteins come in a range of colours, with the Green Fluorescent Protein (GFP) being commonly used (Yang, et al., 1996). Fluorescent proteins are typically large molecules with a molecular weight in the region of tens of kilo dalton. Another category of fluorophores are small molecules such as fluorescein and rhodamine. In recent years the use of Quantum Dot (QD) is also becoming more widespread (Bustos, et al., 2012). A quantum dot is a very small semiconductor crystal

(in the range of nanometres), with size dependant optoelectronic properties that can be used for creating a tracing dye at a controlled emission spectrum. A quantum-dot-based assay has been used for measuring progesterone level in milk (Trapiella-Alfonso, et al., 2011) achieving $0.3\ \mathrm{ng/ml}$ accuracy in cow's milk. However this method requires the use of a lab-based microplate reader, therefore is not suitable as an inline progesterone measurement system (see Section 3.4.4).

3.3 Fluorescence Resonance Energy Transfer (FRET)

Fluorescence Resonance Energy Transfer (FRET) is a form of non-radiative energy transfer from an excited molecule (donor) to an adjacent molecule (acceptor). This phenomenon could result in the excitation of the acceptor and consequently fluorescent emission (Jue, et al., 2009). The acceptor can be considered a quencher, which prevents the donor fluorescing and instead enables energy transfer to the acceptor, causing it to fluoresce.

FRET often takes place in circumstances where the acceptor absorption and donor emission spectra overlap (see Figure 3.2). Dipole-dipole coupling which is dependent upon the molecules spatial orientation is the main reason for FRET. Therefore, the donor and acceptor molecules need to be in close vicinity of each other, often in the range of $1 - 10\ \mathrm{nm}$, and have relatively parallel transition dipole orientations (Held, 2005).

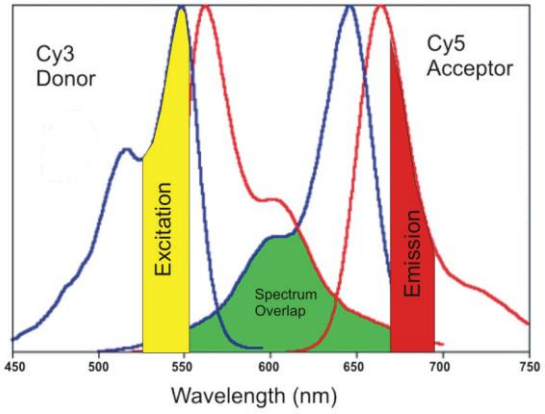

Figure 3.2 FRET overlapping spectra (Held, 2005)

The distance between donor and acceptor molecules (r) greatly influences resonance energy transfer. The extent of spectral overlap and dipole alignment are other key factors in the FRET level. The rate of fluorescence resonance energy transfer, $k_T(r)$, is expressed as follows:

$$k_T(r) = \frac{1}{\tau_D}(\frac{R_0}{r})^6 \tag{3.6}$$

The donor lifetime in the absence of FRET is represented by τ_D. R_0 is the Forster distance (Lakowicz, 2006) calculated based on equation (3.8). At this distance half the donor molecules decay as a result of FRET and the other half due to normal radiative and non-radiative rates. The efficiency of transfer is defined as below:

$$E = \frac{{R_0}^6}{{R_0}^6 + r^6} \tag{3.7}$$

The Forster distance can be formulated as below (Lakowicz, 2006):

$$R_0^6 = \frac{9000(ln\,10)\kappa^2 Q_D}{128\pi^5 N n^4}\int_0^\infty F_D(\lambda)\,\varepsilon_A(\lambda)\lambda^4 d\lambda \tag{3.8}$$

The quantum yield of the donor, Q_D, is related to the donor alone without the acceptor; n, represents the refractive index; N, is the Avogadro's number; $F_D(\lambda)$, the normalised fluorescence intensity at wavelength of λ; and $\varepsilon_A(\lambda)$, the acceptors molar extinction coefficient. The factor κ^2 describes the relative orientation transition diploes of the acceptor and donor, which can be assumed $^2/_3$ based on dynamic random averaging of the acceptor and donor. Equation (3.8) shows R_0 is representative of all important factors in resonance energy transfer. Forster distances of $2 - 9\ \mathrm{nm}$ are most suitable for FRET-based studies of biological macromolecules. Due to the presence of r^6 term in the level of energy transfer, equation (3.6), FRET efficiency is greatly dependant on the distance. For example at $r = 2R_0$, the FRET efficiency stands at 1.5% significantly reduced compared to 50% at $r = R_0$.

3.4 Principles of Commercial Fluorometers

As mentioned before intensity, quantum yield, and lifetime are the main attributes of fluorescence effect. The measurement of average fluorescence intensity reveals information about the concentration of the substance of interest, whereas the study of lifetime of a fluorophore reveals information about the environment that it exists in. Fluorescence measurements are therefore considered in two categories; namely time-resolved and steady-state. The time-resolved fluorometry is based on illuminating the sample using a pulse of light and measuring the fluorescence decay by the means of an ultra-high speed detection circuit. This type of fluorospectroscopy requires expensive equipment to be able to measure fluorescence response in the space of picoseconds to nanoseconds, therefore is not deemed as a suitable method for a low-cost portable progesterone measurement.

Steady-state fluorometry however is based on illuminating the sample over a period of time much longer than the fluorescence lifetime. The excitation light results in fluorescence emission that can be measured using a suitable fluorescence measurement device. As the fluorescence lifetime is in the region of nanoseconds, the steady state is reached quickly afterwards. This type of fluorometry in essence creates an averaging effect over time.

A typical fluorometer or fluorimeter consists of a light source, a filter or monochromator to separate the wavelength of interest from the rest, collimator, sample holder, emission filter or monochromator and finally a sensor for detecting the fluorescence emission. Figure 3.3 shows a generic schematic diagram for a fluorometer. The choice of excitation source, filtering, light channelling and detection depends on the required sensitivity and versatility of the fluorometer. Time-resolved fluorometers have the same structure as the steady-state fluorometer, however as they need to react in sub nanoseconds, they require sophisticated quick-response

excitation and emission circuitry. Therefore, these devices are more expensive and suitable for laboratory use.

3.4.1 Excitation Light Source

In a fluorometer the excitation source generates a beam of light, in a particular wavelength suited for the specific application of the fluorometer. Devices that are designed for general-purpose use often have a wide spectrum so they can be used for different fluorophores, offering greater flexibility. Xenon arc lamps or xenon flash lamps are examples of light sources for these applications. The light intensity of a lamp is controlled to remain constant over a wide bandwidth (see Figure 3.4).

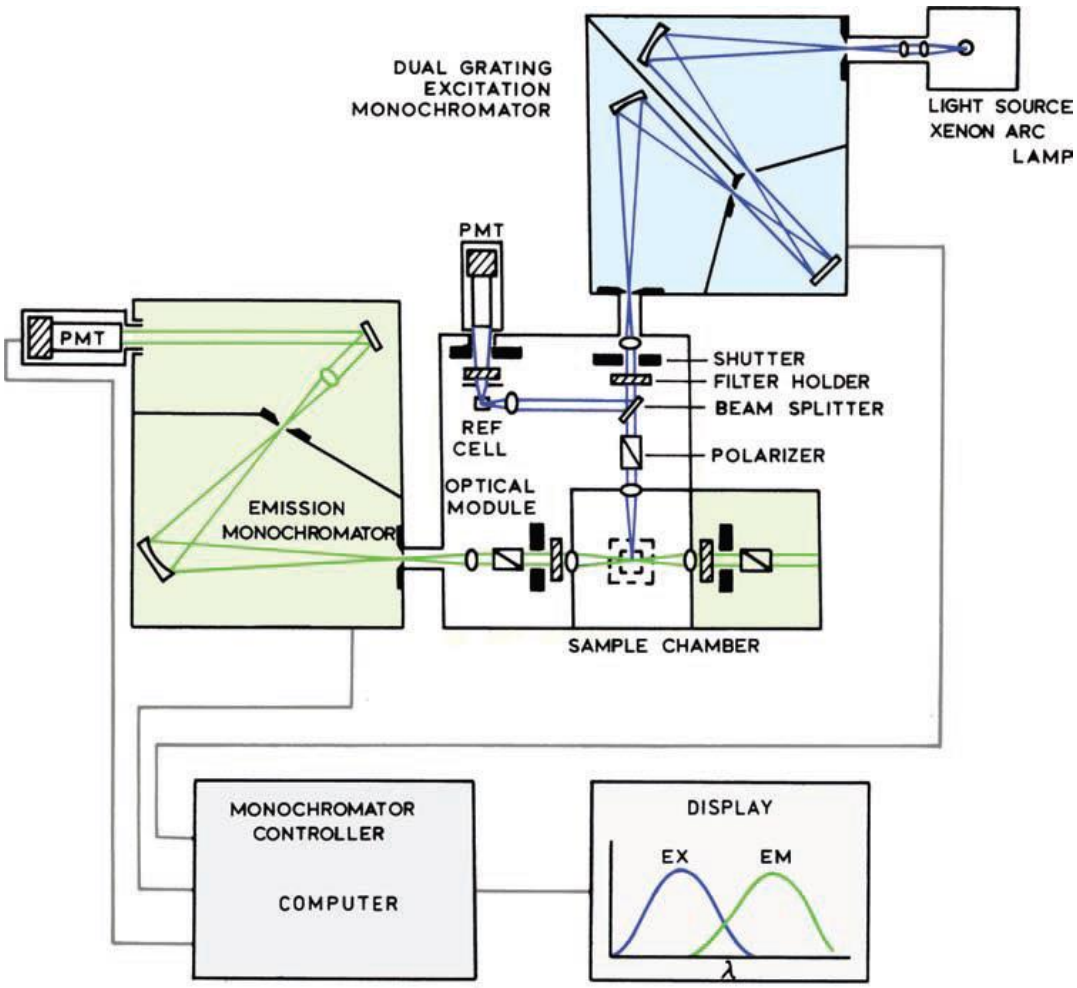

Figure 3.3 Generic fluorometer schematic diagram (Lakowicz, 2006)

These light sources have a limited lifetime, are generally expensive, contain high-pressure gas and generate significant amount of heat during the operation, therefore require special considerations for the electrical circuit and housing.

In applications where a limited excitation bandwidth is sufficient, LEDs (Mizuno, et al., 2012) or laser diodes can be used. Traditionally xenon lamps were the primary sources of excitation light, however the use of LEDs is becoming more widespread. One of the benefits of the laser diode is the monochromatic radiation, which makes it suitable for single fluorophore applications. LEDs and laser diodes can be pulsed or modulated at 100MHz or several GHz, respectively (Lakowicz, 2006). Due to the fast response time of laser diodes, they are mainly used in time-resolved fluorometry.

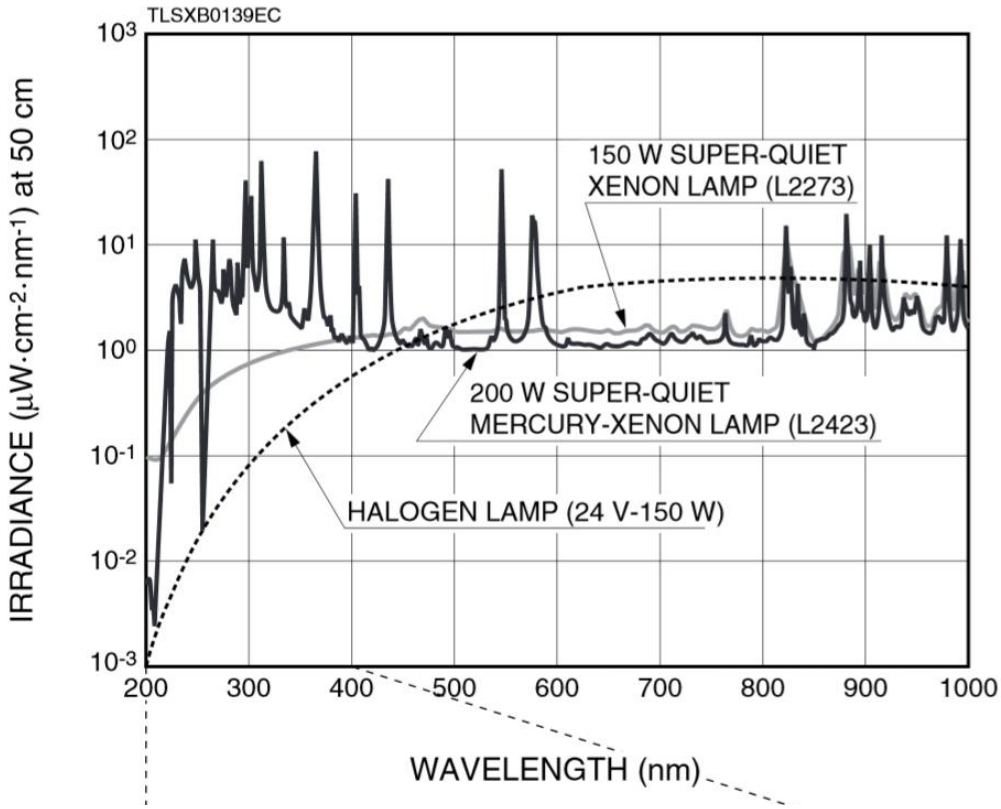

Figure 3.4 Hamamtsu Xenon and Xenon-Mercury irradiance spectra (Photonics, 2012)

3.4.2 Wavelength Selection

Once the excitation source is generated, the wavelength of interest needs to be selected. The light ray at the selected wavelength is then collimated using a collimator. The wavelength selection is carried out using optical filters in a filter-based fluorometer or monochromators in a spectrofluorometer. Optical filters can be considered in two categories of coloured filters and dichroic or thin film filters. The thin film filter (see Figure 3.5) gives a very accurate bandwidth selection, however at a higher cost compared to the normal coloured ones.

Figure 3.5 Dichroic filter (Filters, 2015)

For example Figure 3.6 shows the transmission efficiency of a cool green filter. In order to achieve a more accurate pass band, a combination of filters can be used. In a fluorometer often a minimum of two optical filters are needed, one on the excitation and the other on the emission optical paths. The mechanism to change these filters is often a physical changeover, either manually or automatically to suit different applications.

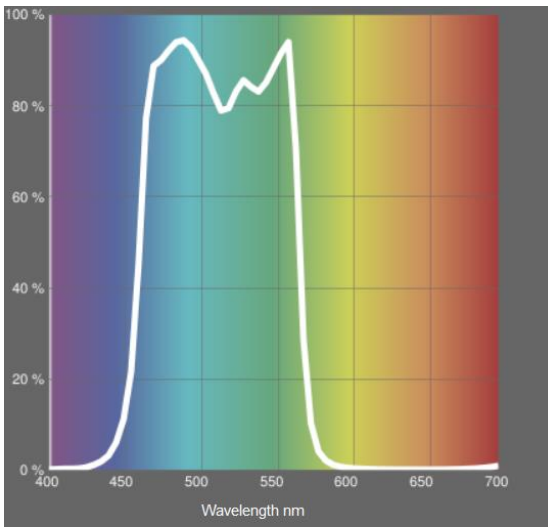

Figure 3.6 Frequency response of Lee Filters cool green filter (LEEFilters, 2015)

A monochromator normally operates based on optical dispersion using a prism or diffraction using diffraction grating. In principle a monochromator first produces a light spectrum from white light source by means of a prism or diffraction grating as shown in Figure 3.8 (Lee, et al., 2010). The desired wavelength is then selected using a combination of mirrors or lenses and a mechanical arrangement to move these components against the separation mechanism. For example in a grating based monochromator (Figure 3.8) different wavelengths can pass through the exit slit by changing the angle of diffractive grating.

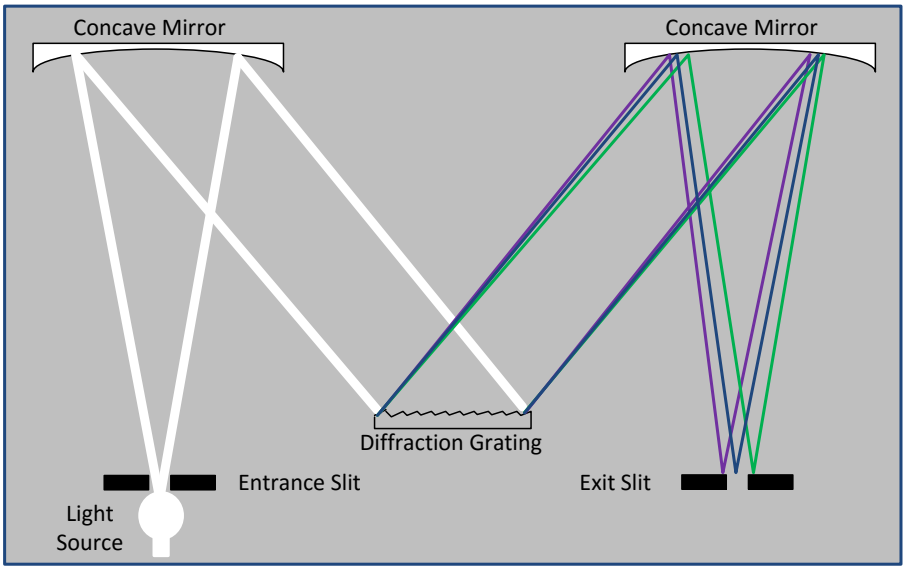

Figure 3.7 Diffraction monochromator based on Czerney-Turner model (Lee, et al., 2010)

The ability to select a specific wavelength enables the user to run a scan over a range of wavelengths, a feature useful for analytical studies. Filter-based fluorometers are normally cheaper than monochromator-based spectrofluorometers.

3.4.3 Detection Circuit

The emitted photons from the fluorophore molecules once passed through a filter or monochromator need to be detected by a detector circuit. Most fluorometers use Photo Multiplier Tubes (PMT) for this purpose, although photodiodes and CCD (Charged Coupled Device) have also been used in recent applications. Figure 3.8 shows the basic structure of a photomultiplier tube. The body of a photomultiplier is a vacuum tube with a window for the incoming photons. The window is often made out of quartz or glass and has a photosensitive surface acting as the photocathode. It releases electrons, which are multiplied by dynode electrodes. There is a series of dynodes in order to multiply the number of electrons several times. The anode at the end of dynode series is the collection electrode, producing a current proportional to the number of photons received through the window.

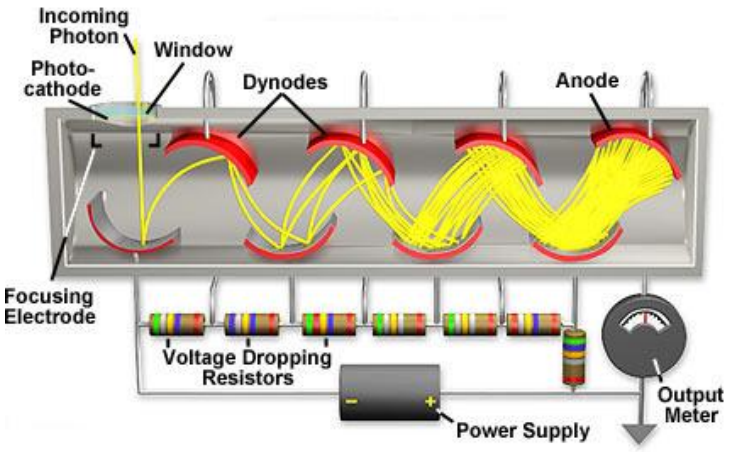

Figure 3.8 Construction of a photomultiplier tube (Abramowitz & Davidson, 2012)

PMT devices are more sensitive, but more expensive than photodiodes. Photodiodes offer a low cost solution for photon detection; however these devices are not as sensitive and have temperature dependant dark current which makes the use of them for detecting small number of photons difficult. Nevertheless the photodiode fabrication technology has significantly improved recently and some with a dark current in the range of pico ampere is now readily available. CCD technology has also been used for developing a lens-less CCD-based fluorometer (Balsam, et al., 2012).

3.4.4 Review of Commercially Available Fluorometers

A review of various commercially available fluorometers from the top of the range Spectrofluorometers and microplate readers to handheld filter-based fluorometers was undertaken. Microplate readers offer a great degree of flexibility and accuracy and can be based on the use of a monochromator and/or dichroic filters. In contract handheld filter-based fluorometers, with LED and photodiodes, provide low cost solutions with less accuracy, and are more suited for specific applications. In this section, some of the commercial fluorometers are briefly presented to provide an overview of the features of the currently available devices.

CLARIOstar® is a high performance monochromator multimode microplate reader, developed by BMG LABTECH. This device is based on Linear Variable Filters (LVF) technology. It uses xenon flash lamp for excitation, and photomultiplier or CCD for detection. A linear variable filter technology is an advanced filter based monochromator that provides a means of selecting a particular wavelength by mechanical movement of various filtering stages as shown in Figure 3.9.

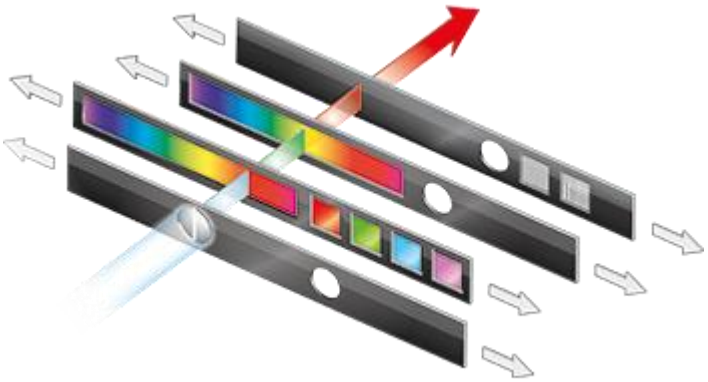

Figure 3.9 BMG Linear variable filtering technology (LABTECH, 2014)

CLARIOstar offers a selection bandwidth of $8-100\,\mathrm{nm}$ over $320-850\,\mathrm{nm}$ range. The measurement accuracy is better than $1\,\mathrm{pM}$ for Fluorescein. This is an expensive device (in the region £40-50K) suitable for research and lab-based use (LABTECH, 2014).

Figure 3.10 CLARIOstar fluorometer (LABTECH, 2014)

Jenway has developed the 62 Series filter-based fluorometers all with pulsed xenon lamp and with photodiode or PMT options. Jenway 6270 uses photodiodes and provides a sensitivity of $1\,\mu\mathrm{g/ml}$ for quinine sulphate. The 6280 and 6285 versions offer much improved sensitivity of $1\,\mathrm{ng/ml}$ using photomultiplier tubes. 6285 has an extended wavelength coverage. The retail price of this product ranges from £4.9K for the photodiode version to £6.3K for 6285 version with a photomultiplier tube (Jenway, 2006)

Figure 3.11 Jenway 62 series fluorometers (Jenway, 2006)

NanoDrop 3300 from Fisher Scientific is a filter fluorometer, which utilises three types of LED for excitation and 2048-element CCD for detection. The LED can be UV, blue or white. This device has a fluorescein detection level of $100\ \mathrm{pM}$ and at a retail price £8.9K (Thermo Scientific, 2013).

Figure 3.12 NanoDrop 3300 fluorometer (Thermo Scientific, 2013)

DS-11 FX series are a group of fluorometers from DeNovix, which use both xenon flash lamp and LEDs for excitation and photodiode or CCD for the detection. This device has four fluorometer channels for UV, blue, green and red measurement. The reported accuracy for BSA protein is $2\ \mu\mathrm{g/ml}$. The molecular weight of BSA is approximately $66.5\ \mathrm{kDa}$, therefore the accuracy level for this device is $30\ \mathrm{nM}$ (DeNovix, 2015).

Figure 3.13 DS-11 FX fluorometer (DeNovix, 2015)

Qubit® 3.0 Fluorometer is a handheld device, developed by Thermo Fisher Scientific. This is a filter based fluorometer, which uses blue and red LEDs for excitation, blue and green filters for excitation and emission filtering, and a photodiode for detecting wavelengths of $300 - 1000\ \mathrm{nm}$ (Scientific, 2014). The retail price of this product is £1.6K. This device although substantially cheaper compared to other lab-based equipment, does not have the molar accuracy required for detecting oestrus cycle. There is no specific progesterone test for this device, however the enzyme based cholesterol test can only detect down to $200\ \mathrm{nM}$ of cholesterol, which is a molecule with similar size to progesterone at 387 molecular weight (Thermo Fisher Scientific, 2012).

Figure 3.14 Qubit® 3.0 Fluorometer (Thermo Fisher Scientific, 2012)

3.5 Fluorescence-Based Progesterone Assays

There have been several studies on the measurement of progesterone level in milk using fluorescence spectroscopy as follows.

3.5.1 Total Internal Reflection Fluorescence (TIRF)

When a light beam reaches a medium other than the one it is travelling in, refracts or reflects depending on the angle of incident light and relative refractive index of the second medium. The Total Internal Reflection (TIR) takes place when the second medium has a lower refractive index than the first one and the angle of incident is more than the critical angle (Millis, 2012).

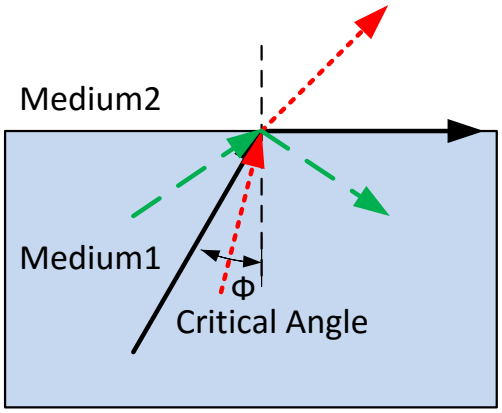

Figure 3.15 Light refraction, critical angle, internal reflection

The critical angle depends on the relative refractive index of the two media and can be worked out using Snell's formula. The critical angle for a light beam travelling through glass with refractive index of 1.5 and entering water with refractive index of 1.3 is approximately 60°.

TIR-based fluorescence spectroscopy relies on the formation of evanescent waves, which penetrate the interface between the two materials, glass and water in this

instance. This is due to the fact that electromagnetic waves cannot discontinue when reach an interface, instead they turn into evanescent wave which dissipates in an exponential fashion at a level depending on the distance from the point of reflection. Figure 3.16 demonstrates this concept, which is used for measuring fluorescence effect from a sample present at glass-water interface. The illuminating light can come from laser or other sources, directed in an angle that results in TIR.

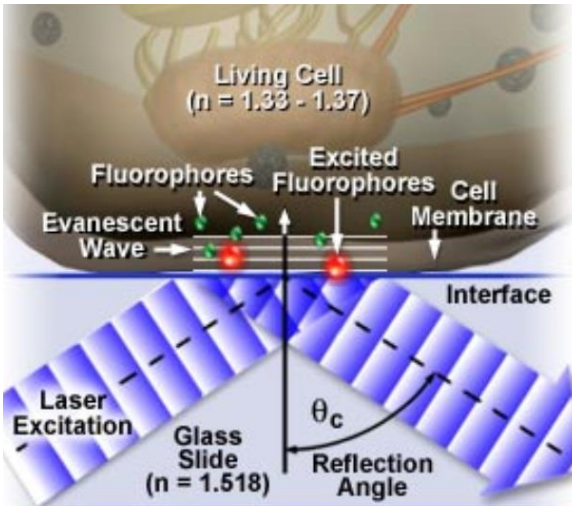

Figure 3.16 Total Internal Reflection Fluorescence (Axelrod & Davidson, 2012)

TIRF can be used for developing very sensitive analytical assays (Engström, et al., 2006). Mozaz et al., used this technique to develop River Analyser RIANA for monitoring different organic pollutants in water (Rodriguez-Mozaz, et al., 2009).

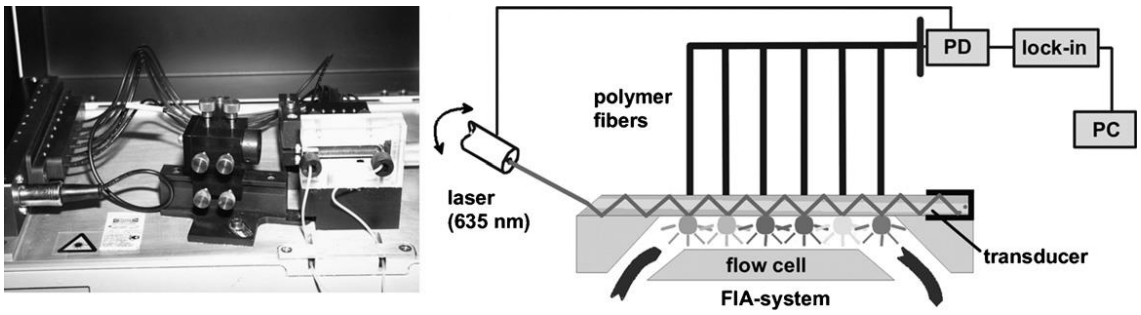

Figure 3.17 RIANA system (Rodriguez-Mozaz, et al., 2009)

This system was utilised as a basis for the development of a TIRF system for measuring progesterone concentration in milk (Tschmelak, et al., 2007), (Kappel, et al., 2007). Using this immunoassay, Tschmelak, et al., monitored the progsterone level in milk over a 25-day period in order to detect the onset of oestrus. In their method progseterone molecules were immobiled on the glass surface and monoclonal antibody was used for recognition. The result is an accurate progesterone measurement, around $12\ \mathrm{pg/ml}$ in 1:10 milk dilution. Although TIRF systems provide accurate results, they are expensive tools. The milk sample also needs to be diluted in order to go through the liquid channels in the sensor.

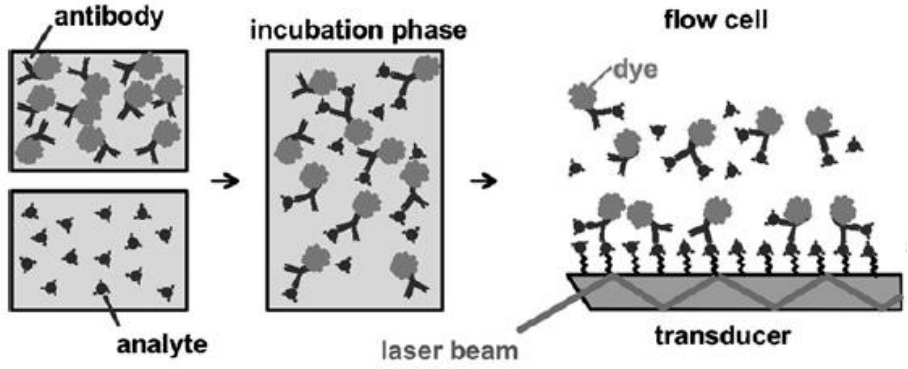

Figure 3.18 Use of biological samples in the TIRF technique for measuring progesterone level in milk (Tschmelak, et al., 2007)

3.5.2 SPR (Surface Plasmon Resonance)

Surface Plasmon Resonance (SPR) spectroscopy enables the implementation of label-free immunoassay for biological analysis. The key element of SPR is a thin layer of a metal like gold covering a glass slide. The light beam that enters the glass from the uncoated side, at a certain angle, wavelength and polarisation is absorbed by the free electrons on the surface of the metal, causing them to resonate and form surface plasmon waves. This oscillation of electrons creates an electromagnetic field, which exponentially decays as moving away from the gold surface but is still relatively strong at $300\ \mathrm{nm}$ (Mitchell, 2010). The incident light beam need to go through total internal

reflection, however as a result of resonance at the particular angle there is a significant reduction in the reflection intensity (Homola, et al., 1999).

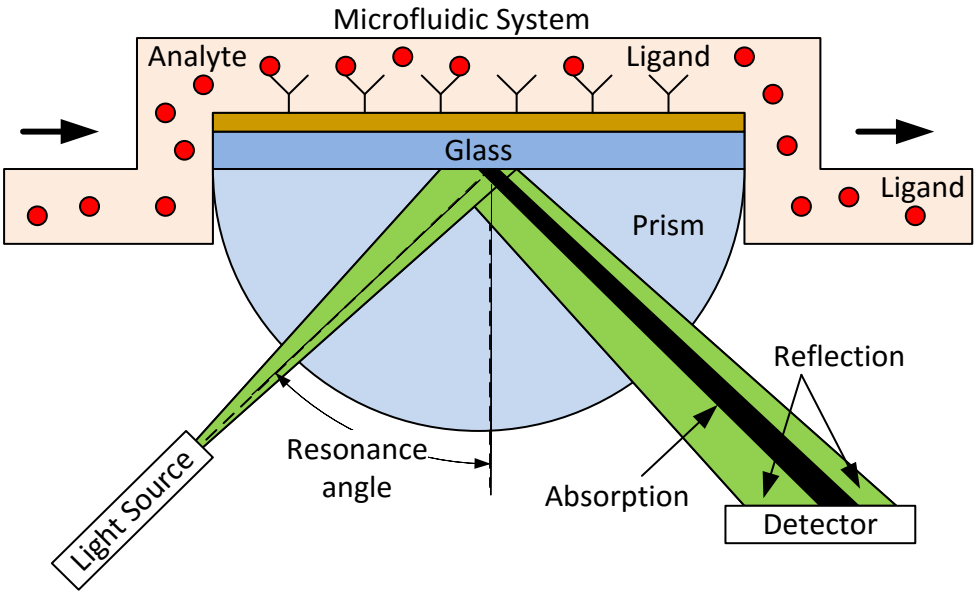

Figure 3.19 A typical setup for one flow cell in a SPR instrument

In an SPR-based immunoassay the gold surface is coated with antibody or other biomolecules that can capture the analyte of interest (Sabban, 2011). The immobilised biomolecule is referred to as the ligand. The analyte often flows through a microfluidic system over the sensor chip as demonstrated in Figure 3.19 (Stahelin, 2013). The resonance angle depends on the refractive index of the substance on the gold surface, which in turn varies based upon the number of ligand-analyte bindings. This method can be used for evaluating various properties of the analyte including concentration, affinity and kinetics.

SPR can be used for developing label-free immunoassays and has been utilised in numerous commercial systems including GE BIACORE system (Healthcare, GE, 2015). Gillis, et al., used BIACORE to measure progesterone level in milk (Gillis, et al., 2002). They reported an accuracy level of $3.56\ \mathrm{ng/ml}$. Mitchel, et al., used nano gold particles to improve the accuracy of progesterone measurement in buffer from $387\ \mathrm{pg/ml}$ to

$8\ \mathrm{pg/ml}$ using a secondary antibody and nano particles (Mitchell, et al., 2005). The detection level was further improved by Yuan, et al., to $4.9\ \mathrm{pg/ml}$. The SPR based systems offer accurate measurement, however they require complex fluidic and optical systems, which makes them more suitable for laboratory use. Besides due to the distance dependency of the SPR wave, the progesterone measurement accuracy in milk is limited to $3.56\ \mathrm{pg/ml}$, which is worse than the results provide by ELISA. The lower detection levels can only be achieved when sample pre-processing is applied and complex set up for the tests are considered. These processes will increase the cost for the use of this method.

3.5.3 Fluorescence Polarisation Immunoassay

A Fluorescence Polarisation Immuno-Assay (FPIA) operates based on polarisation of the fluorescence effect depending on the size of the molecule. When a polarised beam hits a fluorophore, it excites the molecule resulting in fluorescent emission. If the fluorophore compound is heavy, the fluorescent light will also be polarised. If the molecule is small it emits light in an unpolarised fashion due to the molecule's fast Brownian movement (Smith & Eremin, 2008). This phenomenon can be used in the design of homogeneous competitive assays, for example where the analyte is an antigen, competing with fluorescent-tagged antigen to bind with the antibody. When the concentration of antigen high, the majority of fluorophores are free resulting in a reduced level of polarised emission. However when the antigen concentration is low, a higher number of fluorophore-tagged antigen and antibody complex is formed, which due to their large size produce polarised emission. Therefore low analyte concentration results in highly polarised fluorescent emission and vice versa.

Due to the complex molecular structure of milk, the application of this method for detecting analyte in milk has been limited. However recently Varriale, et al. used FPIA for measuring concentration level of some steroid hormones, including eostrogen in a significantly diluted milk samples and achived an accuracy of $2.2\ \mathrm{pmol}$ in a

$2\ \mathrm{ml}$ solution, i.e. $1.1\ \mathrm{nM}$ (Varriale, et al., 2015). FPIA requires expensive equipment making it more suitable for lab-based assays.

3.5.4 Time-Resolved

Oku, et al., used time-resolved fluorscence spectroscopy to measure the progesterone concentration in milk (Oku, et al., 2011). The minimum detection level they achieved was $1.53\ \mathrm{ng/ml}$, approximately $5\ \mathrm{nM}$, which is not always a suitable accuracy level for detecting oestrus cycle. The experiments however proved this minimum detection level is enough for monitoring oestrus cycle in Holstein-Friesian and Japanese Black cows. Time-resolved fluourescence spectroscopy requires expensive equipment to detect changes in fluourscnce level within picosecond to nanosecond of excitation. The procedure followed by the authors of the paper includes several hours incuabtion time for the bimolecules in the microtitre plate wells, which is a limiting factor for on-site measurement of progesterone in milk. This method is more suitable for laboaratory use.

3.5.5 Fluorescence Resonance Energy Transfer (FRET)

The application of Fluorescence Resonance Energy Transfer (FRET) to direct measurement of progesterone in milk has been limited with the only one reported being a homogeneous immunoassay for progesterone measurement in human serum (Tan, et al., 2015). This work is based on tagging a monoclonal anti-progesterone antibody with a fluorescent label as shown in Figure 3.20. The progesterone molecules compete with the quencher-tagged Bovine Serum Albumin (BSA) and β estradiol molecules in forming the antibody-antigen complexes. This complex has been referred to as eBSAq. Progesterone concentration has a direct relationship to the fluorescence level. At low concentration levels the quenching is more prominent as more eBSAq molecules bind with the antibody molecules, resulting in a higher quenching level. This effect is reversed at high progesterone concentration levels. The fluorophore used for

labelling antibody has an emission maximum of $664\,\mathrm{nm}$, while the quencher's excitation is at $777\,\mathrm{nm}$ and emission at $791\,\mathrm{nm}$. The limit of detection in serum has been reported at $0.1\,\mathrm{pg/ml}$

Although this method shows promising results, it has only been applied to human serum but not bovine milk. It also requires two types of tagged molecules and the use of a lab-based microplate reader fluorescence spectrometer, adding to the complexity of preparation work and analysis compared to the method proposed in this PhD. In addition the presence of BSA in the eBSAq molecules can have an adverse effect on the formation of antibody-progesterone bonds. As progesterone is a small molecule it cannot instigate an immune response, therefore in order to produce anti-progesterone antibody, progesterone is often conjugated with BSA. This results in the production of some antibodies with affinity to BSA, which will attract some of the eBSAq complexes.

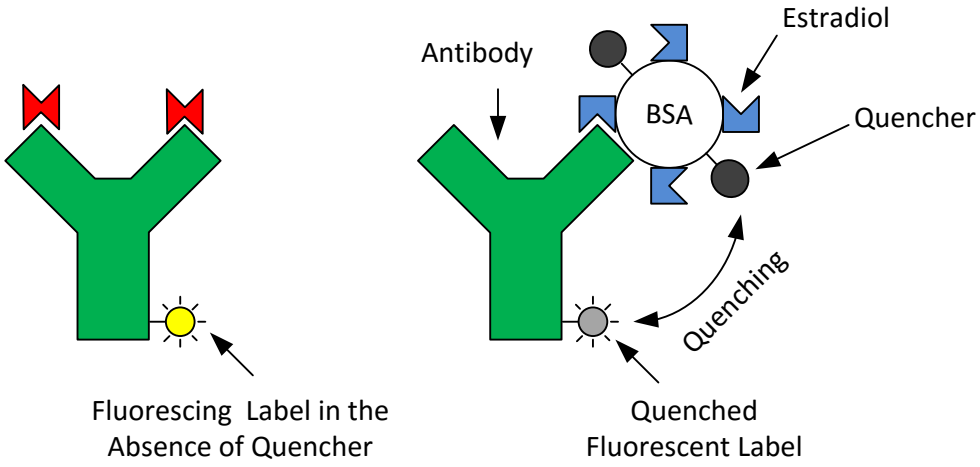

Figure 3.20 Quenching effect in a competitive progesterone assay

3.6 Summary

This chapter provided an introduction into fluorescence spectroscopy. A review of the underlying principles was presented, covering fundamental aspects such depopulation pathway for excited molecules, quantum yield and quenching. Florescence resonance

energy transfer as an essential part of the proposed solution was also reviewed. This was followed by a brief overview of various types of commercially available fluorometers and then the details of state of the art fluorescence-based immunoassays used for measuring progesterone. Table 3.1 shows a summary of some of the commercially available fluorometers reviewed in this chapter. Qubit 3.0, the only portable and low cost device in the table, cannot provide the accuracy required for detecting oestrus cycle. This review demonstrated that a fluorescence-based immunoassay can offer the level of accuracy required for progesterone measurement and consequently detecting the onset of oestrus. The downside however is the need for using expensive and complex lab-oriented equipment based on techniques such as total internal reflection, polarisation, time-resolved and surface plasmon resonance fluorescence spectroscopy.

Table 3.1 A summary of commercially available fluorometers

Name	Source	Detection	Filter	Price	Accuracy	Use Case
CLARIOstar	Xenon lamp	PMT/CCD	Linear variable	£40-50K	1pM Fluorescein	Lab
Nanodrop 3300	LED	CCD	Discrete	£8.9K	0.1nM Fluorescein	Lab
Jenway 6285	Xenon lamp	PMT	Discrete	£6.3K	1.3nM Quinine sulphate	Lab
Jenway 6270	Xenon lamp	Photodiode	Discrete	£5K	1.3uM Quinine sulphate	Lab
Qubit 3.0	LED	Photodiode	Discrete	1.6K	200nM Cholesterol	Portable

The remaining of this thesis presents the proposed framework for the transducer and biological design that need to be considered in developing a portable commercially-viable progesterone fluoroimmunoassay. Next chapter in particular provides a detailed account of the transducer design including electronic, mechanical and optical aspects that enable its use as the biosensor for implementing the immunoassay.

4 TRANSDUCER DESIGN

4.1 Introduction

The biosensor design proposed in this chapter is based on principles of fluorescence-spectroscopy, where the excitation light is generated by an LED in a controlled manner and then channelled through a specially designed mechanical arrangement to illuminate the biomolecules of interest in the test tube. The photons generated or scattered as a result of the incident light are then directed through the incorporated light channels and absorbed by the photodiodes. The output signals are captured, processed and analysed by the detection circuit, resulting in a value for the concentration of the analyte of interest. Low cost LEDs and photodiodes with suitable characteristics are readily available and therefore have been used in this work. Analysis of the characteristics and suitability of these components has been covered in this chapter. The proposed system can be used as a generic transducer for fluorescence-based immunoassay applications; however the focus in this work is on bovine milk as the biological sample and progesterone as the analyte of interest.

This chapter presents the details of the electronic and mechanical design of the transducer with a focus on the aspects of the design that make it novel, effective and efficient, without the use of usual optical components such as filters, collimators, lenses and monochromators incorporated into the current commercial fluorometers (see Chapter 3).

The transducer consists of three main elements; namely, the enclosure, emitter and detector, as shown in Figure 4.1. The enclosure accommodates the LEDs and photodiodes, positioning them in a way to reduce the effect of background light and enhance the sensitivity of the detector. The emitter provides the means of powering the LED in regular intervals and controlling the LED output power. The detector is responsible for detecting photons using two photodiodes and a sensitive circuitry. An

intelligent algorithm combines various data and sensor readings and determines the concentration of the analyte of interest.

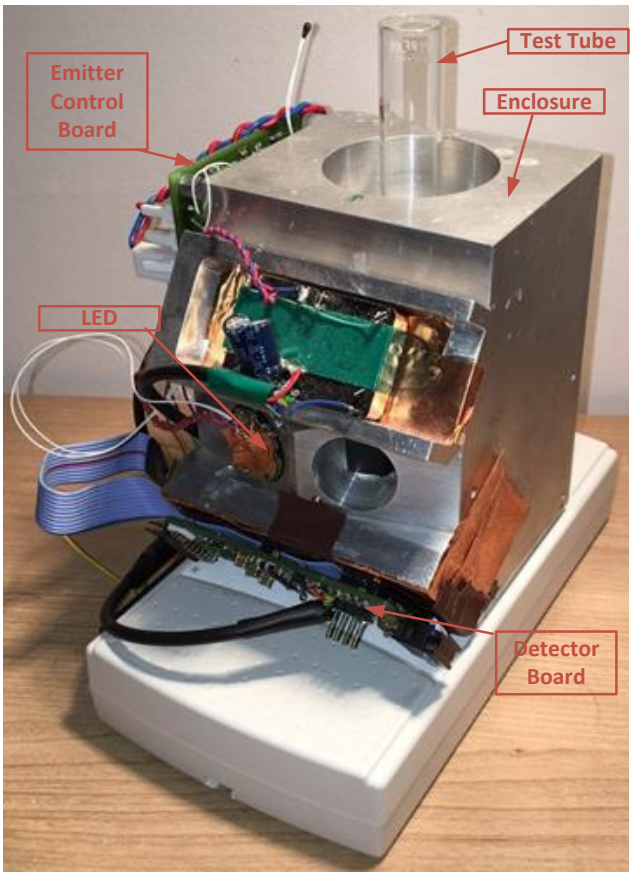

Figure 4.1 Complete transducer prototype designed by A. Ghadar (Ghadar, et al., 2013)

4.2 Enclosure

The enclosure benefits from a novel compact geometric design. The material used is aluminium, which could be accurately machined or moulded into a desirable shape and geometry. It prevents ambient light getting into the test tube chamber and has a high level of heat conductivity, enabling fast and effective heat dissipation from the chamber. The overall size of the enclosure is $80\text{mm} \times 92\ \text{mm} \times 110\ \text{mm}$ (WDH).

The enclosure incorporates three types of light channels; one for the LED, one for the feedback photodiode and one for the green and blue photodiodes on the detector circuit (see Figure 4.2). The feedback photodiodes receive a proportion of the LED light, which can be used to compensate for the variations in the LED light (see Figure 4.3).

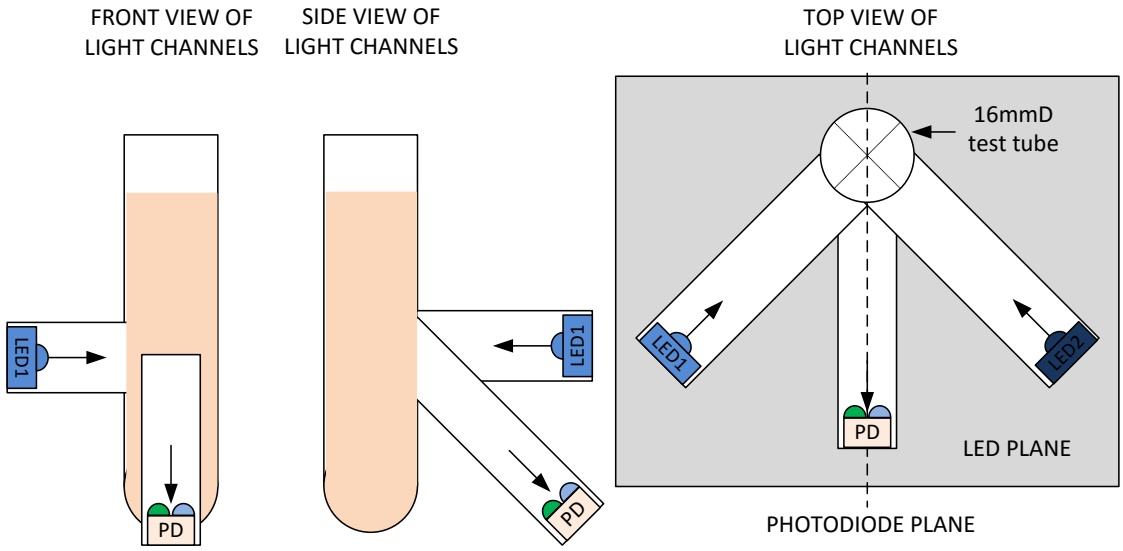

Figure 4.2 Enclosure light channels for the LED and Photodiodes (PD)

In order to facilitate a ratio-metric measurement, the enclosure has been designed to accommodate two sets of LED and detector circuits. The enclosure features a geometric design, in which the photodiodes are on a plane perpendicular to the LED plane, reducing the effect of background LED light on the photodiodes (see Figure 4.2). The LED and photodiode light channels meet at a common circular area on the test tube (see Figure 4.4). As a result the photons generated by the LED do not need to travel far before being absorbed by the fluorescent molecules. This feature is particularly beneficial for opaque media such as milk. The photons generated by the fluorophore will also be close to the detection window and the receiver light channel.

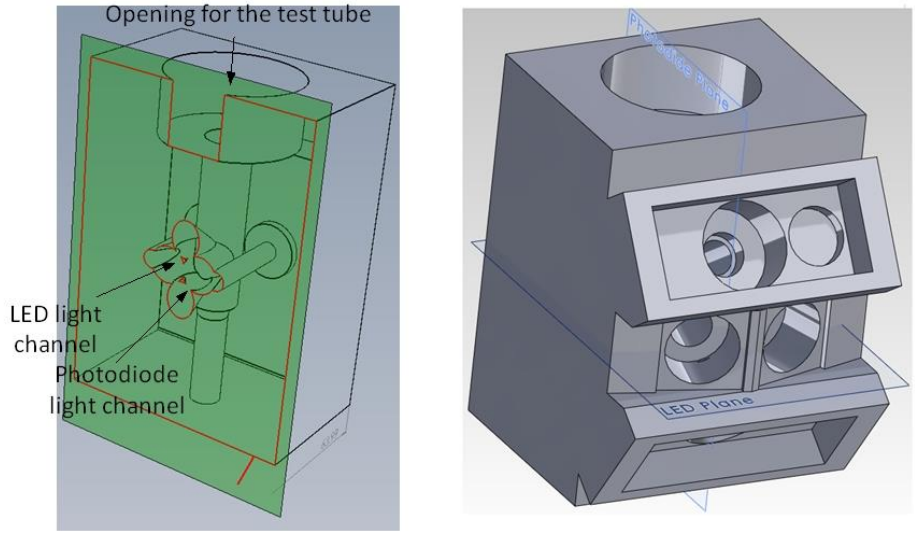

Figure 4.3 Enclosure design, 3D view (Ghadar, et al., 2013)

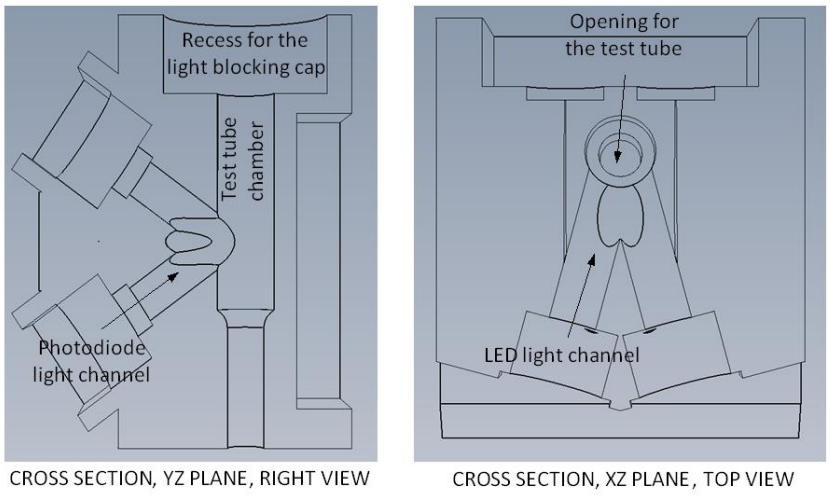

Figure 4.4 Enclosure design, side view

4.3 Emitter Circuit

The LED produces photons required for exciting the fluorophores. The variations in the radiant flux and spectral power of the light emitted by an LED are mainly dependent on the variations of the LED current and junction temperature. The LED used in this design is a blue one from LUXEON Rebel high power coloured LED range (Lumileds, 2010). The dominant wavelength of the blue LED normally shifts by $0.5\ \mathrm{nm}$ per $1°C$ change in

the junction temperature. The radiant flux of the LED is dependent on the LED current (Figure 4.5) and the thermal pad temperature (Figure 4.6).

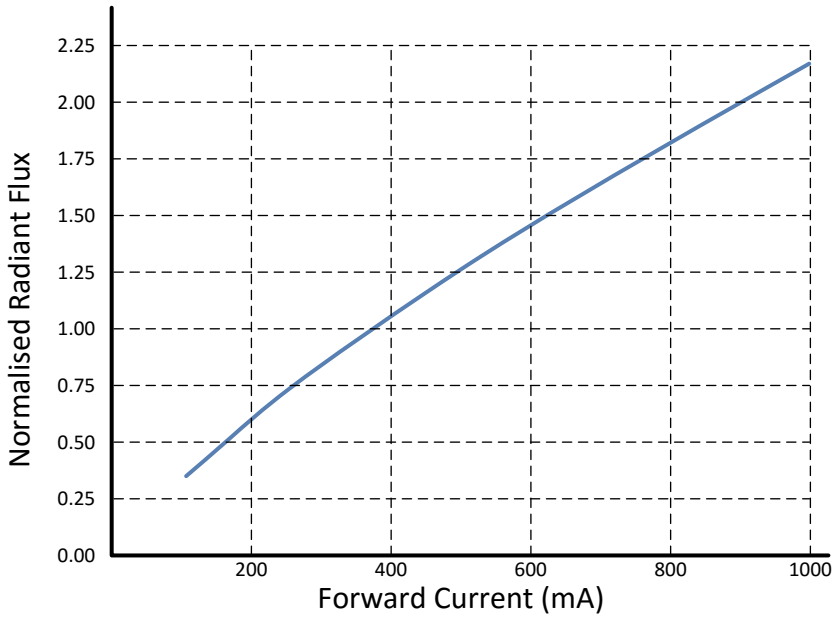

Figure 4.5 Blue LED's radiant flux versus current (Lumileds, 2010)

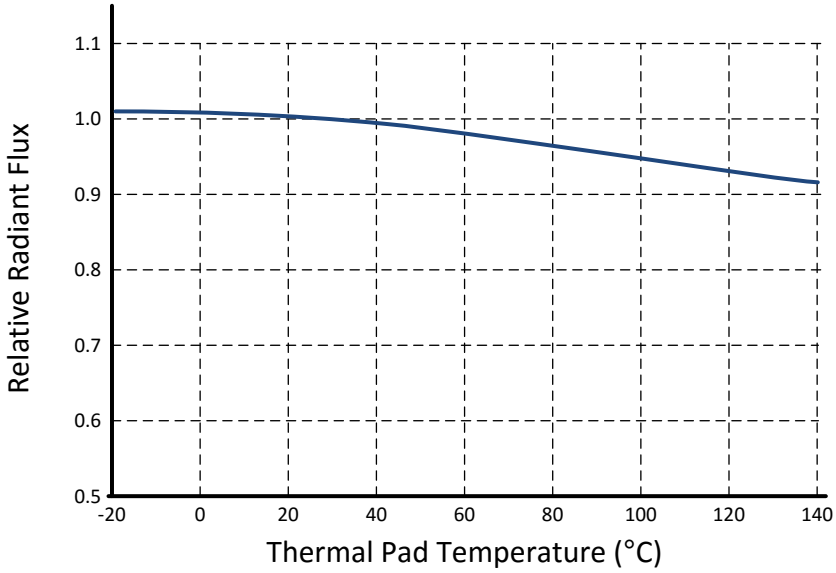

Figure 4.6 Blue LED's radiant flux versus temperature (Lumileds, 2010)

A significant part of photons received by the photodiodes is the background light generated by the LED. Therefore, any slight variations in the spectral power and radiant flux of the LED could be misinterpreted as the photons related to the

fluorescence effect. Depending on the required accuracy of the biosensor such variations must be limited to a certain percentage of the initial system output, ϵ_L, in the absence of analyte. This section focuses on the emitter components in particular the LED and outlines the issues affecting the performance and accuracy of the control system.

4.3.1 LED Parameters

The LED voltage (V_L) can be written as a function of LED current (I), as (Lumileds, 2002).

$$I = I_0(e^{\frac{qV_L}{nkT}} - 1) \tag{4.1}$$

I_0, n, q, k and T are the reverse saturation current, ideality factor (between 1 and 2), electron charge ($1.602\mathrm{e}^{-19}$ C), Boltzmann factor ($1.3805\mathrm{e}^{-23}$ j/°K) and junction temperature. At room temperature kT/q is approximately 25 mV, therefore the exponential term is significantly larger than 1. For electric currents above a few milliampere, the ohmic loss (R_s) must also be considered. The above equation can therefore be simplified as follows:

$$V_L = \frac{kT}{q}\, n\, ln\left(\frac{I}{I_0}\right) + R_s I \tag{4.2}$$

Equation (4.2) has three fundamental parameters; namely, n, I_0 and R_s. By measuring LED voltage at 3 known LED currents, these parameters can be estimated. For example by looking at the LED datasheet (Lumileds, 2010) these parameters for the blue LED are calculated as follows.

$$\begin{Bmatrix} 2.95 = 0.025n(-1.61 - lnI_0) + 0.2R_s \\ 3.11 = 0.025n(-0.92 - lnI_0) + 0.4R_s \\ 3.26 = 0.025n(-0.51 - lnI_0) + 0.6R_s \end{Bmatrix} \rightarrow \begin{Bmatrix} I_0 = 1.28e^{-35} \\ n = 1.43 \\ R_s = 0.677 \end{Bmatrix} \tag{4.3}$$

4.3.2 Control of the LED Current

The LED current in basic terms is controlled using a resistor (R), a transistor (Q) and an Op-Amp (U) as shown in Figure 4.7. By applying a reference voltage to the Op-Amp, the current through the resistor and in effect through the LED is controlled. The voltage applied to the positive terminal of this Op-Amp is a combination of an accurate voltage reference source (V_{REF}) and a DAC voltage (V_{REF}). The DAC is used for calibration as well as estimation of the circuit parameters.

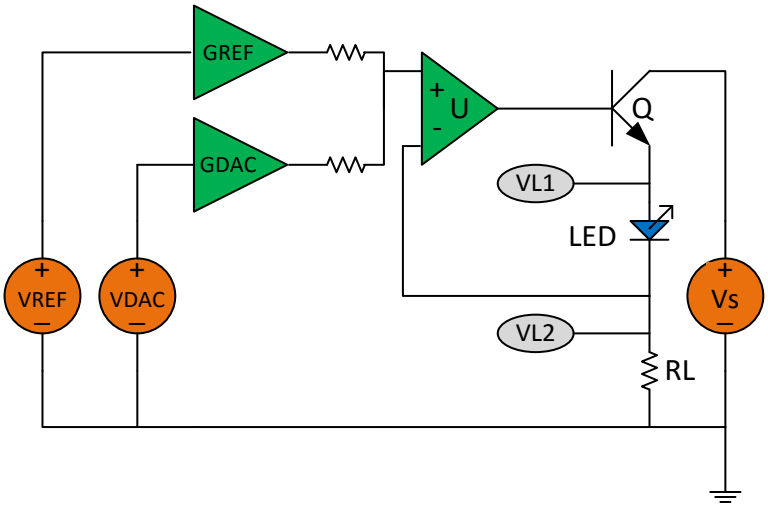

Figure 4.7 Schematic design of LED current control

Defining LED nominal current at I_L and the maximum level of circuit variations to achieve the desired accuracy of ϵ_L, the LED current and voltage variations due to the ambient factors (ΔI_{LED}^{max} and ΔV_{LED}^{max}) must be limited to:

$$\Delta I_{LED}^{max} < \epsilon_L I_L \tag{4.4}$$

$$\Delta V_{LED}^{max} < \epsilon_L R_L I_L \tag{4.5}$$

Considering a DAC with an accuracy of ΔV_{DAC}^{min}, the attenuation required on the DAC output will be:

$$G_{DAC} = \frac{\Delta V_{DAC}^{min}}{\Delta V_{LED}^{max}} = \frac{\Delta V_{DAC}^{min}}{\epsilon_L R_L I_L} \tag{4.6}$$

In order to achieve the ϵ_L variation limit, an accurate reference regulator with an ultra-low temperature drift to match ϵ_L is needed. This can be used as a reference for the DAC as well as the LED drive circuit. The output of the reference regulator needs to be scaled down to the desired voltage of LED resistor (R_L).

$$G_{REF} = \frac{V_{REF}}{R_L I_L} \tag{4.7}$$

$$I_L = \frac{\frac{V_{REF}}{G_{REF}} + \frac{V_{DAC}}{G_{DAC}}}{R_L} \tag{4.8}$$

The LED current is directly related to the DAC and REF voltages, both affected by the temperature drift of the reference voltage. Therefore the temperature drift of the whole circuit can only be as good as temperature drift of the voltage reference, divided by the attenuation factor.

4.3.3 Effect of Junction Temperature

High power LEDs create considerable amount of thermal energy while on. As the majority of the electric power converts to heat, the junction temperature increases rapidly within milliseconds. Yang, et al. carried out a study on dynamic thermal behaviour of high-power LEDs (Yang, et al., 2008). Figure 4.8 shows the junction temperature can change by $1\ ℃$ in less than $1\ \mathrm{msec}$. The figure also demonstrates that following the application of a $50\ \mathrm{Hz}$ pulse, with 50% duty cycle, the temperature stabilises after $20\ \mathrm{sec}$. Figure 4.9 illustrates how the duty cycle of the pulse changes the rise time of the junction temperature. In all instances the temperature rise following the LED pulse remains relatively constant after $20\ \mathrm{sec}$.

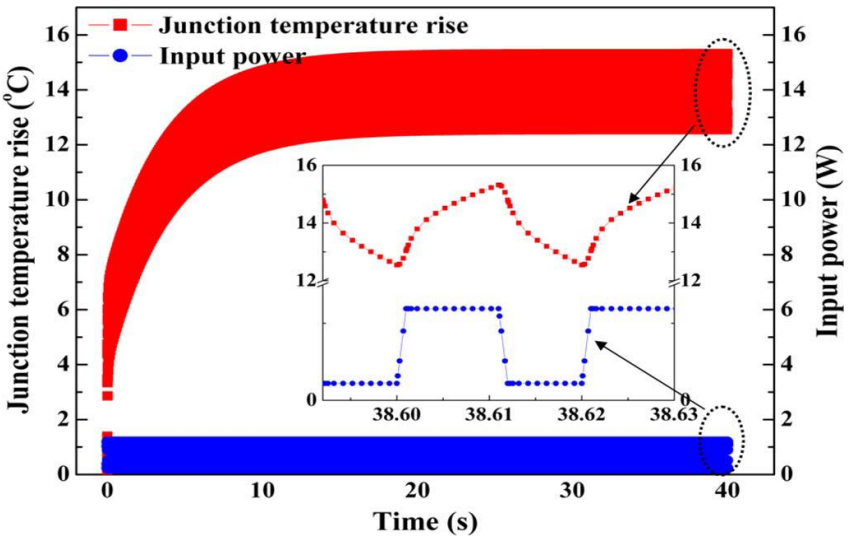

Figure 4.8 LED junction temperature (Yang, et al., 2008)

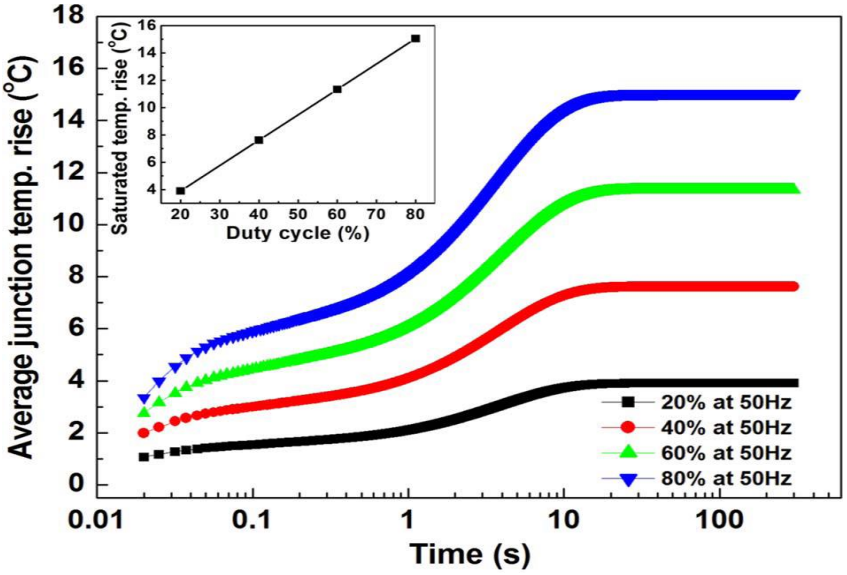

Figure 4.9 Junction temperature rise versus duty cycle (Yang, et al., 2008)

As the LED junction temperature affects both the spectral power and radiant flux, it is best that the detector circuit takes a measurement when the junction temperature reaches a pre-determined point, ensuring the variations in the excitation light are below the limit of ϵ_L.

$$C_T^F \Delta T_j + C_\lambda^F C_T^\lambda \Delta T_j < \epsilon_L \quad (4.9)$$

C_T^F and C_λ^F represent the ratio of change of radiant flux with respect to temperature and wavelength. C_T^λ is the parameter describing the change in wavelength with respect to temperature. The maximum level of variation allowed must therefore be limited to

$$\Delta T_j^{max} = \frac{\epsilon_L}{C_T^F + C_\lambda^F C_T^\lambda} \tag{4.10}$$

Using equation (4.2), it can be shown the variations in the LED voltage and junction temperature are related as follows.

$$dV_{LED} = dT_j \frac{kn}{q} ln\left(\frac{I_L}{I_0}\right) \tag{4.11}$$

Considering the circuit schematic in Figure 4.7, the LED voltage is the difference between VL1 and VL2. By achieving an accurate LED current and using an Op-Amp with low offset voltage drift, VL2 will remain relatively constant. Therefore in order to detect when the LED junction temperature is at a particular point, only VL1 voltage needs to be measured. This is done by amplifying its variations instead of its nominal voltage.

4.3.3.1 Example

Here as an example the blue LED from the LUEXEON range is considered (Lumileds, 2010). For the case of $\epsilon_L = 10$ ppm, $R_L = 0.5\ \Omega$, $I_L = 200$ mA, $V_{REF} = 5$ V, and a 16-bit DAC with 300 μV accuracy over ± 5 V range, G_{DAC} and G_{REF} attenuation factors are calculated as follows:

$$G_{DAC} = \frac{\Delta V_{DAC}^{min}}{\Delta V_{LED}^{max}} = \frac{300e^{-6}}{10e^{-6} \times 0.5 \times 0.2} = 300 \tag{4.12}$$

$$G_{REF} = \frac{5}{0.5 \times 0.2} = 50 \tag{4.13}$$

I_L can therefore be adjusted as below:

$$I_L = \frac{1}{5} + \frac{V_{DAC}}{150} \tag{4.14}$$

For this LED, $C_T^F = 7e^{-4}\ \frac{1}{°C}$, $C_T^\lambda = 0.05\ \frac{nm}{°C}$ and $C_\lambda^F = 0.08\ \frac{1}{nm}$, therefore:

$$\Delta T_j^{max} = \frac{10e^{-6}}{7e^{-4} + \ 0.05 \times 0.08} \sim 0.002\ °C \tag{4.15}$$

According to the Rebel LED datasheet (Lumileds, 2010), the LED voltage changes monotonically with temperature between $2 - 4\ \mathrm{mV}$ per $1\ ℃$. Based on the $2\ \frac{\mathrm{mV}}{℃}$ and the value of ΔT_j^{max}, equation (4.15), the associated variation in the LED voltage will be as low as $4\ \mu\mathrm{V}$. The accuracy of a true 16-bit ADC over $\pm 5\ \mathrm{V}$ range is approximately $152\ \mu\mathrm{V}$. The minimum amplification level required will therefore need to be set to 38. If this level of gain is directly applied to the LED voltage, it will saturate the amplifier output. A DC offset around the nominal LED voltage is required in order to achieve this level of amplification.

4.3.4 Sampling Method

Figure 4.8 shows that after the initial $25\ \mathrm{ms}$ of the application of a $50\ \mathrm{Hz}$ pulse to the LED, the junction temperature rises by approximately $0.2\ ℃$ every millisecond. This means in order to detect a temperature rise of $0.002\ °C$, a sampling rate of $100\ \mathrm{ksps}$ or higher is required. In practice due to the presence of noise and the need for filtering, a much faster rate is necessary. For this reason in this work an alternative approach which does not require a fast ADC has been employed.

In this method LED voltage and detector output are logged over the desired interval of the LED on-time. Then curves $f_V(t)$ and $f_I(t)$ are fitted to the LED voltage and photodiode currents, respectively. As the LED light goes through a highly volatile medium (milk with random movements of large molecules) the data sets contain outliers. Random Sample Consensus (RANSAC) is a well-known algorithm for removing the outliers and fitting a curve to the remaining data. Once the curve is determined, an

estimate of the time t_s at which the LED voltage reaches the desired level of V_L^{th} is used to determine the detector current (I_L^s) at that particular time.

$$I_L^s = f_I\left(f_V^{-1}\left(V_L^{th}\right)\right), \quad \text{where } t_s = f_V^{-1}\left(V_L^{th}\right) \tag{4.16}$$

4.3.5 LED and Lens

LED manufacturers incorporate a glass lens (Figure 4.10) on the LED die in order to create a particular spatial radiation pattern (Figure 4.11). The LED needs to be mounted on the PCB with a special heatsink arrangement.

Figure 4.10 LUXEON Rebel LED (Lumileds, 2010)

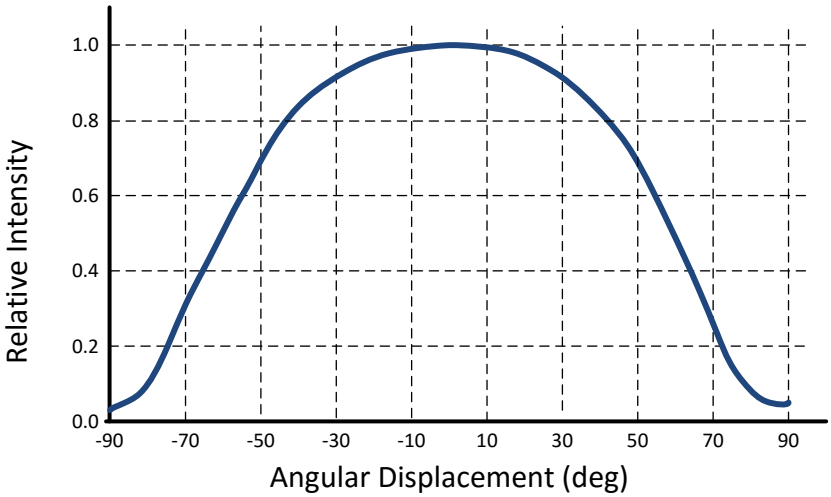

Figure 4.11 Spatial radiation pattern for LUXEON Rebel blue LED (Lumileds, 2010)

These LEDs are often used in conjunction with an external lens in order to narrow down the radiation pattern to within the required range (Figure 4.12). Lenses can be

made out of materials like glass and PMMA (Poly Methyl Meth Acrylate). PMMA is commonly used in particular for LUXEON Rebel Lumiled LEDs. This section provides a review of the factors that can affect the performance of a PMMA lens.

4.3.5.1 Effect of LED Temperature on Lens Properties

Lens has an efficiency factor, which refers to the percentage of light passed through the lens compared to what is absorbed. The PMMA material has an average efficiency of 80-90% (Gilbert, 2011).

Figure 4.12 PMMA lenses by FRAEN (Gilbert, 2011)

The refraction index of PMMA is approximately 1.49 at 600 nm (Polyanskiy, 2008). The focal length and viewing angle of a semi-sphere lens with 1cm radius are calculated as follows (Weisstein, 2007):

$$f = \frac{\frac{1}{R_1}-\frac{1}{R_2}}{n-1} = 2.041\ cm, \text{ where } \quad R_1 = 1cm,\ R_2 = \infty,\ \ n = 1.49 \tag{4.17}$$

$$\theta_{lens} = \tan^{-1}\frac{R_1}{f} = 26.105^{\circ} \tag{4.18}$$

The refractive index of PMMA reduces by 0.012% per $1\ ^{\circ}\text{K}$ increase (Bernini, et al., 1993). Also the PMMA material expands by 0.0075% per $1\ ^{\circ}\text{K}$ (Fellow, 2016). The focal length and the viewing angle after $1\ ^{\circ}\text{K}$ increase are calculated as follows:

$$\hat{R}_1 = (1 + 0.0075\%) \times 1cm, \;\; \hat{n} = 0.9999 \times 1.49 \rightarrow \hat{f} \approx 2.04159cm \tag{4.19}$$

$$\hat{\theta}_{lens} = \tan^{-1}\frac{\hat{R}_1}{\hat{f}} = 26.098^{\circ} \tag{4.20}$$

Considering equations (4.18) and (4.20), the percentage of change in LED lens viewing angle per each degree increase in lens temperature will be:

$$\frac{\Delta\theta_{lens}}{\theta_{lens}} = \frac{26.104854 - 26.098}{26.104854} = 0.02625\% = 262\ ppm \tag{4.21}$$

This is significantly higher than the limit of variations ($\epsilon_{\mathrm{L}} = 10$ ppm) used in the example in Section 4.3.3.1. In order to minimise the effect of lens temperature on the transducer performance, either the lens temperature variation must be limited to a fraction of 1 ℃, or the lens is removed from the transducer design. Lens temperature can be affected by the LED heat while it is on or by the ambient temperature. These aspects are reviewed in the next two sections.

4.3.5.2 Effect of LED Light on the Lens

PMMA has a density of $\rho = 1.8\,\frac{g}{cm^3}$ and specific heat of $C_{lens} = 1.450\,\frac{J}{g.K}$ at room temperature (Fellow, 2016). For a semi sphere with 1cm radius the total mass is:

$$m_{lens} = \frac{1}{2}.\frac{3}{4}\pi r^3\rho = 2.12\ g \tag{4.22}$$

For a 1 W LED (W_{LED}), with 35% efficiency (E_{LED}), based on 1 sec on-time (Δt_{ON}), and using a PMMA lens with 80% efficiency (E_{lens}), if the total thermal energy produced by the LED is absorbed by the lens the temperature rise will be:

$$\Delta T_{lens} = \frac{\Delta t_{ON} W_{LED}(1 - E_{lens})E_{LED}}{m_{lens}C_{lens}} = \frac{1 \times 1 \times (1 - 0.8) \times 0.35}{2.12 \times 1.450} = 0.0227\ ^{\circ}\mathrm{C} \tag{4.23}$$

Based on the same method used for (4.21), the ratio of change in the viewing angle is estimated to be 4.33 ppm. This is less than ϵ_L value considered in Section 4.3.3.1. In

practice the LED will only be on for a fraction of a second, which will further reduce the effect of LED on the lens temperature.

4.3.5.3 Effect of Ambient Temperature on Lens

Effect of ambient temperature on lens can be considered in the same way as the temperature change caused by the LED. Equation (4.21) shows that the lens viewing angle changes by ambient temperature at 262 ppm per $1\ ^{\circ}C$. As the transducer is used in ambient temperature, the lens temperature can vary several degrees. Therefore the use of lens could have a significant adverse effect on the performance of the transducer.

4.3.5.4 Sensor Design without a Lens

Due to the temperature dependency of the PMMA lens and high cost of better quality lenses such as a glass lens, in the proposed solution the lens has been removed from the design. The special geometrical features of the transducer enclosure and also as a result of the dynamic offset cancellation introduced in this thesis, the proposed transducer would work without a lens.

4.4 Detector Circuit

The detector circuit (Figure 4.13) in principle consists of a set of blue and green photodiodes with the associated electronic circuitry for converting the photodiode current to an amplified and filtered voltage, ready to be captured by the analogue to digital converters.

The green and blue photodiodes receive photons from two main sources. The first one is a proportion of the LED light, referred to as the background light, which makes its way through the test tube to the photodiode. The second source is the emission from the fluorophores as a result of the incident light. The background light is several orders

of magnitude higher than the current of interest generated by the fluorescence effect. The background light creates a significant offset level, preventing direct amplification of the signal with the high gain required for fluorescence-related portion of the signal. A novel dynamic offset cancellation method has been proposed to allow for a high level amplification.

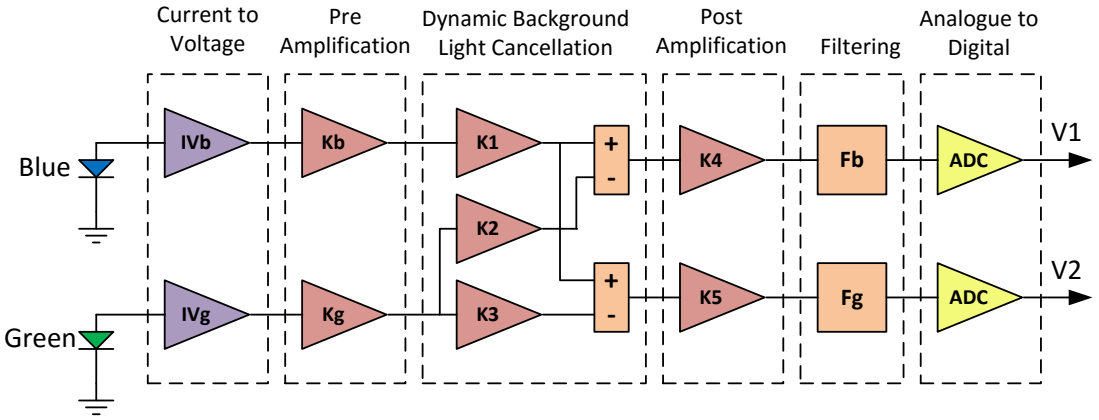

Figure 4.13 Detector block diagram

4.4.1 Main Circuit Components

4.4.1.1 Current to Voltage Conversion and Amplification

A photodiode is a solid-state device, which releases electrons by receiving photons within its spectral response curve. A photodiode is modelled as shown in the dotted section of Figure 4.14, with equation (4.24) governing the model.

$$I_0 = I_L - I_D - I' = I_L - I_S(e^{\frac{qV_D}{kT}} - 1) - I' \quad (4.24)$$

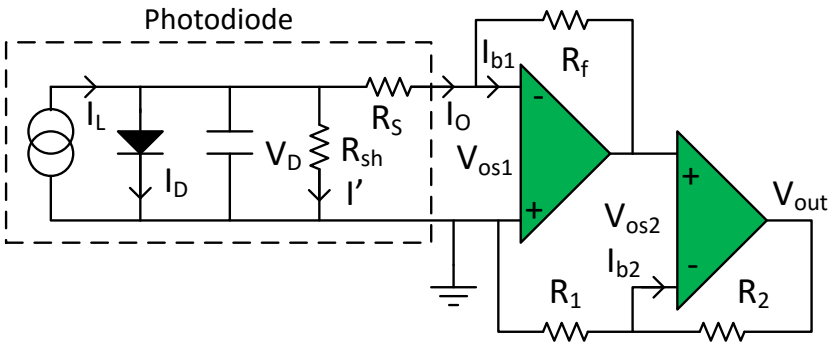

Figure 4.14 Photodiode current to voltage conversion

I_L is the current produced by the photodiode as the result of incident light, I_D the dark current, and $\acute{I}$ the current going through the equivalent shunt resistor of the diode. The term kT/q was described previously in Section 4.3.1 and is approximately $25\ \mathrm{mV}$ at room temperature. The current-to-voltage conversion and the further amplification stages are undertaken using the circuit shown in Figure 4.14. In this circuit, the diode voltage (V_D) is near zero; therefore equation (4.24) can be simplified as follows:

$$I_O = I_L - I_S\left(\frac{qV_D}{kT} + 1 - 1\right) - I' = I_L - I_S\frac{qV_D}{kT} - I', \quad V_D \approx 0 \tag{4.25}$$

Introducing R_{sh} into the equation results in the following:

$$I_O = I_L - \frac{V_D}{R_T} - \frac{V_D}{R_{sh}} \text{ , where } R_T = \frac{kT}{qI_S} \tag{4.26}$$

Substituting $V_D = I_0R_s - V_{os1}$ into the above equation will lead to the following formula for I_O:

$$I_O = \frac{I_LR_{eq}+V_{os1}}{R_{eq}+R_s} \text{ , where } \frac{1}{R_{eq}} = \frac{1}{R_T} + \frac{1}{R_{sh}} \tag{4.27}$$

The output of first stage amplification, V_{out}, is calculated as below:

$$V_{out} = R_2I_{b2} - (1 + \frac{R_2}{R_1})[(I_0 - I_{b1})R_f + V_{os1} + V_{os2}] \tag{4.28}$$

After combining equations (4.27) and (4.28) the following general equation for V_{out} is derived:

$$V_{out} = -\frac{R_1+R_2}{R_1}\frac{R_{eq}R_f}{R_{eq}+R_s}I_L + R_2 I_{b2} + \frac{R_1+R_2}{R_1}R_f I_{b1} - \frac{R_1+R_2}{R_1}\left(\frac{V_{os1}R_f}{R_{eq}+R_s} + V_{os1} + V_{os2}\right) \quad (4.29)$$

If $R_{sh} \gg R_s$, $R_{sh} \gg R_f$ and $I_s < 25$ pA then the equation above can be simplified as below.

$$V_{out} \approx -KR_f\left[I_L + I_{b1} - \frac{V_{os1}+V_{os2}}{R_f}\right], \text{ where } K = \frac{R_1+R_2}{R_1} \quad (4.30)$$

Now let's assume ΔI_L is the minimum level of change in the photodiode current that the circuit is supposed to measure. In order to ensure this level is amplified and passed on to the next stage, the changes in the Op-Amp bias current and the offset voltages divided by the feedback resistance must be significantly less than ΔI_L.

$$|\Delta I_{b1}| + \left|\frac{\Delta V_{os1} + \Delta V_{os2}}{R_f}\right| \ll |\Delta I_L| \quad (4.31)$$

The above equation uses the absolute values as the worst case scenario. This is due to the fact that the offset voltage and input bias current can be positive or negative.

4.4.1.2 Dynamic Background Cancellation

The photodiode fluorescence-related current needs to be significantly amplified before it can be measured. The photodiode current, however, includes some background light which is several orders of magnitude higher than the fluorescence-related current. Therefore direct amplification is not possible as it would lead to a saturated amplifier output.

One solution could be to use a DC offset and amplify the difference. However as the level of background light depends on various factors such as milk sample and temperature, which could vary from time to time, a constant DC offset is not a suitable solution.

In order to enable a high amplification level suitable for a wide range of milk samples with different opacity levels, here a novel dynamic background light cancellation is proposed. The method requires two photodiode in two nearby colours, green and blue for example. Both photodiodes detect a proportion of the LED background light. The ratio of the electric current produced by either photodiodes from the LED light depends on their spectral responses, which is a relatively steady one. As an example if a blue LED is used, the blue photodiode compared to the green one is far more sensitive to the blue light; therefore produces a much higher background current. On the other hand if a fluorescing molecule produces photons in the region of green (as a result of blue excitation light), the emitted photons affect the green photodiode more than the blue one. This concept has been used for the design of a dynamic background offset cancellation.

Let's assume V_b and V_g are the electric voltages produced by two independent circuits based on the circuit depicted in Figure 4.14. These voltages have been shown in Figure 4.15. If gains K_b and K_g are selected in a way to make V_b and V_g nearly the same, then any variations in the background light changes both voltages at nearly the same ratio, which keeps the voltage difference between the two small.

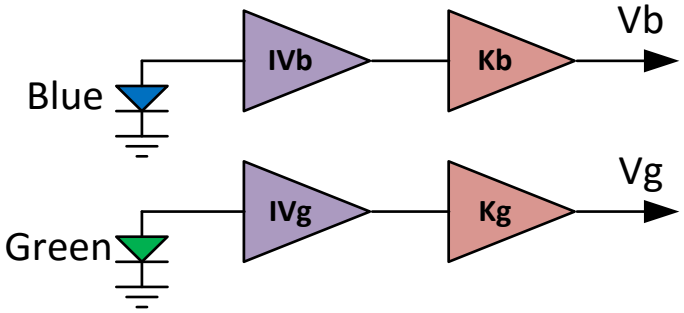

Figure 4.15 Blue and green photodiode voltages

$$\Delta v = V_b - V_g \approx 0 \tag{4.32}$$

In the next stage although further direct amplification will saturate the output, the high gain can be applied to the voltage difference (Δv) due to its small value. The circuit diagram in Figure 4.16 shows this concept.

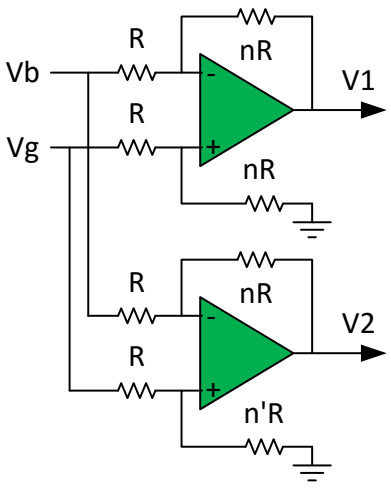

Figure 4.16 Basic dynamic background cancellation circuit

The idea behind the circuit is to use eight gain resistors, seven of them having the same value and one slightly different. The governing equations are summarised here:

$$n\left(V_b - V_g\frac{n}{n+1}\right) = V_g\frac{n}{n+1} - V_1 \rightarrow V_1 = n(V_g - V_b) \tag{4.33}$$

$$n\left(V_b - V_g\frac{n'}{n'+1}\right) = V_g\frac{n'}{n'+1} - V_2 \rightarrow V_2 = n'\frac{n+1}{n'+1}V_g - nV_b \tag{4.34}$$

Now Let's define $K_{\Delta v}$ as below:

$$K_{\Delta v} = \begin{pmatrix} n & -n \\ n'\dfrac{n+1}{n'+1} & -n \end{pmatrix}, |K_{\Delta v}| = n\left(\frac{n'-n}{n'+1}\right) \neq 0, \quad if\ n \neq 0\ , n \neq n' \tag{4.35}$$

Equations (4.33) and (4.34) can therefore be simply expressed as a set of linear equations:

$$\begin{pmatrix} V_1 \\ V_2 \end{pmatrix} = K_{\Delta v}\begin{pmatrix} V_b \\ V_g \end{pmatrix} \rightarrow \begin{pmatrix} V_b \\ V_g \end{pmatrix} = K_{\Delta v}^{-1}\begin{pmatrix} V_1 \\ V_2 \end{pmatrix} \tag{4.36}$$

The determinant of $K_{\Delta v}$ is a non-zero value. This means by knowing V_1 and V_2, the photodiode voltages V_b and V_g can be estimated using (4.36). The above equation is based on an ideal Op-Amp. A normal Op-Amp however has an input bias current and offset voltage (Figure 4.17), with more complex equation governing its operation.

$$\frac{V_b - V_g\frac{n}{n+1} + \frac{nR}{n+1}I'_{b1} - V_{os1}}{R} = I_{b1} + \frac{V_g\frac{n}{n+1} - \frac{nR}{n+1}I'_{b1} + V_{os1} - V_1}{nR} \tag{4.37}$$

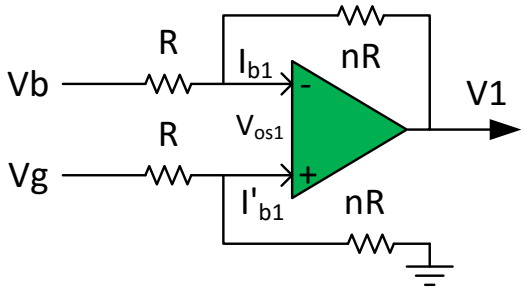

Figure 4.17 Difference amplifier including offset voltage and input bias current

It can be shown that V_1 has the following relationship to V_b and V_g.

$$V_1 = n(V_g - V_b) + nRI_{b1} - nRI'_{b1} + (n+1)V_{os1} \tag{4.38}$$

For the V_2 circuit the following relationship to V_b and V_g applies.

$$\frac{V_b - V_g\frac{n'}{n'+1} + \frac{n'R}{n'+1}I'_{b2} - V_{os2}}{R} = I_{b1} + \frac{V_g\frac{n'}{n'+1} - \frac{n'R}{n'+1}I'_{b2} + V_{os2} - V_2}{nR} \tag{4.39}$$

Similarly V_2 is formulated as follows:

$$V_2 = \frac{n+1}{n'+1}n'V_g - nV_b + nRI_{b2} - \frac{n+1}{n'+1}n'RI'_{b2} - (n+1)V_{os2} \tag{4.40}$$

Let's define ΔV_g as the smallest variation in the green photodiode voltage that the transducer needs to detect. Assuming that $n \approx \acute{n}$ and $n \gg 1$, the combined effect of variations in the input bias current ($\Delta I_{b1}, \Delta I_{b2}$) and offset voltage ($\Delta V_{os1}, \Delta V_{os2}$) need to remain very small in order to ensure they do not affect the performance of the transducer:

$$\begin{aligned} |R\Delta I_{b1}| + |R\Delta I'_{b1}| + |\Delta V_{os1}| &\ll \Delta V_g \\ |R\Delta I_{b2}| + |R\Delta I'_{b2}| + |\Delta V_{os2}| &\ll \Delta V_g \end{aligned} \tag{4.41}$$

4.4.1.3 Filtering

A two-stage low-pass filtering using Sallen-Key design is considered as the anti-aliasing filter before analogue to digital conversion.

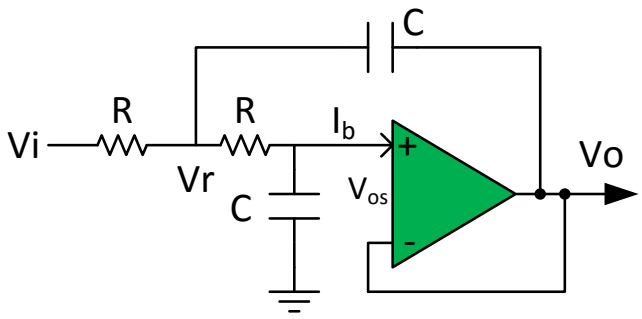

Figure 4.18 Sallen-Key low pass filter

Figure 4.18 shows a basic Sallen-Key filter using a non-ideal Op-Amp. The governing equations are:

$$\begin{aligned} V_i &= (2 + RCs)V_r - (1 + RCs)V_o - V_{os} \\ &= (1 + RCs)^2 V_o + (1 + RCs)^2 V_{os} + RCsV_{os} + (2 + RCs)RI_b \end{aligned} \tag{4.42}$$

V_o will have the following relationship to V_i , the Op-Amp offset voltage and input bias currents.

$$V_o = \frac{V_i}{(1 + RCs)^2} + V_{os} + \frac{RCsV_{os}}{(1 + RCs)^2} + \frac{RI_b}{1 + RCs} + \frac{RI_b}{(1 + RCs)^2} \tag{4.43}$$

In equation (4.43) the term $\frac{RCs}{(1+RCs)^2}$ has a maximum absolute value of 0.25. Other terms have their maximum value at $s = 0$. Using the same definition for ΔV_g as in (4.41), the maximum combined variation in the circuit parameters must be limited to $n\Delta V_g$ as per equation (4.38). If we consider the filter cut-off point of $\frac{V_i}{\sqrt{2}}$ and the worst case for other terms in equation (4.43), the following relationship for the offset voltage

and bias currents must hold in order to ensure the variations in the circuit parameters do not affect the transducer accuracy.

$$\frac{\sqrt{2}}{n}(1.25\Delta V_{os} + 2R\Delta I_b) \ll \Delta V_g \tag{4.44}$$

Assuming that the Op-Amps used for filtering and background cancellation have similar input bias currents and offset voltages and also the criteria set in (4.41) are met, criteria (4.44) will also be satisfied if $n > 1.25\sqrt{2}$.

4.4.2 Calibration

The combined effect of circuit parameters such as offset voltage and input bias current can be estimated during the off period of the LED. This can be done regularly in order to compensate for the effects of temperature and aging, enabling the application of auto calibration. Here equation (4.30) is re-written for both blue and green photodiodes:

$$V_b \approx -K_b R_f \left[I_b + I_{b1,b} - \frac{V_{os1,b}+V_{os2,b}}{R_f} \right], \text{ where } K_b = \frac{R_{1,b}+R_{2,b}}{R_{1,b}} \tag{4.45}$$

$$V_g \approx -K_g R_f \left[I_g + I_{b1,g} - \frac{V_{os1,g}+V_{os2,g}}{R_f} \right], \text{ where } K_b = \frac{R_{1,g}+R_{2,g}}{R_{1,g}} \tag{4.46}$$

Letters b and g represent the blue and green photodiodes, respectively. I_b and I_g are the corresponding I_L current for the blue and green photodiodes. When the LED is off both I_b and I_g are zero. The output voltage in this case is referred to as V_{b0} and V_{g0}. The above equations can therefore be simplified as follows:

$$V_b \approx -K_b R_f I_b + V_{b0} \tag{4.47}$$

$$V_g \approx -K_g R_f I_g + V_{g0} \tag{4.48}$$

In addition when the LED is off equations (4.38) and (4.40) take the following form:

$$V_{10} = n(V_{g0} - V_{b0}) + nRI_{b1} - nRI'_{b1} - (1+n)V_{os1} \tag{4.49}$$

$$V_{20} = \frac{\acute{n}+1}{n+1} nV_{g0} - \acute{n}V_{b0} + \acute{n}RI_{b2} - \frac{\acute{n}+1}{n+1} nRI'_{b2} - (1+\acute{n})V_{os2} \tag{4.50}$$

V_{10} and V_{20} are the output voltages of the background cancellation stage while the LED is off. The equations above can be used to derive the general equations for when the LED is on and measurements are being taken.

$$V_1 = n(V_g - V_b) + [V_{10} - n(V_{g0} - V_{b0})] \quad (4.51)$$

$$V_2 = \frac{\acute{n}+1}{n+1} n V_g - \acute{n} V_b + \left[V_{20} - \frac{\acute{n}+1}{n+1} n V_{g0} + \acute{n} V_{b0}\right] \quad (4.52)$$

The simplified version of the above can be presented in matrix format as below:

$$\begin{pmatrix} V_b - V_{b0} \\ V_g - V_{g0} \end{pmatrix} = K_{\Delta v}^{-1} \begin{pmatrix} V_1 - V_{10} \\ V_2 - V_{20} \end{pmatrix} \quad (4.53)$$

The above equation can be used to calculate the effect of LED light and associated fluorescence effect on the blue and green photodiode voltages, by measuring circuit output voltages when the LED is off and then on.

4.4.3 Measuring Photodiode Current

The photodiodes current is measured while the LED is on. During that time equation (4.53) applies. Using equations (4.47) and (4.48) the photodiode currents are calculated as follows:

$$I_b = -\frac{V_b - V_{b0}}{K_b R_f} \quad (4.54)$$

$$I_g = -\frac{V_g - V_{g0}}{K_g R_f} \quad (4.55)$$

The combination of blue and green photodiode currents can be used for measuring the concentration of analyte of interest, which in this case is progesterone. However as this relationship depends on the biomolecular setup of immunoassay, this aspect is presented in the next chapter.

4.5 Summary

This chapter outlined the theory behind the electronic and mechanical design of the transducer. The sensor enclosure benefits from a novel geometrical design in order to reduce the effect of background light and increase the amount of fluorescent light received by the photodiodes. Milk is an opaque medium, where light cannot travel far. The specific mechanical design creates a feature where both LEDs and photodiodes face the same area in order to increase the number of photons reaching photodiodes, therefore increasing the sensitivity of the sensor.

The emitter design provides a means of accurate control of the LED current. This chapter also reviews the effect of ambient and LED junction temperature on the characteristics of light entering the medium. In order to minimise the effect of LED junction temperature on the performance of the transducer, a sampling algorithm for estimating the best time for triggering the measurement was proposed.

The transducer requires a high level of amplification in order to detect the small changes in the photodiode current produced by the fluorophores of interest. Various parameters of the circuit were studied and their effects on the accuracy of the transducer were investigated. In order to achieve a high level of gain, a novel dynamic background cancellation mechanism was proposed and the associated parameters were evaluated.

The presented transducer design does not need the expensive optical components of filter, dichroic mirror and photo-multiplier, typically employed in standard fluorescence spectroscopy. As a result of the proposed innovative algorithms and hardware design the transducer provides a high degree of accuracy and can be used as a biosensor for measuring concentration of various analytes using fluorescence effect.

Next chapter provides the details of the biological setup proposed for developing the immunoassay, followed by an evaluation of the parameters affecting the immunoassay performance and finally offering a number of procedures for measuring progesterone level in milk.

5 PROGESTERONE MEASUREMENT AND THE IMMUNOASSAY FRAMEWORK

5.1 Introduction

The progesterone assay proposed in this chapter is a competitive immunoassay, based on Fluorescence Resonance Energy Transfer (FRET). There are two main aspects to the immunoassay; namely the transducer design as well as the biomolecular and procedural framework. The transducer including the LEDs, photodiodes and associated electronic circuits incorporated into the purpose-built housing, provides a means of measuring the green and blue emissions produced as a result of fluorescence effect. The transducer design has been fully explained in Chapter 4.

The biological and procedural framework required for measuring progesterone level in milk is presented in this chapter. The relationship between FRET signal and various related elements are also covered and an evaluation of effects of biological and optical parameters on optimum performance of the immunoassay is provided. Finally a general framework for different stages required to measure progesterone level in milk is outlined and then three solutions as a trade-off between hardware requirements and algorithmic and procedural complexity are proposed.

5.2 Principle of Operation

Figure 5.1 provides a schematic diagram of the immunoassay. The LED is used for generating excitation photons, while the photodiodes detect photons coming from the sample (for details of transducer design including the excitation and detection circuitry refer to Chapter 4).

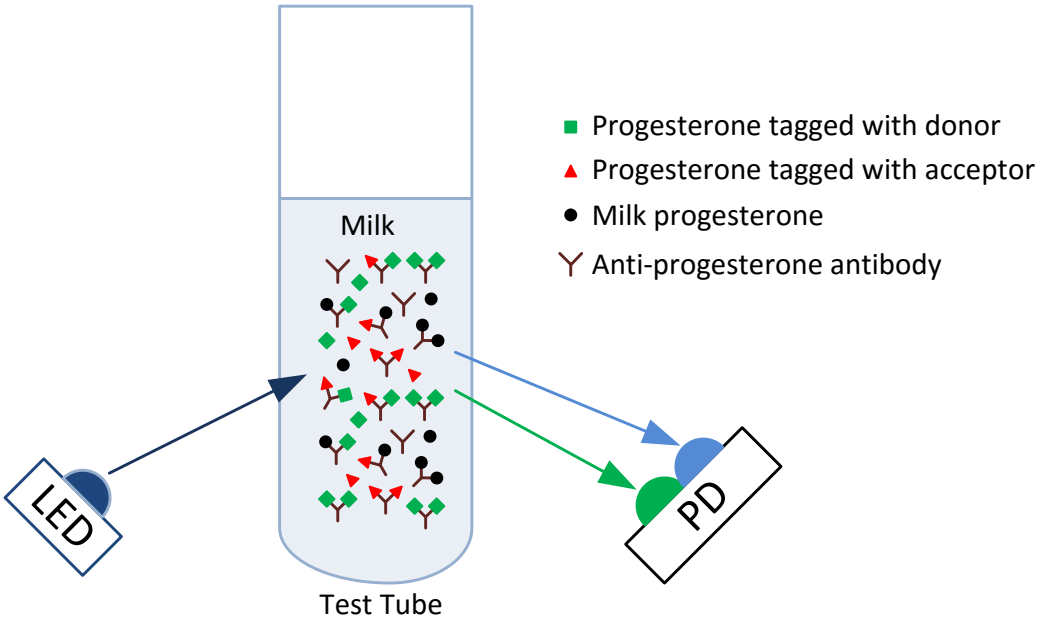

Figure 5.1 Basic components of the proposed immunoassay

The immunoassay works in a competitive manner, where milk progesterone molecules compete with the fluorescent-tagged progesterone molecules in order to bind with the binding sites of the anti-progesterone antibody. The antibody and tagged progesterone molecules are external molecules added to the milk sample in order to facilitate the immunoassay operation. The fluorescent tags are in the form of a pre-determined mixture of Green Fluorescent Protein (GFP) and Red Fluorescent Protein (RFP) molecules. When a pair of GFP and RFP tagged progesterone molecules bind to the two binding sites of an antibody, FRET signal is produced. The level of FRET is used to estimate the concentration of progesterone in milk. The GFP in this case acts as the donor of photon, while the RFP is a photon acceptor in the case of FRET. Therefore the GFP and RFP tagged progesterone molecules are referred to as donor (P_D) and acceptor (P_A) progesterone molecules, respectively. GFP and RFP tags can act as a pure source of fluorescence (without taking part in FRET), when they are moving freely in milk without being bound to an antibody, or when they are bound to an antibody but not in the form of GFP-RFP pair.

The binding sites of a Y-shape antibody can be occupied by any of the milk, donor and acceptor progesterone molecules. In the next section the probability of formation of FRET pair, compared to other combinations is investigated and the relationship between the FRET signal and progesterone concentration is presented.

5.2.1 FRET signal and Progesterone Concentration

There are four essential molecules in the proposed assay. These are anti-progesterone antibody (N), GFP (donor) tagged progesterone (D), RFP (acceptor) tagged progesterone (A) and the milk progesterone (P). The molar concentration of these molecules are represented by M_N, M_D, M_A and M_P. The total concentration of all progesterone molecules, M_T, will therefore be:

$$M_T = M_D + M_A + M_P \tag{5.1}$$

If the number of antibodies is significantly less than the total number of tagged progesterone molecules, all binding sites of the antibodies will eventually be occupied. Consequently after a period of time all antibodies have a pair of antigens attached to their binding sites. This pair can be one of the nine combinations; namely AA, AD, AP, DA, DD, DP, PA, PD and PP. Out of all these combinations only AD or DA form a FRET pair. In order to determine the probability of forming a FRET pair we first need to calculate the probability of forming any combination of an antibody-progesterone pair in a solution where there is only one antibody molecule available. Under such an assumption, all progesterone molecules compete with each other to occupy the binding sites of the antibody molecule. The chance of each type of progesterone molecules forming such a bond depends on the relative concentration of that type of progesterone to the total number of progesterone molecules. The probability of having an AD or DA pair of progesterone-antibody is:

$$p_{AD} = 2\frac{M_D M_A}{{M_T}^2} \tag{5.2}$$

The probability of forming a pair of native milk progesterone compound is

$$p_P = \left(\frac{M_P}{M_T}\right)^2 \tag{5.3}$$

It must be noted that in theory probabilities should be calculated based on picking a molecule from a pool without replacement. However as there are a large number of molecules present this effect can be ignored. Assuming that the number of antibodies is significantly less than the total number of progesterone molecules, over time the binding sites of all antibodies will be occupied by tagged and native progesterone molecules. Therefore p_{AD} represents the proportion of antibody complexes that produce FRET signal, resulting in the following for the concentration of FRET pair (M_F):

$$M_F = p_{AD} M_N \tag{5.4}$$

5.2.2 Relationship between FRET and Milk Progesterone

In order to understand the relationship between the concentration of RFP-GFP pair and progesterone concentration, (5.2) is inserted into (5.4) resulting in the following:

$$M_F = p_{AD} M_N = 2\frac{M_D M_A}{{M_T}^2} M_N = 2\frac{M_D M_A M_N}{(M_D + M_A + M_P)^2} \tag{5.5}$$

Considering equation (5.4) it can be seen that the progesterone concentration (M_P) is inversely related to FRET concentration (M_F). This demonstrates the principle of a competitive immunoassay. The concentration of milk progesterone can therefore be derived from the FRET concentration as per the equation below:

$$M_P = \sqrt{\frac{2M_D M_A M_N}{M_F}} - (M_D + M_A) \tag{5.6}$$

5.3 Photonic Interactions

When the LED emits light, the photons go through the light channel specifically designed in the transducer casing and enter the milk sample. They can reflect back from the channel wall, absorbed or enter gaps or other light channels in the casing. The photons entered the milk sample are absorbed, reflected by the larger milk biomolecules or scattered by the smaller ones. Some will also reflect from the test tube or the internal wall of the test tube chamber. This section describes various processes involved in photonic interactions.

5.3.1 Number of Photons Generating Fluorescence

The majority of light entered the test tube is scattered by milk molecules before exciting the fluorophores. In general the scattering effect takes place when an electromagnetic wave reaches a small particle, creating an induced dipole and as a result scattered light at every direction. The majority of the scattering effect is elastic, meaning that the light is scattered at the same wavelength of the scattered light (Hahn, 2009). The scattering by spherical particles is generally described by Mie solution. This solution is simplified as Rayleigh scattering for small particles where the following criterion is met:

$$r = \frac{2\pi d}{\lambda} \ll 1 \tag{5.7}$$

In the above criterion d is the diameter of the molecule and λ the wavelength of the incident light. Rayleigh scattering is wavelength-dependant, which takes place in every direction. The wavelength dependency of Rayleigh scattering results in more prominent effect in the blue spectrum. This is the reason for seeing the sky above in blue, as the scattered light is mainly in blue region (see Figure 5.2). For larger molecules, where Mie scattering in general applies, the scattered light is more concentrated in the direction of incident light. The Mie scattering is not very

wavelength-dependent. That's why the sky in the direction of sun is in near white colour.

Within the milk sample due to the presence of colloidal molecules, Rayleigh scattering is prominent. The photons are scattered through the milk without a significant loss of energy. The intensity of Rayleigh scattering is inversely related to the wavelength (λ) as follows:

$$I_s = k_s \frac{I_0}{\lambda^4}, \quad \text{where} \quad k_s = \frac{\pi^4}{4}\left(\frac{1+\cos^2\theta}{2R^2}\right)\left(\frac{n^2-1}{n^2+2}\right)^2\left(\frac{d}{2}\right)^6 \tag{5.8}$$

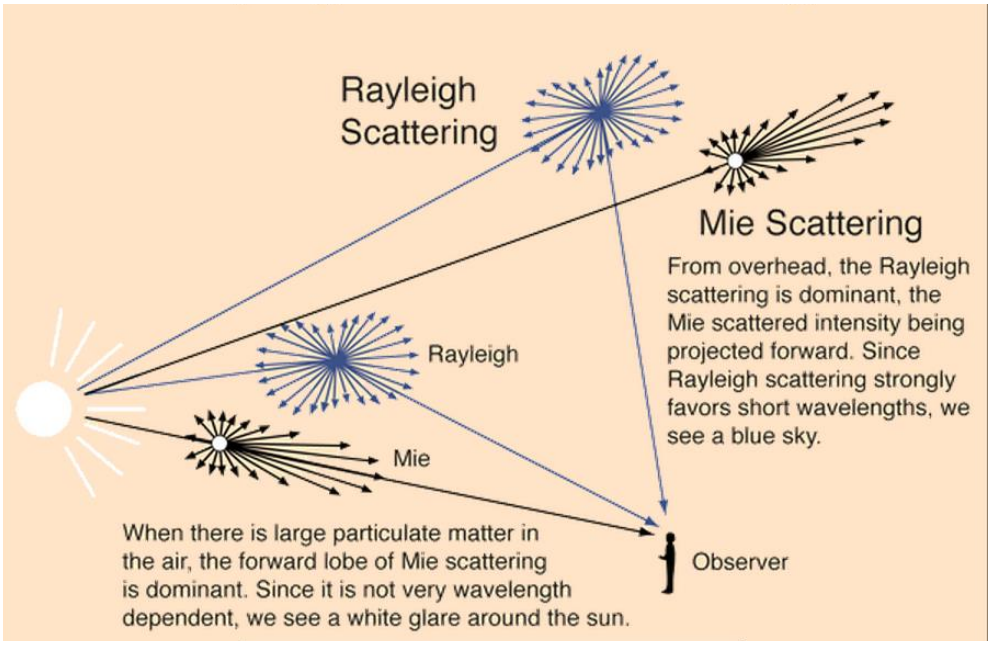

Figure 5.2 Rayleigh vs Mie scattering (Nave, 2016)

I_s is the intensity of scattering effect, I_0 is the light intensity before the interaction with the particle, R is the distance between the particle and the observer, θ is the scattering angle, n is the refractive index of the particle, and d is the diameter of the particle. The location of the test tube with respect to the photodiodes and LEDs, and also the size of the test tube chamber are fixed and specific to the transducer design, therefore θ and R are on average fixed for each transducer. In addition, due to the use

of the same milk sample during a test the value of n and d and consequently k_s remain constant.

The Rayleigh scattering model breaks down when the particle size becomes larger than approximately 10% of the wavelength of the incident radiation. Casein micelles, with an average diameter of 200nm (Glantz, et al., 2010), are the main source of Rayleigh scattering in milk. The larger molecules however produce Mie scattering, which is relatively wavelength independent and scatter more prominently in the direction of incident light. Due the special design of the transducer (photodiode are not in the direction of the incident light) such photons do not generally reach the photodiodes, instead are absorbed by the black surface of internal wall of the test tube chamber, or reach other molecules in milk. In addition to scattering, large biomolecules of milk such as fat globules behave as normal objects, reflecting light depending on their surface geometry.

Considering the above analysis, in order to establish a relationship between the LED current (I_L) and the actual number of photons (N_L) that can potentially generate fluorescence effect in the area of interest in the milk sample, a conversion factor μ_L needs to be defined.

$$N_L(\lambda) = \mu_L \phi(\lambda) S_L(\lambda) I_L \tag{5.9}$$

Parameter μ_L relates the LED current to the number of photons that can instigate the fluorescence process. $S_L(\lambda)$ is the probability of emission at wavelength λ. k_s is as defined in (5.7) and $\phi(\lambda)$ as below:

$$\phi(\lambda) = k_s \lambda^{-4} \tag{5.10}$$

$\phi(\lambda)$ shows the wavelength dependency of the Rayleigh scattering. As the intensity of Mie scattering and light reflection is not wavelength dependent, their effect can be considered in the μ_L factor.

Due to the unknown mix of other molecules (other than the progesterone molecules tagged with donor and acceptor fluorophores) it is hard to estimate exactly what percentage of the N_L photons is received by acceptor or donor fluorophores. However as both donor and acceptor fluorophores have similar physical shapes and properties, the milk and environmental factors affect them both in the same way, represented by a factor (C_m) as follows:

$$N_{L,A}(\lambda) = C_m M_A \, N_L(\lambda) \tag{5.11}$$

$$N_{L,D}(\lambda) = C_m M_D \, N_L(\lambda) \tag{5.12}$$

The ratio of number of fluorophores of each type receiving the photon will therefore be the same as their molar concentrations (M_D and M_A).

$$\frac{N_{L,D}(\lambda)}{N_{L,A}(\lambda)} = \frac{M_D}{M_A} N_L(\lambda) \tag{5.13}$$

5.3.2 Donor and Acceptor Excitation

Once a fluorophore moves to an excited state it may lose its energy as a result of dynamic or static quenching, may transfer its energy due to FRET or emit a photon through fluorescence effect.

Once a photon is absorbed by a fluorophore it may excite the fluorophore and cause the emission of a lower energy photon within a short period of time. The probability of excitation is wavelength dependant based on the excitation spectrum of the fluorophore, $S_E(\lambda)$. Figure 5.3 shows the excitation spectrum for FRET donor and acceptor fluorophores $S_{E,D}(\lambda)$, $S_{E,A}(\lambda)$ respectively.

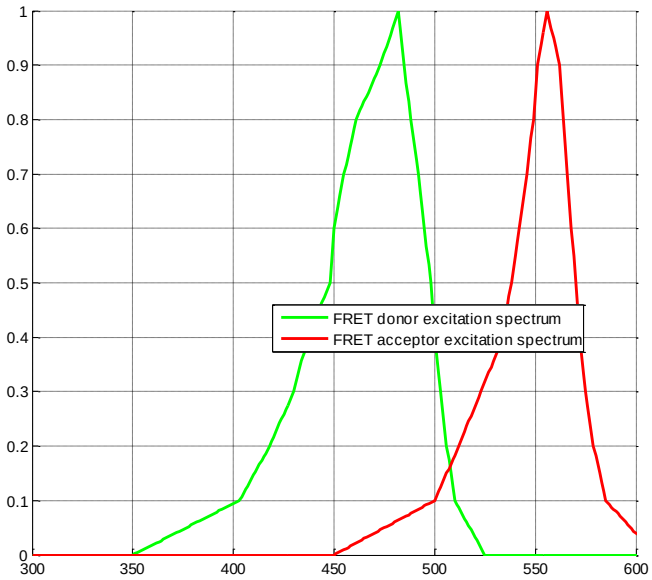

Figure 5.3 The emission spectrum of FRET donor (green) and acceptor (red) fluorophores.

By knowing the number of photons at a particular wavelength and the probability of excitation at that wavelength the total level of excitation, $I_{X,D}$ and $I_{X,A}$, over the entire frequency spectrum of FRET donor and acceptor fluorophores are calculated as follows.

$$I_{X,D} = \int S_{E,D}(\lambda) N_{L,D}(\lambda) d\lambda \tag{5.14}$$

$$I_{X,A} = \int S_{E,A}(\lambda) N_{L,A}(\lambda) d\lambda \tag{5.15}$$

Inserting equations (5.9), (5.10), (5.11) and (5.12) into the above results in:

$$I_{X,D} = \int S_L(\lambda) S_{E,D}(\lambda) C_m M_D \, \mu_L k_s \lambda^{-4} I_L d\lambda \tag{5.16}$$

$$I_{X,A} = \int S_L(\lambda) S_{E,A}(\lambda) C_m M_A \, \mu_L k_s \lambda^{-4} I_L d\lambda \tag{5.17}$$

$k_s, C_m, M_A, M_D, \mu_L, k_\phi$ and I_L are independent of wavelength and can be taken out of the integral.

$$I_{X,D} = C_m M_D \, \mu_L I_L k_s \int S_L(\lambda) S_{E,D}(\lambda) \lambda^{-4} d\lambda \tag{5.18}$$

$$I_{X,A} = C_m M_A \, \mu_L I_L k_s \int S_L(\lambda) S_{E,A}(\lambda) \lambda^{-4} d\lambda \tag{5.19}$$

Now $\bar{S}_{LD}$ and $\bar{S}_{LA}$ are defined as follows:

$$\bar{S}_{LD} = \int S_L(\lambda) S_{E,D}(\lambda) \lambda^{-4} d\lambda \tag{5.20}$$

$$\bar{S}_{LA} = \int S_L(\lambda) S_{E,A}(\lambda) \lambda^{-4} d\lambda \tag{5.21}$$

$\bar{S}_{LD}$ and $\bar{S}_{LA}$ are constant values which can be calculated off-line using the emission and excitation spectra of the LED and RFP/GFP fluorophores. Substituting these definitions into (5.18) and (5.19) results in the following:

$$I_{X,D} = C_m M_D \, \mu_L \bar{S}_{LD} k_s I_L \tag{5.22}$$

$$I_{X,A} = C_m M_A \, \mu_L \bar{S}_{LA} k_s I_L \tag{5.23}$$

5.3.3 Photon Detection

A proportion of the original LED light after elastic scattering reaches the photodiodes on the detection circuit, and detected by the receiver as the LED background light. Some of the reflected photons may also reach the photodiodes, however due to the particular angle of the receiver channel in relation to the emitter channel and also the relatively small size of the window, the reflected photons are far more likely to be scattered by milk molecules and then reach the photodiodes.

The LED photons, including those reflected or scattered, may be absorbed by fluorophores in milk and emit a secondary photon; absorbed by other molecules and lose their energy; or leave the test tube, which will either be reflected back in or absorbed by the transducer casing.

In summary the photons detected by photodiodes are sourced either by the LED in the form of LED background light mainly through scattering effect in milk, or the emission by the donor or acceptor of the FRET pair.

$$I_P = I_{P,A} + I_{P,D} + I_{P,K} \tag{5.24}$$

I_P is the total photodiode current, and $I_{P,K}$, $I_{P,A}$ and $I_{P,D}$ are the current produced as a result of LED light, donor and acceptor emission, respectively.

5.3.3.1 Effect of Donor and Acceptor on Photodiode

The emitted photons from the free donor and acceptor molecules are absorbed by each photodiode and converted to electric current. The amplitude of the electric current depends on the emission level, emission spectrum of the fluorophores in relation to the spectral response of the photodiode and a constant factor, μ_P, related to the geometry of the transducer housing with respect to the photodiode and also the milk sample.

$$I_{P,D} = \mu_P I_{X,D} \int S_D(\lambda) S_P(\lambda) d\lambda \tag{5.25}$$

$$I_{P,A} = \mu_P I_{X,A} \int S_A(\lambda) S_P(\lambda) d\lambda \tag{5.26}$$

$S_D(\lambda)$ and $S_A(\lambda)$ are the emission spectra of donor and acceptor respectively. The quantum yield of each fluorophore will also be included in the μ_P factor. $S_P(\lambda)$ is the spectral response of the photodiode. Here $\bar{S}_{DP}$ and $\bar{S}_{AP}$ are defined as follows:

$$\bar{S}_{DP} = \int S_D(\lambda) S_P(\lambda) d\lambda \tag{5.27}$$

$$\bar{S}_{AP} = \int S_A(\lambda) S_P(\lambda) d\lambda \tag{5.28}$$

$\bar{S}_{DP}$ and $\bar{S}_{AP}$ can be calculated offline using the emission and response spectra provided in the datasheets. Using the above definition and (5.22) and (5.23), equations (5.25) and (5.26) will be simplified as below:

$$I_{P,D} = \mu_P \mu_L k_s \bar{S}_{DP}\, \bar{S}_{LD} C_m M_D\, I_L \tag{5.29}$$

$$I_{P,A} = \mu_P \mu_L k_s\, \bar{S}_{AP}\, \bar{S}_{LA} C_m M_A\, I_L \tag{5.30}$$

$I_{P,D}$ and $I_{P,A}$ are measured by the detector circuit. I_L is known as the LED current is controlled to be at this level. M_D and M_A are also known as the donor and acceptor are added at predetermined molar concentration levels.

5.3.3.2 Effect of LED Background Light on a Photodiode

The background light is the proportion of the LED light received by a photodiode. Once a photon is absorbed by a photodiode it generates an electric current which depends on the sensitivity of the photodiode at that particular wavelength. The proportion of scattered light, which reaches the photodiode, μ_K, is wavelength-independent and depends on the physical construction of the transducer housing. In summary $I_{P,K}$, which is the electric current generated by the photodiode as a result of LED background light is calculated as follows:

$$I_{P,K} = \mu_K \int S_P(\lambda) N_L(\lambda) d\lambda \tag{5.31}$$

Substituting (5.9) and (5.10) in the above results in the following:

$$I_{P,K} = \mu_K \mu_L k_s I_L \int S_P(\lambda) \lambda^{-4} d\lambda \tag{5.32}$$

Now $\bar{S}_P$ is defined as below:

$$\bar{S}_P = \int S_P(\lambda) \lambda^{-4} d\lambda \tag{5.33}$$

$\bar{S}_P$ is a constant value which can be calculated offline using the spectral response curve of the photodiode. The above equation can therefore be simplified.

$$I_{P,K} = \mu_K \mu_L k_s \bar{S}_P I_L \tag{5.34}$$

5.3.3.3 Total Photodiode Current

The total current produced by the photodiode is as a result of LED background light and also the photons received from the donor and acceptor fluorophores. The total current based on (5.24), considering (5.29), (5.30) and (5.32) will therefore be:

$$I_P = \left[c_{D,P}^{L} M_D \; + \; c_{A,P}^{L} M_A \; + c_{K,P}\right] I_L \tag{5.35}$$

Where $c_{D,P}^{L}$, $c_{A,P}^{L}$ and $c_{K,P}$ are defined as follows:

$$c_{D,P}^{L} = \; \mu_P \mu_L k_s \bar{S}_{DP} \, \bar{S}_{ED} C_m \tag{5.36}$$

$$c_{A,P}^{L} = \; \mu_P \mu_L k_s \, \bar{S}_{AP} \, \bar{S}_{EA} C_m \tag{5.37}$$

$$c_{K,P} = \; \mu_K \mu_L k_s \bar{S}_P \tag{5.38}$$

The transducer developed for this PhD accommodates two LEDs and two photodiodes (see Chapter 4), with the associated electronic circuits to drive the LEDs and measure the fluorescence-related current produced by the photodiodes. Therefore equation (5.35) can be expanded to cover any combination of (L_1, L_2) LEDs and (P_1, P_2) photodiodes.

$$I_{P_i}^{L_j} = \left(c_{D,P_i}^{L_j} M_D \; + \; c_{A,P_i}^{L_j} M_A \; + c_{K,P_i}\right) I_{L_j} \;\; , \;\; L_j \in (L_1, L_2) \text{ and } P_i \in (P_1, P_2) \tag{5.39}$$

5.3.4 Effect of FRET on Photodiode Current

When an antibody is added to the milk sample, the donor and acceptor tagged progesterone molecules as well as milk progesterone molecules compete to bind with the antibody. When a FRET pair is formed, the donor emission level reduces, while the acceptor's increases. Therefore the concentration of FRET (M_F) will have the following effect on the current produced by each photodiode (P_1, P_2) as a result of each LED (L_1, L_2).

$$\hat{I}_{P_i}^{L_j} = \left(c_{D,P_i}^{L_j} (M_D - M_F) \; + \; c_{A,P_i}^{L_j} (M_A + M_F) \; + c_{K,P_i}\right) I_{L_j} \tag{5.40}$$

5.3.5 Effect of Empty Test Tube on Photodiode Current

When there is no milk sample, the LED light reflects back from internal wall of the test tube and chamber and is then detected by the photodiode. There is no scattering in this case and the governing equation is as follows.

$$I_P = \mu_E I_L \int S_L(\lambda) S_P(\lambda) d\lambda \tag{5.41}$$

μ_E is the conversion constant which depends on the geometry of the sensor housing. $\bar{S}_{LP,E}$, defined below, is a constant value determined using the emission and response spectra of the LED and photodiode.

$$\bar{S}_{LP,E} = \int S_L(\lambda) S_P(\lambda) d\lambda \tag{5.42}$$

The current produced by each photodiode for each LED is therefore expressed as follow:

$$I_{P_i}^{L_j} = \mu_C \bar{S}_{L_j P_i} I_{L_j} \ , \ L_j \in (L_1, L_2) \ , P_i \in (P_1, P_2) \tag{5.43}$$

5.4 General Progesterone Measurement Framework

As described earlier in Section 5.2.2, milk progesterone concentration is inversely related to the FRET concentration. In general in order to accurately measure FRET level, the following stages need to be considered:

a) The background offset is estimated and compensated for. This can be achieved using the transducer in the absence of any RFP or GFP tagged progesterone molecules.
b) Fluorescence level produced by RFP and GFP tagged progesterone molecules in the absence of anti-progesterone antibody is measured. As there is no antibody, there

will be no competition and no FRET signal produced. This will provide a sound basis for measuring FRET concentration, when antibody is introduced.

c) Anti-progesterone antibody is introduced into the milk sample, creating an environment for the progesterone molecules to compete and consequently forming FRET pairs. The FRET concertation is used to estimate the concentration of progesterone.

In this section a general measurement process, based on the stages described above and using the two LEDs and photodiodes is proposed. The method presented here, provides a general framework, without any particular focus on the colours of the LEDs and photodiodes.

5.4.1 Background Offset Measurement

This stage requires the transducer to be set up for normal operation after initialisation and the test tube containing milk sample is inserted into the test tube chamber. In order to determine the electric current produced by each photodiode as a result of the background LED light, the LEDs are turned on one at a time. The photodiode currents for each LED are measured at the same time. As there is no fluorophore in the milk, the LED background light ($I_{P_i,K}^{L_j}$) will be expressed based on (5.39) as follows:

$$I_{P_i,K}^{L_j} = c_{K,P_i} I_{L_j} \ , \ \ L_j \in (L_1, L_2) \ \text{and} \ P_i \in (P_1, P_2) \tag{5.44}$$

5.4.2 Donor Injection

At this stage the milk sample is mixed with donor tagged progesterone molecules at the pre-determined concentration level of M_D. The photodiode current for each LED is measured resulting in the following 4 linear equations.

$$I_{P_{i,D}}^{L_j} = \alpha_j (c_{D,P_{i1}}^{L_j} M_D I_{L_j} + I_{P_i,K}^{L_j}) \ \text{where} \ \ L_j \in (L_1, L_2) \ \text{and} \ P_i \in (P_1, P_2) \tag{5.45}$$

α_1 and α_2 factors represent the combined effect of changes in each LED current and optical properties of the LED and milk since the background offset measurement stage. For each LED both background light and the donor emission change at the same rate, as both go through the same milk and are directly or indirectly generated by the photons emitted from the LED.

There are 8 unknown parameters in these equations; namely, $c_{D,P_1}^{L_1}$, $c_{D,P_2}^{L_1}$, $c_{D,P_1}^{L_2}$, $c_{D,P_2}^{L_2}$, I_{L_1}, I_{L_2}, α_1 and α_2. Looking at equation in Section 5.3, I_{L_1} is always used in conjunction with $c_{D,P_1}^{L_1}$ and $c_{D,P_2}^{L_1}$. The same also applies to I_{L_2} in relation to $c_{D,P_1}^{L_2}$ and $c_{D,P_2}^{L_2}$. Therefore the above equations are reformulated as follows, reducing the number of unknown parameters to 6:

$$I_{P_{i,D}}^{L_j} = \alpha_j (C_{D,P_{i1}}^{L_j} M_D + I_{P_{i,K}}^{L_j}), \quad \text{where } C_{D,P_{i1}}^{L_j} = c_{D,P_{i1}}^{L_j} I_{L_j}, \quad i,j \in (1,2) \tag{5.46}$$

5.4.3 Acceptor Injection

At this stage the milk sample is mixed with acceptor tagged progesterone molecules at a pre-determined concentration level of M_A. The photodiode current for each LED is measured resulting in the following 4 linear equations.

$$I_{P_{i,AD}}^{L_j} = \beta_j (c_{A,P_i}^{L_j} M_A I_{L_j} + c_{D,P_i}^{L_j} M_D I_{L_j} + I_{P_{i,K}}^{L_j}) \text{ , where } i,j \in (1,2) \tag{5.47}$$

As for the case of donor injection, β_1 and β_2 represent the combined effect of the changes in each LED current and optical properties of milk and LED since the background offset measurement stage, for the first and second LEDs, respectively. By moving LED currents into the c coefficients and combining with set of equations in (5.46) the following yields:

$$I_{P_{i,AD}}^{L_j} = \beta_j (C_{A,P_i}^{L_j} M_A + \frac{I_{P_{i,D}}^{L_j}}{\alpha_j}), \text{ where } i,j \in (1,2) \tag{5.48}$$

5.4.4 Antibody Injection

At this stage antibody is added to the solution. The process of FRET formation results in a reduction in the donor emission and an increase in the acceptor emission. Equations (5.40) is used to arrive at the following:

$$I_{P_{i,F}}^{L_j} = \gamma_j \left[c_{D,P_i}^{L_j} (M_D - M_F) I_{L_j} + c_{A,P_i}^{L_j} (M_A + M_F) I_{L_j} + I_{P_i,K}^{L_j} \right], i,j \in (1,2) \quad (5.49)$$

As for the case of donor injection, γ_1 and γ_2 represent the combined effect of changes in each LED current and optical properties of milk and LED since the background offset measurement stage, for the first and second LEDs, respectively. Moving LED currents into the *c* coefficients and combing with equations (5.47) results in the following:

$$I_{P_{i,F}}^{L_j} = \gamma_j \left[\frac{I_{P_{i,AD}}^{L_j}}{\beta_j} + \left(C_{A,P_i}^{L_j} - C_{D,P_i}^{L_j} \right) M_F \right], i,j \in (1,2) \quad (5.50)$$

5.4.5 Progesterone Measurement

Equation sets (5.46), (5.48) and (5.50) are 12 individual equations with 15 unknown parameters; namely, α_1, α_2, β_1, β_2, γ_1, γ_2, $C_{D,P_1}^{L_1}$, $C_{D,P_2}^{L_1}$, $C_{D,P_1}^{L_2}$, $C_{D,P_2}^{L_2}$, $C_{A,P_1}^{L_1}$, $C_{A,P_2}^{L_1}$, $C_{A,P_1}^{L_2}$, $\mathrm{C}_{\mathrm{A,P}_2}^{\mathrm{L}_2}$ and M_{F}. In Section 5.5 a number of methods are presented where under some circumstances some parameters are removed and/or extra equations are created in order to solve the equations and determine the value of M_F. Once M_F is known using equation (5.6) the progesterone concentration level is calculated as follows.

$$M_P = \left[\sqrt{\frac{2\alpha M_N}{M_F}} - (\alpha + 1) \right] M_A, \quad M_D = \alpha M_A \quad (5.51)$$

5.5 Specific Progesterone Measurement Procedures

Section 5.4 presented four basic stages for measuring progesterone level; namely, background offset measurement, donor, acceptor and antibody injection, formulated by equations (5.44), (5.46), (5.48), (5.50). The progesterone concentration is measured at the end using the detected FRET signal as per equation (5.51). The unknowns in the above equations are α_i, β_i, γ_i, $C_{D,P_i}^{L_j}$,$C_{A,P_i}^{L_j}$ and M_F, where $i,j \in (1,2)$. The number of equations in total is 12, whereas the unknowns are 15 in total. This section proposes a 5-stage method, a 4-stage method and finally a 2-stage method based on the above equations in order to solve or omit the unknown parameters and ultimately determine the concentration of progesterone.

5.5.1 Progesterone Measurement – 5 Stage Method

This method is based on using one LED and 2 photodiodes in 5 stages. The specific conditions for this method are the injection of donor in two stages; and also the use of a second photodiode that has a spectral response with no or very small overlap with the emission spectrum of the acceptor for the chosen LED. The combination of blue LED in conjunction with blue and green photodiodes satisfies this condition (see Chapter 7 for details).

Stage1 – Background Offset Measurement

Milk is added to the test tube and LED background currents $I_{P_{1,K}}$ and $I_{P_{2,K}}$ detected by photodiodes P_1 and P_2, are measured.

Stage2 – Partial Donor Inclusion

The milk sample is then mixed with donor-tagged progesterone molecules to reach a percentage (e.g. 90%) of the predetermined concentration level of M_D. The photodiode currents are measured resulting in the following two linear equations.

$$\begin{pmatrix} C_{D,P_1} \\ C_{D,P_2} \end{pmatrix} = \begin{pmatrix} \frac{I_{P_{1,D}} - \alpha I_{P_{1,K}}}{0.9\alpha M_D} \\ \frac{I_{P_{2,D}} - \alpha I_{P_{2,K}}}{0.9\alpha M_D} \end{pmatrix} \quad \text{where} \begin{Bmatrix} I_{P_{1,D}} = \alpha(C_{D,P_1}\ 0.9M_D + I_{P_{1,K}}) \\ I_{P_{2,D}} = \alpha(C_{D,P_2}\ 0.9M_D + I_{P_{2,K}}) \end{Bmatrix} \tag{5.52}$$

It is assumed that although the LED current, ambient temperature and optical properties of milk have changed since background current measurement, the changes have the same proportional effect (α) on the current measured by both photodiodes.

Stage3 – Full Donor Inclusion

The milk sample is mixed with donor-tagged progesterone molecules to increase the concentration level to M_D. The photodiode currents are measured resulting in the following two linear equations.

$$\begin{pmatrix} C_{D,P_1} \\ C_{D,P_2} \end{pmatrix} = \begin{pmatrix} \frac{\acute{I}_{P_{1,D}} - \varepsilon I_{P_{1,K}}}{\varepsilon M_D} \\ \frac{\acute{I}_{P_{2,D}} - \varepsilon I_{P_{2,K}}}{\varepsilon M_D} \end{pmatrix} \quad \text{where} \begin{Bmatrix} \acute{I}_{P_{1,D}} = \varepsilon(C_{D,P_1}\ M_D + I_{P_{1,K}}) \\ \acute{I}_{P_{2,D}} = \varepsilon(C_{D,P_2}\ M_D + I_{P_{2,K}}) \end{Bmatrix} \tag{5.53}$$

Parameter ε is defined in the same way as α in (5.52) to represent the changes since stage 1. Combining equations (5.52) and (5.53) leads to the following:

$$\begin{pmatrix} \frac{1}{\alpha} \\ \frac{1}{\varepsilon} \end{pmatrix} = \begin{pmatrix} 10I_{P_{1,D}} & -9\acute{I}_{P_{1,D}} \\ 10I_{P_{2,D}} & -9\acute{I}_{P_{2,D}} \end{pmatrix}^{-1} \begin{pmatrix} I_{P_{1,K}}^{L_1} \\ I_{P_{2,K}}^{L_1} \end{pmatrix} \tag{5.54}$$

Due to the presence of term $0.9M_D$ in equation (5.52) compared to (5.53), the equations are not linearly dependant therefore the matrix in (5.54) has a non-zero determinant and can therefore be inversed. By inserting α value into equation (5.52) coefficients C_{D,P_1} and C_{D,P_2} are calculated.

Stage4 – Acceptor Inclusion

Here the milk sample is mixed with acceptor-tagged progesterone molecules at a predetermined concentration level of M_A. The second photodiode is chosen so that its

spectral response does not overlap with the acceptor emission ($C_{A,P_2} = 0$). Therefore the governing equations in this case are:

$$\left\{\begin{matrix} I_{P_{1,AD}} = \beta(\frac{\acute{I}_{P_{1,D}}}{\varepsilon} + C_{A,P_1} M_A) \\ I_{P_{2,AD}} = \frac{\beta}{\varepsilon} \acute{I}_{P_{2,D}} \end{matrix}\right\} \quad (5.55)$$

β and C_{A,P_1} can therefore be calculated as follows:

$$\beta = \varepsilon \frac{I_{P_{2,AD}}}{\acute{I}_{P_{2,D}}}, \quad C_{A,P_1} = \frac{I_{P_{1,AD}} \acute{I}_{P_{2,D}} - I_{P_{2,AD}} \acute{I}_{P_{1,D}}}{\varepsilon M_A I_{P_{2,AD}}} \text{ and } C_{A,P_2} = 0 \quad (5.56)$$

Stage5 – Antibody Inclusion

The milk sample is mixed with antibody at a predetermined concentration level of M_N. The governing equations are:

$$\left\{\begin{matrix} I_{P_{1,F}} = \gamma(\frac{I_{P_{1,AD}}}{\beta} + (C_{A,P_1} - C_{D,P_1}) M_F) \\ I_{P_{2,F}} = \gamma(\frac{I_{P_{2,AD}}}{\beta} - C_{D,P_2} M_F) \end{matrix}\right\} \quad (5.57)$$

This results in calculating M_F and γ values using the parameters known by this stage.

$$M_F = \frac{\gamma I_{P_{2,AD}} - \beta I_{P_{2,F}}}{\beta \gamma C_{D,P_2}} \text{ where } \gamma = \beta \frac{I_{P_{1,F}} C_{D,P_2} + I_{P_{2,F}} (C_{A,P_1} - C_{D,P_1})}{I_{P_{1,AD}} C_{D,P_2} + (C_{A,P_1} - C_{D,P_1}) I_{P_{2,AD}}} \quad (5.58)$$

Using (5.6) progesterone level is estimated as follows:

$$M_P = \sqrt{2 M_D M_A M_N \frac{\beta \gamma C_{D,P_2}}{\gamma I_{P_{2,AD}} - \beta I_{P_{2,F}}}} - M_A - M_D \quad (5.59)$$

5.5.2 Progesterone measurement – 4 Stage Method

The method proposed here is based on using two LEDs and two photodiodes, in four stages. The specific condition for this method is that both LEDs must have the same

ratio of change in the LED current from stage 3 to stage 4 and from stage 2 to stage 3. This condition is met if the LED current to the junction temperature can be assumed linear around the operating condition. In addition the second photodiode frequency response must not overlap with emission spectrum of the acceptor for both LEDs. The combination of blue and cyan LEDs in conjunction with blue and green photodiodes satisfies this imposed condition (see Chapter 7 for details).

Stage1 – Background Measurement

Milk is added to the test tube. The background currents measured by the photodiodes for each LED are $I_{P_{1,K}}^{L_1}$, $I_{P_{2,K}}^{L_1}$, $I_{P_{1,K}}^{L_2}$ and $I_{P_{2,K}}^{L_2}$.

Stage2 – Donor Inclusion

Milk sample is mixed with donor tagged progesterone molecules at a pre-determined concentration level, $\mathrm{M_D}$. The photodiode current for each LED is measured resulting in the following 4 linear equations.

$$\begin{Bmatrix} I_{P_{1,D}}^{L_1} = \alpha_1 (C_{D,P_1}^{L_1} M_D + I_{P_1,K}^{L_1}) \\ I_{P_{2,D}}^{L_1} = \alpha_1 (C_{D,P_2}^{L_1} M_D + I_{P_2,K}^{L_1}) \\ I_{P_{1,D}}^{L_2} = \alpha_2 (C_{D,P_1}^{L_2} M_D + I_{P_1,K}^{L_2}) \\ I_{P_{2,D}}^{L_2} = \alpha_2 (C_{D,P_2}^{L_2} M_D + I_{P_2,K}^{L_2}) \end{Bmatrix} \quad (5.60)$$

Stage3 – Acceptor Inclusion

Milk sample is mixed with acceptor at a predetermined concentration level of M_A. The second photodiode is chosen so that its response spectrum does not overlap with the acceptor emission. Therefore the governing equations in this case are:

$$\left\{\begin{array}{c} I_{P_{1,AD}}^{L_1} = \beta_1(C_{A,P_1}^{L_1} M_A + \frac{I_{P_{1,D}}^{L_1}}{\alpha_1}) \\ I_{P_{2,AD}}^{L_1} = \beta_1(\frac{I_{P_{2,D}}^{L_1}}{\alpha_1}) \\ I_{P_{1,AD}}^{L_2} = \beta_2(C_{A,P_1}^{L_2} M_A + \frac{I_{P_{1,D}}^{L_2}}{\alpha_2}) \\ I_{P_{2,AD}}^{L_2} = \beta_2(\frac{I_{P_{2,D}}^{L_2}}{\alpha_2}) \end{array}\right\} \text{where } C_{A,P_2}^{L_1} = 0, C_{A,P_2}^{L_2} = 0 \quad (5.61)$$

Stage4 – Antibody Inclusion

Milk sample is mixed with antibody at a predetermined concentration level of M_N. The governing equations are:

$$\left\{\begin{array}{c} I_{P_{1,F}}^{L_1} = \gamma_1(\frac{I_{P_{1,AD}}^{L_1}}{\beta_1} + (C_{A,P_1}^{L_1} - C_{D,P_1}^{L_1})M_F) \\ I_{P_{2,F}}^{L_1} = \gamma_1(\frac{I_{P_{2,AD}}^{L_1}}{\beta_1} - C_{D,P_2}^{L_1} M_F) \\ I_{P_{1,F}}^{L_2} = \gamma_2(\frac{I_{P_{1,AD}}^{L_2}}{\beta_2} + (C_{A,P_1}^{L_2} - C_{D,P_1}^{L_2})M_F) \\ I_{P_{2,F}}^{L_2} = \gamma_2(\frac{I_{P_{2,AD}}^{L_2}}{\beta_2} - C_{D,P_2}^{L_2} M_F) \end{array}\right\} \text{where } C_{A,P_2}^{L_1} = 0, C_{A,P_2}^{L_2} = 0 \quad (5.62)$$

The above 12 equations have 13 unknown parameters; namely, α_1, α_2, β_1, β_2, γ_1, γ_2, $C_{D,P_1}^{L_1}$, $C_{D,P_2}^{L_1}$, $C_{D,P_1}^{L_2}$, $C_{D,P_2}^{L_2}$, $C_{A,P_1}^{L_1}$, $C_{A,P_1}^{L_2}$, and M_F. We now assume the variations in both LED lights over time is on a linear curve, and taking into account that the milk media is the same for both LEDs the following relationship can be established:

$$\frac{\gamma_1 - \beta_1}{\beta_1 - \alpha_1} = \frac{\gamma_2 - \beta_2}{\beta_2 - \alpha_2} \quad (5.63)$$

The combination of (5.60) to (5.63) provides 13 equations that are used for calculating the value of M_F, from which progesterone concentration can be calculated using (5.6).

5.5.3 Progesterone Measurement – 2 Stage Method

The method proposed here is based on using one LED and 2 photodiodes, assuming that FRET formation is a first order process.

Stage1 – Acceptor and Donor Inclusion

Both donor and acceptor molecules at the predetermined concentrations of M_D and M_A are added at the same time, resulting in the following two linear equations.

$$\begin{Bmatrix} I_{P_{1,AD}} = C_{A,P_1} M_A + C_{D,P_1} M_D + I_{P_{1,K}} \\ I_{P_{2,AD}} = C_{A,P_2} M_A + C_{D,P_2} M_D + I_{P_{2,K}} \end{Bmatrix} \quad (5.64)$$

Assuming that $C_{A,P_2} = 0$ by measuring $I_{P_{2,K}}$ when there is no donor, then $I_{P_{2,AD}}$once the donor is added, C_{D,P_2} can be calculated.

Stage2 – Antibody Inclusion

At this stage the milk sample is mixed with antibody at a predetermined concentration level of M_N. Note that β and M_F are considered time dependant. The formation of FRET pairs is a gradual first order process, following an exponential path:

$$M_F(t) = M_{F,\infty}(1 - e^{-\frac{t}{\tau}}) \quad (5.65)$$

The governing equations are:

$$\begin{Bmatrix} I_{P_{1,F}}(t) = \beta(t)\left(I_{P_{1,AD}} + \Delta C_{P_1} M_{F,\infty}(1 - e^{-\frac{t}{\tau}})\right) \\ I_{P_{2,F}}(t) = \beta(t)\left(I_{P_{2,AD}} + \Delta C_{P_2} M_{F,\infty}(1 - e^{-\frac{t}{\tau}})\right) \end{Bmatrix} \text{ where } \begin{pmatrix} \Delta C_{P_1} \\ \Delta C_{P_2} \end{pmatrix} = \begin{pmatrix} C_{A,P_1} - C_{D,P_1} \\ -C_{D,P_2} \end{pmatrix} \quad (5.66)$$

The unknown parameters in the above equations are τ, $M_{F,\infty}$, , ΔC_{P_1}, and $\beta(t)$, which are all assumed constant expect for $\beta(t)$. After the addition of antibody, while the FRET pairs are being formed by measuring photodiode currents at regular sampling intervals (t_n), a new dual set of equations are formed every time, with all parameters remaining constant except for $\beta(t)$.

$$\left\{\begin{matrix} I_{P_{1,F}}(t_n) = \beta(t_n)\left(I_{P_{1,AD}} + \Delta C_{P_1} M_{F,\infty}(1 - e^{-\frac{t_n}{\tau}})\right) \\ I_{P_{2,F}}(t_n) = \beta(t_n)\left(I_{P_{2,AD}} + \Delta C_{P_2} M_{F,\infty}(1 - e^{-\frac{t_n}{\tau}})\right) \end{matrix}\right\} \quad n \in (1..N) \tag{5.67}$$

After taking N measurements, there will be $2N$ equations and $3 + N$ unknown parameters. To solve the unknown parameters, the following relationship should hold:

$$2N = N + 3 \rightarrow N = 3 \tag{5.68}$$

Therefore in order to estimate $M_{F,\infty}$ as the steady state concentration of FRET pairs, measurements at a minimum of 3 sampling times are required. $M_{F,\infty}$ is used for estimating the concentration of progesterone as per equation (5.6).

5.6 Summary

This chapter provides the theoretical framework for fluorescence based progesterone measurement using FRET. The probability of formation of FRET pair in relation to the concentration of milk progesterone was formulated. The effects of fluorophores emission and excitation spectra in conjunction with photodiodes spectral sensitivity and LED emission spectrum were assessed and entered into the associated formulas. At the end a generic framework for progesterone measurement was presented, followed with specific measurement procedures as a trade-off between hardware cost versus algorithmic and procedural complexity.

The first method is a 5-stage process requiring one LED and 2 photodiodes. It consists of background light measurement, two stages for adding donor-tagged progesterone molecules to the milk samples, one stage for adding acceptor-tagged progesterone and finally one stage for adding antibody and measuring FRET level. This method requires minimum hardware components and is independent of the LED current, with no need for any additional assumptions on the parameters of the system. Therefore this is a more robust method and can be used in wider ambient conditions and over longer

periods. The downside of this method is the number of stages needed to perform the test.

The second method is a 4-stage process with an additional LED compared with the first method. This extra LED needs extra control circuit. Also the receiver circuit needs a selectable gain due to the fact that the ratio of background light on the blue and green photodiodes is different for blue and cyan LEDs. In comparison the second method requires extra electronic circuitry and a more complex casing in order to house the second LED, all at extra cost. However progesterone measurement under this method is carried out over 4 stages instead of 5, with some savings on the cost of each test. This saving in an automated test solution is likely to be insignificant.

The third method is a 2-stage process with similar hardware setup as the 5-stage method. The computational cost of this method is significantly higher than the first method and requires a more sensitive analogue circuitry in order to detect changes during the process. However due to its simplicity will have a great advantage in farms and will be the favourable method in practice.

In the next chapter the effects of milk composition and molecular interactions on the formation of FRET and fluorescence effect are evaluated.

6 ANALYSIS OF THE EFFECT OF MILK COMPOSITION ON THE IMMUNOASSAY PERFORMANCE

6.1 Introduction

Milk is an opaque aqueous colloidal liquid, containing three major classes of molecules; namely lactose, lipids and proteins. In addition, the milk sample will also contain molecules essential for the operation of the proposed immunoassay. These molecules are natural milk progesterone, anti-progesterone antibody and tagged progesterone molecules. Chapter 5 described the general framework for interaction of molecules of interest and formation of FRET pair, which is essential for measuring the progesterone level. Milk however is a complex medium with various biomolecules that could affect the performance of the immunoassay. In order to understand these effects it is paramount to investigate how various biomolecules dissolve in the aqueous medium of milk; their interactions with the immunoassay specific biomolecules in particular antibody and colloidal globules such as fat; the distribution of progesterone and the effect of its physical shape and the accompanying molecules on the probability of binding with antibody; and the interaction of GFP and RFP tags with the milk molecules.

This chapter first provides a brief overview of the elementary concepts required for understanding the analysis. Then the molecular composition of milk is detailed, with a focus on the biomolecules that could affect the performance of the immunoassay. This will then be followed by an analysis of the intermolecular interactions between milk and immunoassay biomolecules.

6.2 A Brief Review of Relevant Chemistry Concepts

In order to comprehend the topics presented in this chapter, it is important to have a degree of understanding of the relevant chemistry concepts. These are briefly reviewed in this section however the reader is invited to refer to the relevant chemistry books for an in depth understanding of these concepts.

6.2.1 Chemical Bonds

Molecules and atoms can form chemical bonds through different mechanisms at various strength levels. Ionic, covalent, hydrogen and van der waal bonds are the main categories of chemical bonds, with ionic being the strongest and van del waal the weakest. Ionic bonds are formed as a result of electrostatic attraction between ions and cations. Table salt (NaCl) is an example of an ionic bond. A covalent bond is established where the two parties share valence electrons. Water ($\mathrm{H_2O}$) is a molecule with covalent bonds between hydrogen and oxygen atoms.

Hydrogen bond or H-bond is formed due to the attraction of hydrogen to highly electronegative atoms, such as nitrogen and oxygen. This type of bond holds the $\mathrm{H_2O}$ molecules together and creates the liquid water. Van der Waal bonds are basically as a result of dipole-dipole attractive and repulsive forces. The dipoles can be momentarily produced while the electrons orbit around the nucleus, or induced, or permanently exist for example in ions. Hydrogen and van der Waal bonds exist as an external force between molecules, in another word at the intermolecular level. All molecules experience van der Waal bonding, however as it is a weak bond, it only manifests itself when no other chemical bond exists. Hydrogen and van der wall bonds are the key forces related to the interaction of biomolecules pertaining to this PhD work.

6.2.2 Acidity, Basicity and pH Level

The pH is a scale related to the number of hydrogen ions in a water solution, showing the degree of acidity or basicity of the solution. Solutions with a pH level of 7 are neutral, those with a lower value are acidic and those at a higher level are basic. Acidic solutions have a high level of hydrogen ions. Milk pH is around 6.7 so is slightly acidic.

6.2.3 Zeta Potential and Isoelectric Point

When large colloidal molecules move in an aqueous medium, a charged double layer is formed around them. The inner or stern layer is produced as a result of ions being absorbed to the surface. This in turn attracts counter ions to the molecule forming the outer or diffuse layer. As a result of charge separation a potential gradient is created, the value of which depends on the charge concentration and dielectric constant of the aqueous medium. The first layer generally moves with the molecule, whereas the diffuse layer consisting of loose counter ions does not. This voltage potential at the point of stern layer is referred to the Zeta (ζ) potential, which is a measure of stability of the colloidal liquids. Where the level of zeta potential is higher than $30\ \mathrm{mV}$ (either positive or negative), the colloidal solution is stable with no flocculation taking place.

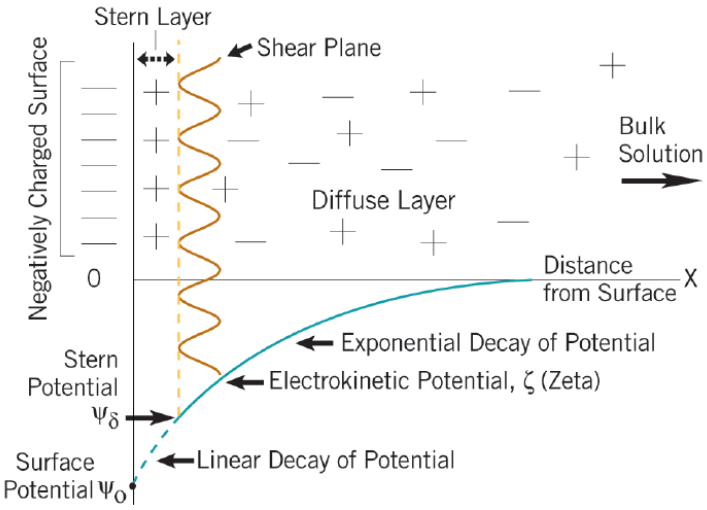

Figure 6.1 Schematic diagram of zeta potential concept (Particle Sciences, 2012)

Zeta potential for a solution is pH dependant. At low pH levels due to the presence of hydrogen ions, the colloidal particles gather more positive charge shifting their zeta potential towards positive voltages. The opposite effect takes place for high pH solutions.

Isoelectric point (pI) is the pH level at which the solution is neutral. If a protein for example is present in a solution with a pH level lower than its pI, the proteins gather positive charge, creating a positive zeta potential. The same protein gathers negative charge in a solution with a higher pH level than its pI value. Isoelectric point and zeta potential could affect the formation of progesterone-antibody bonds.

6.2.4 Polar vs Non-Polar Molecules

Some molecules have an imbalanced electron distribution within their structure, due to their geometrically imbalanced atomic arrangement. This will produce a positive charge on one side and a negative one on the other. Such molecules, such as water, are referred to as polar molecules. This property allows water to be an ideal solvent for many solutes. Two good examples are table salt (NaCl) and sugar ($\mathrm{C_{12}H_{22}O_{11}}$). Salt is an ionic compound, which when dissolved in water breaks down into positive sodium ions and negative chloride ions. The chloride ions are attracted to the hydrogen side of water molecules, which is positively charged due to its polar property. The sodium ions on the other hand are attracted to the oxygen side. This will create uniformly distributed sodium and chloride ions in water. Sugar is a covalent compound and retains its molecular structure in water. However due to the presence of polar HO bonds it can form H-bond with water molecules.

6.2.5 Hydrophilic, Hydrophobic and Amphiphilic Properties

A polar molecule that can dissolve in water is referred to as having hydrophilic property, whereas non-polar molecules that move away from water molecules are specified as having hydrophobic property. Most hydrophobic molecules are lipophilic, meaning that they have the tendency to join with other lipids. However there are some exceptions such as silicone which are neither hydrophilic nor lipophilic. Molecules that have both hydrophilic and lipophilic parts are referred to amphiphilic. These properties play an important role in the molecular behaviour of the proposed immunoassay.

6.3 Milk Composition and Molecular Structure

At molecular level, bovine milk consists of four main elements; namely, water (87.3%w/w), lactose (4.8%), lipid (3.7%) and proteins (3.4%) (Fox, et al., 2015, p. 2), (Goff & Hartel, 2013). Approximately 20% of bovine milk protein content is whey and the remaining casein. These figures vary significantly depending on some factors such as the breed of cow, time of milk production, diet and so on.

6.3.1 Lactose

Lactose is the main carbohydrate in milk, which along with milk lipids, is the primary source of energy for the new-borns. Lactose is a disaccharide, formed by glucose and galactose linked together. There are two types of lactose; namely α-lactose and β-lactose. Lactose is a polar molecule and therefore will dissolve in water. When one type dissolves in water, due to its instability, gradually turns into the other type (from α to β and vice versa) until an equilibrium is reached. The initial solubility of α and β lactose are 7 g and 50 g in 100 g water, respectively. It is therefore apparent that β-lactose is far more soluble than α-lactose. However the two types convert to each

other until reaching equilibrium at β/α ratio of 1.6 at 20 ℃. Therefore the total solubility at equilibrium is 18.2 g $= 7$ g (α-lactose) + 1.6×7 g (β-lactose).

The milk density is in the range of $1.026 - 1.034$ g/ml at 20 ℃ (Anton Paar GmbH, 2009). The weight of water and lactose in 100 ml water is therefore calculated at 89.9 g and 4.6 g (based on average milk density of 1.03 g/ml), which is an equivalent of 5.2 g of lactose per 100 g water. This amount is significantly lower than the solubility limit of 18.2 g, meaning that lactose is fully dissolved in fresh milk. During lactation period the lactose concentration gradually declines while lipid and protein concentrations increase. The lactose concentration is therefore at the lowest level and easier to dissolve at the end of lactation period, where the progesterone level is of a particular interest.

Substances such as lactose, minerals and casein which can dissolve in water affect the refractive index of milk. Studies show that bovine milk's refractive index varies between 1.344 and 1.3485 (McCarthy & Singh, 2009).

6.3.2 Casein

Casein molecules in milk form large aggregates called casein micelles, consisting of four types of casein (α_{S1}, α_{S2}, β and κ-casein) as well as some minerals prominently Colloidal Calcium Phosphate (CCP), which are responsible for holding the casein molecules within the micelle structure together. Casein micelles account for 93% of dry material of casein content of milk. Amongst the four types κ-casein is calcium-insensitive water-soluble, whereas the other three types are water-insoluble calcium-sensitive. Several models have been suggested for the structure of casein micelles. Earlier models suggest a sub-micellar structure where sub-micelles are joined by CCP. The sub-micelles with no or few κ-casein come together inside the micelle, while κ-casein molecules form the shell, resulting in the water-solubility of the micelle due to the presence of hydrophilic κ-casein on the surface.

The most recent models propose a gel-like nano-clusters (Figure 6.2), linked together by means of CCP in a structure similar to polymers' (Horne, 2006). Recent studies carried out using small-angle neutron, X-ray and light scattering show that only the nano-cluster model can explain the scattering behaviour of casein micelles (De Kruif, et al., 2012).

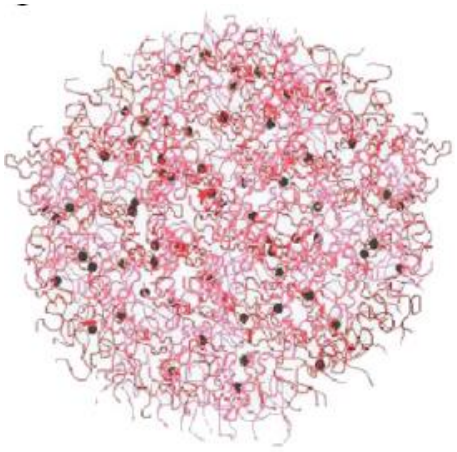

Figure 6.2 Casein micelle nano-cluster structure (De Kruif, et al., 2012)

In all models κ-casein remains on the outer surface of the micelle, effectively wrapping the hydrophobic casein molecules (α and β types) inside the micelle, preventing them from precipitation by stabilising the micellar structure. The diameter of casein micelles in milk can vary from $60\,\mathrm{nm}$ to $600\,\mathrm{nm}$, on average $200\,\mathrm{nm}$ (Glantz, et al., 2010). Figure 6.3 shows the size distribution of casein micelles, with the majority around $200\,\mathrm{nm}$. The casein micelle zeta potential has been shown to be approximately $-19\,\mathrm{mV}$ (Glantz, et al., 2010a). The zeta potential will increase by lowering the pH level of milk, until it reaches zero at its isoelectric point of 4.6, where the casein micelles begin to precipitate (Rahimi Yazdi & Corredig, 2012).

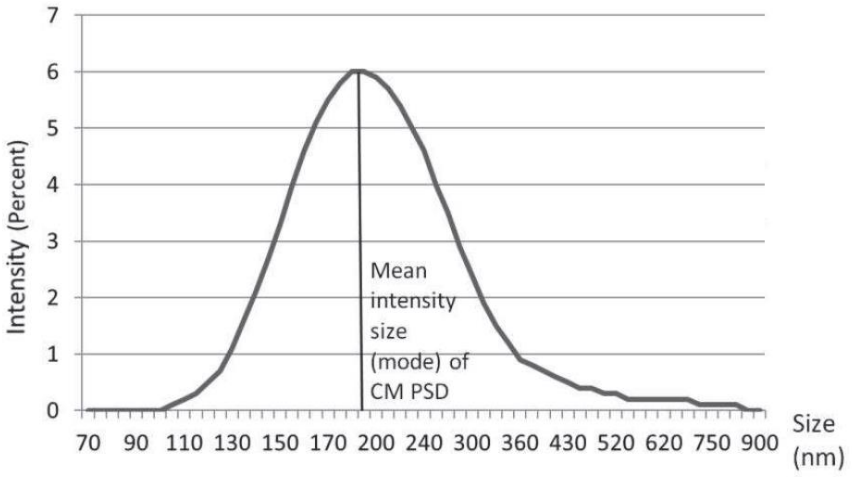

Figure 6.3 Casein micelle size distribution (Mootse, et al., 2014)

6.3.3 Whey

Whey form approximately 20% of protein in bovine milk and mainly constitutes β-lactoglobulin (BLG), α-lactalbumin (α-la), bovine serum albumin (BSA), and immunoglobulins (Ig) (Fox, et al., 2015, p. 188). If the milk pH is reduced to 4.6 at $25\ ^{\circ}\mathrm{C}$ (its normal pH value is around 6.7), the casein part precipitates but the whey remains soluble in water (Rahimi Yazdi & Corredig, 2012).

6.3.3.1 Beta Lacto-Globulin (BLG)

BLG forms $50-60\%$ of whey protein. It is a relatively small molecule with molecular weight of $18\ \mathrm{kDa}$ as a monomer. At normal milk pH level, beta lactoglobulins create dimers (Kontopidis, et al., 2004) with molecular weight of $36\ \mathrm{kDa}$, as shown in Figure 6.4. BLG is a lipocalin, a category of proteins that can transport small hydrophobic molecules such as steroids and fatty acids. This biomolecule has a complex structure, including a central calyx which acts as a ligand-binding pocket. Access to this calyx is pH dependant. The calyx is open at milk normal pH level (6.7), enabling its ligand binding function (Loch, et al., 2011).

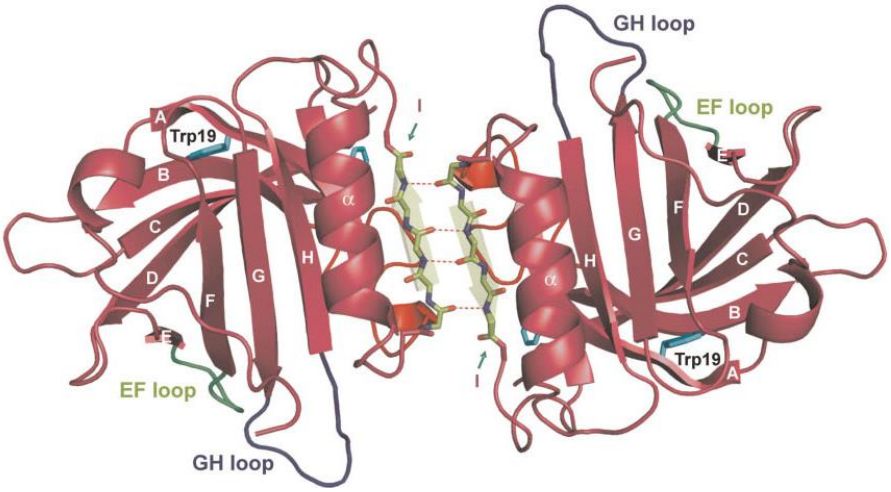

Figure 6.4 Two β-lactoglobulins create a dimer at normal milk pH level. The β-sheets form the β-barrel or central calyx. The EF loop is the opening to the calyx (Loch, et al., 2011)

Progesterone is one of the ligand types that can bind to BLG (Ragona, et al., 2000), although there is very little study on the binding mechanism. However cholesterol as a precursor to progesterone has been shown to bind to BLG (Wang, et al., 1997). The molar concentration of BLG in whole milk is estimated to be around $200\ \mu\mathrm{M}$. This is based on milk density of $1.033\ \frac{g}{ml}$ and assuming that 3.5% of milk weight is protein, out of which 20% is whey, with 50% being BLG.

$$M_{\beta-lg} = 50\% \times 20\% \times 1.033\frac{g}{ml} \times 3.5\% \times 1000 \times \frac{1}{18k} \sim 200\mu M \tag{6.1}$$

This concentration level is several orders of magnitude higher than the progesterone level in milk, which is typically less than $50\ \mathrm{nM}$ (see Chapter 1). Therefore it is expected that the majority of progesterone molecules are bound to BLG. The molecular weight of GFP and RFP are both in the region of $27\ \mathrm{kDa}$ similar to BLG dimer. This will give both native and tagged progesterone molecule relatively equal chance of binding to the antibody binding sites.

BLG has an isoelectric point of 5.1 with zeta potential of lower than $-30\ \mathrm{mV}$ at near neutral pH. Figure 6.5 shows the zeta potential versus pH level. The isoelectric point is at pH of 5.1, where the zeta potential reaches zero (Engelhardt, et al., 2013). Due to

the relatively high zeta potential at standard milk pH, BLG remains stable in milk under normal conditions.

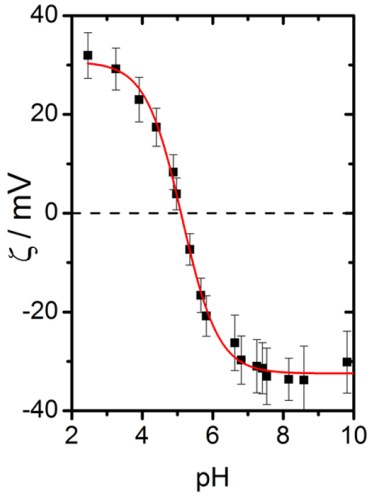

Figure 6.5 BLG zeta potential versus pH level (Engelhardt, et al., 2013)

6.3.3.2 Alpha Lactalbumin

α-lactalbumin is a water soluble protein, which forms 20% of milk whey. It has a molecular weight of $14.2\,\mathrm{kDa}$ (Le Maux, et al., 2014), isoelectric point of 4.8 and ellipsoid molecular dimensions of approximately $2.5\,\mathrm{nm} \times 4\,\mathrm{nm}$ (Fox, et al., 2015, p. 194). Alpha-lactalbumin has a strong affinity to Ca^{2+} and generally metal cations although its association constant for calcium is several orders of magnitude higher than sodium's (Permyakova, 2000). This molecule is not expected to interact with the immunoassay-specific biomolecules.

6.3.3.3 Bovine Serum Albumin (BSA)

BSA is a protein forming $0.2\,\mathrm{mg/ml}$ of whole milk (Santos & Lies, 2013), with molecular weight of $66\,\mathrm{kDa}$, isoelectric point of 4.7 and ellipsoid shape of approximately $4\,\mathrm{nm} \times 14\,\mathrm{nm}$ (Sigma Aldrich, 2000). It is a part of albumin family and therefore is water soluble. BSA is used in producing the majority of anti-progesterone antibodies. As progesterone is a small molecule, it cannot instigate an immune response therefore often it is conjugated with BSA in order to produce anti-

progesterone antibody. As a result two types of antibody is produced, one for BSA and one for progesterone. The BSA fragment is washed away, however there may be some residual amount left in the progesterone antibody solution used for this immunoassay. Such antibody molecules however will not have an effect on the performance of the proposed immunoassay, as they will not interact with any of the 3 basic biomolecules of the immunoassay; namely anti-progesterone antibody, progesterone and FP-tagged progesterone.

6.3.3.4 Immunoglobulins

Milk contains a variety of immunoglobulins, constituting between $0.3 - 1\ mg/ml$ of whole milk (Fox, et al., 2015, p. 198). Antibodies are highly specific and only bind to their specific antigen (see Section 6.4.1 for the properties of antibodies). Milk does not contain a significant level of native anti-progesterone antibody as the mammals' body use progesterone receptor to detect progesterone. The native antibody is therefore progesterone receptor antibody which has low affinity to the progesterone molecule itself. Therefore the milk immunoglobulins are not expected to have a significant effect on the performance of the proposed immunoassay.

6.3.4 Milk Lipid and Milk Fat Globule Membrane (MFGM)

Lipids are water-insoluble biomolecules that form $3 - 5\%$ (on average 3.7%,) of bovine milk. Lipids are produced by mammals as Milk Fat Globules (MFG), which are colloidal molecules dispersed in the aqueous medium of milk. The fat globules come in a wide range of diameters, from a fraction of μm to more than $10\ \mu m$. Lopez, et al. state a range from $0.1\ \mu m$ to $10\ \mu m$, with the majority of them being from $1.6\ \mu m$ to $6.6\ \mu m$ (Lopez, et al., 2011). In another study Singh specifies a range from $0.2\ \mu m$ to $15\ \mu m$, with very few larger than $10\ \mu m$. Different figures are as a result of variations in the breed of cow, method of sample preparation, separation and measurement. The average diameter however is around $4\ \mu m$. The fat globule has a slight negative

charge, which in fresh milk is around $9 - 12\ \mathrm{mV}$ zeta potential (Singh, 2006), (Ménard, et al., 2010).

During MFG secretion by a mammal, a thin layer of $10 - 20\ \mathrm{nm}$ thickness is formed around the globule core, protecting the globule against enzymatic reactions and enabling its emulsifying properties. The majority of fat globule core content is triglyceride, whereas the Milk Fat Globule Membrane (MFGM) mainly consists of proteins and polar lipids.

Triglycerides, steroids and phospholipids are three major classes of lipids. Triglyceride is a hydrophobic molecule, meaning that it is insoluble in water. These molecules tend to get together and move away from water molecules. This is the reason for the triglyceride-dense core in the fat globule. The polar lipids on the MFGM are mainly phospholipids, which are amphiphilic compounds consisting of hydrophobic and hydrophilic ends. The hydrophobic end joins with the hydrophobic ends of other lipids, whereas the polar hydrophilic end forms a bond with water molecules. The process creates a ball-like fat globule with triglycerides in the middle, wrapped around by the membrane (see Figure 6.6), which on one hand contains the core and on the other facilitates the formation of emulsion in milk (Dewettincka, et al., 2008).

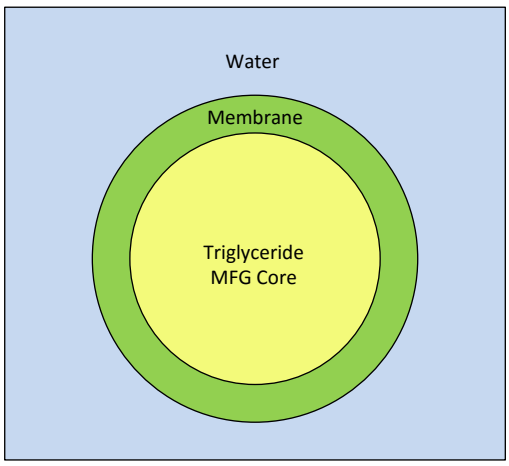

Figure 6.6 Milk Fat Globule and its membrane in water

There have been many studies on the structure of the bilayer of membrane and its various constituents, primarily lipids and proteins. This layer is particularly important for our study due to its potential interactions with antibody and antigens used in the design of the proposed immunoassay. H. Mather (Mather, 2011), Lopez (Lopez, 2011), Gallier et al. (Galliera, et al., 2011), Fong et al. (Fong, et al., 2007), and Singh (Singh, 2006) have worked on the nutritional and compositional aspects, while Zheng et al. (Zheng, et al., 2014), Lopez et al. (Lopez, et al., 2011), (Lopez, et al., 2010), and Dewettinck et al. (Dewettincka, et al., 2008) have also focused on the structural aspects of MFGM.

The fat globule membrane consists of 5 essential types of polar lipids; namely Phosphatidyl Ethanolamine (PE), Phosphatidyl Linositol (PI), Phosphatidyl Serine (PS), Phosphotidyl Choline (PC) and Sphingo Myelin (SM). Various figures have been stated for the percentage of these lipids in the membrane, depending on the milk sample and isolation method used. Zheng et al, estimated 27%, 6%, 14%, 27%, 26% for PE, PI, PS, PC and SM (Zheng, et al., 2014) whereas Dewettinckres's estimate was 30%, 5%, 3%, 35% and 25%, respectively (Dewettincka, et al., 2008). Nonetheless PE and PC and SM concentration in both studies are roughly in the same region and form the majority of polar lipids. Figure 6.10 shows the structure of phospholipids and triglycerides (glycerol and fatty acid).

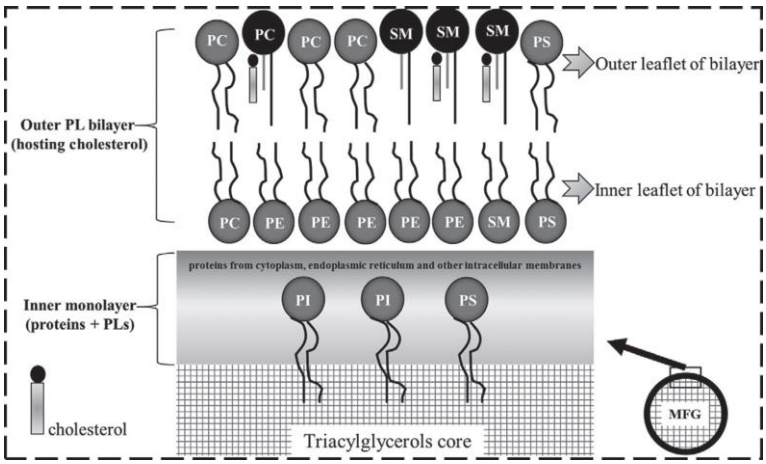

Figure 6.7 Structural schematic of MFGM in relation to the triglyceride core (Zheng, et al., 2014).

The MFGM consists of an inner monolayer and an outer bilayer, filled with cytoplasm between the two layers as shown in Figure 6.7. The MFGM polar lipids have different Hydrophilic-Lipophilic Balance (HLB) values. HLB is a measure in the scale of 0-20 developed by Griffin (Griffin, 1954) to indicate the relative activity of the hydrophilic section of a surfactant compared to its lipophilic element. Surface active agents or Surfactants are amphipathic molecules, meaning that they consist of amphiphilic and hydrophobic parts (Tadros, 2005). The polar lipids are classed as surfactants. Water-in-oil emulsifiers have a HLB value of $3-6$, wetting agents between $7-9$ and oil-in-water emulsifiers between $8-18$ (Tadros, 2005, p. 134). The HLB value of PI lipids in milk is approximately 8, making it suitable for residing on the inner layer and therefore emulsifying the triglyceride fat droplet. PS has the second highest HLB value at 3.9. SM, PC and PE have HLB values of 3.7, 3.6 and 2.6. These lipids are those that have the highest concentration of polar lipids in the membrane, more than 20% each, and form the majority of membrane outer layer. Experiments carried out by Zheng et al. show that PI and PS are relatively hard to remove from MFG after wash, indicating that the majority of these lipids are on the inner layer (Zheng, et al., 2014).

Lopez et al. (Lopez, et al., 2011) have carried out several experiments using Rh-PE fluorescent tags for labelling phospholipids. The results show that the membrane has a heterogeneous bilayer structure with Liquid-Ordered (LO) and Liquid-Disordered (LD) regions (Lopez, et al., 2010) as shown in Figure 6.8.

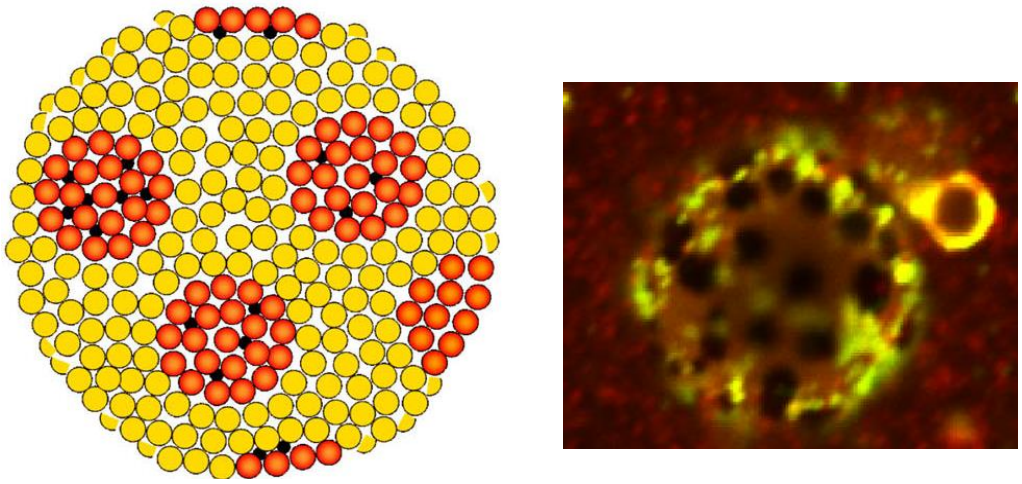

Figure 6.8 LH image: the orange circles (SM) with small back circles (cholesterol) show the liquid-ordered rafts. The yellow circles are the liquid-disordered regions containing phospholipids. RH image: The black circles show the SM-rich liquid-ordered region (Lopez, et al., 2011) (Lopez, et al., 2010)

The MFGM also includes some proteins, most prominently mucins, CD36, PS6/7, ADPH and XO as shown in Figure 6.9. The XO and ADPH proteins remain inside the membrane structure and the remaining proteins protrude through the external surface of the LD region of the membrane.

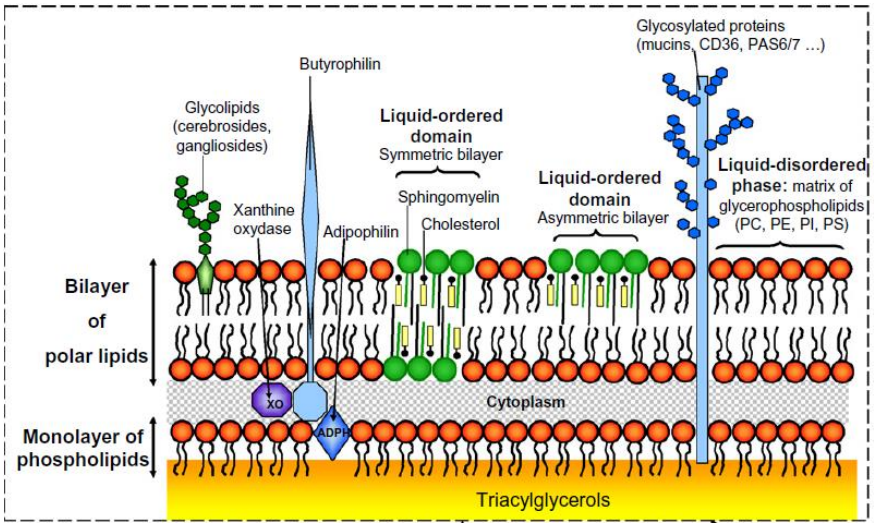

Figure 6.9 Structural schematic of MFGM with liquid-ordered rafts, consisting of SM and cholesterol (Lopez, et al., 2011)

6.4 Molecular Structure of Molecules Affecting the Immunoassay Performance

The proposed immunoassay relies on four different biomolecules to operate. These molecules are progesterone antibody, GFP-tagged progesterone, RFP-tagged progesterone and progesterone, which are described in the following subsections.

6.4.1 Antibody

The antibody used in this work is a monoclonal IgG type, with a high specificity for progesterone, and low cross reactivity to other progestogen molecules (Novus Biologicals, 2013). A monoclonal antibody is a Y shape protein, with two identical sides, each side consisting of a heavy (H) and a light (L) chain. The light chain has two domains and the heavy one four. Each chain has a variable domain (Fv) and the remaining constant domains (Fc). Each domain is formed by two anti-parallel beta sheets joined together by a disulphide link (Liu & May, 2012). A beta sheet consists of beta strands, a long chain of amino acids linked together via covalent bonds. In order to understand the structure of antibody, first a brief review of amino acids and beta sheets is provided.

6.4.1.1 Amino Acid

Amino acid is a biomolecule consisting of an amine ($\mathrm{NH_2}$) and a carboxyl (COOH), as well as side chain (R), which is responsible for creating the variety of amino acids. Amino acids are the building blocks of proteins. At midrange pH levels the carboxyl side loses a hydrogen atom, while the amine side gains one. The effect is a zwitterion, with negative $\mathrm{COO^-}$ and positive $\mathrm{NH_3^+}$ sides. This effect is critical in forming protein and its water solubility property.

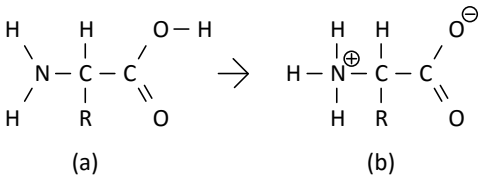

(a) (b)

Figure 6.10 Molecular structure of an amino acid, including amine and carboxyl heads, where (a) shows the original format and (b) the zwitterion format.

The C-terminus (negative end) of an amino acid can form a covalent bond with the N-terminus (positive end) of another one, creating a long chain, referred to as a polypeptide or beta strand. Beta strands can then join in a parallel or an anti-parallel format, by forming hydrogen bonds between the NH of one amino acid and the CO of the adjacent one. The ends of two nearby strands are connected by a beta turn consisting of a number of amino acids. Figure 6.11 shows the typical structure of anti-parallel beta sheet. A beta sheet will have a pair of free positive N-terminus and negative C-terminus.

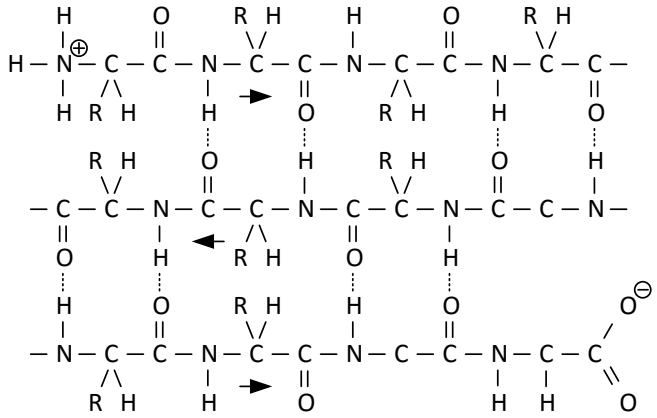

Figure 6.11 Anti-parallel beta-sheet used in the structure of antibody. The arrow points towards the C-terminus

6.4.1.2 Antibody Structure

Each constant and variable domain of an antibody consists of two beta sheets, forming a beta barrel, joined together by a disulphide link. Each variable domain has 3 hyper variable loops or complementarity Determining Regions (CDR). These regions are the antigen binding sites (Berg, et al., 2002).

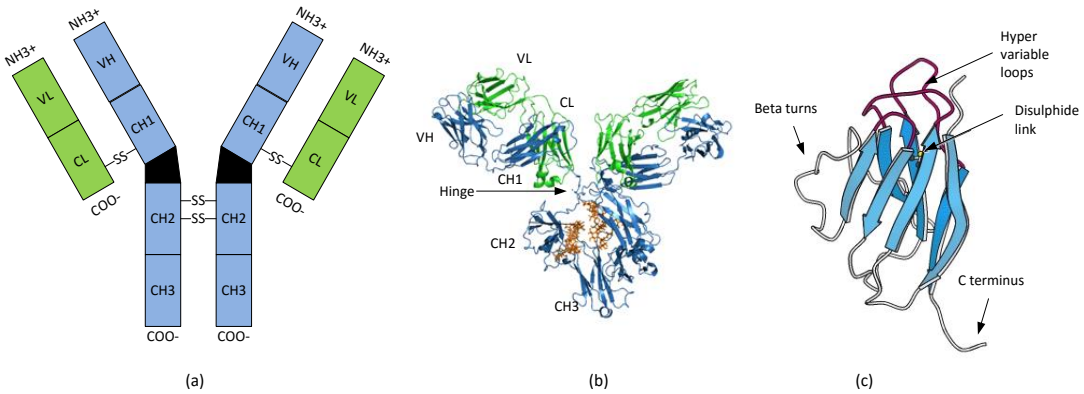

Figure 6.12 (a) Schematic structure of antibody with positive amine, negative carboxyl and disulphide links (Fox, et al., 2015, p. 199); (b) Beta sheets as a part of variable and constant domains (Berg, et al., 2002); (c) Structure of a variable domain with hyper variable loops (Absolute Antibody, 2016)

Figure 6.12 (a) shows that although the beta barrels are joined together, the head groups of amine and carboxyl retain their positive and negative charges.

The molecular weight of atypical IgG antibody is approximately $150\ \mathrm{kDa}$, with the heavy chain weighing $50\ \mathrm{kDa}$ and light one $25\ \mathrm{kDa}$. Figure 6.13 shows the dimensions for a typical IgG antibody (Tan, et al., 2008).

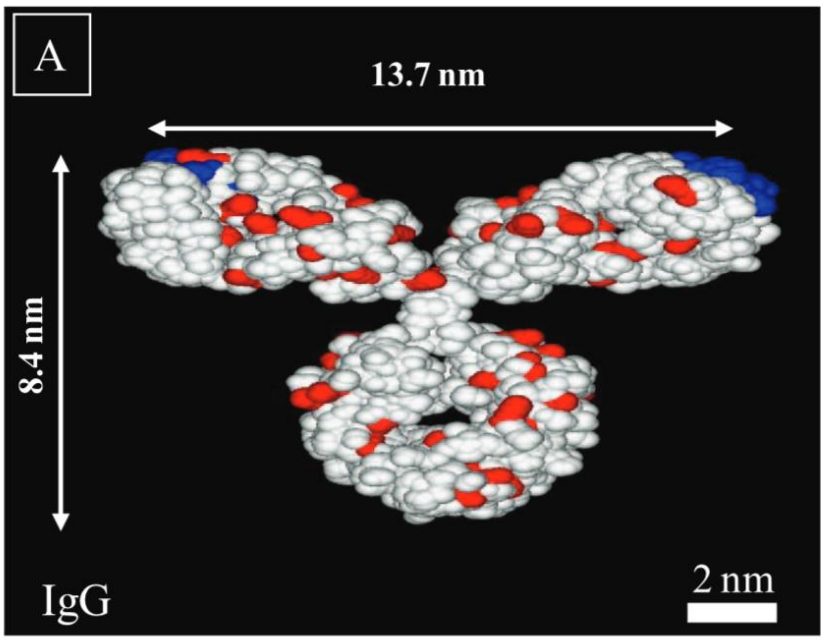

Figure 6.13 Dimensions of a typical IgG antibody (Tan, et al., 2008)

6.4.1.3 Analysis of Antibody Motion in Milk

Immunoassay tests that require antibody for their function, such as enzyme based methods described in chapter 2, often need to immobilise the antibody on a solid surface. The antibody can attach to the surface in various ways, as shown in Figure 6.14.

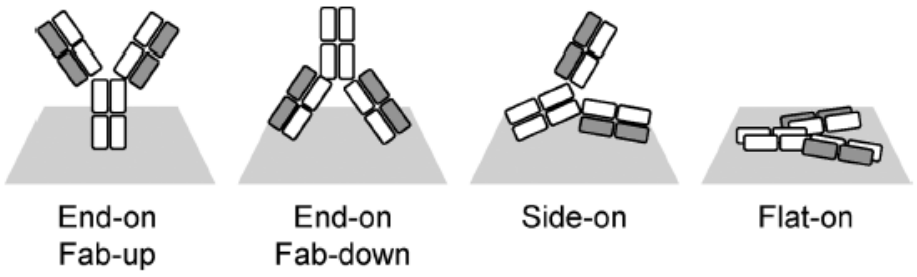

Figure 6.14 Immobilisation of antibody on a flat surface (Wiseman & Frank, 2012)

Schramm, et al. conducted a study on the formation of antibody-antigen complexes, where two types of tagged progesterone antigens were used. Some progesterone molecules were tagged with large Horseradish Peroxidase (HRP) molecules and some other with a small iodine radioactive tag (Schramm & Paek, 1992). Figure 6.15 shows the 4 distinct scenarios. The results show that at low antibody concentration levels, the antibody attaches to the surface in any format. When the binding site is faced down, there is a greater possibility for the smaller antigens to bind. As the concentration increases more antibodies face upwards, giving a good chance to both small and large progesterone molecules to bind. At high antibody concentration levels, the close vicinity of binding sites again reduces the chance of large progesterone molecules to bind.

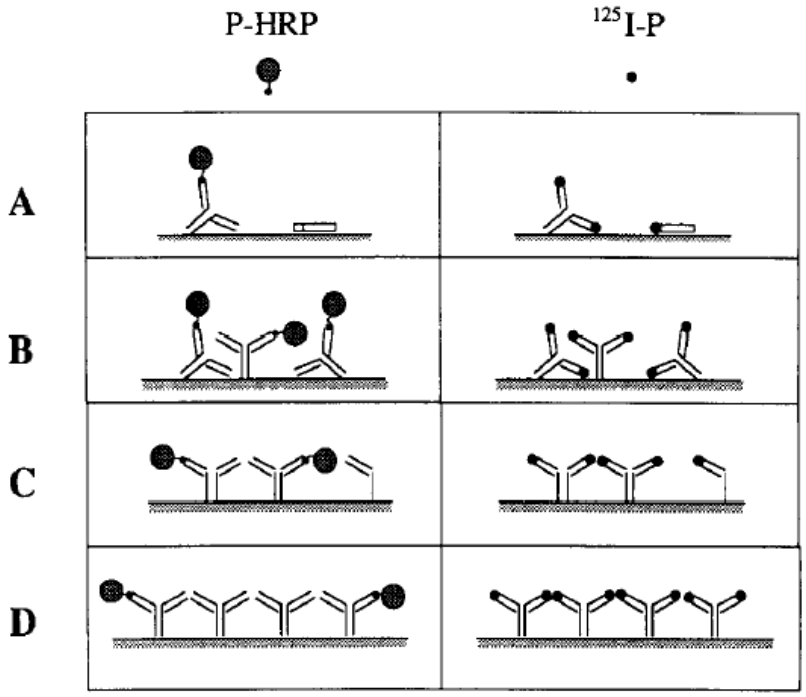

Figure 6.15 Formation of antigen-antibody complex using HRP and iodine tagged progesterone (Schramm & Paek, 1992).

In the immunoassay method proposed in this PhD, the antibodies are mobile, therefore both tagged and native progesterone molecules have a similar chance of binding. In addition a significant part of native progesterone molecules will be carried by BLG molecules (see Section 6.3.3.1), which has a similar size to RFP and GFP tags. The issue however is around the large milk fat globules which due to their large surface area (relative to the size of antibody) there is a risk that they can immobilise antibody molecules. The progesterone molecules in the area around fat globules also exist in their small form and are able to freely move within the fat membrane.

The antibody as shown in Figure 6.12(a) is a zwitterion, meaning that has both the positive and negative ends. At normal milk pH level (6.7), due to the slightly higher concentration of hydrogen ions compared to a neutral solution, some antibodies gain an extra hydrogen ion and turn into a positive cation. This theory can be verified by the work carried out by Lehermayr, et al., who studied the isoelectric point of a number of monoclonal antibodies (Lehermayr, et al., 2011). The study shows that the majority of

antibodies have an isoelectric point above of 7, meaning that they have a positive zeta potential at the normal milk pH level.

The milk fat globulin has a negative zeta potential, therefore a cation stern layer is formed around the core. Due to the relative abundance of small cations such as Na^{+} and Ca^{+2} in milk and also the presence of H^{+} and OH^{-} in the close vicinity of the membrane (Naumowicz & Figaszewski, 2014), the majority of the layer is formed by these smaller atoms that are relatively free to move. As a result large molecules such as anti-progesterone antibody are far more likely to stay in the diffuse layer as shown in Figure 6.1. The negative C-terminus of the antibody will therefore move towards the fat membrane and the N-terminus (the binding site end) away from it. As a result the base rotates towards the stern layer, moving the binding sites facing away from this layer and consequently being made available for binding with native and tagged progesterone molecules. This analysis shows the anti-progesterone antibodies in milk, are either freely moving in the aqueous medium or are in the diffuse layer near the fat globules facing away from the fat globulin. As a result, all antibodies can be considered mobile and therefore the issues with regards to antibodies immobilised on the surface of fat globulin membrane does not apply to the proposed immunoassay solution.

6.4.2 Progesterone Tagged with Green and Red Fluorescent Proteins

In the proposed competitive immunoassay Green Fluorescent Protein (GFP) and Red Fluorescent Protein (RFP) are used for labelling progesterone molecules. There are dedicated GFP-RFP molecules, specifically produced for FRET applications, such as Evrogen Tag-GFP2-TagRFP FRET pair that has been used in this PhD (JSC, Evrogen, 2016).

GFP is a barrel-like protein with 11 beta sheets, an alpha helix inside and short segments capping the top and bottom of the barrel. The fluorophore resides in the centre of the barrel, and is therefore protected by the barrel structure (Yang, et al.,

1996). The molecular weight of Evrogen GFP2 is $27\ \mathrm{kDa}$, its quantum yield 0.59, the excitation peak at $483\ \mathrm{nm}$ and emission peak at $506\ \mathrm{nm}$ (Xia, et al., 2002).

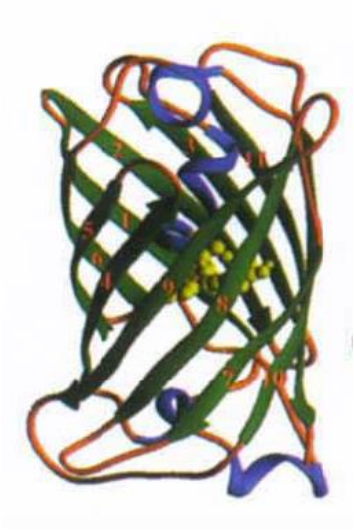

Figure 6.16 Structure of GFP structure (Yang, et al., 1996)

RFP in the form of DsRed has a nearly identical structure to GFP (see Figure 6.16), with 11 beta sheets and a central alpha helix. The top and bottom of the barrel are capped by proteins, protecting the fluorescing core and providing a stable structure (Wall, et al., 2000). The molecular weight of Evrogen RFP (Merzlyak, et al., 2007) is $27\ \mathrm{kDa}$, has a quantum yield of 0.48, excitation peak at $555\ \mathrm{nm}$ and emission peak at $584\ \mathrm{nm}$ (Evrogen, 2016).

6.4.3 Progesterone

Progesterone is a steroid hormone, which due to its hydrophobic property has a strong affinity to milk lipids and because of its small size can diffuse freely though the plasma membrane. Waldmann, et al. measured the progesterone level in milk fat at $9.7 \pm 4.5\ \mathrm{ng/ml}$ at the time of first insmeination (Waldmann, et al., 2001). This level corresponds to the $0.3\ \mathrm{ng/ml}$ progestreone level in whole milk. This stark difference indicates that the majority of progesterone molecules gather around the fat globules. Although it may appear due to the abundance of progesterone in fat, measuring its

level directly from fat is a more suitable approach in practice due the need for a fat separation stage, this method is not suitable for on-line progesterone measurement systems.

Other progesterone molecules in milk are either accompanied by BLG (see Section 6.3.3.1) or are single progsterone molecules moving in the milk aqueous medium. Due to the signficantly higher concentration of BLG compared to serium progesterone, it is extected that the majorty are acompanied by BLG. As the molecular weight of BLG ($36\ \mathrm{kDa}$) is close to RFP and GFP molecular weight ($27\ \mathrm{kDa}$), the native and tagged progesterone moleuclss will have a similar chance of binding to antibody binding sites.

6.5 Optical Properties of Milk

As discussed in Section 6.3.1 milk refractive index can be between 1.3440 and 1.3485 at room temperature. The variation in refractive index is mainly between milk samples, which will be taken into account during background light measurement. Temperature could change the density of milk and hence its refractive index. Temperature changes during the experiment and its effect on the optical properties of milk have been taken into consideration by the introduction of parameters α, β and γ in Chapter 5.

Milk contains carotenoid pigments, which absorb photons in the wavelength range of $400\ \mathrm{nm}$ to $520\ \mathrm{nm}$ (Fox, et al., 2015, p. 341), overlapping with the emission spectrum of blue LED light and GFP tags. The absorption of the LED photons will be accounted for during the background measurement stage. The absorption of GFP emission however affects the FRET measurement. The reason is that in the absence of antibody a proportion of the GFP emitted photons will be absorbed by carotenoids rather than being detected by the photodiodes. When antibody is added, some GFP tags instead of emitting photons cause FRET and instigate photon emission by the RFP. FRET measurement relies on a reduction in GFP emission and a similar increase in RFP emission. The photon absorption by carotenoids reduces the variations in GFP

emission but does not change the RFP emission, thus affecting the level of FRET measured by the photodiodes. Carotenoids concentration in milk is in the region of $200\ \mu g/l$ (Fox, et al., 2015, p. 74). As proteins form 3.4% of milk, 80% of which being casein micelles, which are responsible for light scattering, the ratio of concentration of carotenoids to casein per a litre of milk, (with density of $1.033\ g/ml$) is approximately:

$$r = \frac{200 \times 10^{-6}}{0.8 \times 3.4\% \times 1.033 \times 1000} = 7.11 \times 10^{-6} \quad (6.2)$$

This means the photons emitted from GFP have approximately five orders of magnitudes higher chance of being scattered by caseins than absorbed by carotenoids. Therefore, the presence of carotenoids does not have a noticeable effect on the level of FRET signal produced.

Another constituent of milk, which has an optical effect is riboflavin. This is a fluorophore, which fluoresces on excitation in the range of $400 - 500\ nm$, with the emission spectrum in the region of $500 - 600\ nm$ (Maiti, et al., 2014). Similar to the analogy used for carotenoids, the effect of these molecules on the LED light in the milk sample can be compensated for during background light measurement stage. The effect of riboflavin on FRET is however two folds. It absorbs GFP emission and emits photons which partly overlap with the RFP emission range.

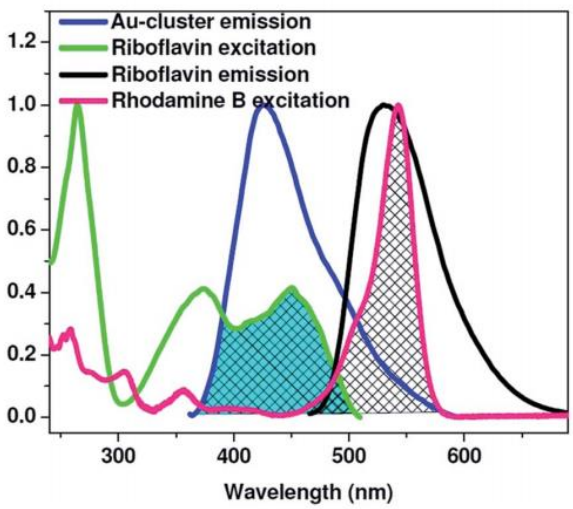

Figure 6.17 Excitation and emission spectra of riboflavin (Maiti, et al., 2014)

The concentration of riboflavin is approximately $1.62\ \mathrm{mg/kg}$, which compared to $34\ \mathrm{g/kg}$ casein is still several orders of magnitude lower. As a result riboflavin is not expected to have a significant effect on the performance of the immunoassay.

6.6 Summary

This chapter provided an analysis on the effects of various immunoassay and milk molecules, their structures and interactions on the performance of the immunoassay. Lactose, its solubility and the effect on the refractive index of milk were reviewed. The molecular structure of proteins including casein micelles and whey protein were outlined. The affinity of BLG as the main constituent of whey on progesterone was reviewed. Milk fat globules and the fat membrane covering the fat globules were discussed in details, explaining the zeta potential, stern layer and how individual un-accompanied progesterone molecules can diffuse freely within the fat membrane. Finally the molecular structure of antibody was reviewed and was concluded that the binding sites of anti-progesterone antibodies face away from the fat membrane, dramatically reducing the potential for steric hindrance in relation to native and tagged-progesterone molecules.

The next chapter provides the results of parameter optimisation; the rationale behind choosing the particular FRET pair, photodiode and LED; and finally the results of all experiments carried out on various aspects of the proposed solution.

7 VERIFICATION, ANALYSIS AND EXPERIMENTATION RESULTS

7.1 Introduction

Earlier in Chapter 4 the electronic, optical and mechanical design of the proposed transducer was presented in details. A prototype transducer was designed and developed as shown in Figure 7.1. A labview program was developed in order to control and monitor various hardware elements, capture sensor output, analyse data and provide quantitative results (see Figure 7.2).

Figure 7.1 The biosensor developed by A. Ghadar (Ghadar, et al., 2013)

The hardware design incorporates a cylindrical chamber used for inserting the test tube, which contains the milk sample. The milk sample will have natural progesterone molecules along with anti-progesterone antibody as well as RFP and GFP tagged progesterone molecules, added in various stages of the assay. These aspects of the

immunoassay, including photonic interactions, FRET generation and photon detection were covered in Chapter 5.

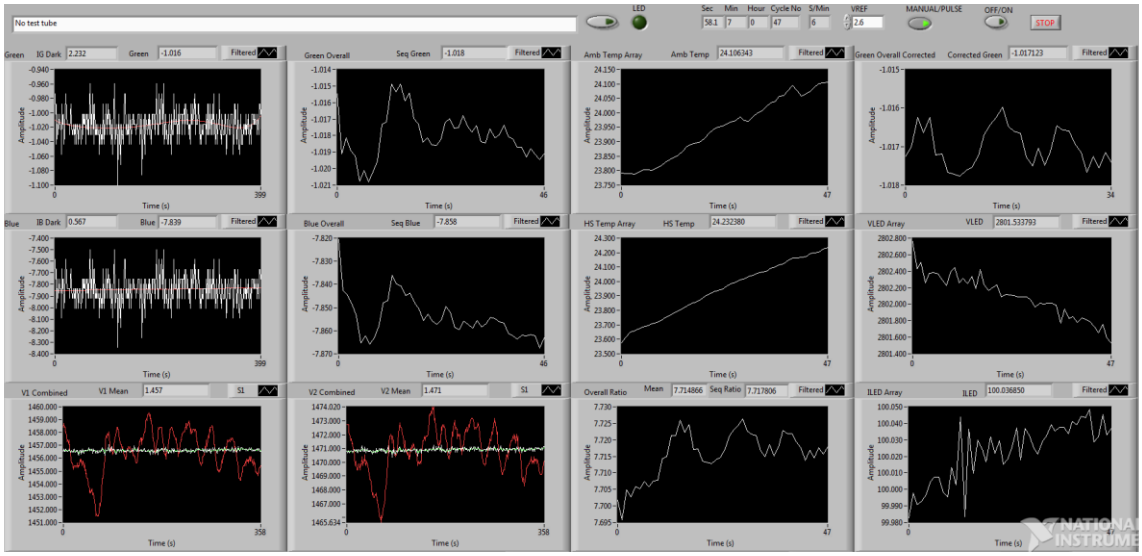

Figure 7.2 Front panel of the labview program

This chapter provides an analysis and optimisation of various parameters related to the antibody and tagged antigens used for implementing the immunoassay. This is then followed by a detailed review of emission and excitation of LED and fluorescent tags along with the spectral response of photodiodes in order to select the best combination of LED, fluorophore and photodiode colour. The chapter will then focus on experimentation results, starting from circuit parameters, leading to the use of fluorescein, GFP, RFP and design verification using a commercial high performance CLARIOstar spectrofluorometer.

7.2 Analysis and Optimisation of Immunoassay Parameters

Referring to chapter 5, the FRET concentration will have the following relationship with the concentration of antibody, progesterone and tagged progesterone molecules:

$$M_F = 2\frac{M_D M_A M_N}{(M_D + M_A + M_P)^2} \tag{7.1}$$

M_F, M_P, M_D and M_A are the molar concentrations of FRET, milk progesterone, donor-tagged progesterone and acceptor-tagged progesterone, respectively. By defining parameter α as the ratio of donor to acceptor concentrations, the above equation can be expressed as follows:

$$M_F = \frac{2\alpha M_N}{\left((1+\alpha) + \frac{M_P}{M_A}\right)^2} \tag{7.2}$$

In order to ensure all tagged and untagged progesterone molecules bind to the two antibody binding sites, the concentration level of antibody, M_N, must be less than half the total concentration of tagged and untagged progesterone molecules. As the progesterone level in milk is not known, the antibody concentration is considered a factor of total concentration of acceptor and donor tagged progesterone molecules together.

$$M_N = k(M_A + M_D) = k(1+\alpha)M_A, \;\; k < 0.5 \tag{7.3}$$

k is a factor that relates to the reaction time of the immunoassay. Where k is small, the binding process completes in a short time as there are less antibodies to provide binding sites. A small k however requires a more sensitive transducer, suggesting a trade- off between sensor complexity and cost versus response time. Substituting (7.3) into (7.2) results in the following:

$$M_F(M_P) = \frac{2k\alpha(1+\alpha){M_A}^3}{[M_A(1+\alpha) + M_P]^2} \tag{7.4}$$

Now let's assume the progesterone level of interest is in the range of $M_P \in \left(M_P^{min}, M_P^{max}\right)$. This indicates that the transducer must be able to detect the minimum level at M_P^{min} in order to determine the onset of oestrus. It also must be able to provide a detectable FRET difference between the minimum and maximum progesterone concentration levels, M_P^{min} to M_P^{max}, providing a means of verifying the occurrence of minimum by following the progesterone trend from high to low concentration over time. Therefore ΔM_F is defined as below:

$$\Delta M_F = M_F(M_P^{max}) - M_F\left(M_P^{min}\right) \tag{7.5}$$

Looking back at the diagram in Figure 1.3, the minimum progesterone concentration level during an oestrus cycle is $2\ \mathrm{ng/ml}$, which equates to $6.3\ \mathrm{nM}$ based on the progesterone molecular weight of $314\ \mathrm{g/mol}$. Therefore for the purpose of oestrus detection, M_P^{min} at $2\ \mathrm{nM}$ is sufficiently low to be able to detect the oestrus. Also for a transducer with $\pm 1\ \mathrm{nM}$ accuracy, having 5 samples at $2\ \mathrm{nM}$ intervals allows for detecting the downward trend on a 3rd order polynomial with 4 unknown parameters, verifying the presence of the 5th point as its minimum at M_P^{min}. Therefore M_P^{max} is considered at $10\ \mathrm{nM}$, which is roughly equivalent to $3\ \mathrm{ng/ml}$. Figure 7.3 shows the FRET concentration (M_F) versus acceptor concentration (M_A) and donor to acceptor ratio (α). The figure is based on $k = 0.35$ and $M_P \in (2\ \mathrm{nM}, 10\ \mathrm{nM})$. It is apparent that somewhere around $\alpha = 1$ the highest level of FRET difference between low and high progesterone levels is produced. In addition FRET level increases by an increase in the M_A level for any given α value. The next sections cover the analytical evaluation of the FRET formula.

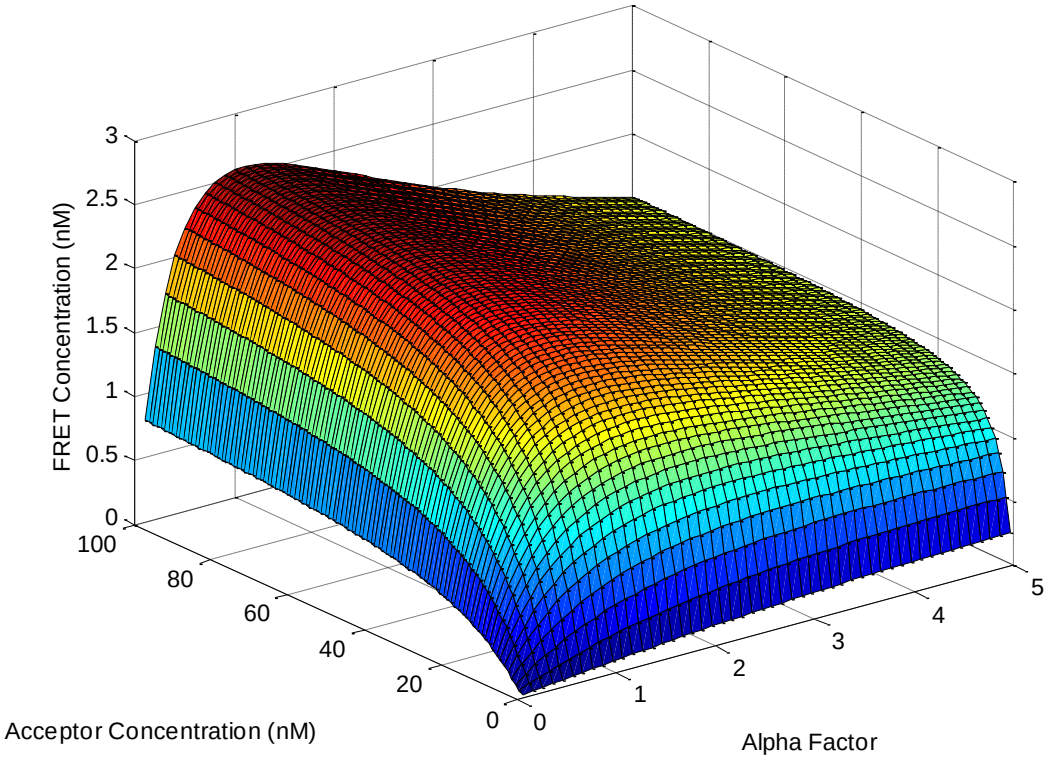

Figure 7.3 FRET concentration versus M_A and α, based on $M_P \in (2\text{ nM}, 10\text{ nM})$ and $k = 0.35$

7.2.1 Effect of Acceptor and Donor Concentrations on FRET Signal

One of the factors that has a significant effect on the sensitivity of the proposed solution is parameter α, the ratio of donor to acceptor concentrations. The optimum value for this parameter can be determined using two different criteria. The first approach is to maximise ΔM_F with respect to α as per equations (7.4) and (7.5).

$$\Delta M_F = \frac{2k\alpha(1+\alpha){M_A}^3}{\left(M_A(1+\alpha)+M_P^{min}\right)^2} - \frac{2k\alpha(1+\alpha){M_A}^3}{(M_A(1+\alpha)+M_P^{max})^2} \tag{7.6}$$

The maximum ΔM_F occurs where the partial derivative with reference to α is zero.

$$\frac{\partial \Delta M_F}{\partial \alpha} = 2k{M_A}^3\left[\frac{M_A(\alpha+1)+(2\alpha+1)M_P^{min}}{\left(M_A(\alpha+1)+M_P^{min}\right)^3} - \frac{M_A(\alpha+1)+(2\alpha+1)M_P^{max}}{(M_A(\alpha+1)+M_P^{max})^3}\right] \tag{7.7}$$

Therefore α value which generates the maximum ΔM_F must hold the following relationship.

$$\frac{M_A(\alpha+1)+(2\alpha+1)M_P^{min}}{\left(M_A(\alpha+1)+M_P^{min}\right)^3}-\frac{M_A(\alpha+1)+(2\alpha+1)M_P^{max}}{(M_A(\alpha+1)+M_P^{max})^3}=0 \tag{7.8}$$

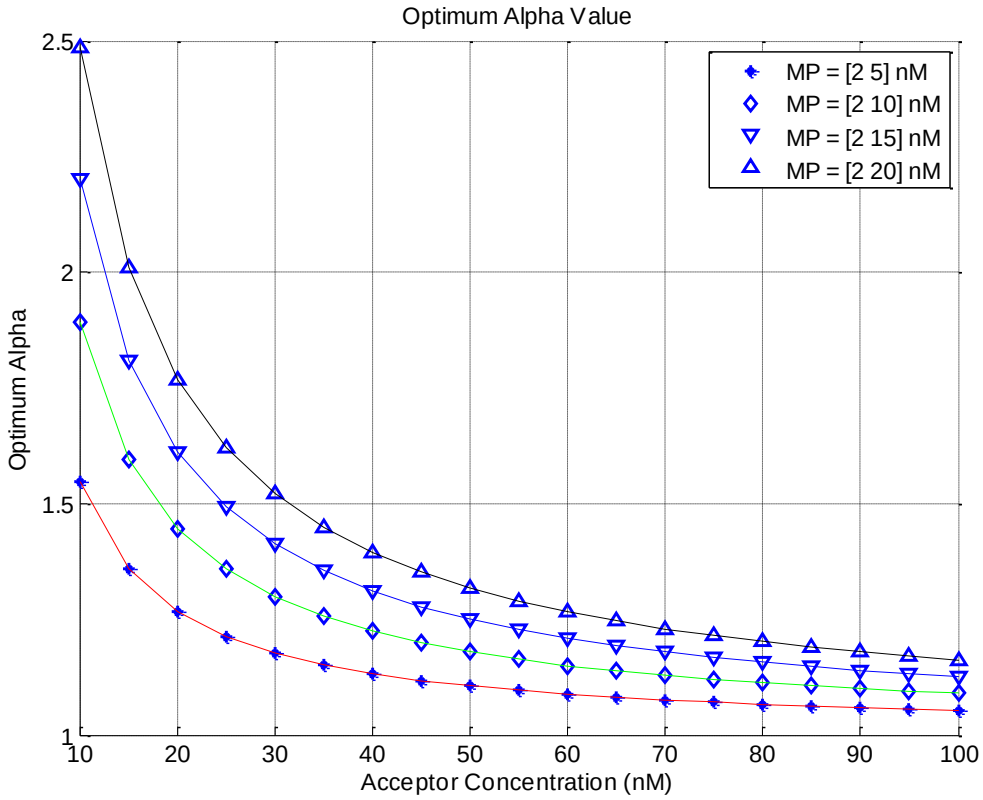

Figure 7.4 Optimum α value to maximise ΔM_F

It can be shown that the equation (7.8) results in a 4th order polynomial, solved by MATLAB as shown in Figure 7.4. This graph shows the optimum α based on acceptor concentration from $10\ \mathrm{nM}$ to $100\ \mathrm{nM}$ and 4 different ranges of progesterone, all with a minimum of $2\ \mathrm{nM}$ but the maximum of 5, 10, 15 and $20\ \mathrm{nM}$. The figure shows that as the concentration level of acceptor increases the optimum value varies less with the acceptor concentration.

Another factor that affects the performance of the sensor is the level of change in FRET concentration per unit change in the progesterone concentration.

$$\left|\frac{\partial}{\partial M_P} M_F(M_P)\right| = \left|\frac{\partial}{\partial M_P} \frac{2k\alpha(1+\alpha){M_A}^3}{(M_A(1+\alpha)+M_P)^2}\right| = \frac{4k\alpha(1+\alpha){M_A}^3}{(M_A(1+\alpha)+M_P)^3} \tag{7.9}$$

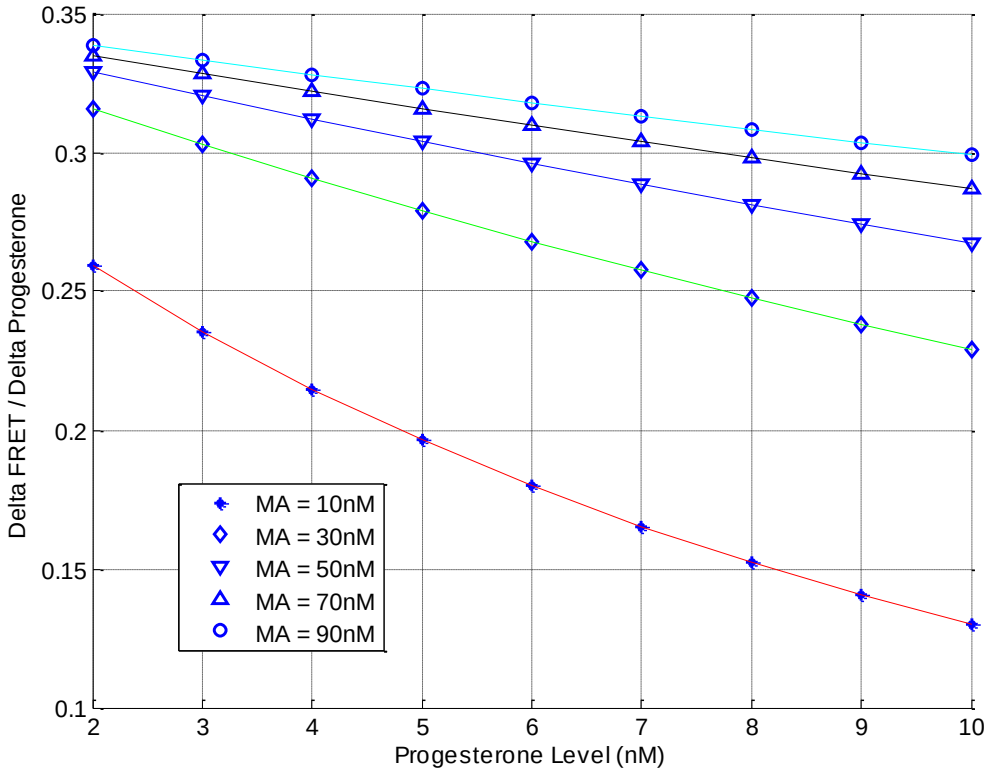

Figure 7.5 ΔM_F vs ΔM_P using optimum α and for acceptor concentrations from 10 nM to 90 nM

Figure 7.5 illustrates the change in the FRET signal per unit change in progesterone concentration level for a number of acceptor concentration levels from $10\,\mathrm{nM}$ to $90\,\mathrm{nM}$, assuming the use of optimum α based on $M_P \in (2\,\mathrm{nM}, 10\,\mathrm{nM})$. The figure shows that at the lowest acceptor concentration, $10\,\mathrm{nM}$, $\frac{\partial}{\partial M_P} M_F$ for $2\,\mathrm{nM}$ and $10\,\mathrm{nM}$ progesterone concentration is $0.26\,\mathrm{nM}$ and $0.13\,\mathrm{nM}$, respectively, meaning that the immunoassay is 50% less sensitive at progesterone level of $10\,\mathrm{nM}$, compared to $2\,\mathrm{nM}$. This ratio reduces to 11.7% at $90\,\mathrm{nM}$ acceptor concentration, from $0.34\,\mathrm{nM}$ to $0.30\,\mathrm{nM}$ for $2\,\mathrm{nM}$ and $10\,\mathrm{nM}$ progesterone concentrations. This means that the minimum accuracy required for the case of $10\,\mathrm{nM}$ acceptor concentration is 2.3 times the sensing accuracy needed for the case of $90\,\mathrm{nM}$. In general higher acceptor concentration levels offer a stronger and more uniform response, requiring a less

sensitive transducer. The downside however is the cost associated with a high concentration of acceptor-tagged progesterone.

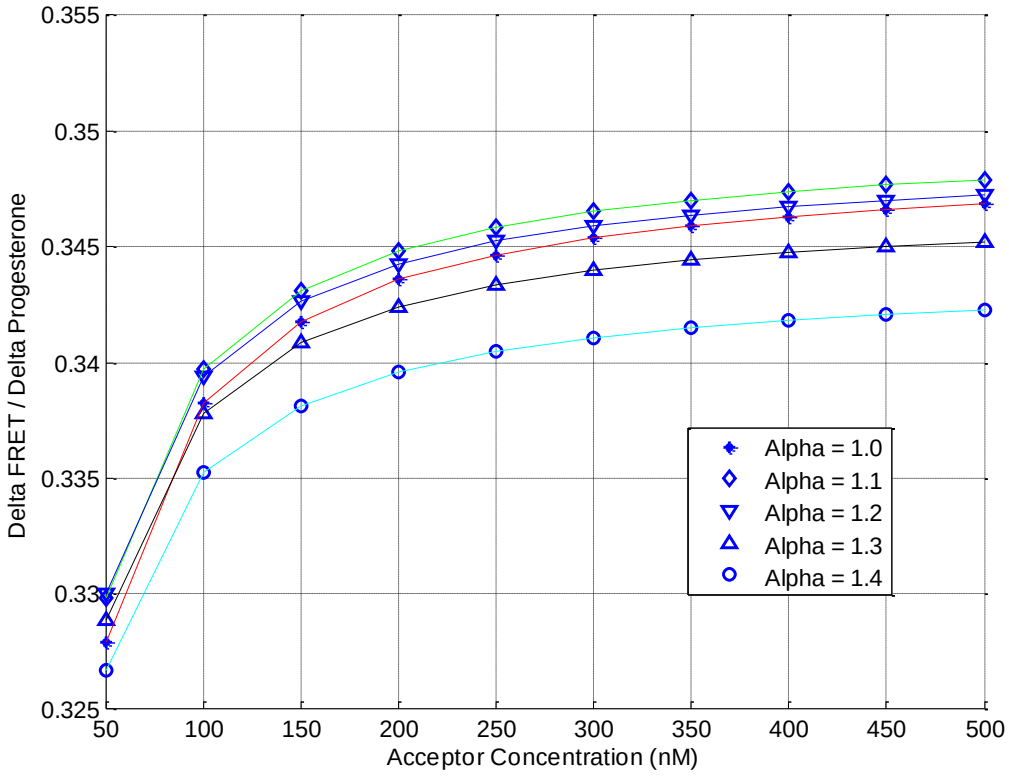

Figure 7.6 $\partial \mathrm{M_F} / \partial \mathrm{M_P}$ versus acceptor concentrations as different α values

Figure 7.6 illustrates that the slope of $\partial \mathrm{M_F} / \partial \mathrm{M_P}$ dramatically reduces at high acceptor concentration levels, reaching to a constant value at infinity.

$$\lim_{M_A \to \infty} \left| \frac{\partial}{\partial M_P} M_F \right| = \lim_{M_A \to \infty} \left| \frac{-4k\alpha(1+\alpha){M_A}^3}{(M_A(1+\alpha)+M_P)^3} \right| = \frac{4k\alpha}{(1+\alpha)^2} \tag{7.10}$$

The analysis above demonstrates the importance of the ratio of change in FRET concentration to progesterone and its relationship to the sensitivity of the sensor. Therefore here a different approach is taken to estimate the optimum value of α, this time to maximise $\partial M_F / \partial M_P$, by equating its partial derivative with reference to α to zero. Using equation (7.9) this leads to the following.

$$\frac{\partial}{\partial \alpha}\frac{\partial M_F}{\partial M_P} = -4k{M_A}^3 \frac{\partial}{\partial \alpha}\frac{\alpha(1+\alpha)}{(M_A(1+\alpha)+M_P)^3} = 0 \tag{7.11}$$

This results in a 2nd order polynomial for the optimum value of α.

$$(1+2\alpha)(M_A(1+\alpha)+M_P)-3\alpha M_A(1+\alpha)=0 \tag{7.12}$$

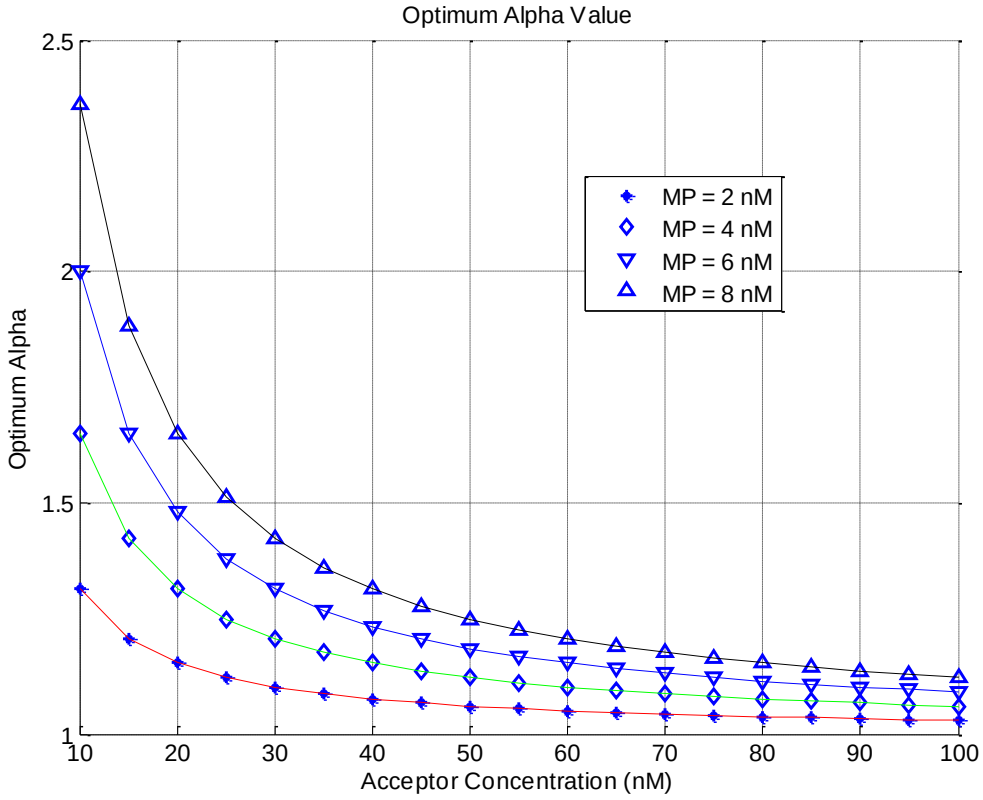

Figure 7.7 Optimum α value to maximise $\frac{\partial M_F}{\partial M_P}$

Figure 7.7 shows the optimum α value to maximise $\partial \mathrm{M_F}/\partial \mathrm{M_P}$ around progesterone concentration of $2\,\mathrm{nM}$, $4\,\mathrm{nM}$, $6\,\mathrm{nM}$ and $8\,\mathrm{nM}$ and for a range of acceptor concentration levels from $10\,\mathrm{nM}$ to $100\,\mathrm{nM}$. As an example for the case of progesterone level of interest at $2\,\mathrm{nM}$ and acceptor concentration of $50\,\mathrm{nM}$, the optimum α is 1.06. However if the optimisation approach based on equation (7.8) is considered, the optimum alpha value will be 1.179.

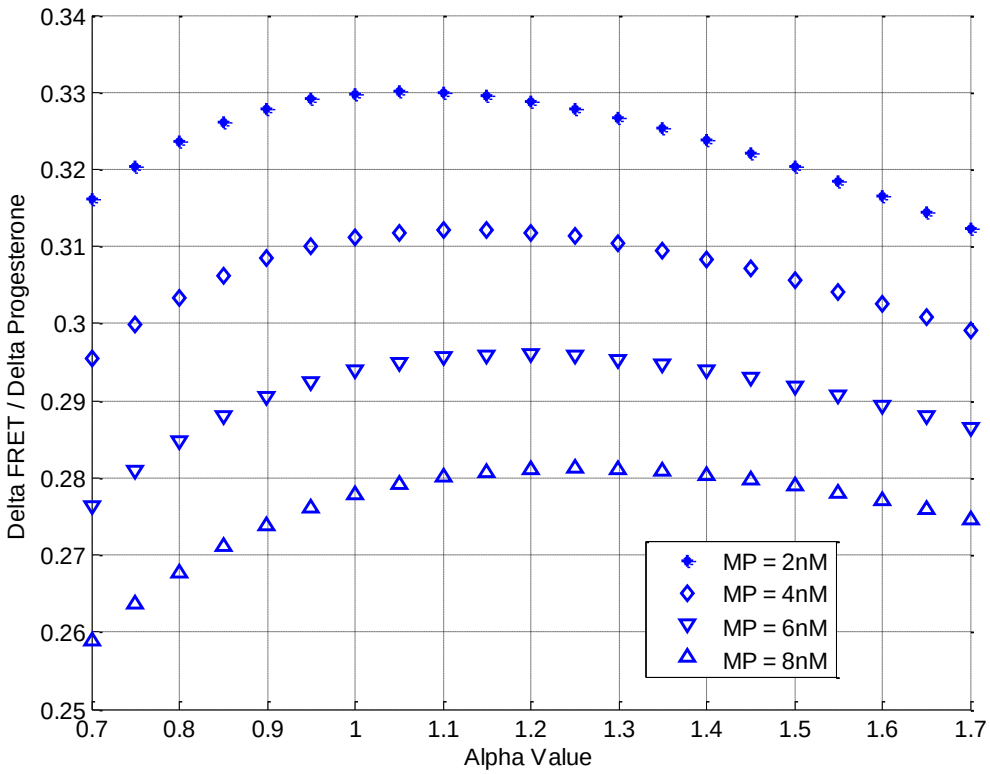

Figure 7.8 $\frac{\partial \mathrm{M_F}}{\partial \mathrm{M_P}}$ versus α for $\mathrm{M_A} = 50\ \mathrm{nM}$

Maximising $\partial \mathrm{M_F}/\partial \mathrm{M_P}$ around $2\ \mathrm{nM}$, $4\ \mathrm{nM}$, $6\ \mathrm{nM}$ or $8\ \mathrm{nM}$ progesterone concentrations results in different α values of 1.06, 1.12, 1.19 and 1.25. In order to evaluate the effect of choosing an α value other than its optimum value, $\partial \mathrm{M_F}/\partial \mathrm{M_P}$ has been shown in Figure 7.8 for progesterone concentration levels of $2\ \mathrm{nM}$, $4\ \mathrm{nM}$, $6\ \mathrm{nM}$ and $8\ \mathrm{nM}$ and acceptor concentration of $M_A = 50\ \mathrm{nM}$. Focusing on the range of $\alpha \in (1, 1.5)$, the maximum variations in $\partial \mathrm{M_F}/\partial \mathrm{M_P}$ is approximately 3% in the case of $2\ \mathrm{nM}$ progesterone level, which will not have a significant effect on the required sensitivity of transducer. Therefore for commercial purposes in order to reduce production cost, it is suggested to standardise the concentration of reagents to 50nM acceptor solution, $60\ \mathrm{nM}$ donor solution based on $\alpha = 1.2$ and $40\ \mathrm{nM}$ antibody solution based on $\mathrm{k} = 0.33$.

7.2.2 Analysis of LED, FRET Pair and Photodiode

In order to produce a high quality FRET signal, it is best to use verified FRET pairs for tagging progesterone molecules. One of such pairs is TagGFP2-TagRFP pair supplied by Evrogen (Evrogen, 2016). The peak wavelength of the donor excitation spectrum is $483\ \mathrm{nm}$, causing photon emission at the peak wavelength of $506\ \mathrm{nm}$. The excitation spectrum of the acceptor FRET peaks at $555\ \mathrm{nm}$ and the emission at $584\ \mathrm{nm}$, in the red region.

The milk sample is illuminated using one or more LEDs at predetermined intervals, one at a time. Whilst an LED is emitting photons, the fluorescence level is measured using two photodiodes. High power LEDs are required for fluorescence measurement. These LEDs are chosen from Luxeon rebel series (Philips Lumileds, 2010). Table 1.2 shows the maximum output power, peak wavelength and spectral half width for blue, cyan, green, amber and orange version.

Table 7.1 LED specification for each colour (Philips Lumileds, 2010)

LED Specification	Blue	Cyan	Green	Amber	Orange
Max Luminous Flux (lm) @350mA	40	80	100	40	70
Peak Wavelength (nm)	470	505	530	590	617
Spectral Half Width (nm)	20	30	30	20	20

Sensitive photodiodes must be used for detecting fluorescence level. The Hamamtsu S6429, S6429 and S6430 photodiodes are suitable for this purpose. These are sensitive photodiodes with a low dark current and the specification as detailed in Table 7.2 (Hamamtsu, 2015).

Table 7.2 Photodiode Specification (Hamamtsu, 2015)

Photodiode Specification	Blue	Green	Red
Photo Sensitivity (A/W)	0.22	0.27	0.45
Peak Wavelength (nm)	460	540	660
Spectral Half Width (nm)	90	70	20
Dark Current (pA)	5	5	5

In order to select the right combination of LED(s) and photodiodes, their effect on the sensitivity and effectiveness of the immunoassay is reviewed in the following sections.

7.2.3 Effect of LED Background Light on Photodiode

As described in Chapter 4 the LED creates a background light on the photodiode. Figure 7.9 shows the blue LED wavelength spectrum along with the photodiodes response spectra. By multiplying the LED emission spectrum and each photodiode response spectrum over the specified wavelength range and then integrating over the entire range the relative σ_{LED1}^{n} can be calculated as follows:

$$\sigma_{LED1}^{n} \propto \int_{\lambda=300nm}^{800nm} S_{\lambda}^{n}\ PD_{LED1}^{n}\delta\lambda, \quad n \in \{R, G, B\} \tag{7.13}$$

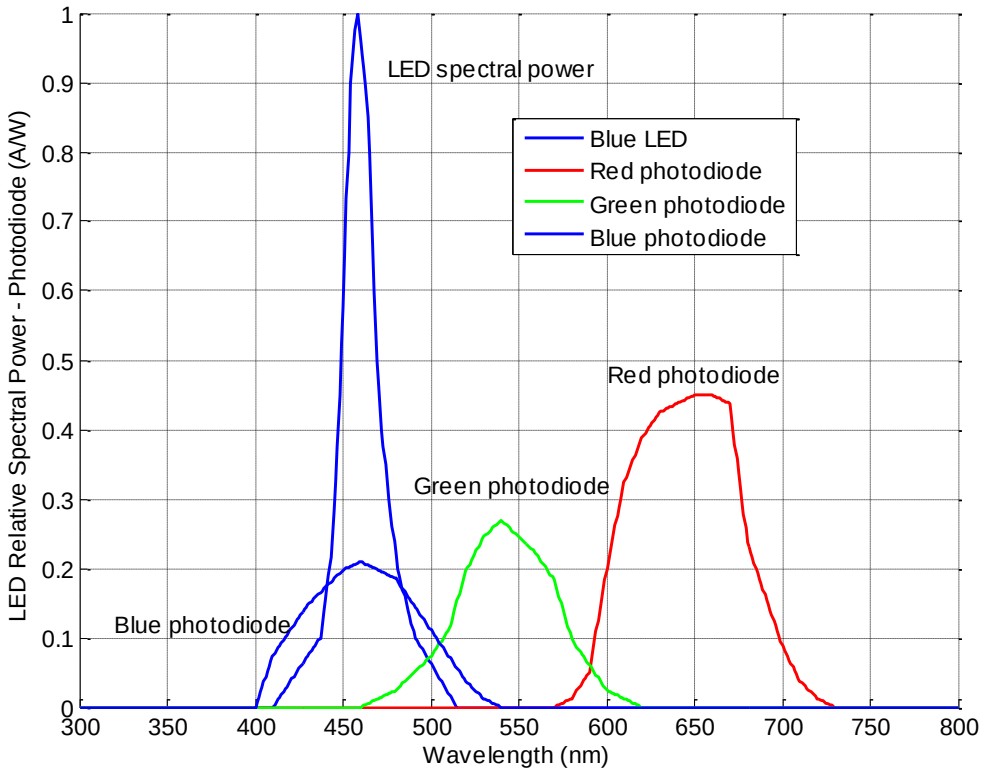

Figure 7.9 The blue LED emission spectrum and photodiode frequency response, based on the LED and photodiode datasheets

In order to select the most suitable set of LEDs for the sensor, the background light generated by different colour LEDs has been estimated using MATLAB based on Figure 7.9 and presented in Table 7.3, assuming that all LEDs have $1\ \mathrm{W}$ radiometric power.

Table 7.3 Effect of each LED on each photodiode in units of $\frac{lm.A}{W}$

	Photodiode Colour		
LED Colour	**Red**	**Green**	**Blue**
Blue	0	0.2504	5.2384
Cyan	0.0006	4.6313	3.3228
Green	0.1854	9.0894	1.3977
Amber	2.6965	1.3401	0
Orange	9.6218	0.0671	0

It must be noted that only a proportion of the LED light reaches the photodiodes. This factor depends on the geometry and mechanical features of the enclosure, the level of Rayleigh scattering, the radiation pattern and properties of different colour LEDs. However the focus at this stage is on comparing the LED and photodiode sets based on background light in order to find the most suitable set.

7.2.4 Effect of LED on FRET excitation

In the presence of donor and/or acceptor in the milk sample, the LED photons will create primary emissions through direct excitation of the donor and acceptor fluorophores, while donor also produces secondary emission through FRET. Figure 7.10 shows the excitation spectra of the FRET donor and acceptor fluorophores (dotted lines) in comparison with the emission spectra of various LEDs (Shcherbo, et al., 2009). The level of excitation for different colour LEDs have been estimated using MATLAB and presented in Table 7.4. The figure shows the maximum excitation levels for the donor fluorophores is achieved by blue LED.

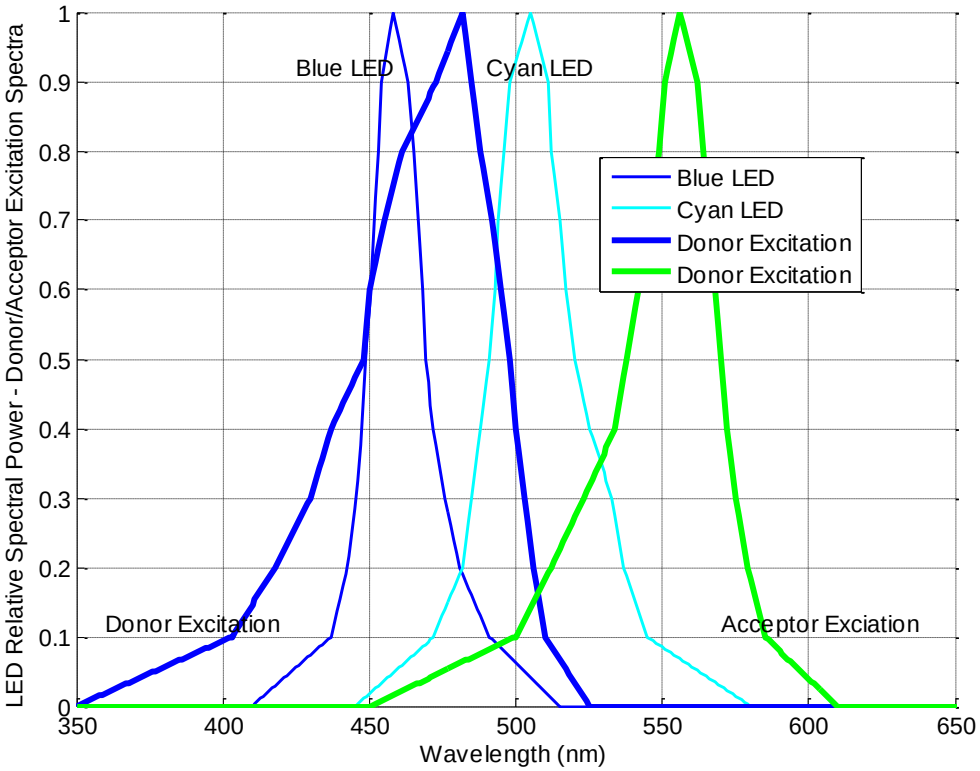

Figure 7.10 The excitation spectrum of FRET donor and acceptor fluorophores in comparison with the LED emission spectrum

Table 7.4 Relative FRET Excitation Level

	FRET Excitation Level	
LED Colour	**Donor**	**Acceptor**
Blue	19.6547	0.7261
Cyan	11.7796	8.0431
Green	3.3256	18.95
Amber	0	2.4566

Although the level of donor excitation is important, it is also important that a good level of emission is produced by these fluorophores and well detected by the photodiodes, while the LED background signal is as low as possible.

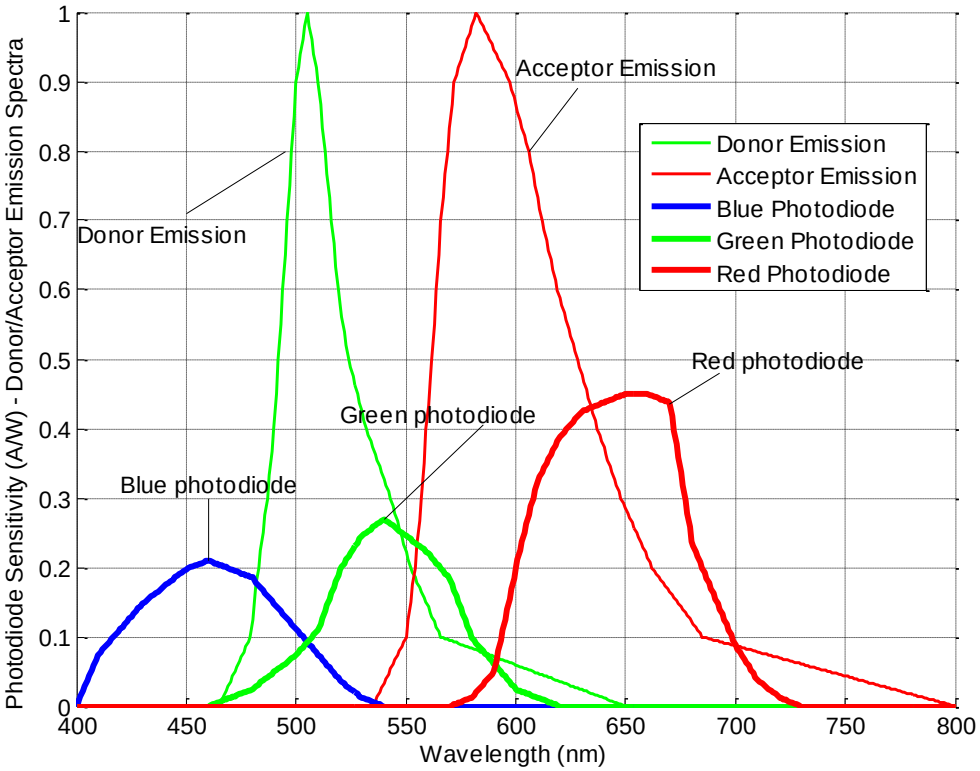

Figure 7.11 The emission spectrum of FRET donor and acceptor fluorophores in comparison with the photodiodes frequency response

Figure 7.11 shows the emission spectra of FRET pair against the photodiodes response spectra. Table 7.5 presents the photodiodes' detection sensitivity for donor and acceptor emission, estimated using MATLAB for each photodiode.

Table 7.5 Relative Emission Detection

	Relative Emission Detection	
Photodiode Colour	**Donor**	**Acceptor**
Red	0.6204	14.0401
Green	6.138	4.7066
Blue	2.8453	0.0002

Here in order to assess the effect of each LED on the donor and acceptor emission, and consequently detection by the photodiodes, Table 7.3, Table 7.4 and Table 7.5 are combined into Table 7.6 below.

Table 7.6 Combined table for background light, donor emission and acceptor emission. The columns represent photodiode and rows represent LEDs.

	Background Light			Donor Emission			Acceptor Emission		
LED/PD	**Red**	**Green**	**Blue**	**Red**	**Green**	**Blue**	**Red**	**Green**	**Blue**
Blue	0	0.2504	5.2384	12.195	120.64	55.923	10.194	3.4174	0.0001
Cyan	0.0006	4.6313	3.3228	7.3086	72.303	33.516	112.93	37.856	0.0013
Green	0.1854	9.0894	1.3977	2.0634	20.413	9.4622	266.06	89.191	0.0031
Amber	2.6965	1.3401	0	0	0	0	34.491	11.562	0.0004
Orange	9.6218	0.0671	0	0	0	0	0.9511	0.3188	0

The above table shows that amber and orange LEDs do not excite donor tagged progesterone, therefore are not suitable for this application. Blue LED generates the highest amount of emission from donor, detected at a high level by blue and green photodiodes. At the same time the blue LED does very little to the acceptor, resulting in a low output on the green photodiode and nearly none on the blue one. Therefore the combination of blue LED and green and blue photodiodes provides a balanced set in terms of relatively low background signal and direct acceptor emission in comparison to the donor emission. The choice of blue photodiode also satisfies the criteria set out in 5-satge and 4-stage solutions in Chapter 5, where the response spectrum of the second photodiode shall not overlap with the emission spectrum of acceptor.

7.3 Transducer Parameters and Experimentation Results

7.3.1 System Set up

The transducer uses a LXML-PB01-0040 blue Luxeon Rebel LED (Lumileds, 2016), mounted on a $20\,\mathrm{mm}$ star CoolBase (see Figure 7.12), emitting $70\,\mathrm{lm}$ at $700\,\mathrm{mA}$ (Leuxeon Star, 2012). The photodiodes are Hamamatsu S6428-01 (blue) and S6429-01 (green) (Hamamtsu, 2015).

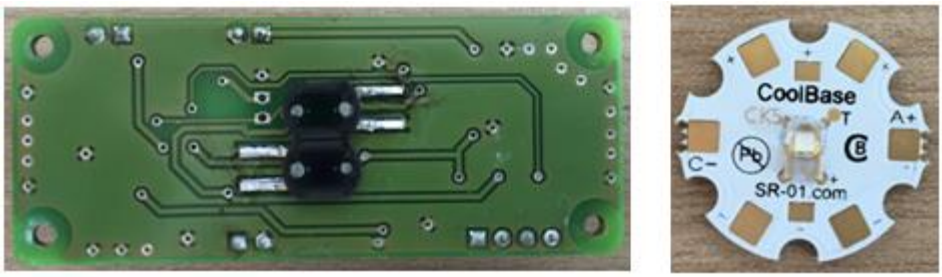

Figure 7.12 The image on the left shows the bottoms side of the first stage detector board including the two photodiodes. The image on the right shows the LED on the heatsink arrangement.

The detector consists of two boards. The first board accommodates the photodiodes (Figure 7.12), amplification, basic filtering and dynamic offset measurement circuit The second board includes output filtering and A/D conversion circuitry (Figure 7.13). The detector circuits have been designed to implement $\mathrm{n} = 25$ and $\mathrm{n}' = 50$, used in calculating $\mathrm{K}_{\Delta \mathrm{v}}$ as referred to in Chapter 4. K_{b} and K_{g}, the total gain level on the blue and green photodiode currents, are $4\ \mathrm{M}$ and $24\ \mathrm{M}$, respectively. Therefore based on detector circuit equations in Chapter 4, voltages V_1 and V_2 (outputs of the background offset measurement stage) have the following relationship to the photodiode currents.

$$\begin{pmatrix} V_1 \\ V_2 \end{pmatrix} = K_{\Delta v} \begin{pmatrix} K_b I_b \\ K_g I_g \end{pmatrix}, \text{ where } K_b = 4M, K_g = 24M, K_{\Delta v} = \begin{pmatrix} 25 & -25 \\ 25.49 & -25 \end{pmatrix} \quad (7.14)$$

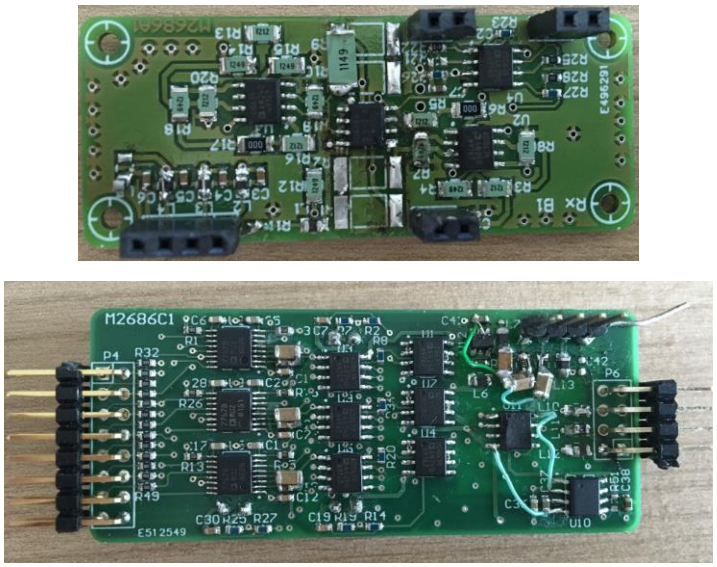

Figure 7.13 The top image shows the top side of the first stage detector board. The bottom image shows the top side of the second stage detector board, including filtering and A/D conversion. The board size is 70 mm x 30 mm.

The emitter circuit has $0.5\,\Omega$ LED resistor, providing $1\,\mathrm{A}$ at approximately $3\,\mathrm{V}$ LED voltage. Figure 7.14 shows the emitter boards with the associated drive circuit, including, LED control, filtering, amplification, ADC and DAC circuits.

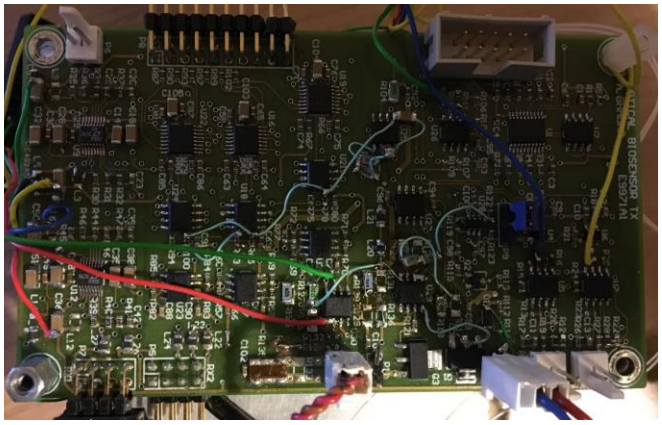

Figure 7.14 Top side of the emitter board. The board size is 110 mm x 63 mm.

The LED is turned on for $20\,\mathrm{ms}$ every $10\,\mathrm{sec}$. Samples at taken at $20\,\mathrm{kHz}$ with the first $2\,\mathrm{msec}$ considered as the transition period.

7.3.2 Filtering

V1 and V2 voltages are monitored over the LED on-time. As both voltages are generated using similar circuits, the effect of noise on both voltages is similar (see Figure 7.15). After removing outliers and fitting a curve to both voltages, the average noise profile over the entire period is calculated and used to provide voltage profiles with significantly improved signal to noise ratio.

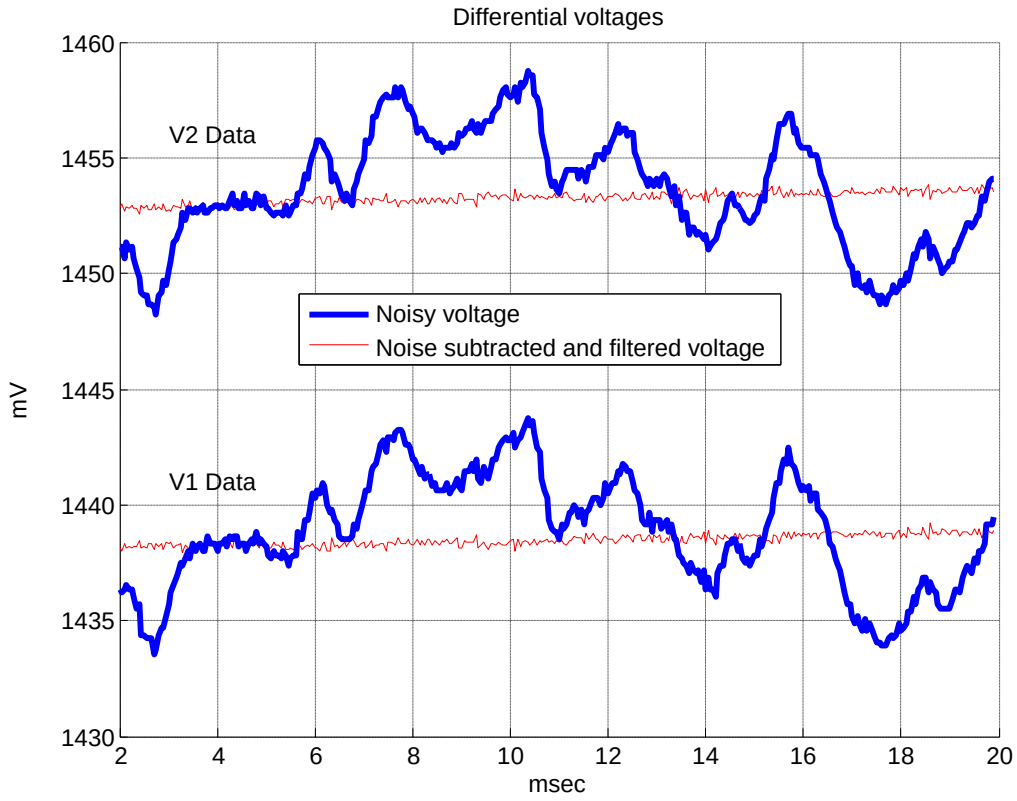

Figure 7.15 V1 and V2 voltages over the on time of LED. The initial 2 msec transition period has been removed

7.3.3 Effect of LED current on Photodiode Output

The photodiode current is calculated using equation (4.36). Figure 7.16 shows the photodiodes current measured for LED currents from 60 mA, 70 mA, 80 mA, 90 mA, 100 mA, 120 mA, 130 mA and 150 mA. The test tube was filled with 4 ml of 10 mM Tris-Hcl buffer. The output of the transducer was monitored over 10 min for each LED current.

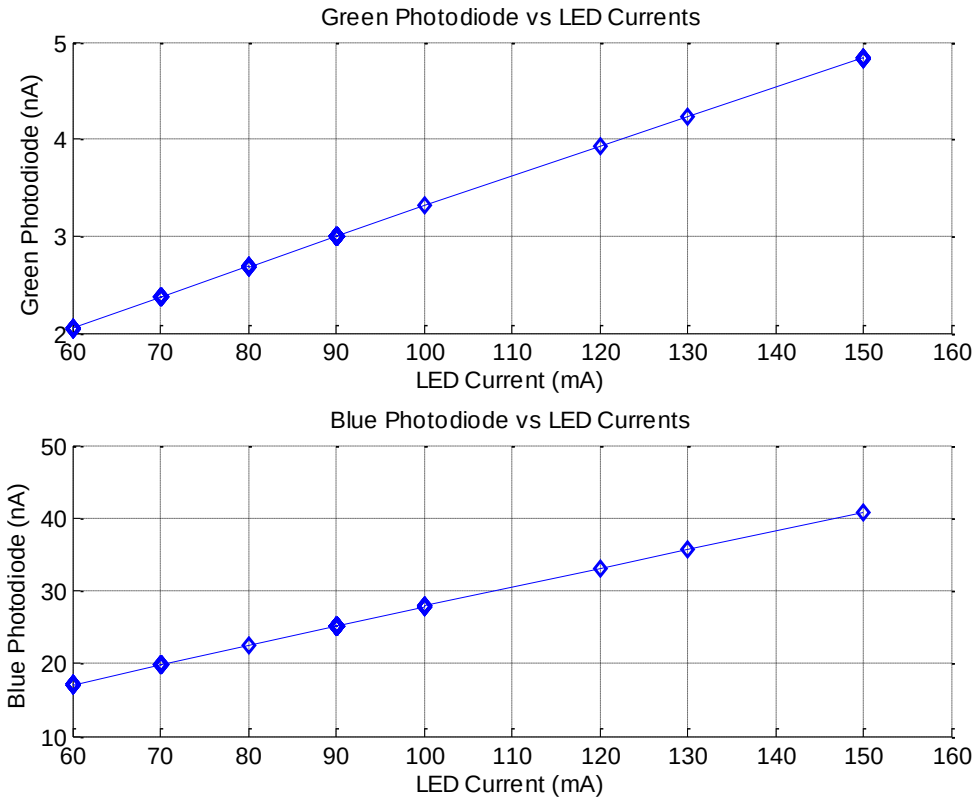

Figure 7.16 Photodiode current vs LED current

The figure shows that the photodiode current has a linear relationship with the LED current. The maximum current that the LED can withstand is $1\,\mathrm{A}$. The LED in this design is set to run at $100\,\mathrm{mA}$, which is significantly less than $1\,\mathrm{A}$ maximum and $350\,\mathrm{mA}$ test current used in the datasheet (Leuxeon Star, 2012), resulting in a relatively stable output. Due to the linear relationship around the working current of 100mA, the sensor output is normalised to the LED current to cancel the effect of LED current variations. Figure 7.17 shows the blue and green photodiode current normalised to the LED current. The figure shows green normalised photodiode current is not constant and depends on the LED current. The normalised current varies from $3.407\,\mathrm{nA}$ at $60\,\mathrm{mA}$ to $3.312\,\mathrm{nA}$ at $100\,\mathrm{mA}$ and finally $3.221\,\mathrm{nA}$ at $150\,\mathrm{mA}$ LED current. Around $100\,\mathrm{mA}$ the ratio of change in photodiode current to LED current is $\pm 0.06\,\frac{\%}{\mathrm{mA}}$.

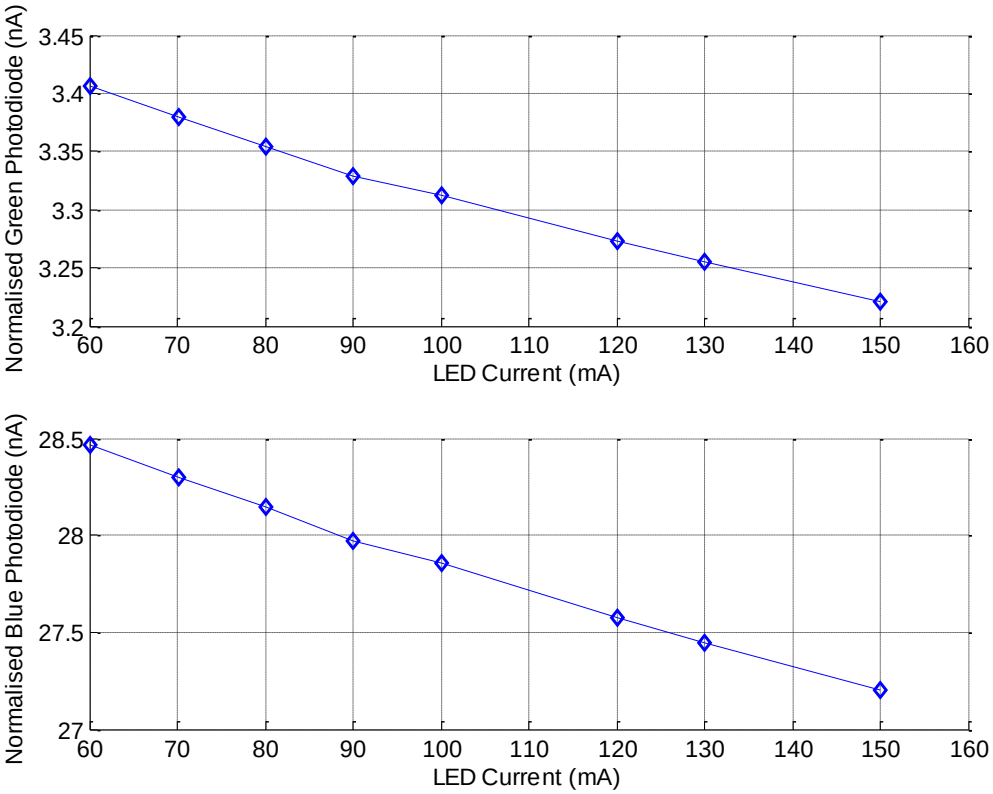

Figure 7.17 Normalised Photodiode current vs LED current

Figure 7.18 shows the green photodiode current at $100\ \mathrm{mA}$ LED current over a $10\ \mathrm{min}$ interval. The figure demonstrates that LED current is being controlled with an accuracy of $\pm 10\ \mu\mathrm{A}$. Considering $\pm 0.06\ \frac{\%}{\mathrm{mA}}$ variations in photodiode current and $10\ \mu\mathrm{A}$ accuracy of LED current control, the total error due to LED variations is limited to $6\ \mathrm{ppm}$, significantly less than $10\ \mathrm{ppm}$ allowance specified in Section 4.3.3.1.

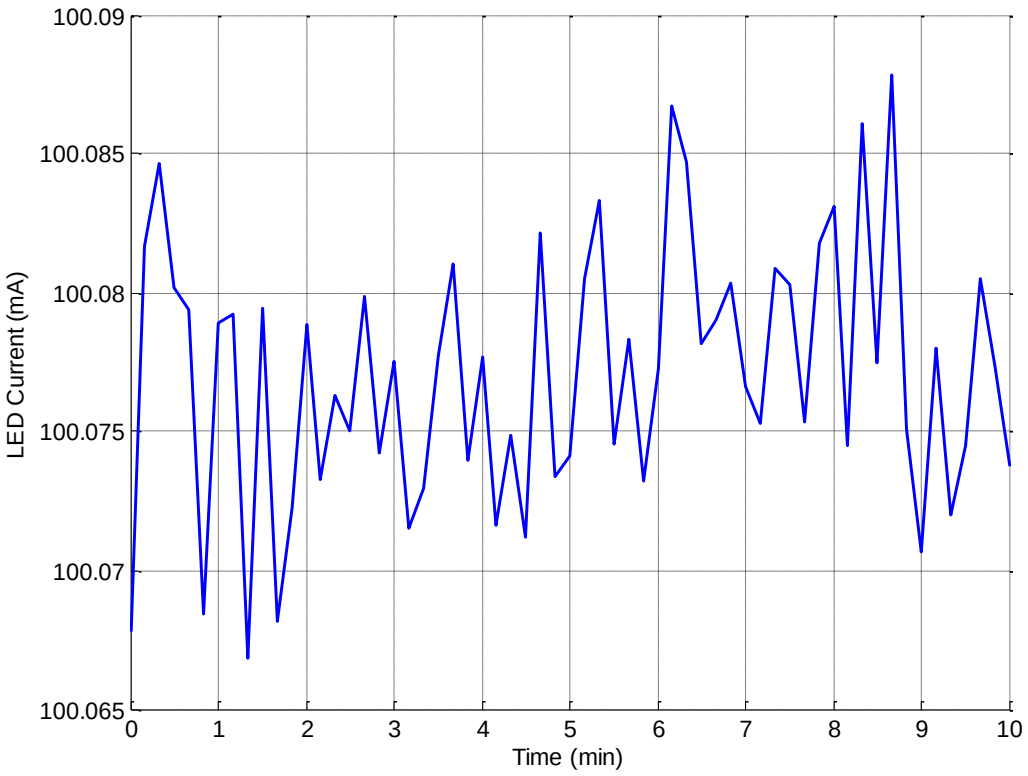

Figure 7.18 LED current variations at $100\ \mathrm{mA}$ over $10\ \mathrm{min}$ interval

7.3.4 Effectiveness of Dynamic Background Offset Cancellation

In order to demonstrate the effectiveness of the dynamic offset cancellation, the transducer is used in 4 different scenarios; namely, no test tube, with empty test tube, then test tube filled with transparent buffer solution and finally test tube with full fat milk, each monitored over $10\ \mathrm{min}$. Figure 7.19 shows despite several orders of magnitude change in the photodiode current from no test tube to full fat case, the circuit can still measure the photodiode current at the same LED current level of $100\ \mathrm{mA}$, without changing the circuit settings. This demonstrates the wide dynamic measurement range that the transducer design can provide. The total gain levels applied by the circuit to the green and blue photodiodes are $600\ \mathrm{M}$ and $100\ \mathrm{M}$. In the absence of dynamic offset cancellation this level of gain will clearly push the output of the circuit to a saturated state.

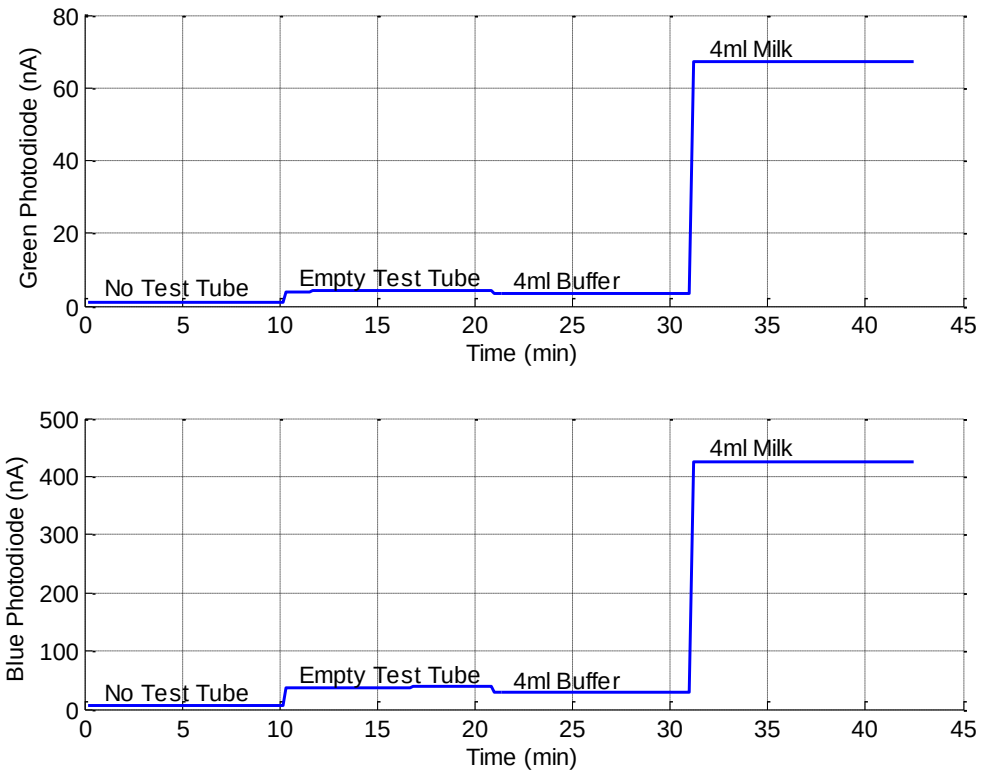

Figure 7.19 Photodiode current with no test tube, then empty test tube, test tube with buffer and finally full fat milk

7.3.5 Effect of Test Tube, Milk and Buffer

Table 7.7 lists the average green and blue photodiodes current for each case, which shows that the current produced by the photodiodes in the case of buffer is less than empty test tube. This can be explained by looking at the concept of critical angle.

Table 7.7 Green and blue photodiode currents

Photodiode	No Test Tube	Empty Tube	4ml Buffer	4ml Milk
Blue	7.432 nA	38.039 nA	28.663nA	424.407 nA
Green	0.983 nA	4.339 nA	3.265 nA	67.287 nA

When LED photons hit the test tube, they enter the glass wall and then pass through to reach inside of the test tube. As the refractive index of air (1.003), water (1.33) or milk

(1.35) inside the test tube is less than the refractive index of glass at 1.5, in theory some photons that have entered the glass wall may not leave the wall and go through total internal reflection, as shown in Figure 7.20.

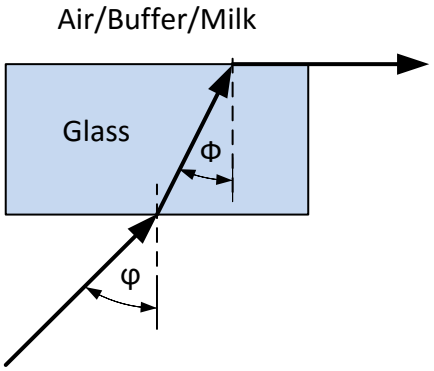

Figure 7.20 Total internal reflection in test tube

The minimum angle to create this effect, ϕ, is $41.8°$ for the case of air and $62.5°$ for buffer (water). As the light inside the glass comes from the LED, in order to create the critical angle inside the glass, the LED incident light must be tangent at the point of incident, which is not possible due to the geometry of the transducer. The critical angle for the case of water is even higher meaning that no internal reflection takes place. Therefore if the LED light enters the glass wall, it passes through and enters the test tube without internal reflection. The LED light that has entered the glass could reflect back by the internal aluminium wall of the enclosure and eventually reach the photodiode window. When the medium is clear water, some of the photons are absorbed by water, and some other reach the glass in the front of the photodiodes window. As the medium between the glass and photodiodes is air, the critical angle is $41.8°$. The incident light from the reflected light within the test tube needs to hit the test tube at angle greater than $48.7°$ to go through total internal reflection and reflect back into the water. This is clearly possible, which means a significant amount of light within the test tube never leave the test tube and do not reach the photodiodes. As a result 25% reduction has been observed when the test tube is filled with water. Calculating the exact reduction requires complex geometrical modelling of the system, which is outside the scope of this PhD work.

Another interesting aspect of this experiment is the photodiode current in the case of milk, which is an order of magnitude higher compared to when the test tube is filled with milk. This is the result of Rayleigh scattering where the majority of photons in the blue and green range scatter in every direction, resulting in a dramatic increase in the signal level.

7.3.6 Compensated Green Photodiode Current

In order to evaluate the effect of temperature and LED current and voltage on the photodiode current, $4\ \mathrm{ml}$ full fat pasteurised homogenised milk was poured into the test tube. In the first experiment the transducer started from cold. Figure 7.21 shows the measured photodiode current as well as LED voltage and current. The blue photodiode current rises by $1.3\ \mathrm{nA}$ and the green one by $220\ \mathrm{pA}$ during the $20\ \mathrm{min}$ period. The ambient and heatsink temperatures have been depicted in Figure 7.23.

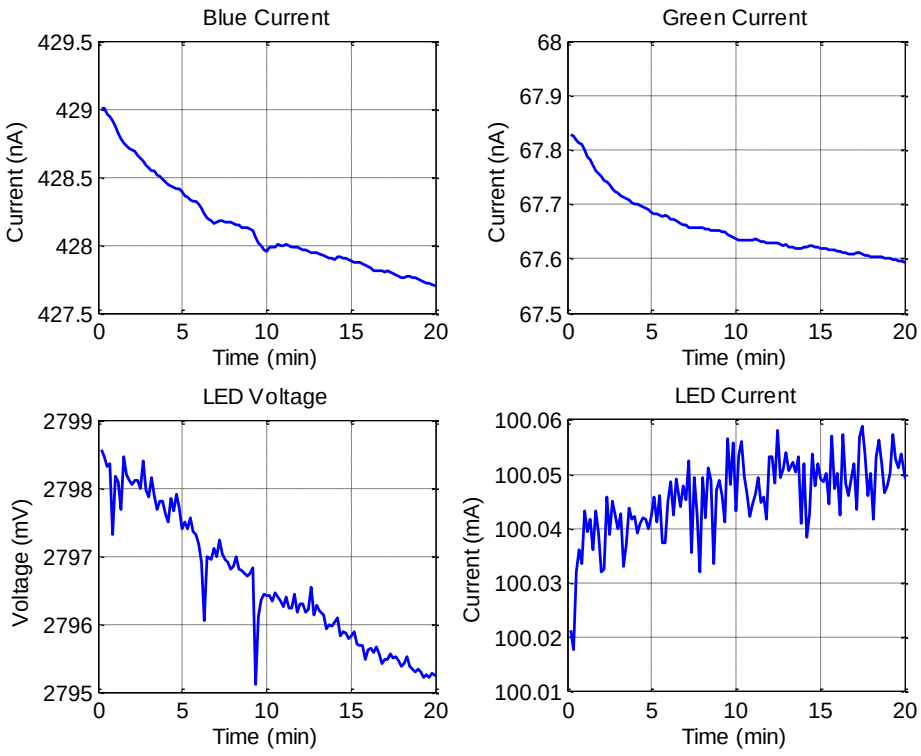

Figure 7.21 Photodiode current along with LED voltage and current obtained from full fat milk sample. The green current varies by $200\ \mathrm{pA}$ over the $20\ \mathrm{min}$ period.

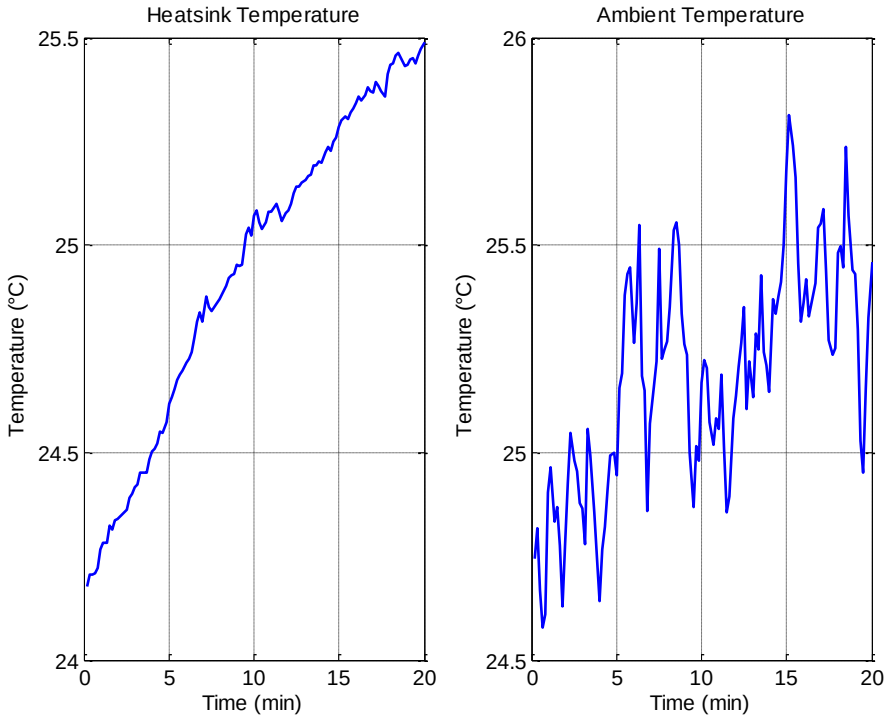

Figure 7.22 The heat sink temperature rises during the 20-min start up period, while ambient temperature remains relatively constant in the region of 25 °C

If the value of the blue photodiode and LED currents are used to compensate for the associated changes in the green photodiode current, the compensated green current has significantly less variations, making it a suitable measure for detecting the fluorescence level. Figure 7.23 shows the range of variations of the compensated current, which is only 20 pA after the initial transition period and 10 pA during the last 10 minutes. This is an order of magnitude less than the variations in the raw data obtained from the green photodiode.

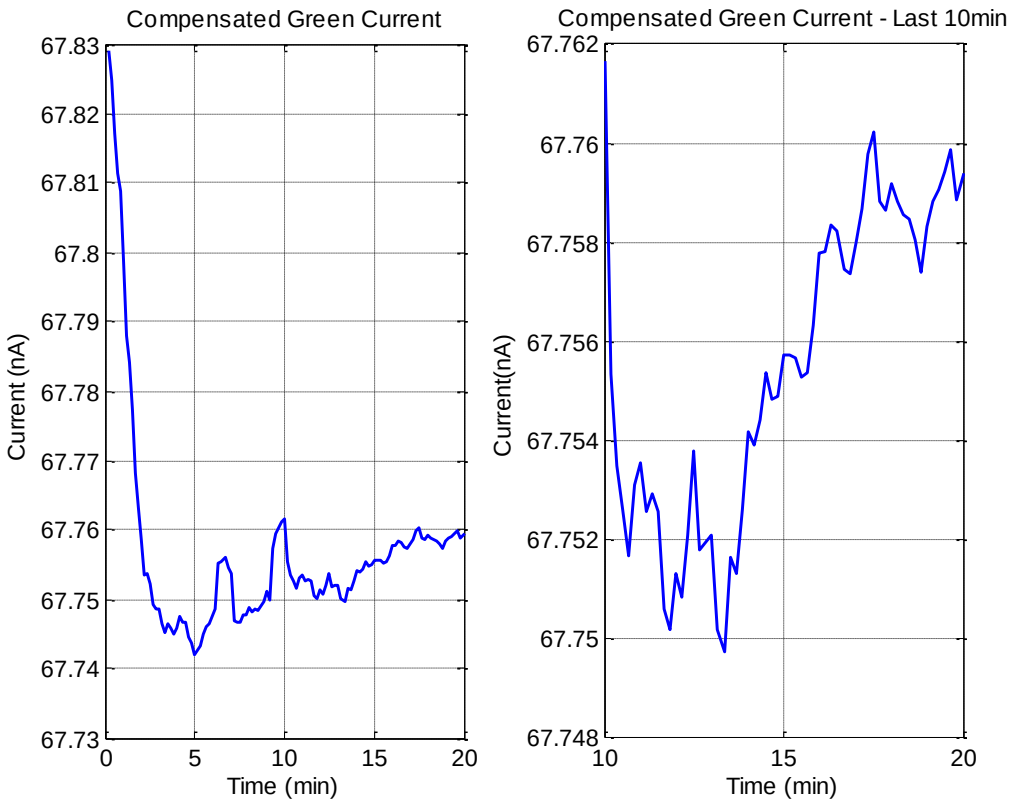

Figure 7.23 The image on the left displays the compensated green photodiode current over the 20min period. The figure on the right shows that after the initial transition period this current only changes by approximately 10 pA over the last 10 min of this period.

The compensated green current is monitored again for a period of 10 min, as shown in Figure 7.24. The results show that the variations of the compensated current remains within 10 pA over the 10 min period. Later on in this chapter it will be shown that a 1 nM increase in the fluorescence level, increases the compensated green current by approximately 20 pA, therefore 10 pA variation over this period will not obscure the actual signal level that needs to be measured. The immunoassay test is carried out over 10-15 minutes. In addition using a moving average will further reduce the variations of the compensated green current.

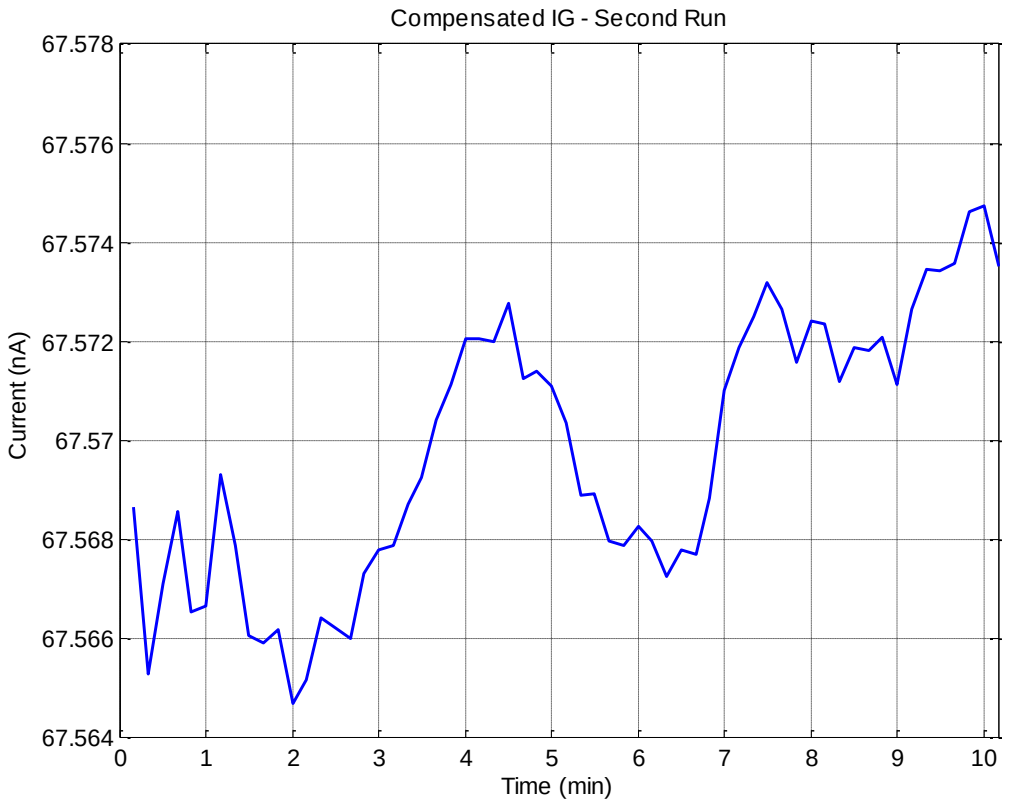

Figure 7.24 The images above show the compensated green photodiode current over a further 10-min data capture period.

7.3.7 Results of Measuring FITC Concentration in Milk

In order to evaluate the sensitivity of the transducer, fluorescein-milk solutions at different concentration levels were made. Fluorescein is a well-known organic compound with molecular formula of C20H12O5. In the experiments Fluorescein disodium salt hydrate, C20H10Na2O2xH2O, CAS 518-47-8 was used. The molecular weight of this formula is 376.28, with excitation peak wavelength at $488 - 491$ nm.

Fluorescein (FITC) solution needed to be made using a suitable buffer. In this experiment a 0.5 M Tris-Hcl, 6.8 pH buffer was used. This buffer was chosen to have a pH similar to milk's average pH level which is around 6.7. The molar concentration was first reduced to 10 mM by adding 5 ml of 0.5 M buffer to 245 ml of sterile water. The

sterile water was passed through a filter, using a 50 ml syringe, before being mixed with the 0.5 M buffer. The resultant 10 mM Tris-Hcl buffer had a pH of 6.71. The pH level of milk was 6.69.

At the next stage 7.7 mg of FITC was added to 10 ml of 10 mM Tris-Hcl buffer. As the molecular weight of FITC is 376.28, this mass amounts to 0.020463 mol of FITC. The result is 10 ml of 2.0463 mM FITC-Tris solution.

$$C = \frac{7.7 \times 10^{-3} g}{376.28 g} \times \frac{1}{10 \times 10^{-3} l} = 2.0463 mM \tag{7.15}$$

In order to evaluate the performance of the transducer, FITC-milk solutions at 1 nM, 5 nM, 10 nM, 20 nM and 50 nM FITC were made. Full fat pasteurised homogenised milk was obtained from supermarket. The transducer needs to detect as low as 2 nM. FITC-Tris is a transparent solution (with lower opacity compared to pure milk) therefore in order to maintain similar optical properties one part FITC-Tris solution at an appropriate concentration was mixed with 9 part milk. To provide the $1/10$ ratio, FITC-Tris solutions at 10 nM, 20 nM, 50 nM, 100 nM, 200 nM, 500 nM were made.

The initial FITC-Tris concentration was 2.0463 mM, from which first 10 µM concentration was made using 48.84 µl of 2.0463 mM FITC-Tris and 9951.13 ml of Tris buffer. The 10 µM was then used to make 10 ml of 1 µM, 500 µM and 200 µM of FITC-Tris. This was done using 1 ml, 500 µl, and 200 µl of 10 µM FITC-Tris solution added to 9 ml, 9.5 ml, and 9.8 ml of Tris buffer, respectively. The 1 µM FITC-Tris was subsequently used to make 100 nM, 50 nM and 20 nM of FITC-Tris by using 1 ml, 500 µl, and 200 µl of 1 µM FITC-Tris solution added to 9 ml, 9.5 ml, and 9.8 ml of Tris buffer, respectively.

The FITC-milk solutions were made by mixing 4.5 ml of Tris buffer and 0.5 ml of 500 nM, 200 nM, 100 nM, 50 nM and 10 nM of FITC-Tris, resulting in Milk-FITC solutions of 50 nM, 20 nM, 10 nM, 5 nM and 1 nM.

Several experiments were carried out using different samples over several days. The transducer was run for approximately $10\ \mathrm{min}$ for $4\ \mathrm{ml}$ of each sample, the test tube was then emptied and the content replaced with the next sample. The sample tubes were wrapped in tin foil and kept in the fridge while not in use. Figure 7.25 shows the compensated green photodiode current (IGC) for the entire period.

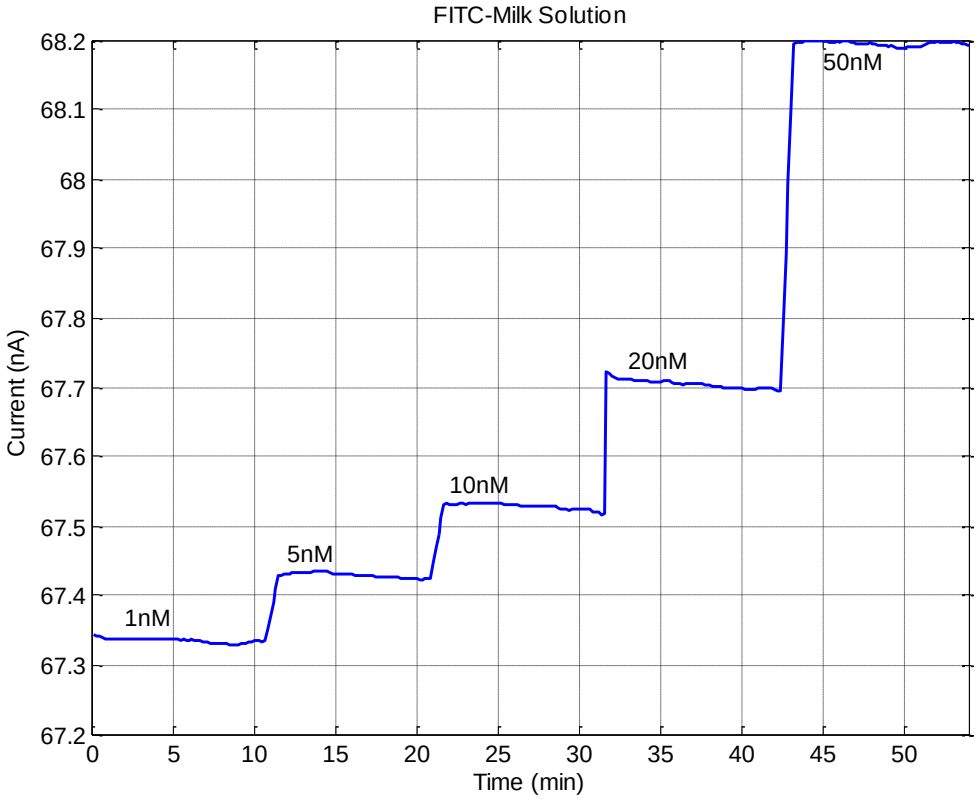

Figure 7.25 Compensated green photodiode current for FITC-milk solution at 5 different concentrations, monitored at a minimum of $10\ \mathrm{min}$ test for each sample

The average value for each sample was calculated and presented in Figure 7.26. The diagram shows there is a linear relationship between FITC concentration and compensated green photodiode current (IGC). The results of some of other experiments carried out using FITC-Milk samples have been shown in Figure 7.27. On average the transducer has a sensitivity of $19\ \frac{\mathrm{pA}}{\mathrm{nM}}$. However if individual FITC samples above concentration of $10\ \mathrm{nM}$ are considered, this conversion factor varies in the range of $15.75 - 17\ \mathrm{pA/nM}$, with an average of $16.4\ \mathrm{pA/nM}$. It must be noted that in all the immunoassay procedures suggested in Chapter 5, antibody is added at the last

stage. As a result, there is always a level of fluorescence produced by GFP and RFP labels before FRET is generated. This base level can be used for estimating FRET level, while compensating for the variations in the ambient and milk sample. Once antibody is added, FRET is produced which is essentially a reduction in GFP and an increase of RFP signals, respectively. Using the equation presented at the beginning of Section 7.2 for M_F, and based on $60\,\mathrm{nM}$, $50\,\mathrm{nM}$ and $40\,\mathrm{nM}$ for donor, acceptor and antibody concentration levels (based on the calculations at the end of Section 7.2.1), FRET level for $0, 3, 6, 9, 12, 15\,\mathrm{nM}$ concentration levels of progesterone is estimated to be $19.83, 18.80, 17.84, 16.95, 16.13, 15.36\,\mathrm{nM}$. As FRET production amounts to the same level of decrease in GFP signal level as the increase in RFP, the signal level is effectively amplified by a factor of two, while the variations level due to ambient and milk remain the same as both GFP and RFP are in the same milk and ambient conditions. This is assuming that electronic circuits can be made accurate enough with a negligible effect on the variations. To put the above discussion into perspective, let's assume there are two milk samples, one with $3\,\mathrm{nM}$ and the other $6\,\mathrm{nM}$ progesterone level. In the absence of antibody, both samples produce no FRET. The GFP and RFP signals are used as baseline offset for FRET measurement. When Antibody is added, using the $15.75 - 17\,\mathrm{pA/nM}$ range for the conversion factor and the gain of two that was explained above, the variation range for sample one is $18.45 - 18.8\,\mathrm{nM}$ and sample two $17.5 - 17.84\,\mathrm{nM}$. These two ranges do not overlap, therefore despite variations in the conversion factor it is still possible to detect the minimum of oestrus cycle.

It must be mentioned that the data in Figure 7.27 has been gathered from a proof of concept sensor, developed during the course of the PhD. The current system although serves this purpose, can be improved significantly during the commercialisation phase both in terms of electronic and mechanical design, in particular after miniaturisation of the sensor. In addition, the use of a second set of LED and photodiodes, as well as background measurement photodiode will provide additional means of compensation for ambient effect and variations in milk samples. Unfortunately due to the limited

resources during this multi-disciplinary PhD, these features were not used though have been suggested as future work in the final chapter.

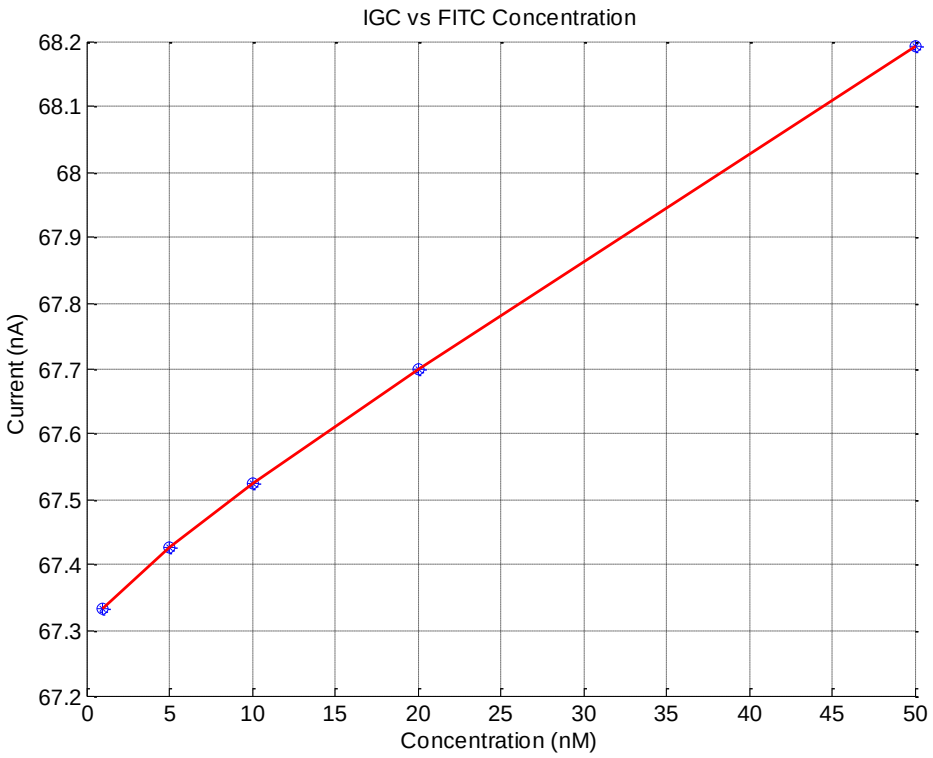

Figure 7.26 Compensated green photodiode current vs concentration of FITC in full fat milk

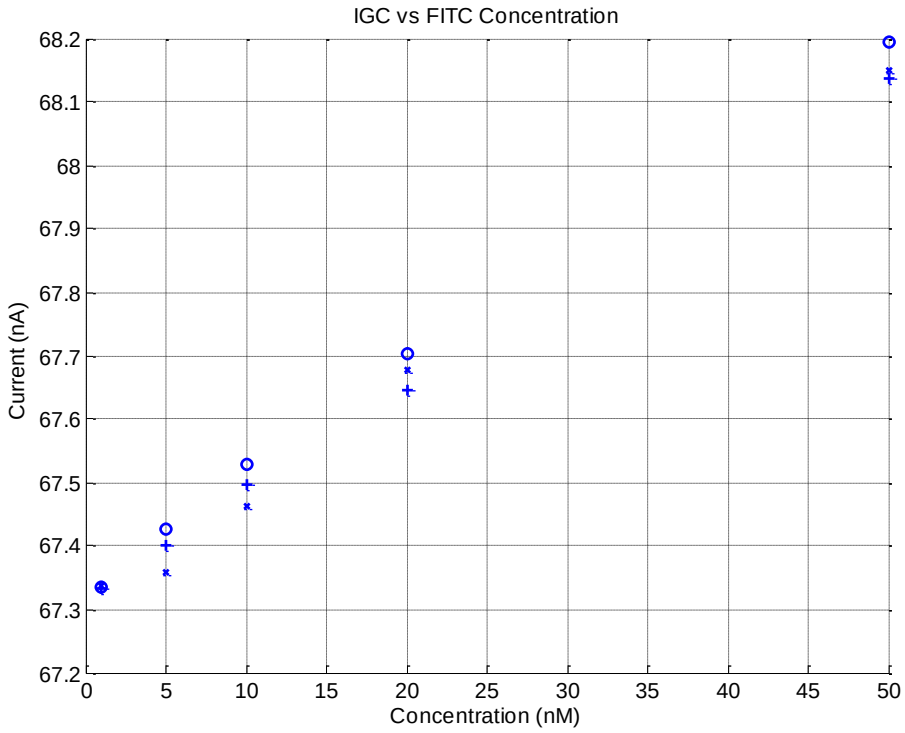

Figure 7.27 A number of datasets collected for the compensated green photodiode current vs concentration of FITC in full fat milk

7.3.8 Results of Measurements Using GFP Tags

The initial his-GFP product was provided by the School of Life Sciences, University of Warwick. The GFP-solution had a concentration of $1\ \mu M$ in $10\ mM$ Tris buffer. In order to produce GFP-Milk solutions at $2\ nM$, $7\ nM$, $15\ nM$, $30\ nM$ and $70\ nM$ with a ratio of $1/10$, GFP-Tris solutions of $20\ nM$, $70\ nM$, $150\ nM$, $300\ nM$ and $700\ nM$ were required. This was done by adding $7\ \mu l$, $36\ \mu l$, $71\ \mu l$, $143\ \mu l$ and $357\ \mu l$ of $700\ nM$ GFP to $493\ \mu l$, $464\ \mu l$, $429\ \mu l$, $357\ \mu l$ and $142\ \mu l$ buffer, respectively.

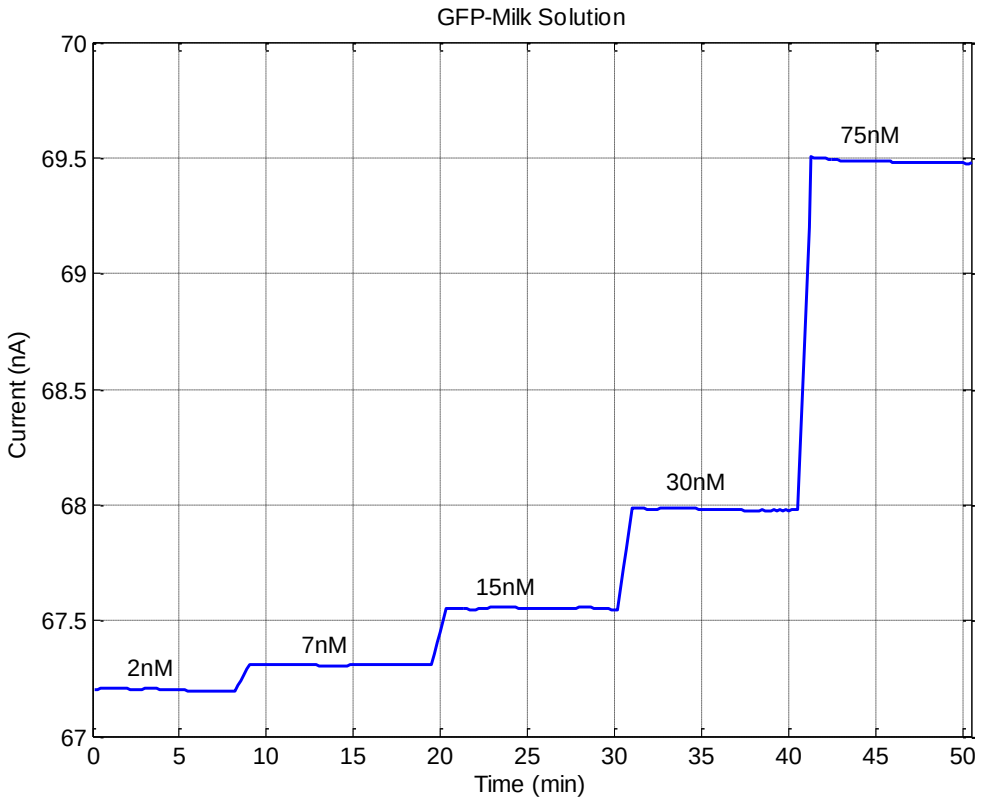

Figure 7.28 The fluorescence level for GFP-milk solutions at a number of concentration levels were monitored for a minimum of 10min each.

$500\ \mu l$ of each GFP-buffer solution was then mixed with $4.5\ ml$ of full fat milk to produce the GFP-milk solutions of interest. The fluorescence level for GFP-milk solutions were monitored over a minimum of $10\ min$ period for each sample, with the results shown in Figure 7.28. The average value for each sample was calculated, as presented in Figure 7.29, showing a linear relationship. On average the transducer has a sensitivity of $19.5\ pA/nM$. GFP has the excitation peak wavelength of $483\ nm$ and peak emission of $506\ nm$, whereas FITC peak excitation wavelength is $494\ nm$ and emission of $512\ nm$. The shift of GFP excitation towards the blue LED peak wavelength, results in more excited photons. On the other hand the GFP emission peak shifts away from the green photodiode peak, with the combined effect producing the same results for GFP and FITC milk solutions.

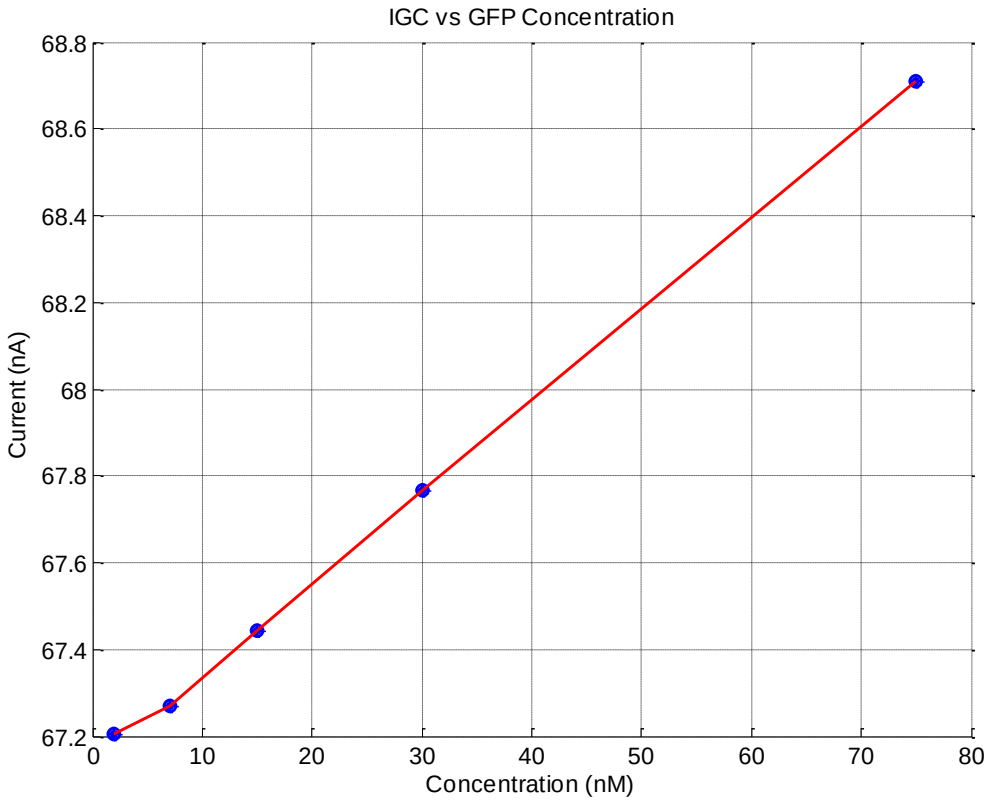

Figure 7.29 The fluorescence level for GFP-milk solutions at a number of concentration levels shows a linear relationship between IGC and concentration level.

7.3.9 Verification Using CLARIOstar™

In order to verify the correct operation of the transducer, BMG Labtech CLARIOstar™, a high performance monochromator and spectrometer microplate reader was used to measure the fluorescence level from the same FITC samples. An NUNC™ 384-well microtiter plate with transparent bottom was used, requiring the bottom optics to be enabled. Figure 7.30 shows the transducer in front CLARIOstar™ microplate reader and the 384-well microtiter plate. The figure demonstrates the small size of the transducer compared to the desktop lab-based equipment.

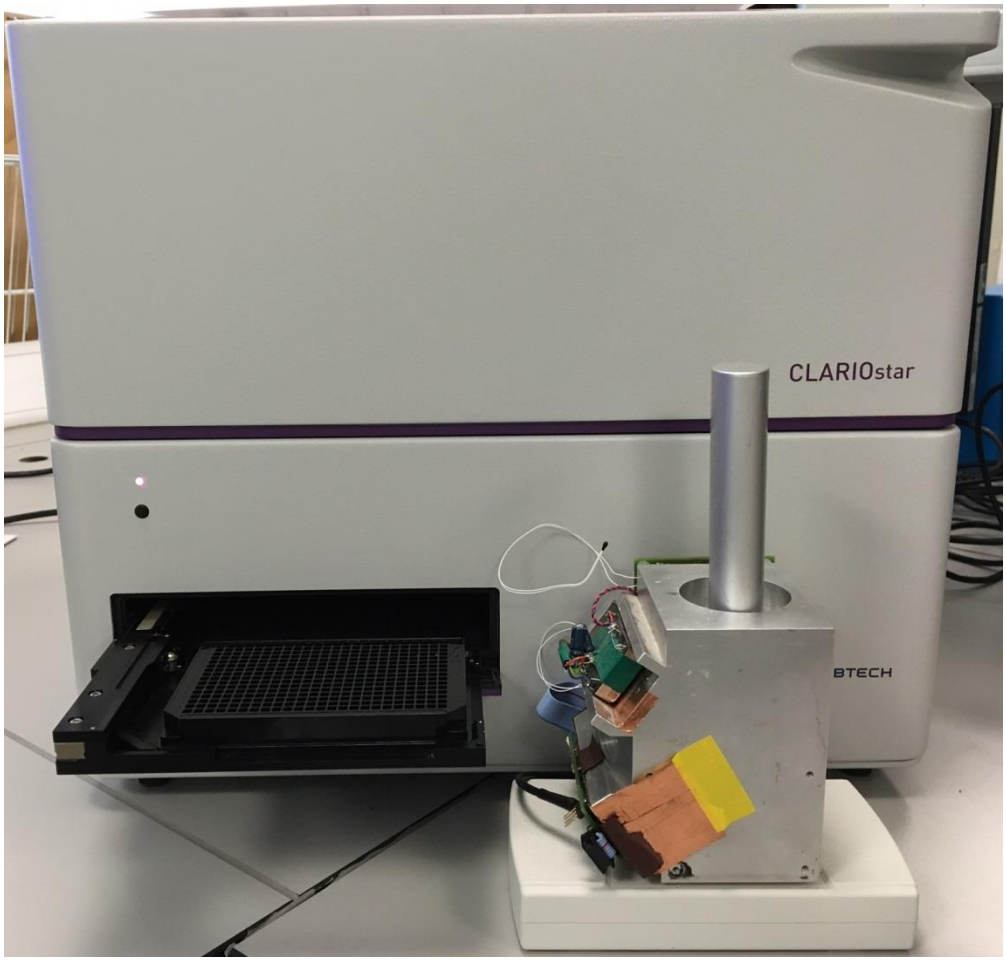

Figure 7.30 The developed immunoassay in comparison with CLARIOstar

The excitation peak wavelength was set to $470\ \mathrm{nm}$ and the emission to $540\ \mathrm{nm}$ to match the blue LED and green photodiode excitation and emission wavelengths. The monochromator gain was set to 500 and the focal point to $2.8\ \mathrm{mm}$. The dichroic filter wavelength was automatically adjusted by the system between the excitation and emission spectra. Several tests were carried out, on 3 wells of the microtiter plate filled with $50\ \mu\mathrm{l}$ of each sample. The results for 7 sets of measurements taken over time have been presented in Figure 7.31.

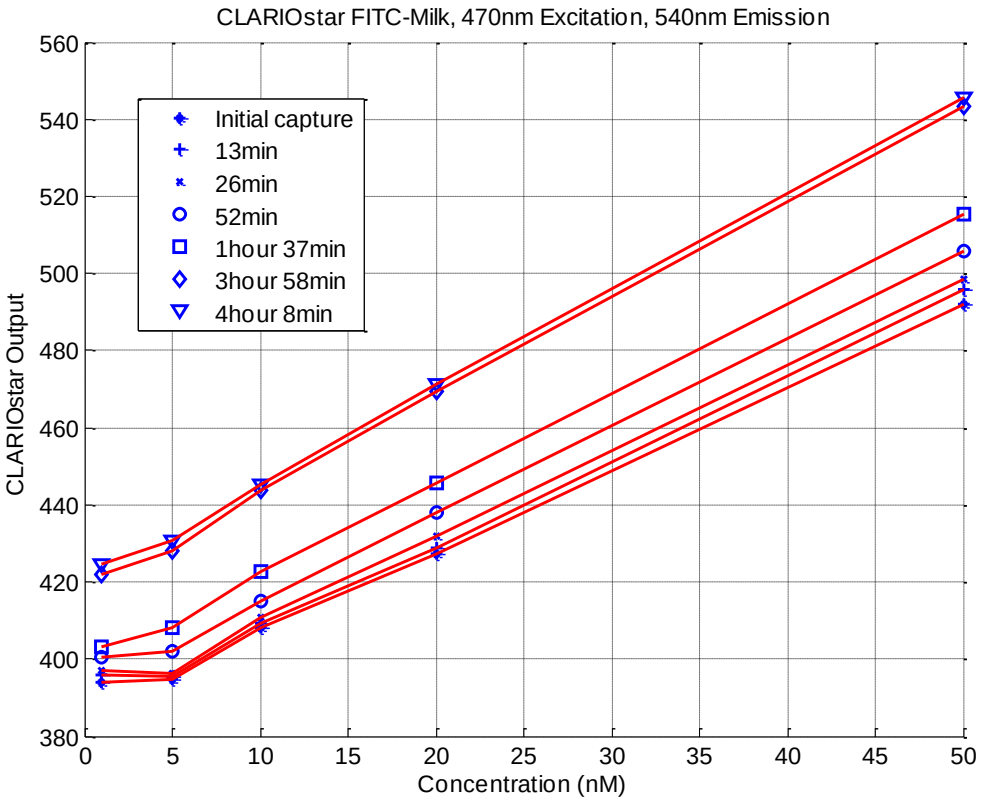

Figure 7.31 Data collected by CLARIOstar™ for FITC-milk solution at different concentration levels.

The figure shows a linear relationship between the FITC concentration level and the monochromator output, at higher concentration levels. Table 7.8 shows the initial measurement for each well. The output is not distinguishable between the two lower concentrations in the initial data captures.

Table 7.8 The initial CLARIOstar output for the three rows of samples.

	1 nM	5 nM	10 nM	20 nM	50 nM
First row	395	394	407	429	491
second	394	395	410	427	494
Third row	393	395	407	426	491

Due to the small volume of sample in each well (50 µl) and the viscosity of milk, initially after filling up the well, the surface profiles are not all the same. These variations cancel the effect of small fluorescence change that should be observed between 1 nM and 5 nM samples. As time goes on, however, the surface of each

sample spreads evenly and the small bubbles are released, allowing for the difference between the low-concentration samples to appear. In addition over time the aqueous part evaporates leading to an increased density and therefore increased signal. This effect will also increase the slope of the linear curve as all samples are affected at the same rate. Table 7.9 demonstrates the CLARIOstar output for the same samples captured after nearly 4 hours.

Table 7.9 CLARIOstar output after 4 hours for the three rows of samples.

	1 nM	5 nM	10 nM	20 nM	50 nM
First row	422	431	445	475	542
second row	426	429	444	468	546
Third row	426	432	447	471	549

In order to evaluate the effect of detection wavelengths on the output, a number of scenarios were examined and presented in Table 7.10. The table demonstrates the adverse effect of choosing a small bandwidth on the strength of output signal.

Table 7.10 Effect of detection wavelength on the output

		FITC Concentration				
Excitation	**Emission**	1 nM	5 nM	10 nM	20 nM	50 nM
$450-490\ nm$	515 – 590 nm	403.33	408	422.67	445.67	515.33
450 – 490 nm	510 – 550 nm	348.67	352.67	367.67	390.67	462
455 – 485 nm	505 – 535 nm	192.33	196	203.67	217.33	260

The results show that after adjusting the CLARIOstar wavelength profile as well as offset and gain, the data from CLARIOstar and the proposed transducer match, verifying the correct functionality of the developed transducer.

7.3.10 Verification Using a FRET Pair

CLARIOstar is a powerful analysis tool widely used by the research community for spectrofluorometry. Once a satisfactory comparison between the CLARIOstar results

and output of the developed transducer was drawn, further experiments were carried out using CLARIOstar. This is due to the fact that it offers a powerful means of spectrum analysis for assessing the molecular behaviour also because it only requires a small volume of sample in the region of microliters as otherwise the cost of experimental work would have been substantial and prohibitive.

In order to evaluate the performance of the proposed immunoassay solution using FRET pair, recombinant red, green and blue fluorescent proteins were obtained from Evrogen (Evrogen, 2016). The proteins are supplied with 6xHis-tag, a polyhistidine with 6 histidine residues attached. Histidine or His is a type of amino acid, with a molecular weight of 155g/mol. This molecule is widely used in protein biosynthesis. $100\ \mu l$ of rTagBFP (Blue Fluorescent Protein, catalogue number FP155), rTagGFP2 (Green Fluorescent Protein, catalogue number FP152) and rTagRFP (Red Fluorescent Protein, catalogue number FP154), each with the density of $1\ g/l$ were obtained. The rTagBFP has a molecular weight of $26\ kDa$, concentration of $38.5\ \mu M$ and was used to simulate milk natural progesterone by enabling effective monitoring of molecular behaviour of the system. The other two proteins had a molecular weight of $27\ kDa$ and concentration of $37\ \mu M$. In addition to these proteins, anti-His antibody was also required to bind with their His elements. Anti-His mouse monoclonal antibody from Roche, catalogue number 11922416001, was obtained from Sigma-Aldrich. The antibody has a molecular weight of $150\ kDa$ and was supplied in $100\ \mu g$ lyophilized format. This was then turned into $1\ ml$ of $0.1\ g/l$ anti-His antibody solution, with concentration of $666\ nM$ as recommended by the manufacture.

A number of samples were made using equal amounts of rTagGFP, rTagRFP, Anti-His Antibody and rTasgBFP. Therefore in order to arrive at the final concentration levels of $60\ nM$ and $50\ nM$ for donor and acceptor molecules as suggested in Section 7.2.1, TagGFP and TagRFP solutions of $240\ nM$ and $200\ nM$ were prepared. This was done first by making $1.2\ \mu M$ and $1\ \mu M$ GFP and RFP samples through diluting the original $37\ \mu M$ sample using 1xPBS (Phosphate Buffered Saline). These were then further

diluted using full fat milk to a ratio of $1/5$ to produce the $240\ \mathrm{nM}$ and $200\ \mathrm{nM}$ required for this test. These concentrations were chosen four times the actual required level so that after mixing all four constituents of each sample, the final concentration will become the desired $60\ \mathrm{nM}$ and $50\ \mathrm{nM}$.

The antibody concentration in the final solution was considered at $33\ \mu\mathrm{M}$, based on $\mathrm{k} = 0.25$ (Section 7.2) for $60\ \mathrm{nM}$, $50\ \mathrm{nM}$ and $20\ \mathrm{nM}$ donor, acceptor and progesterone concentrations, respectively. As explained above, a 4-times higher concentration level of $133\ \mathrm{nM}$ antibody-milk dilution was required, made by mixing the original 666nM antibody-buffer dilution with milk at a ratio of $1/5$ (4 parts milk, 1 part antibody dilution).

To assess the FRET concentration in relation to the native antigen, 4 different concentrations of $30\ \mathrm{nM}$, $60\ \mathrm{nM}$, $120\ \mathrm{nM}$ and $240\ \mathrm{nM}$ for TagBFP in the final samples were considered. As stated above 4 times higher concentration samples of TagBFP-Milk at $960\ \mathrm{nM}$, $480\ \mathrm{nM}$, $240\ \mathrm{nM}$ and $120\ \mathrm{nM}$ were made.

Once the samples were prepared three wells of a 384-well microtiter plate were filled with $20\ \mu\mathrm{l}$ of each sample. GFP and RFP form a FRET pair, therefore by illuminating the samples using the excitation wavelength of GFP at around $480\ \mathrm{nm}$ it is expected to see various levels of emission at $580\ \mathrm{nm}$, which is the peak emission wavelength of RFP. On the other hand if the molecules are illuminated using $545\ \mathrm{nm}$ light, which is the excitation peak of RFP, no significant difference between FRET concentrations should be observed as resonance energy transfer from donor to acceptor would not take place in this case.

Inserting donor, acceptor antibody concentrations at $60\ \mathrm{nM}$, $50\ \mathrm{nM}$ and $33\ \mathrm{nM}$ into equation (7.1) results in the following equation:

$$M_F = \frac{198000}{(110 + \mathrm{BFP})^2} \tag{7.16}$$

The amount of FRET produced in each, estimated to be at $10.1\ \mathrm{nM}$, $6.85\ \mathrm{nM}$, $3.75\ \mathrm{nM}$ and $1.61\ \mathrm{nM}$ for $30\ \mathrm{nM}$, $60\ \mathrm{nM}$, $120\ \mathrm{nM}$ and $240\ \mathrm{nM}$ concentrations of TagBFP, respectively.

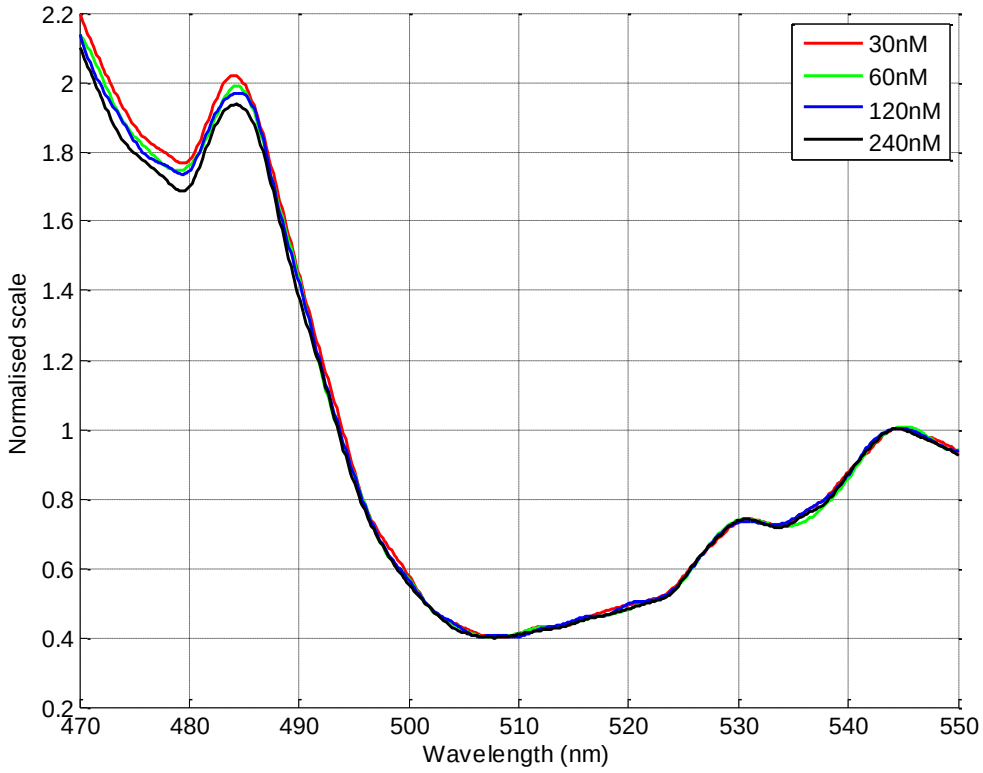

Figure 7.32 Excitation wavelength scan and the effect on the emission peak wavelength at $580\ \mathrm{nm}$.

Several experiments were carried out using different samples, wells and CLARIOstar optical and gain settings. The outcomes were downloaded as excel files for further analysis. Figure 7.32 shows the results for one of the experiments. The emission strength at $580\ \mathrm{nm}$ wavelength (the peak emission wavelength of RFP) was monitored for a sweep of excitation wavelengths from $470\ \mathrm{nm}$ to $550\ \mathrm{nm}$. The curves were normalised to their average value to take into account variations in the instrument and samples. An average of three wells was then used to produce the final curves. The results show that at the excitation wavelength around 480nm (peak excitation of green protein), a peak in red emission takes places which is different for each sample. As this excitation wavelength is far away from the actual excitation wavelength of the red protein, the effect on the red emission can only be produced by resonance energy

transfer. According to the calculations above the maximum and minimum FRET signals are for $30\ \mathrm{nM}$ and $240\ \mathrm{nM}$, respectively. This can be clearly seen from the figure, with the highest level for $30\ \mathrm{nM}$ step by step reducing to reach the minimum at $240\ \mathrm{nM}$.

Figure 7.32 also demonstrates that the red emission again reaches a local peak at a wavelength around $545\ \mathrm{nm}$. This is the peak excitation wavelength for the red protein and as expected due to the presence of same amount of RFP in all samples and in the absence of FRET, the emission levels at this excitation wavelength are very similar.

Another observation that can be made from this figure is the effect of Rayleigh scattering. At blue and green wavelengths the scattering effect is much stronger acting as a natural amplifier, whereas this effect is significantly less prominent at higher wavelengths.

7.4 Summary and Conclusion

This chapter provided an analysis on various parameters affecting the performance of the proposed immunoassay framework, leading to the calculation of the optimum concentration levels for donor, acceptor and antibody molecules depending on the expected range of progesterone or analyte of interest in the solution. This was then followed by evaluating the effect of excitation, emission and detection spectra of the LED, fluorescent proteins and photodiodes and finally determining the right combination of these components for an acceptable performance.

In this chapter also the effects of various features of electronic design were investigated and it was shown, through a number of experiments, that the LED current is effectively controlled providing the required accuracy by the transducer. The experiments also demonstrated that adaptive offset cancellation was working effectively, providing a wide dynamic range without the need to change the circuit parameters. This also enabled the application of photodiode current compensation,

which was shown to be a greatly beneficial feature in providing a stable and clean output signal. As a result the transducer is capable of measuring stabilised picoampere currents produced from milk which is an inherently volatile medium.

Once the transducer design was verified it was used to measure fluorescence signal from a variety of fluorophores including fluorescein, GFP, RFP and BFP. The results show that the developed system can reliably measure down to $\pm 5\,\mathrm{pA}$ current, equivalent to approximately $\pm 250\,\mathrm{pM}$ accuracy of fluorophore concentration based on GFP. This is significantly better than the accuracy required for detecting the onset of oestrus.

In order to verify the functionality of the system, it's outcome was compared against the results produced by CLARIOstar, an advanced lab-based analysis tool for spectrofluorometry. It was shown that the developed transducer provides a comparable detection level meaning that the current measurement limitations of the developed transducer is as a result of the tests being carried out in milk as a volatile complex medium, rather than the transducer characteristics itself. The FRET formation was also tested in a number of experiments and was illustrated that the proposed biological framework is capable of providing a sound platform for a competitive homogeneous immunoassay, with the precision required for measuring progesterone level in milk and detecting the onset of oestrus as the main aim of this PhD work.

8 SUMMARY, DISCUSSION AND FUTURE WORK

8.1 Summary

Profitability of a dairy farm directly relates to the amount of milk produced per cow. A cow needs to give birth in order to produce milk, therefore effective reproductive management with the aim to maximise the pregnancy rate when the milk production is declining, is an essential part of most modern dairy farms. Detecting the onset of oestrus is a fundamental element of this process. Progesterone as a hormone that signals the body to provide the necessary condition for enabling and maintaining bovine pregnancy is a key indicator that can be used for detecting the onset of oestrus. These aspects were reviewed in the initial chapters of the thesis, setting out the case for the design of a portable commercially-viable transducer and associated immunoassay, able to measure progesterone on-site at dairy farms. This PhD work provided the details of the proposed hardware solution along with a biological framework for developing a homogeneous competitive immunoassay suitable for measuring progesterone concentration in milk.

In the initial stage of this thesis, a review of the current reproductive management schemes, including methods of determining the reproductive cycle, oestrus synchronisation and artificial insemination was carried out. The chapter then continued with a financial analysis of the market size, benefits and potential revenues that the proposed system can bring to the dairy industry. It was concluded that there is a significant market for on-site progesterone measurement, with a multi-million pound annual revenue in particular for the consumable element of the assay.

Once a valid case for developing the transducer was established, a detailed study of the essential concepts in the currently available immunoassay technologies was undertaken. In basic terms an immunoassay requires a set of antibody, antigen and label molecules interacting in a controlled environment and through predetermined

procedural stages. The output produced as a result of the presence of label molecules is detected by a specific detection mechanism and subsequently correlated to the concentration level of the analyte of interest.

In recent years there have been numerous studies with regards to progesterone measurement in bovine milk. The majority of these methods are based on the concept of heterogeneous immunoassay where sample incubation and several wash stages are required in order to measure the progesterone concentration. Nonetheless there have been few cases based on homogeneous methodology, without the need for physical separation. The equipment necessary for these tests are however expensive and suitable for laboratory use. Lateral flow test is the only simple and low-cost commercial test offered so far, albeit it does not provide the level of accuracy needed for progesterone measurement.

One of the prominent methods of detection in an immunoassay setup is fluorescence spectroscopy. In order to understand the work undertaken in this area, a review of the relevant concepts was carried out. In addition, a range of methods that have been applied to the measurement of progesterone concentration was investigated and outlined. As an example, surface plasmon resonance technology can be used for developing a label-free progesterone immunoassay. These methods however often rely on expensive lab-based instruments for detection and sample handling. Due to the existence of a wide range of fluorescent labels and technologies available to achieve fluorescence spectroscopy with a potential to design a commercially-viable portable system, this method was used as a basis for developing the proposed transducer and the associated immunoassay.

Once the case for a fluorescence-based immunoassay was made, a detailed account of the proposed design of the electronic hardware, enclosure and optical features needed for the transducer was provided. The electronic design benefits from a unique adaptive offset cancellation mechanism, which compensates for the effect of

background LED light. It eliminates the need for expensive optical components such as lens, collimator and dichroic mirror; and offers a wide dynamic range without having to change circuit parameters. In addition, due to the novel design of the enclosure, the effect of background light on the detector circuit has been substantially reduced, whilst fluorescent light capture inside the milk sample improved. In order to provide a reliable design, capable of offering detection level of $2\,\mathrm{nM}$ progesterone in milk, various parameters that could influence the performance of the transducer were studied and measures were put in place to compensate for their likely adverse effects.

The developed prototype transducer provides the means to measure fluorescence concentration at the required accuracy. Building on this platform a framework for a competitive homogeneous immunoassay based on fluorescence resonance energy transfer was proposed. The immunoassay benefits from the use of three fundamental external biomolecules. These are anti-antigen antibody, donor-labelled antigen and acceptor-labelled antigen added at various stages during the procedure. In the context of progesterone measurement and based on the developed transducer, the antigen is progesterone and the donor and acceptor labels are green and red fluorescent proteins. Once the biological framework was developed, three specific procedures were suggested to offer a compromise on hardware cost versus procedural and algorithmic complexity.

Milk as a medium with a complex mix of molecules at various sizes, shapes and functionalities, greatly influences the performance of the immunoassay. It mainly consists of lactose, proteins including casein and whey, and finally lipids as an emulsion in an aqueous medium. The biomolecular interactions in milk, in particular between immunoassay molecules and milk's, were investigated in some depth and analysed.

The proposed biological framework requires a mix of antibody and labelled antigens at predetermined concentration levels. The formulated model was analysed with respect to these parameters and optimised values were determined.

Numerous experiments were carried out on different aspects of the transducer and immunoassay as a whole. The results show that the adaptive offset cancellation mechanism works effectively, providing a wide dynamic measurement range. In addition the developed transducer can comfortably measure down to $\pm 5\ \mathrm{pA}$ current, equivalent to approximately $\pm 250\ \mathrm{pM}$ accuracy of fluorophore concentration based on GFP. It is worth noting that the developed prototype is not a commercial device and further significant improvement on the accuracy of measurement can be expected during miniaturisation and commercialisation of the system.

The sensor was also tried with a number of fluorophores including fluorescein and GFP. The results demonstrate the sensor's ability to measure below $1\ \mathrm{nM}$ concentration, which is suitable for measuring progesterone level in milk and detecting the on-set of oestrus. Furthermore an rTagGFP and rTagRFP FRET pair was used to observe and evaluate the formation of FRET on antibody binding sites, depending on the concentration of the analyte of interest which in this case was rTagBFP. The outcome clearly demonstrates that FRET is formed and can be detected as it produces distinguishable signal levels between different test concentrations used in the experiments. Therefore it is concluded that the proposed transducer design and the associated immunoassay framework are able to provide the necessary accuracy and meet the requirements set out in the beginning of the PhD.

8.2 Discussion

The outcome of investigation into current immunoassays shows that, although various methods for measuring progesterone have been proposed by the research community, the complexity and cost of developing these methods into commercially-viable products for use in dairy farms have been a prohibiting factor. The majority of these methods are based on enzyme-linked immunoassay principles, which require extensive

incubation periods often over many hours, as well as several wash stages to separate the labelled antibody-antigen complexes from the free labels in the solution.

The sensor system developed here has addressed all these issues, by offering a compact portable design, with standard electronics, an easy-to-make machined or moulded enclosure and without the need for expensive optical and optoelectronic components found in the standard lab-based fluorimeters. In addition, the proposed immunoassay framework is a homogeneous one, which does not require any wash stages nor a pre-test incubation period. The procedural complexity can also be tailored to achieve a lower hardware cost.

The sensor system also offers a generic framework that can be employed for measuring the concentration of a variety of molecules in complex liquids, potentially in blood. However as the characteristics of these molecules and the environment of test are different, various parameters of the system need to be assessed and possibly optimised before this can be achieved.

One of the major limitations of the developed prototype is the volume of sample required for each test, which currently stands at $4\ \mathrm{ml}$. This is significantly more than the sample size needed in the lab-based commercial equipment, which tends to be in the region of tens to hundreds of micro litres. Although due to the abundance of milk in a dairy farm providing $4\ \mathrm{ml}$ milk sample per test is not an issue, the cost of antibody and labelled antigen molecules may become prohibitive. This however will not be a limiting factor in the final commercial product as the current design can easily be scaled down to reduce the required volume to below $100\ \mu\mathrm{l}$. This sample size can simply be achieved by reducing the height and radius of test tube to a quarter of their current values.

This work has been mainly focused on offering a theoretical solution in terms of sensor hardware design, algorithms and immunoassay framework. Extensive work was carried

out to capture all parameters and system features that can affect the measurement performance. Unfortunately, due to the limited resources, especially as a multi-disciplinary project, a thorough verification of all aspects of the design was not possible. Some of the areas, which need further work are as follows.

Milk and ambient temperatures affect the results. The experiments in this work were carried out with milk at room temperature. While a degree of variations in temperature were taken into account using the specific hardware design, dynamic offset cancelation and measurement methodology proposed in Chapter 4, further analysis and verification is highly recommended.

The milk samples were obtained from supermarket fresh products. Such samples although useful for verification do not exactly match the characteristics of a freshly produced milk at farm. Test on fresh milk needs to be considered as future work. Also it is recommended that an artificially-made colloidal liquid with a known concentration of scattering particles to simulate milk with known parameters is utilised in order to understand the performance of the sensor using different types of milk.

To deal with the above issues additional measures such as use of extra temperature sensors, a secondary test tube chamber as well as another set of LED and photodiodes will be required. Such investigations are suggested to be considered as a part of future work.

Another limitation of the experimental work in this PhD was the absence of RFP and GFP tagged progesterone molecules as well as anti-progesterone antibody. These samples were not available off-the-shelf and had to be made specifically for the project, which due to the lack of resources was not possible. Consequently, the process was only simulated using His tags and anti-His antibody, which were available to purchase, although even use of these samples were limited due to the cost and support issues. For the commercialisation, a complete programme of work needs to be

considered in order to focus on the production of the required biological samples, more likely as a part of another PhD to focus on the biological aspects of the immunoassay.

The proposed immunoassay framework and measurement methodology make significant use of the way the sensor has been designed, where both green and blue photodiodes outputs are available for analysis at the same time. However, commercial spectrometers such as CLARIOstar only provide one reading at a time per specific excitation wavelength. As a result, measurement of FRET and estimation of progesterone concentration level using the existing commercial systems in the way that is intended in this proposal was not possible. At the same time due to the volume of the samples and cost implications, use of the current sensor in some verification phases was limited. Therefore, it is suggested that for any future work the prototype sensor is further developed and miniaturised first. Additional experiments on the biological samples need to be carried out using the newly developed sensor rather than the commercial lab-based spectrometers.

One of the immunoassay procedures proposed here offers a two-stage solution for measuring progesterone, where labelled progesterone molecules are added to milk in stage one, then antibody is added and the system behaviour is monitored over time. The reaction time depends on the volume of the sample and other factors such as temperature. As a result monitoring changes over time due to the effects of noise and variations in milk density may not be possible for small volumes. Therefore, this solution is expected to need a higher volume of sample, resulting in an increased cost per test.

The developed transducer requires the samples to be poured into the test tube. There is however the possibility to use this transducer as a part of an on-line automated system, where milk along with other necessary reagents is added to the test tube by an automatic nozzle. In such circumstances there is no need to have a test tube,

instead the common end of the light channels can be capped by a glass window or alternatively a cylindrical test tube without a bottom end is inserted into the chamber. The automated system can flush the test tube or the empty chamber with buffer, eliminating the need to replace the test tube after each test.

8.3 Future Work

Automated on-line measurement

The proposed immunoassay solution can be further developed in order to integrate into an automated on-line progesterone measurement system. Such a solution is likely to need a custom-designed and miniaturised liquid handling system. This will obviously require a significant change to the electronics as well as the mechanical and optical design of the enclosure, resulting in consequential effects on the behavioural response and performance of the immunoassay, which all can be the subject of a new study.

Lab-On-Chip

Lab on Chip technology is finding its way into many new monitoring and diagnostic tools, particularly in in-vitro diagnostics and point of care devices. This is due to the advances in precision engineering, microfluidic systems and microelectronics. The use of this technology in progesterone measurement needs a careful consideration due to the viscosity, opacity and complex molecular structure of milk.

Application to Other Molecules

The focus in this PhD has been on measuring progesterone level in bovine milk. As milk is a fluid produced by the mammals' body it carries various biomolecules that some can be used as a measure for a certain body condition or disease. One such condition is mastitis that is commonly seen in dairy farms, with significant economic benefits if detected early. Mastitis often results in symptoms such as red or hard udder with the associated changes in the molecular composition of the milk, such as increased level of

white blood cell or a reduction in the concentration of casein, potassium and lactoferrin (Kandasamy, et al., 2011). These molecules have a different structure and property to progesterone, requiring a different type of antibody, antigen and fluorescent label for detection. Their manner of interaction with milk molecules will also be different. These all can be the subject of a new research.

Application to Other Fluids

The proposed solution has been mainly concentrated on milk, though in principle it is applicable to a variety of fluids such as urine and blood. Urine as an easily accessible bodily fluid can be used for carrying out a variety of diagnostic tests. This is particularly useful in GP surgeries where urine or blood samples need to be taken and sent off-site for further analysis. The ability to carry out on-site tests even as a purely indicative tool in order to determine whether or not off-site test is required, will be appealing to most GP surgeries as it will bring in significant cost savings.

Improved Stage Transition Model

The procedures suggested for adding various reagents to milk in order to measure progesterone level in two, four or five stages assume a degree of change in the optical properties of milk over time based on only one coefficient. This holds true if the test is undertaken over tens of minutes rather than hours, and where the ambient temperature variations are not substantial. The reaction time also depends on the molecular structure of the analyte, its environment and the required reagents and is likely to vary significantly case by case. However it is possible to develop a more complex model to take these effects into account or alternatively try to control the temperature of the milk chamber. The former option is likely to add to the procedural complexity of progesterone measurement, due to the need to have more equations to be able to solve the increased number of unknown parameters. The latter option on the other hand increases the complexity of hardware and will add to the cost of transducer.

8.4 Final Remarks

The aim of this PhD was to propose a solution for the design of a portable commercially-viable transducer to be used in conjunction with a specifically developed immunoassay framework. It is the author's belief that taking into account the proposed detailed design of the transducer and immunoassay framework; the development, fabrication and test of the transducer; together with the analysis, optimisation, evaluation and verification carried out and presented in this thesis, this aim has been fulfilled within the defined scope. The discussion and future work sections however set out the recommendations for further work in order to provide a more robust and easy to use solution and also expand the reach of the proposed solution beyond the defined aims of this PhD.

REFERENCES

Abcam, 2015. *A comparison between polyclonal and monoclona.* [Online]
Available at: http://www.abcam.com/protocols/a-comparison-between-polyclonal-and-monoclonal
[Accessed 09 12 2015].

Abramowitz, M. & Davidson, M. W., 2012. *Photomultiplier Tubes.* [Online]
Available at:
http://www.olympusmicro.com/primer/digitalimaging/concepts/photomultipliers.html
[Accessed 05 09 2015].

Absolute Antibody, 2016. *Antibody Structure.* [Online]
Available at: http://absoluteantibody.com/antibody-resources/antibody-overview/antibody-structure/
[Accessed 11 07 2016].

Agency, F. S., 2015. *UK Producer Numbers.* [Online]
Available at: http://dairy.ahdb.org.uk/market-information/farming-data/producer-numbers/uk-producer-numbers/#.VejE5pc8qmB
[Accessed 03 09 2015].

Anton Paar GmbH, 2009. *Density Measurement in Dairy Industry,* s.l.: Anton Paar.

Axelrod, D. & Davidson, M., 2012. *Total Internal Reflection Fluorescence, Introduction and Theoretical Aspects.* [Online]
Available at:
http://www.olympusmicro.com/primer/techniques/fluorescence/tirf/tirfintro.html
[Accessed 11 07 2016].

Ball, P. & Peters, A., 2004. Reproduction in Cattle. In: B. Publishing, ed. *Reproduction in Cattle.* Oxford: Blackwell Publishing, p. 95.

Balsam, J., Ossandon, M., Bruck, H. & Rasooly, A., 2012. Modeling and design of micromachined optical Soller collimators for lensless CCD-based fluorometry. *Analyst,* 137(21), pp. 5011-5017.

Banu, T. et al., 2012. Milk progesterone enzyme-linked immunosorbent assay as a tool to investigate ovarian cyclicity of water buffaloes in relation to body condition score and milk production. *Acta Veterinaria Scandinavica,* pp. 1-7.

Berg, J. M., Tymoczko, J. L. & Stryer, L., 2002. The Immunoglobulin Fold Consists of a Beta-Sandwich Framework with Hypervariable Loops. In: *Biochemistry.* New York: W H Freeman.

Bernini, U. et al., 1993. Temperature dependent optical properties of a synthesis blend of poly(methyl methacrylate) and vinyl rubber. *Journal of Materials Science,* 28(23), pp. 6399-6402.

Biotechnology Information, N. I. o. H., 2015. *Progesterone.* [Online]
Available at: http://pubchem.ncbi.nlm.nih.gov/compound/progesterone#section=Top
[Accessed 05 12 2015].

Birdi, K. S., 2009. Emulsions, Microemulsions, and Lyotropic Liquid Crystals. In: *Surface and Colloid Chemistry: Principles and Applications.* s.l.:CRC Press, p. 203.

Bustos, A. R. M., Trapiella-Alfonso, L., Encinar, J. R. & Costa-Fernández, J. M., 2012. Elemental and molecular detection for Quantum Dots-based immunoassays: A critical appraisal. *Biosensors and Bioelectronics,* 33(1), pp. 165-171.

Claycomb, R. W. & Delwiche, M. J., 1998. Biosensor for on-line measurement of bovine progesterone during milking. *Biosensors & Bioelectronics,* 13(11), p. 1173–1180.

Claycomb, R. W., Delwiche, M. J., Munro, C. J. & BonDurant, R., 1998. Rapid enzyme immunoassay for measurement of bovine progesterone. *Biosensors & Bioelectronics,* 13(11), p. 1165–1171.

Colazo, M., Ambrose, D. & Small, J., 2008. Comparison of 2 enzyme immunoassays and a radioimmunoassay for measurement of progesterone concentrations in bovine plasma, skim milk, and whole milk. *Canadian Journal of Veterinary Research,* 72(1), pp. 32-36.

De Kruif, C. G., Huppertz, T., Urban, V. S. & Petukhov, A. V., 2012. Casein micelles and their internal structure. *Advances in Colloid and Interface Science,* Volume 171-172, pp. 36-52.

DEFRA, 2015. *UK Cow Numbers.* [Online]
Available at: http://dairy.ahdb.org.uk/market-information/farming-data/cow-numbers/uk-cow-numbers/#.VejNDZc8qmA
[Accessed 03 09 2015].

DeJarnette, M. & Nebel, R., 2016. *Reproductive Anatomy and Physiology of Cattle,* s.l.: Select Reproductive Solutions.

DeNovix, 2015. *The DS-11 Spectrophotometers & FX Flurometer Series.* [Online]
Available at: http://www.denovix.com/ds-11-specifications/
[Accessed 11 07 2016].

Dewettincka, K. et al., 2008. Nutritional and technological aspects of milk fat globule membrane material. *International Dairy Journal,* 18(5), pp. 436-457.

Dransfield, M., Nebel, R., Pearson, R. & Warnick, L., 1998. Timing of Insemination for Dairy Cows Identified in Estrus by a Radiotelemetric Estrus Detection System. *Journal of Dairy Science,* 81(7), pp. 1874-1882.

Encylopedia, N. W., 2011. *Estrous cycle.* [Online]
Available at: http://www.newworldencyclopedia.org/entry/Estrous_cycle
[Accessed 04 07 2015].

Engelhardt, K. et al., 2013. pH Effects on the Molecular Structure of β-Lactoglobulin Modified Air−Water Interfaces and Its Impact on Foam Rheology. *Langmuir,* 29(37), pp. 11646-11655.

Engström, H. A., Andersson, P. O. & Ohlson, S., 2006. A label-free continuous total-internal-reXection-Xuorescence-based immunosensor. *Analytical Biochemistry,* 357(2), pp. 159-166.

Evrogen, 2016. *High effective FRET pairs.* [Online]
Available at: www.evrogen.com/flyers/FRET_pair_flyer.pdf
[Accessed 11 07 2016].

Evrogen, 2016. *Red fluorescent protein TagRFP.* [Online]
Available at: http://evrogen.com/products/TagRFP/TagRFP_Detailed_description.shtml
[Accessed 11 07 2016].

FAO, 2015. *World Milk Production.* [Online]
Available at: http://dairy.ahdb.org.uk/market-information/supply-production/milk-production/world-milk-production/#.VejEm5c8qmA
[Accessed 03 09 2015].

Fellow, G., 2016. *Poly Methyl Methacrylate Material Peroperties.* [Online]
Available at: http://www.goodfellow.com/E/Polymethylmethacrylate.html
[Accessed 08 11 2015].

Ferguson, J. & Skidmore, A., 2013. Reproductive performance in a select sample of dairy herds. *Journal of Dairy Science,* 96(2), p. 1269–1289.

Filters, L., 2015. *Dichroic Glass Series.* [Online]
Available at: http://www.leefilters.com/architecture/arch-dl.html
[Accessed 04 09 2015].

Firk, R., Stamer, E., Junge, W. & Krieter, J., 2002. Automation of oestrus detection in dairy cows: a review. *Livestock Production Science,* 75(3), p. 219–232.

Fong, B. Y., Norris, C. S. & MacGibbon, A. K. H., 2007. Protein and lipid composition of bovine milk-fat-globule membrane. *International Dairy Journal,* 17(4), pp. 275-288.

Fox, P., Uniacke-Lowe, T., McSweeney, P. & O'Mahony, J., 2015. *Dairy Chemistry and Biochemistry.* Cork, Ireland: Springer.

Friggen, N. C. & Chagunda, M. G., 2005. Prediction of the reproductive status of cattle on the basis of milk progesterone measures: model description. *Theriogenology,* 64(1), pp. 155-190.

Galliera, S., Gordon, K. C., Jiménez-Flores, R. & Everett, D. W., 2011. Composition of bovine milk fat globules by confocal Raman microscopy. *International Dairy Journal,* 21(6), pp. 402-412.

Gan, S. & Patel, K., 2013. Enzyme Immunoassay and Enzyme-Linked Immunosorbent Assay. *Investigative Dermatology,* 133(12), pp. 1-3.

Ghadar, A., Gardner, J. W. & Dowson, C. G., 2013. *Precision Transducer for Fluorescence-Based Immunoassays.* Baltimore, USA, IEEE Sensors Conference.

Gilbert, J., 2011. *FLP Lens Series for LUXEON Rebel and Rebel ES LEDs.* s.l.:Fraen Corporation.

Gillis, E., Gosling, J., Sreenan, J. & Kane, M., 2002. Development and validation of a biosensor-based immunoassay for progesterone in bovine milk. *Immunological Methods,* 267(2), p. 131–138.

Giordano, J., Fricke, P., Wiltbank, M. & Cabrera, V., 2011. an economic decision-making support system for selection of reproductive management programs on dairy farms. *Journal of Dairy Science,* 94(12), p. 6216–6232.

Glantz, M. et al., 2010a. Importance of casein micelle size and milk composition for milk gelation. *Dairy Science,* 93(4), pp. 1444-1451.

Glantz, M., Hakansson, A. & Mansson, H., 2010. Revealing the Size, Conformation, and Shape of Casein Micelles and Aggregates with Asymmetrical Flow Field-Flow Fractionation and Multiangle Light Scattering. *Langmuir,* p. 12585–12591.

Goff, H. D. & Hartel, R. W., 2013. Ice Cream. In: *Mix Ingredients.* New York: Springer, p. 49.

Griffin, W. C., 1954. Calculation of HLB Values of Non-Ionic Surfactants. *Journal of the Society of Cosmetic Chemists ,* 5(4), pp. 249-256.

Grimard, B. et al., 2006. Genetic and environmental factors influencing first service conception rate and late embryonic/foetal mortality in low fertility dairy herds. *Animal Reproduction Science,* 91(1-2), p. 31–44.

H., M. I., 2011. Milk Lipids - Milk Fat Globule Membrane. In: F. J. W., F. P. F. & M. P. L. H., eds. *Encyclopedia of Dairy Sciences.* s.l.:s.n., p. 680–690.

Hahn, D. W., 2009. *Light Scattering Theory,* Florida: Department of Mechanical and Aerospace Engineering, University of Florida.

Hamamtsu, 2015. *Si Photodiodes.* [Online]
Available at: https://www.hamamatsu.com/resources/pdf/ssd/s6428-01_etc_kspd1013e.pdf
[Accessed 11 07 2016].

Healthcare, GE, 2015. *Surface Plasmon Resonance.* [Online]
Available at:

http://www.gelifesciences.com/webapp/wcs/stores/servlet/catalog/en/GELifeSciences-uk/products/surface-plasmon-resonance/
[Accessed 20 08 2015].

Held, P., 2005. *An Introduction to Fluorescence Resonance Energy Transfer (FRET) Technology and its Application in Bioscience.* Winooski: BioTek Instruments.

Homola, J., Sinclair, S. & Gauglitz, G., 1999. Surface plasmon resonance sensors: review. *Sensors and Actuators,* 54(1-2), pp. 3-15.

Horne, D. S., 2006. Casein micelle structure: Models and muddles. *Colloid & Interface Science,* 11(2-3), pp. 148-153.

Huppertz, T. & Kelly, A. L., 2006. Physical Chemistry of Milk Fat Globules. In: P. F. Fox & P. L. H. McSweeney, eds. *Advanced Dairy Chemistry Volume 2: Lipids.* s.l.:Springer, pp. 173-174.

Ivanovaa, T. & Godjevargova, T., 2015. Sensitive Progesterone Determination Using a Magnetic Particle-Based Enzyme-Linked Immunosorbent Assay. *Analytical Letters,* 48(5), pp. 843-860.

Jenway, 2006. *Jenway 62 series fluorometers.* s.l.:Jenway.

JSC, Evrogen, 2016. *TagFPs: protein localization tags.* [Online]
Available at: http://evrogen.com/products/TagFPs.shtml
[Accessed 11 07 2106].

Jue, T., Yeh, Y., Fore, S. & Wu, H., 2009. *Fundamental concepts in biophysics.* New Yor: Springer.

Kandasamy, S., Green, B. B., Benjamin, L. & Kerr, D. E., 2011. Between-cow variation in dermal fibroblast response to lipopolysaccharide reflected in resolution of inflammation during Escherichia coli mastitis. *Journal of Dairy Science,* 94(12), p. 5963–5975.

Kappel, N. D., Proll, F. & Gauglitz, G., 2007. Development of a TIRF-based biosensor for sensitive detection of progesterone in bovine milk. *Biosensors and Bioelectronics,* 22(9-10), p. 2295–2300.

Keski-Rahkonena, P., Huhtinenb, K., Poutanenb, M. & Auriolaa, S., 2011. Fast and sensitive liquid chromatography–mass spectrometry assay for seven androgenic and progestagenic steroids in human serum. *Journal of Steroid Biochemistry and Molecular Biology,* 127(3-5), pp. 396-404.

King, T. L. & Brucker, M. C., 2010. Progesterone. In: *Pharmacology for Women's Health.* s.l.:Jones & Bartlett Publishers, p. pp. 372–373.

Kontopidis, G., Holt, C. & Sawyer, L., 2004. Invited Review: β-Lactoglobulin: Binding Properties,. *Dairy Science,* 87(4), pp. 785-796.

LABTECH, B., 2014. *CLARIOstar, High Performance Microplate Reader with Advanced LVF Monochromators.* [Online]
Available at: http://www.bmglabtech.com/en/products/clariostar/
[Accessed 05 09 2015].

Laitinen, M. & Vuento, M., 1996a. Immunochromatographic assay for quantitation of milk progesterone. *Acta Chemica Scandinavica,* Volume 50, pp. 141-145.

Laitinen, M. & Vuento, M., 1996b. Affinity Immunosensor for Milk Progesterone: Identification of Critical Parameters. *Biosensors & Bioelectronics,* 11(12), pp. 1207-1214.

Lakowicz, J., 2006. Instrumentation for fluorescence spectroscopy. In: *Principles of Fluorescence Spectroscopy.* Baltimore, Maryland, USA: Springer, p. 28.

Lakowicz, J., 2006. *Principles of Fluorescence Spectroscopy.* Third ed. Baltimore, Maryland, USA: Springer.

Le Maux, S., Bouhallab, S. & Giblin, L., 2014. Bovine β-lactoglobulin/fatty acid complexes: binding, structural, and biological properties. *Dairy Science and Technology,* 94(5), pp. 409-426.

LEEFilters, 2015. *Cool green dichroic filter.* [Online]
Available at: http://www.leefilters.com/architecture/colour-details.html#G96&filter=dgf
[Accessed 04 09 2015].

Lee, K. S., Thompson, K. P. & Rolland, J. P., 2010. Broadband astigmatism-corrected Czerny–Turner spectrometer. *Optics Express,* 18(22), pp. 23378-23384.

Lehermayr, C., Mahler, H. C., Mader, K. & Fischer, S., 2011. Assessment of Net Charge and Protein–Protein Interactions of Different Monoclonal Antibodies. *Pharameceutical Sciences ,* 100(7), pp. 2551-2562.

Leuxeon Star, 2012. *Blue (470nm) LUXEON Rebel LED.* [Online]
Available at: http://www.luxeonstar.com/blue-20mm-star-coolbase-led-70lm
[Accessed 11 07 2016].

Lima, F. et al., 2010. Economic comparison of natural service and timed artificial insemination breeding programs in dairy cattle. *Journal of Dairy Science,* 93(9), p. 4404–4413.

Liu, H. & May, K., 2012. Disulfide bond structures of IgG molecules, Structural variations, chemical modifications and possible impacts to stability and biological function. *Landes Bioscience,* 4(1), pp. 17-23.

Loch, J. et al., 2011. Two modes of fatty acid binding to bovine β-lactoglobulin- crystallographic and spectroscopic studies. *Molecular Recognition,* 24(2), pp. 341-349.

Lopez, C., 2011. Milk fat globules enveloped by their biological membrane: Unique colloidal assemblies with a specific composition and structure. *Current Opinion in Colloid & Interface Science,* 16(5), p. 391–404.

Lopez, C. et al., 2011. Fat globules selected from whole milk according to their size: Different compositions and structure of the biomembrane, revealing sphingomyelin-rich domains. *Food Chemistry,* 125(2), p. 355–368.

Lopez, C., Madec, M. N. & Jimenez-Flores, R., 2010. Lipid rafts in the bovine milk fat globule membrane revealed by the lateral segregation of phospholipids and heterogeneous distribution of glycoproteins. *Food Chemistry,* 120(1), pp. 22-33.

Lumileds, 2002. *Advanced Electrical Design Models, Application Brief AB20-3A,* San Jose: Lumileds Lighting.

Lumileds, 2016. *LUXEON Rebel and LUXEON Rebel ES Colors.* [Online]
Available at: http://www.lumileds.com/uploads/265/DS68-pdf
[Accessed 11 07 2016].

Lumileds, P., 2010. *Technical Datasheet DS65,* s.l.: Philips Lumileds Lighting Company.

Maiti, D. K., Roy, S., Baral, A. & Banerjee, A., 2014. A fluorescent gold-cluster containing a new three-component system for white light emission through a cascade of energy transfer. *Journal of Materials Chemistry C,* Volume 2, pp. 6574-6581.

Mather, I. H., 2011. Milk Lipids - Milk Fat Globule Membrane. In: F. J. W., F. P. F. & M. P. L. H., eds. *Encyclopedia of Dairy Sciences.* s.l.:s.n., p. 680–690.

McCarthy, O. J. & Singh, H., 2009. Physio-chemical Properties of Milk. In: P. L. H. McSweeney & P. F. Fox, eds. *Advanced Dairy Chemistry: Volume 3: Lactose, Water, Salts and Minor Constituents.* s.l.:Springer Science & Business Media, p. 702.

Ménard, O. et al., 2010. Buffalo vs. cow milk fat globules; Size distribution, zeta-potential, compositions in total fatty acids and in polar lipids from the milk fat globule membrane. *Food Chemistry,* 120(2), pp. 544-551.

Merzlyak, E. M. et al., 2007. Bright monomeric red fluorescent protein with an extended fluorescence lifetime. *Nature Methods,* 4(7), pp. 555-557.

Millis, B., 2012. Evanescent-Wave Field Imaging: An Introduction to Total Internal Reflection Fluorescence Microscopy. *Methods in Molecular Biology,* Volume 823, pp. 295-309.

Mitchell, J., 2010. Small Molecule Immunosensing Using Surface Plasmon Resonance. *Sensors,* 10(8), pp. 7323-7346.

Mitchell, J. S., Wu, Y., Cook, C. J. & Main, L., 2004. Protein Conjugate-Based Immunoassay of Whole Milk Progesterone. *Dairy Science,* 87(9), pp. 2864-2867.

Mitchell, J., Wu, Y., Cook, C. & Main, L., 2005. Sensitivity enhancement of surface plasmon resonance biosensing of small molecules. *Analytical Biochemistry,* 343(1), p. 125–135.

Mizuno, T., Mizutani, Y. & Iwata, T., 2012. Phase-modulation fluorometer using a phase-modulated excitation light source. *Optical Review,* 19(4), pp. 222-227.

Moemeni, A., Ghadar, A. & Tatham, E., 2014. Inertial-Visual Pose Tracking using Optical Flow-aided Particle Filtering. *IEEE Symposium Series on Computational Intelligence (IEEE SSCI 2014).*

Moemeni, A. & Tatham, E., 2010. *A framework for camera pose tracking using stochastic data fusion.* Hongkong, s.n.

Monerris, M. J. et al., 2012. Integrated electrochemical immunosensor with gold nanoparticles for the determination of progesterone. *Sensors and Actuators B,* Volume 166-167, pp. 586-592.

Mootse, M. et al., 2014. Investigation of Casein Micelle Particle Size Distribution in Raw Milk of Estonian Holstein Dairy Cows. *Agronomy Research,* 12(3), pp. 753-758.

Naumowicz, M. & Figaszewski, Z. A., 2014. The Effect of pH on the Electrical Capacitance of Phosphatidylcholine - Phosphatidylserine System in Bilayer Lipid Membrane. *The Journal of Membrane Biology,* 247(4), pp. 361-369.

Nave, R., 2016. *HyperPhysics, Light and Vision.* [Online]
Available at: http://hyperphysics.phy-astr.gsu.edu/hbase/atmos/blusky.html#c2
[Accessed 11 07 2016].

Neave, N., 2008. *Hormones and behaviour: a psychological approach.* s.l.:Cambridge University Press.

Novus Biologicals, 2013. *Progesterone Antibody NB100-62844.* s.l.:Novus Biologicals.

Oku, Y. et al., 2011. Validation of a direct time-resolved fluoroimmunoassay for progesterone in milk from dairy and beef cows. *The Veterinary Journal,* 190(2), pp. 244-248.

Overton, M., 2005. Cost comparison of natural service sires and artificial insemination for dairy cattle reproductive management. *Theriogenology, Elsevier,* 64(3), p. 589–602.

Particle Sciences, 2012. *An Overview of the Zeta Potential,* s.l.: Technical Brief 2012 Volume 2.

Pemberton, R., Hart, J. & Mottram, T., 2001. An electrochemical immunosensor for milk progesterone using a continuous flow system. *Biosensors and Bioelectronics,* 16(9-12), p. 715–723.

Permyakova, E. A. L. J., 2000. α-Lactalbumin: structure and function. *FEBS Letters,* 473(3), pp. 269-274.

Philips Lumileds, 2010. *LUXEON Rebel Color Datasheet DS65,* s.l.: Philips Lumileds.

Photonics, H., 2012. *Super-Quiet Xenon Lamp and Super-Quiet Mercury-Xenon Lamp.* [Online] Available at: http://www.hamamatsu.com/resources/pdf/etd/Xe-HgXe_TLSX1044E.pdf [Accessed 04 09 2015].

Polyanskiy, M., 2008. *Optical Constants of Plastics - PMMA.* [Online] Available at: http://refractiveindex.info/?shelf=3d&book=plastics&page=pmma [Accessed 11 07 2016].

Poock, S., 2009. *Dairy Cattle Reproductive Manual.* [Online] Available at: http://agebb.missouri.edu/dairy/reproduction/ [Accessed 07 11 2016].

Poock, S., Horner, J. & Milhollim, R., 2009. *Dairy Cattle Reproductive Manual,* Missouri: University of Missouri.

Posthuma-Trumpie, G., Korf, J. & Amerongen, A., 2009. Lateral flow (immuno) assay: its strengths, weaknesses, opportunities and threats. A literature survey. Anal Bioanal Chem. *Analytical and Bioanalytical Chemistry,* 393(2), pp. 569-582.

Posthuma-Trumpie, G., Van Amerongen, A., Korf, J. & Van Berkel, W., 2009. Perspectives for on-site monitoring of progesterone. *Trends in Biotechology,* 27(11), p. 652–660.

Ragona, L. et al., 2000. Bovine b-lactoglobulin: Interaction studies with palmitic acid. *Protein Science,* 9(7), pp. 1347-1356.

Rahimi Yazdi, S. & Corredig, M., 2012. Heating of milk alters the binding of curcumin to casein micelles. A fluorescence spectroscopy study. *Food Chemistry,* 132(3), p. 1143–1149.

Rao, T. K. S. et al., 2013. Heat detection techniques in cattle and buffalo. *Veterinary World,* 6(7), pp. 363-369.

Regal, P. et al., 2010. Determination of naturally occurring progestogens in bovine milk as their oxime derivatives using high performance liquid chromatography-electrospray ionization-tandem mass spectrometry.. *Journal of the Science of Food and Agriculture,* 90(10), pp. 1621-1627.

Rodriguez-Mozaz, S., López de Alda, M. & Barceló, D., 2009. Achievements of the RIANA and AWACSS EU Projects: Immunosensors for the determination of pesticides, endocrine disrupting chemicals and pharmaceuticals. *Biosensors for Environmental Monitoring of Aquatic Systems,* Volume 5J, pp. 33-46.

Roelofs, J. et al., 2006. Relationship between progesterone concentrations in milk and blood and time of ovulation in dairy cattle. *Animal Reproduction Science,* 91(3-4), pp. 337-343.

Sabban, S., 2011. *Development of an in vitro model system for studying the interaction of Equus caballus lgE with its high - affinity Fc receptor.* Sheffield: University of Sheffield - PhD Thesis.

Samsonova, J., Safronova, V. & Osipov, A., 2015. Pretreatment-free lateral flow enzyme immunoassay for progesterone detection in whole cows' milk. *Talanta,* Volume 132, pp. 685-689.

Santos, M. & Lies, M., 2013. *Analysis of Casein and Whey Protein in Whole, 2%, and Skim Milk by Capillary Gel Electrophoresis,* Brea, USA: Beckman Coulter Life Sciences.

Sauer, M., Hofkens, J. & Enderlein, J., 2011. *Handbook of Fluorescence Spectroscopy and Imaging: From Single Molecules to Ensembles.* s.l.:Wiley-VCH.

Schramm, W. & Paek, S. H., 1992. Antibody-Antigen Complex Formation with Immobilised Immunoglobulins. *Analytical Biochemistry ,* 205(1), pp. 47-56.

Scientific, T. F., 2014. *Qubit® 3.0 Fluorometer.* s.l.:Thermo Fisher Scientific.

Shakuntala, N. & Manay, O., 2001. Milk and Milk Products. In: *Food: Facts and Principles.* s.l.:Steiner Books, p. 337.

Shcherbo, D. et al., 2009. Practical and reliable FRET/FLIM pair of fluorescent proteins. *BMC Biotechnology,* 9(24), pp. 1-6.

Sigma Aldrich, 2000. *Bovine Serum Albumin.* s.l.:Sigma Aldrich.

Singh, H., 2006. The milk fat globule membrane - A biophysical system for food applications. *Current Opinion in Colloid & Interface Science,* 11(2-3), pp. 154-163.

Smith, S. D. & Eremin, S. A., 2008. Fluorescence polarization immunoassays and related methods for simple, high-throughput screening of small molecules. *David S. Smith, Sergei A. Eremin ,* 391(5), pp. 1499-1507.

Stahelin, R. V., 2013. Surface plasmon resonance: a useful technique for cell biologists to characterize biomolecular interactions. *Molecular Biology of the Cell,* 24(7), pp. 883-886.

Szpocińska, E. & Markiewicz, A., 2007. New RIA Kit for the Determination of Progesterone in Cows' Milk. *Immunoassay and Immunochemistry,* 27(3), pp. 279-288.

Tadros, T. F., 2005. Introduction. In: *Applied Surfactants: Principles and Applications.* s.l.:Wiley-VCH, p. 1.

Tan, C. et al., 2015. A new one-step antigen heterologous homogeneous fluorescence immunoassay for progesterone detection in serum. *Talanta,* Volume 134, pp. 508-513.

Tan, Y. H. et al., 2008. A Nanoengineering Approach for Investigation and Regulation of Protein Immobilization. *ACS Nano,* 2(11), p. 2374–2384.

Thermo Fisher Scientific, 2012. *Amplex Cholesterol Assay manual.* [Online]
Available at: https://www.thermofisher.com/uk/en/home/industrial/spectroscopy-elemental-

isotope-analysis/molecular-spectroscopy/fluorometers/qubit/qubit-assays.html
[Accessed 11 07 2016].

Thermo Scientific, 2011. *Thermo Scientific Pierce Assay Development Technical Handbook.* [Online]
Available at: https://tools.thermofisher.com/content/sfs/brochures/1602127-Assay-Development-Handbook.pdf
[Accessed 11 07 2016].

Thermo Scientific, 2013. *NanoDrop 3300 Fluorospectrometer.* [Online]
Available at: http://www.nanodrop.com/productnd3300overview.aspx
[Accessed 11 07 2016].

Trapiella-Alfonso, L., Costa-Fernández, J. M., Pereiro, R. & Sanz-Medel, A., 2011. Development of a quantum dot-based fluorescent immunoassay for progesterone determination in bovine milk. *Biosensors and Bioelectronics,* 26(12), p. 4753– 4759.

Tschmelak, J., Kappel, N. & Gauglitz, G., 2007. Development of a TIRF-based biosensor for sensitive detection of progesterone in bovine milk. *Biosensors and Bioelectronics,* 22(9-10), p. 2295–2300.

Ullman, E. F., 2013. Homogeneous Immunoassays. In: *The Immunoassay Handbook.* s.l.:Elsevier, pp. 67-86.

Varriale, A. et al., 2015. A Fluorescence Polarization Assay To Detect Steroid Hormone Traces in Milk. *Journal of Agricultural and Food Chemistry,* 63(41), p. 9159−9164.

Velasco-Garcia, M. & Mottram, T., 2003. Biosensor Technology addressing Agricultural Problems. *Biosystems Engineering,* 84(1), pp. 1-12.

Vishwanath, R., 2003. Artificial insemination: the state of the art. *Theriogenology,* 59(2), p. 571–584.

Waldmann, A., 1993. Enzyme Immunoassay (EIA) for Milk Progesterone using a Monoclonal Antibody. *Animal Reproduction Science,* 34(1), pp. 19-30.

Waldmann, A. et al., 2001. Progesterone concentrations in milk fat at first insemination - effects on non-return and repeat-breeding. *Animal Reproduction Science,* 65(1-2), pp. 33-41.

Wall, M. A., Socolich, M. & Ranganathan, R., 2000. The structural basis for red fluorescence in the tetrameric GFP homolog DsRed. *Nature structural biology,* 7(12), pp. 1133-1138.

Walstra, P. & Jenness, R., 1984. *Dairy chemistry and physics.* New York: Wiley Interscience.

Wang, Q., Allen, J. C. & Swaisgood, H. E., 1997. Binding of Vitamin D and Cholesterol to β-Lactoglobulin. *Dairy Science,* 80(6), pp. 1054-1059.

Watch, H., 2006. *Heat watch II.* [Online]
Available at: http://www.cowchips.net/index.html
[Accessed 11 07 2016].

Weisstein, E. W., 2007. *Lens Maker's Formula.* [Online]
Available at: http://scienceworld.wolfram.com/physics/LensMakersFormula.html
[Accessed 11 07 2016].

Wild, D., 2013. Immunoassay Handbook, Theory and Applications of Ligand Binding, ELISA and Related Techniques. In: *Immunoassay Handbook.* 4 ed. s.l.:Elsevier, p. 7.

Wiseman, M. E. & Frank, C. W., 2012. Antibody Adsorption and Orientation on Hydrophobic Surfaces. *Langmuir,* 28(3), pp. 1765-1774.

Xia, N. S. et al., 2002. Bioluminescence of Aequorea macrodactyla, a Common Jellyfish Species in the East China Sea. *Marine Biotechnology,* 4(2), pp. 155-162.

Xu, Y., Velasco-Garcia, M. & Mottram, T. T., 2005. Quantitative analysis of the response of an electrochemical biosensor for progesterone in milk. *Biosensors and Bioelectronics,* 20(10), p. 2061–2070.

Yang, F., Moss, L. G. & Phillips, G. N., 1996. The molecular structure of green fluorescent protein. *Nature Biotechnology,* Volume 14, pp. 1246-1251.

Yang, L., Hu, J. & Shin, M., 2008. Dynamic Thermal Analysis of High-Power LEDs at Pulse Conditions. *IEEE ELECTRON DEVICE LETTERS,* 29(8), pp. 863-866.

Zheng, H., Jiménez-Flores, R. & Everett, D. W., 2014. Lateral lipid organization of the bovine milk fat globule membrane is revealed by washing processes. *Journal of Dairy Science,* 97(10), pp. 5964-5974.